

Lucía González Bermúdez

Iodoethynyl derivatives scaffolds in
supramolecular chemistry: the
interplay of design and synthesis

Departamento
Química Orgánica

Director/es
Uriel Rubio, Santiago
Serrano Ostáriz, José Luis

<http://zaguan.unizar.es/collection/Tesis>



Reconocimiento – NoComercial –
SinObraDerivada (by-nc-nd): No se
permite un uso comercial de la obra
original ni la generación de obras
derivadas.

© Universidad de Zaragoza
Servicio de Publicaciones

ISSN 2254-7606

Tesis Doctoral

IODOETHYNYL DERIVATIVES SCAFFOLDS IN SUPRAMOLECULAR CHEMISTRY: THE INTERPLAY OF DESIGN AND SYNTHESIS

Autor

Lucía González Bermúdez

Director/es

Uriel Rubio, Santiago
Serrano Ostáriz, José Luis

UNIVERSIDAD DE ZARAGOZA

Química Orgánica

2017

TESIS DOCTORAL

Iodoethynyl derivatives scaffolds in supramolecular chemistry: the interplay of design and synthesis.

Departamento de Química Orgánica

Facultad de Ciencias

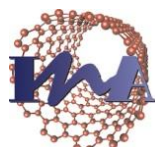
Instituto de Nanociencia de Aragón

Instituto de Ciencia de los Materiales de Aragón

Universidad de Zaragoza



Departamento de
Química Orgánica
Universidad Zaragoza



Instituto de Ciencia
de Materiales de Aragón

**Memoria presentada en la Universidad de Zaragoza para optar al
grado de Doctor en Química por:**

Lucía González Bermúdez

Zaragoza, Mayo 2017

INFORME DIRECTORES

Autorización de presentación de la tesis con mención internacional.

D. SANTIAGO URIEL RUBIO, Profesor Titular del Departamento de Química Orgánica, y D. JOSÉ LUIS SERRANO OSTÁRIZ, Catedrático del Departamento de Química Orgánica,

AUTORIZAN

La presentación de la siguiente memoria, titulada “Iodoethynyl derivatives scaffolds in supramolecular chemistry: the interplay of design and synthesis.”, presentada por Dña. LUCÍA GONZÁLEZ BERMÚDEZ para optar al grado de Doctor por la Universidad de Zaragoza, y certifican que ha sido realizada bajo su dirección en el Departamento de Química Orgánica.

Y para que conste, expiden la presente autorización

En Zaragoza, a 05 de Mayo de 2017

Fdo. Santiago Uriel Rubio

Fdo. José Luis Serrano Ostáriz

TRIBUNAL DESIGNADO PARA LA DEFENSA

DOCTORANDA D^a. Lucía González Bermúdez

TÍTULO DE LA TESIS: “**Iodoethynyl derivatives scaffolds in supramolecular chemistry: the interplay of design and synthesis.**”

PRESIDENTE: LARRY R. FALVELLO

SECRETARIO: GUILLERMO MÍNGUEZ ESPALLARGAS

VOCAL 1: MARC FOURMIGÉ

SUPLENTE 1: TERESA SIERRA TRAVIESO:

SUPLENTE 2: EMMA CAVERO MENÉNDEZ

El tribunal designado para calificar la tesis doctoral arriba indicada y reunido en el día de la fecha, una vez efectuada la defensa por la doctoranda y contestadas las objeciones y/o sugerencias que se le han formulado, ha otorgado por la calificación de:

En Zaragoza, a _____ de _____ de 2017

Agradecimientos

Agradecer a mis directores de Tesis Doctoral el Dr. José Luis Serrano y el Dr. Santiago Uriel por brindarme la oportunidad de realizar este intenso estudio de los enlaces de halógeno dentro del grupo de Cristales Líquidos y Polímeros perteneciente al departamento de Química Orgánica, así mismo agradecer al Ministerio de Economía Industria y Competitividad la financiación que lo ha hecho posible mediante la beca predoctoral FPI 2010, la estancia breve FPI 2013 con el Dr Jagadese Jay Vittal en la Universidad de Singapur, y los proyectos MAT2009-1436-C03-01 y MAT2012-38538-C03-01.

A mi madre

Resumen

El manuscrito de tesis se enmarca dentro del ámbito de la Química Supramolecular, la cual fue definida por Jean Marie Lehn como “la química más allá de la molécula”.¹

Es un campo altamente interdisciplinario que cubre tanto aspectos químicos, como físicos y biológicos, de las especies químicas de complejidad más grande que las moléculas mismas que se mantienen unidas y organizadas por medio de interacciones no covalentes. Uno de los aspectos más importantes y rápidamente desarrollados de la química supramolecular es la síntesis de cristales moleculares, la cual es también un objetivo mayor de otra área relativamente nueva, la ingeniería cristalina. La ingeniería cristalina se define como el estudio de las interacciones intermoleculares en el contexto del empaquetamiento cristalino, por un lado, y como la utilización del dicho entendimiento en el diseño de los sólidos nuevos con las propiedades físicas y químicas deseadas, por el otro. Los cristales moleculares, que consisten de las moléculas orgánicas, organometálicas o de los complejos de coordinación, cuales están ensamblados en el estado sólido como la consecuencia de las interacciones no-covalentes, son los objetos de investigaciones numerosas durante las últimas décadas. El interés hacia tales materiales es el resultado de la posibilidad de manipular con las propiedades de los cristales singulares en el estado sólido a través de la variación sistemática de sus estructuras moleculares y de las propiedades de sus componentes moleculares.

Dentro de la química supramolecular también se encuentran los cristales líquidos. El estado cristal líquido² se define como un estado de agregación de la materia intermedio entre el estado cristalino y el líquido, y surge como consecuencia de fuerzas intermoleculares en un proceso de auto-organización supramolecular. La inusual combinación en estos sistemas de

propiedades, como fluidez y anisotropía, han permitido que estos materiales tengan, desde hace 50 años, una gran cantidad de aplicaciones en la vida cotidiana (relojes, calculadoras, televisores, cosméticos, etc.). No obstante, lo aprendido a lo largo de estos años ha permitido así mismo constatar lo que probablemente en la actualidad suponga el mayor atractivo, interés e innovación de los cristales líquidos: que este estado de agregación de la materia sea considerada como una herramienta de trabajo en la consecución de nuevos sistemas y aplicaciones.

En la última década una de las líneas de investigación del *Grupo de Cristales Líquidos y Polímeros* se ha centrado en la preparación y caracterización de nuevas materiales basados en enlaces de halógeno. Las propiedades de un material no dependen únicamente de las moléculas que lo componen sino también de su organización en estado sólido. Además, de las interacciones clásicas (enlace de hidrógeno, dipolo-dipolo, enlace de coordinación) están cobrando una gran importancia los enlaces de halógeno. Este tipo de interacciones se ha empleado en la preparación de conductores orgánicos y cristales líquidos ya que presentan una fuerza y direccionalidad similar a los enlaces de hidrógeno.

OBJETIVOS Y METODOLOGÍA

Objetivos:

El trabajo que se va a desarrollar en esta Tesis Doctoral tiene como objetivo principal estudiar y aportar nuevas posibilidades de las estructuras basadas en enlace de halógeno en Química Supramolecular, centrándonos nuestra

atención en la fuerza y direccionalidad que posee el enlace de halógeno basado en moléculas con yodo unidas a un carbono con hibridación sp.

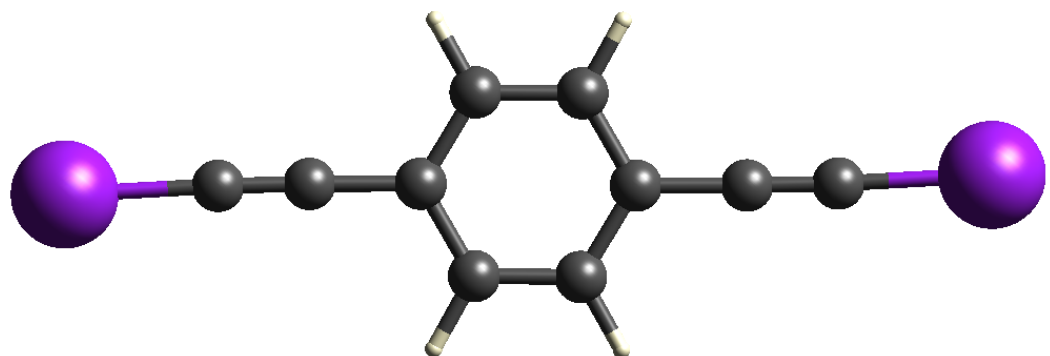


Ilustración 1 Molécula con dos grupos yodoetinil.

El estudio de estos compuesto no solo nos permitirá la obtención de nuevos materiales, como los cristales líquidos tipo bent-core (no descritos hasta la fecha vía enlace de halógeno)², calamíticos y discóticos. Además de materiales porosos.

Así mismo nos permitirá una comparación directa con el enlace de hidrógeno, tanto como la competitividad o/y la cooperatividad entre ambos.

Metodología:

Para la consecución de estos objetivos se han seleccionado y sintetizado moléculas halogenadas con diferentes geometrías. Además de los dadores de enlace de halógeno, se seleccionaron diferentes aceptores de enlace de halógeno: halogenuros y derivados nitrogenados principalmente.

De esta manera, los objetivos particulares y metodología de trabajo de esta tesis doctoral pueden dividirse en los siguientes apartados:

1. Síntesis y caracterización:

- Síntesis y caracterización de derivados de yodoetinil ditópicos y tritópicos con diferentes geometrías. Capítulo 1.
- Síntesis y caracterización de bases de Tröger halogenadas para formación de redes supramoleculares porosas. Capítulo 3.

La síntesis de estos compuestos combina diferentes reacciones de esterificación, halogenación, etc.

Todos los compuestos preparados, tanto intermedios como finales, se caracterizarán según las técnicas habituales para determinar su estructura química: espectroscopia de resonancia magnética nuclear de protón y de carbono ($^1\text{H-RMN}$ y $^{13}\text{C-RMN}$), espectroscopia infrarroja (IR) y espectrometría de masas (MS). Además se estudiarán sus propiedades en el monocrystal.

2. Estudio y caracterización de las propiedades:

- En el capítulo 4 se estudiará la formación de cocróstales mediante enlaces de halógeno como interacción principal, y los enlaces de hidrógeno como herramientas para aumentar la dimensionalidad estructural.
- En el capítulo 5 se estudiarán las propiedades térmicas y mesomorfas de los materiales mediante microscopía óptica con luz polarizada, calorimetría diferencial de barrido (DSC), termogravimetría (TGA) y difracción de rayos X.
- En el capítulo 6 se sintetiza, caracteriza y estudia las propiedades de una molécula con 4 posibilidades diferentes de interacción, además del enlace de halógeno, hilo conductor de esta tesis, la posibilidad de coordinación metálica, enlaces de hidrógeno o interacciones π - π .

Asimismo en el capítulo 5 y en el capítulo 4 se hará uso de otras técnicas como espectroscopia Raman, espectroscopia fotoelectrónica de rayos X

(XPS), calorimetría isoterma de titulación (ITC), difracción de rayos X de monocristal y de polvo para completar los estudios de cristales líquidos del capítulo 5 y en el capítulo 4 también se pretende comparar las propiedades en disolución con las del estado sólido, por ello el uso del ITC.

[1] J.-M. Lehn, *Angewandte Chemie International Edition in English* **1990**, 29, 1304-1319.

[2] L. Gonzalez, N. Gimeno, R. Maria Tejedor, V. Polo, M. Blanca Ros, S. Uriel and J. Luis Serrano, *Chem. Mat.* **2013**, 25, 4503-4510.

Acronyms list

¹³C-NMR	Nuclear Magnetic Resonance Carbon
¹H-NMR	Nuclear Magnetic Resonance Proton
1,3,5-TIEB	1,3,5-tris(iodoethynyl)benzene
1,3,5-TIPCB	tris(3-iodoprop-2-yn-1-yl) benzene-1,3,5-tricarboxylate
A	Halogen-hydrogen bond acceptor
Å	Angstrom ($1 \cdot 10^{-10}$ m)
BET	Brunauer–Emmett–Teller
BPE	bis(4-pyridyl)ethylene
BSSE	“Basis set superposition error”
CDCl₃	Cloroformo deuterado
CDS	“Cambridge structural database”
COF	“Covalent-organic frameworks”
Col.	Colaboradores
Col_h	Columnar hexagonal
Cr	Cristal
DCC	N,N'-diciclohexilcarbodiimida
d_e	Distancia externa a la superficie de Hirshfeld
DFT	“Density functional theory”
d_i	Distancia interna a la superficie de Hirshfeld
DMAP	4-(dimetilamino)piridina

DMSO	dimetilsulfóxido
DSC	“Differential scanning calorimetry” (calorimetría diferencial de barrido)
DTMABr	Deciltrimethyl Ammonium Bromide
EI	Ionización electrónica
ESI	Ionización por electrospray
EtOH	Etanol
FT-IR	espectroscopía infrarroja por transformada de Fourier
HBOF	“Hydrogen bond organic frame-works”
HPLC	“High-Performance Liquid Chro-matography”
HTMA	hexamethylenetetramine
INPBA	4-Iodo-N-(4-pyridyl)benzamide
IUPAC	“Internacional union of pure and applied chemistry”
ITC	Isothermal titration calorimetry
MALDI	“Matrix-assited laser desorption ionization”
mBIEB	1,3-bis(iodoethynyl)benzene
MeOH	Metanol
MOF	Metal-organic frameworks
MOM	Metal-organic materials
Mp	“Melting point”
MS	“Mass Spectrometry”

NBO	“Natural bond orbital”
NPBA	N-(4-pyridyl)benzamide
ORTEP	“Oak Ridge Thermal Ellipsoid” Plot
pBBrEB	1,4-bis(bromoethynyl)benzene
pBIEB	1,4-bis(iodoethynyl)benzene
pBIPT	bis(3-iodoprop-2-yn-1-yl) terephthalate
Ph₄PBr	Tetraphenyl Phosphonium bromide
POCM	porous organic polymers and crystalline materials
Rac	Racemic
STC	“Supramolecular-tilt-chirality”
T	Coordination shape
TB	Tröger´s Base
TBABr	Tetrabutylammonium Bromide
TFA	Ácido trifluoroacético
TGA	Thermogravimetry
THF	Tetrahidrofurane
TPABr	Tetrapropyl ammonium Bromide
TMS	tetrametilsilane

INDEX

Chapter 1	Introduction	1
1.1	Bibliography	6
Chapter 2	Iodoethynyl halogen bond donors	7
2.1	Introduction	9
2.2	Previous works of halogen bond acceptor groups	12
2.3	Objectives	14
2.4	Synthesis of the bis-iodoethynyl synthons and their bis-ethynyl precursors	
15		
2.4.1	Preparation of the ethynyl precursors.....	15
2.4.2	Synthesis of the iodoethynyl derivatives.....	16
2.5	Ethynyl <i>vs</i> iodoethynyl derivatives: A comparative study.	17
2.5.1	1,4-Bis(iodoethynyl)benzene (pBIEB) <i>vs</i> 1,4-bis(ethynyl)benzene (pBEB)	20
2.5.2	1,3,5-Tris(iodoethynyl)benzene (1,3,5-TIEB) <i>vs</i> 1,3,5-tris(ethynyl)benzene	26
2.5.3	1,3-Bis(iodoethynyl)benzene (mBIEB)	29
2.5.4	Bis(3-iodoprop-2-yn-1-yl) terephthalate (pBIPT) <i>vs</i> bispropargyl terephthalate (pBPT)	32
2.5.5	Tris(3-iodoprop-2-yn-1-yl) benzene-1,3,5-tricarboxylate (1,3,5-TIPCB) <i>vs</i> tris(prop-2-yn-1-yl) benzene-1,3,5-tricarboxylate (1,3,5-TPCB) .	34
2.6	Conclusions	38
2.7	Experimental Section.....	39

2.7.2	General method.....	39
2.7.3	Characterization of halogen derivatives	40
2.7.4	X-ray monocrystal diffraction	40
2.7.5	Hirshfeld Surfaces	41
2.8	Final Remarks	43
2.9	Bibliography.....	44
Chapter 3	Iodo Tröger's Base derivatives: Towards halogen bonded porous organic crystalline materials	47
3.1	Introduction	49
3.2	Previous work	50
3.3	Objectives and planning.....	54
3.3.1	Objectives	54
3.3.2	Planning	54
3.4	Results and discussion	57
3.4.1	Preparation of the Tröger's base derivatives	57
3.4.2	X-ray monocrystal structures of iodo Tröger's base derivatives.....	57
3.5	Conclusions	65
3.6	Experimental Section	66
3.6.1	Synthesis and chemical characterization	66
3.6.2	X-ray monocrystal diffraction	67
3.7	Bibliography.....	69
Chapter 4	Supramolecular chemistry: Crystal engineering.....	71
4.1	Introduction	73
4.2	Objectives and work plan.....	76

4.3 Halogen bonding cocrystals.....	77
4.3.1 Previous works	77
4.3.2 X-ray Crystal Structures.....	82
4.3.3 Halogen bonded complexes 1 and 2: Linear XB donor and acceptor	88
4.3.4 Angular polymers	89
4.3.5 Hirshfeld Surface Analysis.....	97
4.3.6 DFT Calculations.	98
4.4 Halogen bonding salts	102
4.4.1 Previous works	102
4.4.2 X-ray Crystal Structures.....	107
4.4.3 pBIEB· TPABr complex, Structure 9.	111
4.4.4 pBIEB ·TBA Br complex, Structure 10.	113
4.4.5 pBIEB ·[TPhPBr] ₂ complex, Structure 11.	115
4.4.6 Hirshfeld Surface.....	117
4.4.7 Isothermal Titration Calorimetry.	122
4.5 Conclusions	127
4.6 Experimental.....	128
4.6.1 Crystal synthesis and characterization	128
4.6.2 X-ray monocrystal diffraction.....	128
4.7 Hirshfeld Surfaces	131
4.8 Computational Methods.	132
4.9 Bibliography	133
Chapter 5 Liquid Crystals: Promesogenic Calamitic, Bent-core and Discotic Shapes by Halogen Bonding.	139

5.1	Introduction	141
5.2	Previous works.....	143
5.2.1	Liquid crystals: Properties and classification	144
5.2.2	Liquid Crystal Characterization.....	149
5.2.3	Liquid crystals by hydrogen bonding	150
5.2.4	Liquid crystals by halogen bonding.....	151
5.3	Objectives and planning work.....	153
5.3.1	Objectives	153
5.3.2	Planned work	153
5.4	Synthesis and Characterization of the precursors and the complexes ...	157
5.4.1	General Synthesis	157
5.4.2	Characterization	158
5.5	Liquid crystal properties of the complexes	167
5.5.1	Series P (rod-like structures)	170
5.5.2	Series M (bent-shaped structures)	171
5.5.3	Series T (disc-like structures)	174
5.6	Crystal and Molecular Structure	177
5.7	Theoretical modeling	180
5.8	Conclusions	182
5.9	Experimental Section	183
5.9.1	Synthesis	183
5.9.2	Computational methods	186
5.9.3	X-ray monocrystal diffraction	187
5.10	Bibliography	189

Chapter 6 Coordination Metal Complexes Based on 4-Iodo-N-(4-pyridyl)benzamide, a Polyfunctional Ligand	193
6.1 Introduction	195
6.2 Previous works	197
6.3 X-ray Crystallography	202
6.3.1 4-iodo-N-(4-pyridyl)benzamide (INPBA)	202
6.4 Hirshfeld Surface Analysis	213
6.5 Quantum Mechanical Calculations.....	215
6.6 Conclusions	217
6.7 Experimental Section.....	218
6.8 Bibliography	222
Chapter 7 Conclusions	225

Chapter 1 Introduction

Non-covalent interactions have become an extraordinary and versatile tool to generate many original and attractive supramolecular architectures and functionalities in different fields.^[1]

Among them, it is worth highlighting the remarkable evolution of hydrogen bonding from being a curious intermolecular interaction between a hydrogen atom and an electron-rich partner to being a powerful tool for molecular control of protein and DNA chemistry, crystal engineering of solid-state materials and also in soft matter assemblies. Regarding soft materials, the use of hydrogen bonding is quite widespread in the field liquid crystals, and crystals engineering in which it has been successfully used to prepare a varied of functional materials.^[2]

In this context, an alternative working strategy to hydrogen bonding (HB) is halogen bonding (XB). Indeed, a great deal of research has recently been carried out with the aim of understanding and harnessing this type of noncovalent interaction, which involves pairing a halogen atom with an electron-rich partner. Although the halogen bond was described more than 150 years ago,^[3] it was not until the 1970s that O.Hassel highlighted the ability of this interaction to manage self-assembly processes.^[4] During the past decade, many applications of halogen bonding in fields as diverse as crystal engineering, enantiomer separation, biology, and supermolecular architectures have been reported and reviewed.^[5] This noncovalent interaction exhibits similar characteristics to HB in directionality and strength and may cooperate with or prevail over HB.^[6]

In the work recovered in this PhD we tried to advance in the knowledge supramolecular organizations based of the XB and other weak interactions. Among the different structural possibilities to introduce XB bonds we have choose the iodoethynyl group as the main halogen bond donor group because their novelty and their excellent geometrical and electronic properties.

Introduction

Thus the chapter 2 is devoted to the new *Iodoethynyl* halogen bond donor molecules designed and synthesized in this PhD. In the synthesis of these compounds the homologous precursors bearing ethynyl moieties instead the iodoethynyl groups are obtained. Both type of compounds form in the solid state to give rise to very interesting isostructural crystalline organizations. A comparative study of these structures has been made.

Chapter 3 is devoted to preparation of porous organic crystalline materials. In order to achieve this objective we are choose *Iodo-containing* Tröger base derivatives functionalized in positions 2 and 8, taking advantage of their rigid geometry and self-complementarity of their enantiomers in racemic mixtures.

In chapter 4 deals with crystal engineering procedures to guide the arrangement adopted by the individual molecules in the solid networks. In our case we use the cocrystallization of two or more components that engage via weak interactions as hydrogen or halogen bond, $\pi\cdots\pi$ staking or a combination of them. This strategy allows obtaining new architectures in a versatile way using previously described compounds.

Chapter 5 is devoted to prepare new ‘supermolecules’ by means of halogen bonding interactions that exhibit liquid crystal properties. Our approach combine halogen bond donors based on bis(iodoethynyl)benzene derivatives and halogen bond acceptors based on basic nitrogen-containing molecules. In order to advance in the knowledge of the liquid crystal state a study of the structure-activity relationship for the complexes have been planned.

Finally chapter 6 explored the design of solid state structures based on molecules that use metal-ligand coordination, hydrogen and halogen bonding, and $\pi\cdots\pi$ stacking interactions as directional motifs to guide the self-assembly of network structures. One of the most powerful strategies for regulating solid-state structure is the arrangement of metallotectons by non-covalent interactions. However, the

presence of halogen bonding in metal coordination polymers has not been received sufficient attention.^[7]

1.1 Bibliography

- [1] a) J. Ř. P. Hobza, *Chem. Rev.* **2016**, 9, 11; b) A. S. M. a. G. N. Sastry, *Chem. Rev.* **2016**, 116, 2775–2825; c) M. Raynal, P. Ballester, A. Vidal-Ferran and P. W. van Leeuwen, *Chem Soc Rev* **2014**, 43, 1660-1733; d) K. T. M. A. M. Maharramov, M. N. Kopylovich, A. J. L. Pombeiro,, *Non-covalent Interactions in the Synthesis and Design of New Compounds*, Wiley, **2016**, p.
- [2] a) M. Meot-Ner., *Chem. Rev* **2011**, 110, 22-103; b) M. B. G. Armstrong, *J Mat. Sci.* **2005**, 40, 547-559; c) M. I.-V. E. D. Głowiak, S. Bauer, N. S. Sariciftci, , *J. Mater. Chem. B* **2013**, 1, 3742-3753; d) T. Steiner, *Angew. Chem., Int. Ed.* **2002**, 41, 48.
- [3] a) F. Guthrie, *J. Chem. Soc.* **1863**, 16, 239; b) I. N. Remses, J. F. , *Am. Chem. J.* **1896**, 18, 90.
- [4] a) O. Hassel and J. Hvoslef, *Acta Chemica Scandinavica* **1954**, 8, 873-873; b) O. Hassel and C. Romming, *Quarterly Rev.* **1962**, 16, 1-18; c) H. A. Bent, *Chem. Rev.* **1968**, 68, 587.
- [5] a) P. Auffinger, F. A. Hays, E. Westhof and P. S. Ho, *Proc. Natl. Acad. Sci. U. S. A.* **2004**, 101, 16789; b) P. Metrangolo, H. Neukirch, T. Pilati and G. Resnati, *Acc. Chem. Res.* **2005**, 38, 386-395; c) A. R. Voth and P. S. Ho, *Curr. Top. Med. Chem.* **2007**, 7, 1336; d) P. Metrangolo, F. Meyer, T. Pilati, G. Resnati and G. Terraneo, *Angew. Chem., Int. Ed.* **2008**, 47, 6114; e) D. W. Bruce in *Halogen-bonded liquid crystals*, Vol. 126 Eds.: P. Metrangolo and G. Resnati), **2008**, pp. 161-180; f) L. A. Hardegger, B. Kuhn, B. Spinnler, L. Anselm, R. Ecabert, M. Stihle, B. Gsell, R. Thoma, J. Diez, J. Benz, J. M. Plancher, G. Hartmann, D. W. Banner, W. Haap and F. Diederich, *Angew Chem Int Ed Engl* **2011**, 50, 314-318; g) H. L. Nguyen, P. N. Horton, M. B. Hursthouse, A. C. Legon and D. W. Bruce, *J. Am. Chem. Soc.* **2004**, 126, 16; h) M. Fourmigue and P. Batail, *Chem. Rev.* **2004**, 104, 5379-5418; i) L. C. Gilday, S. W. Robinson, T. A. Barendt, M. J. Langton, B. R. Mullaney and P. D. Beer, *Chem. Rev.* **2015**, 115, 7118-7195.
- [6] I. I. Ebralidze, M. Hanif, R. Arjumand, A. A. Azmi, D. Dixon, N. M. Cann, C. M. Crudden and J. H. Horton, *J. Phys. Chem. C* **2012**, 116, 4217.
- [7] a) L. Brammer, G. M. Espallargas and S. Libri, *CrystEngComm* **2008**, 10, 1712-1727; b) R. Bertani, P. Sgarbossa, A. Venzo, F. Lelj, M. Amati, G. Resnati, T. Pilati, P. Metrangolo and G. Terraneo, *Coord. Chem. Rev.* **2010**, 254, 677; c) R. Bertani, P. Sgarbossa, A. Venzo, F. Lelj, M. Amati, G. Resnati, T. Pilati, P. Metrangolo and G. Terraneo, *Coord. Chem. Rev.* **2010**, 254, 677-695; d) R. W. Troff, T. Mäkelä, F. Topič, A. Valkonen, K. Raatikainen and K. Rissanen, *Eur. J. Org. Chem.* **2013**, 2013, 1617; e) B. Li, S.-Q. Zang, L.-Y. Wang and T. C. W. Mak, *Coord. Chem. Rev.* **2016**, 308, 1-21.

Chapter 2 Iodoethynyl halogen bond donors

2.1 Introduction

This chapter is devoted to the synthesis and crystal structures of the iodoethynyl derivatives, which were used throughout the work reported here as halogen bonding donors to prepare different kinds of materials.

The first logical step in a planning such a study is to carry out a literature survey in the area of interest. For this reason, section 2.3 of this chapter is devoted to a brief discussion of the prior art on the different groups of halogen bond donors reported to date. Only a few papers dealing with iodoethynyl groups were found in the literature, despite the fact that the iodoethynyl group shows excellent properties as a halogen bond donor.^[1] On the basis of these precedents the iodoethynyl group was selected for the work described in this Ph.D. thesis.

As explained in chapter 1, one of the fundamental objectives of this work was to use halogen bonding interactions as a tool to obtain supramolecular structures in both the solid state (by crystal engineering) and in the liquid crystalline state.

In order to achieve these objectives, the design and synthesis of five ditopic tectons bearing two iodoethynyl groups were planned. Some of these halogen bond donors have been described previously by other authors but many of the compounds are novel and were synthesized for the first time in this study.^[2]

When selecting the appropriate synthons both the electronic parameters, such as conjugation in the molecules, and structural factors, such as rigidity and geometry, were taken into account. The three bis-iodoethynyl and the two tris-iodoethynyl derivatives chosen for this work are shown in Table 2.1 and Figure 2.1.

Some of these difunctional building blocks have been used in the work described in chapter 4, which concerns supramolecular crystalline structures, and in the chapter devoted to liquid crystals.

Iodoethynyl halogen bond donors

Table 2.1- Description of the halogen bond donor derivatives synthesized in this work.

Name	Code	Electronic parameter	Geometry	Rigidity
1,4-bis(iodoethynyl)benzene	pBIEB	Conjugated ^a	Linear	Rigid
1,3-bis(iodoethynyl)benzene	mBIEB	Conjugated	Angular	Rigid
1,3,5-tris(iodoethynyl)benzene	1,3,5-TIEB	Conjugated	Angular	Rigid
bis(3-iodoprop-2-yn-1-yl) terephthalate	pBIPT	Non-conjugated	Linear	Flexible
tris(3-iodoprop-2-yn-1-yl) benzene-1,3,5-tricarboxylate	1,3,5-TIPCB	Non-conjugated	Angular	Flexible

^a the triple bonds are conjugated with the aromatic ring.

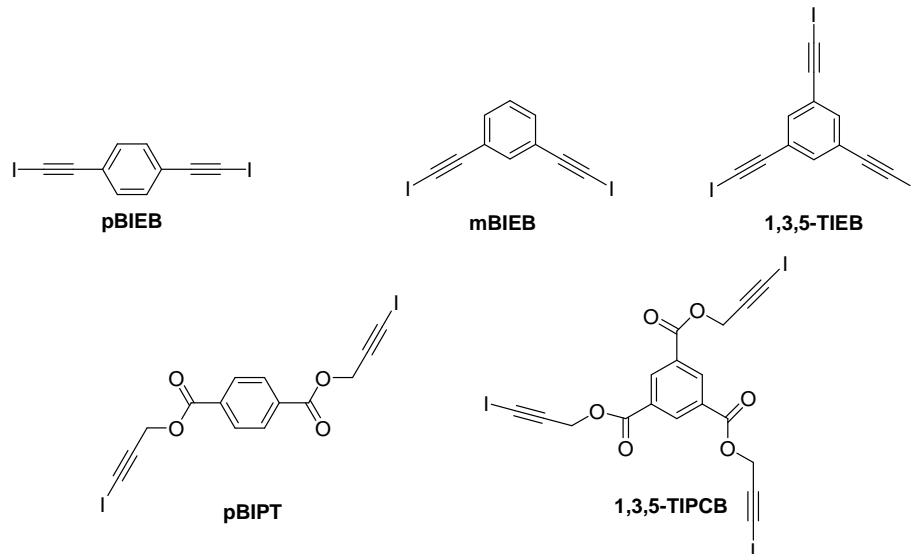


Figure 2.1 The five halogen bond donor derivatives synthesized in this work.

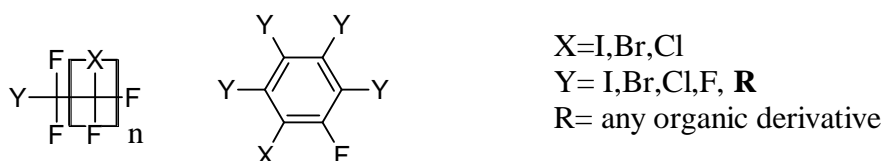
Additionally, two other ditopic synthons derived from Tröger's base derivatives bearing iodo- and iodoethynyl donor groups were prepared. Both of these compounds are included in chapter 3, which is devoted specifically to porous structures obtained by means of crystal engineering using the synthons derived from Tröger's base.

The five ditopic synthons included in this chapter have halogen bond donor and acceptor groups in their structure. These groups interact in the solid state to give rise to very interesting structures. It is worth noting that in the synthesis of these compounds the ethynyl derivatives are the precursors. The latter compounds also form crystal structures that are isostructural with their related iodoethynyl derivatives. Due to the rarity of the phenomenon of isostructuralism in crystal engineering, a comparative study of these crystal structures could be very attractive.

2.2 Previous works of halogen bond acceptor groups

As mentioned in the previous chapter, the first report dealing with halogen bonds was published in 1863. The paper by Frederick Guthrie^[3] concerns $\text{NH}_3 \cdots \text{I}_2$ and pyridine \cdots alkyl iodide adducts. However, it was not until 1994 that halogen bonds were defined for the first time by Muller.^[4] All of the studies in this field were carried out with molecular halogens until 1968, when Bent introduced some halogenated organic compounds.^[5]

With a focus on supramolecular chemistry, and more specifically crystal engineering, it became clear that it was possible to design and fine-tune the structural and functional features of self-assembled adducts by selecting the nature and the structure of the molecules involved in XB formation. The appropriate design of halo-organic molecules with good electron-withdrawing groups increased the atom polarizability and directionality of the halogen bond donor. In this respect, in the 1990s the studies by Politzer and Murray were particularly significant and they demonstrated the anisotropic charge distribution on halogen atoms that form one covalent bond.^[6] In the 2000s the studies by Metrangolo *et al.* concerned the intermolecular interaction involving a representative halogen bond acceptor (ammonia) and halofluoromethanes by quantum chemical calculations (DFT and MP2). The energy values and the defined geometry of the interaction promised to make halogen bonding a very effective tool in the manipulation of haloperfluorocarbons.^[7] It seems clear that in the last 20 years almost all of the studies on halogen bonds are on perfluorocarbons.^[8] A general representation of these compounds is shown in Scheme 2.1.



Scheme 2.1 General representation of perfluorocarbon halogen bond donors.

Despite the presence of electron-withdrawing groups in halocarbons, the ipso carbon hybridization also increases the polarizability of halogen atom. Of particular interest in this respect are the iodoethynyl groups, which are present in 1,4-bis(iodoethynyl)benzene (**pBIB**) and have only been investigated by Yamamoto *et al.*^[9] and Batail *et al.*^[10] in electrocrystallization experiments with non-halogenated tetrathiafulvalene derivatives.

Other diidoalkynes that have been studied as halogen bond donors are iodoacetylene^[11] and polyiodoacetylene.^[12] However, compared to these compounds **pBIB** is easier to prepare and is also more stable. More recently, Aakeröy *et al.* tried to establish a halogen bond donor ranking based on calculated molecular electrostatic potential surfaces (MEPS).^[13] It was found that 1-iodoethyl-iodobenzene (**IEIB**) and 1,4-diiodotetrafluorobenzene (**DITFB**) are halogen bond donors of equal strength.^[13] ^[14]

In the next chapter we will discuss the halogen bond donor capabilities of bisiodoethynyl derivatives.

2.3 Objectives

Taking into account the information outlined above, the main objectives covered in this chapter are:

- The synthesis and characterization of the crystalline structures of the five bis-iodoethynyl halogen bond acceptors and their bis-ethynyl precursors.
- The comparative study of the crystal structures obtained with each pair of isostructural bis-iodoethynyl and bis-ethynyl derivatives.

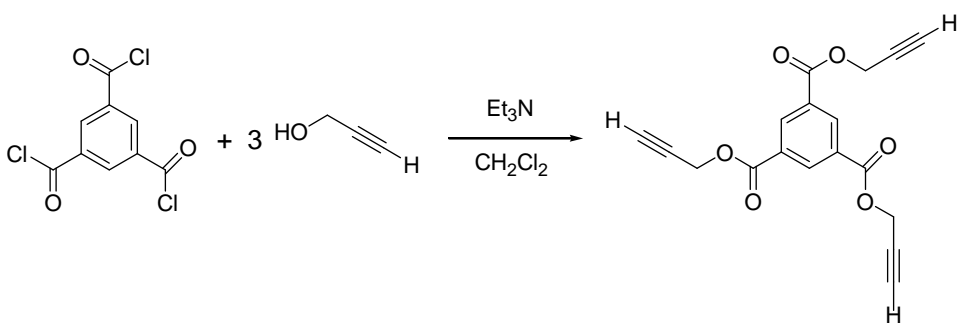
2.4 Synthesis of the bis-iodoethynyl synthons and their bis-ethynyl precursors

A general discussion of the synthetic procedures for both bis- and tris-iodoethynyl and their bis-/tris-ethynyl precursors is included in this chapter. The detailed procedures for the synthesis and characterization of each compound are included in the experimental section.

2.4.1 Preparation of the ethynyl precursors

The synthesis of terminal alkyne derivatives has witnessed significant developments due to the versatility of reactions such as the 1,3-dipolar cycloaddition of azides (click chemistry), amongst others.^[15]

The ethynyl precursors of 1,3- and 1,4-bisethynylbenzene and 1,3,5-triethynylbenzene were used as received from commercial sources. Two strategies were employed to obtain non-commercial precursors: esterification of the appropriate acyl chloride with propargyl alcohol and Sonogashira coupling. The Sonogashira coupling will be described in the next chapter.



Scheme 2.2 Synthesis of tris(prop-2-yn-1-yl) benzene-1,3,5-tricarboxylate by esterification of the acid chloride with propargyl alcohol.

Tris(prop-2-yn-1-yl) benzene-1,3,5-tricarboxylate (**1,3,5-TPCB**) and bis(prop-2-yn-1-yl) terephthalate (**pBPT**) were obtained from the commercial acid chlorides 1,4-benzenedicarbonyl dichloride, 1,3,5-benzenetricarbonyl trichloride and

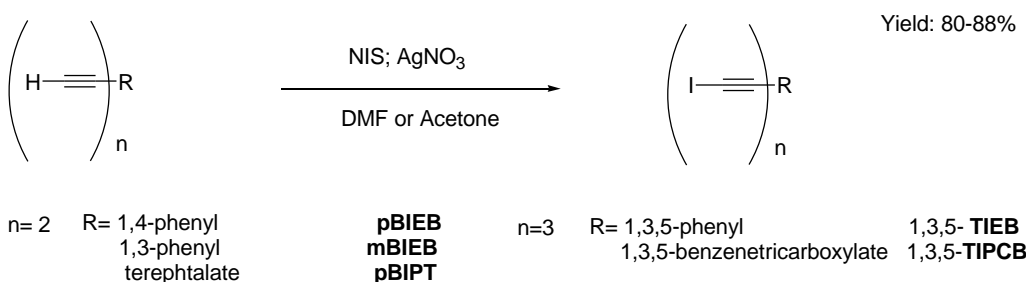
Iodoethynyl halogen bond donors

benzenedicarbonyl dichloride by reaction with propargyl alcohol in dichloromethane and triethylamine with yields of around 90% obtained (See Scheme 2.2).^[16]

2.4.2 Synthesis of the iodoethynyl derivatives

Different methods for the synthesis of iodoalkyne derivatives have been described in the literature. For example, **pBIEB** was first synthesized by Yamamoto *et al.*^[9] by the reaction of 1,4-bis(ethynyl)benzene with *n*-BuLi and subsequent treatment with iodine. In this work a modification of the method described by Bouchemella *et al.* was used.^[17]

In this method the parent compound containing the alkyne terminal group was reacted with N-iodosuccinimide using silver nitrate as catalyst and acetone as solvent. The product was then purified by flash chromatography. In our method, DMF or acetone was used as solvent depending on the starting material in order to favor solubility. The reaction times were reduced to 30 minutes to avoid decomposition of the components. The products were purified by washing the reaction mixture with water and the desired product was extracted with diethyl ether. In all cases high yields in the range 80–88% were obtained (See Scheme 2.3).



Scheme 2.3 General synthesis of halogen derivatives

2.5 Ethynyl vs iodoethynyl derivatives: A comparative study.

In this section, the crystal structures of the iodoethynyl derivatives are compared with those of their alkyne precursors. X-ray quality single crystals were obtained by slow evaporation of solutions of the compounds in the appropriate solvent.

The ethynyl group is comparable to a C–X halogen atom because both have similar anisotropic charge distribution, polarizability and volume. The two moieties contain a partial positive charge at the end of the covalent bond and a negative charge in the perpendicular region (see Figure 2.2).

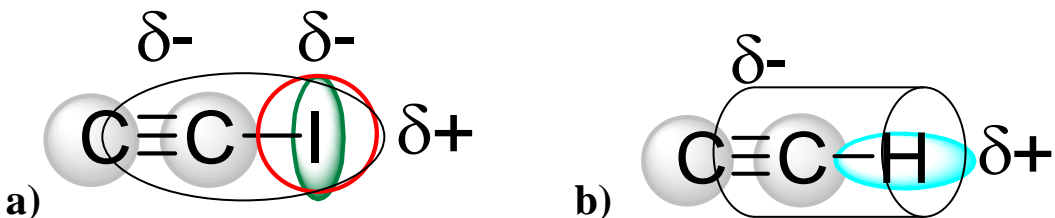


Figure 2.2 Distribution of the partial charge in the a) iodoethynyl and b) ethynyl moieties.

The volume of the ethynyl group (28.81 Å) is intermediate between the volume of Br (24.4 Å) and I (32.96 Å). The bromine and iodine atoms in the C–X bond have an elliptical shape that is flattened along the polar direction, whereas the ethynyl group is cylindrical.

The combination of iodine and a triple bond gives rise to an iodoalkynyl group with two partial negatively charged zones and one partial positively charged zone (see Figure 2.2). The additional negative charge leads to the possibility that iodoalkynyl derivatives can form self-assembled suprastructures. This situation may result in intermolecular interactions with T forms, similar to those observed in crystal structures described for terminal alkynes.^[2] Similar supramolecular organizations can be obtained from terminal alkynes and iodoalkynes. This

Iodoethynyl halogen bond donors

phenomenon is named isostructuralism and is opposite to the polymorphism described in the previous chapter.^[18] The first example of this phenomenon has received relatively little attention due to its rarity (Figure 2.3).

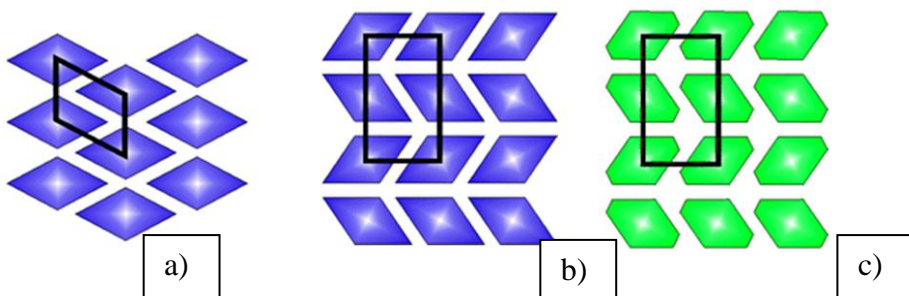


Figure 2.3- Graphical representation of polymorphism and isostructuralism.

Blue represents the same synthons and green different synthons. The structures a) and b) are polymorphs; the structures b) and c) are isostructural.

Adapted from ref.^[19]

Isostructuralism may provide an attractive opportunity to construct materials with different properties following a common structural starting point. Additionally, sets of isostructural compounds rarely include more than two members. It is well known that minor structural changes could result in significant changes in crystal structures. This could explain the difficulty in achieving isostructurality in single compound solids.^[19-20] All-alkyne and -iodoalkyne rigid structures described in this chapter exhibit a characteristic Csp–H \cdots π interaction with a dislocated T form because this interaction is directed to the central point of the triple bond.^[21]

The geometrical parameters of the C–H \cdots π and C–I \cdots π interactions in the compounds 1,4-bisethynylbenzene (**pBEB**), 1,3,5-tris(ethynyl)benzene (**1,3,5-TEB**), tris(prop-2-yn-1-yl)benzene-1,3,5-tricarboxylate (**1,3,5-TPCB**), dipropargylterephthalate (**pBPT**), **pBIEB**, **mBIEB**, **1,3,5-TIEB**, **1,3,5-1,3,5-TIPCB** and **pBIPT** are listed in Table 2.2. Hydrogen and halogen bond distances are determined at the center of the π -system and the position of hydrogen atoms and were normalized to a C–H distance of 1.08 Å.

According to the geometric parameters, the distance interactions are slightly shorter than the sum of the van der Waals radii of hydrogen or iodine and the carbon atom ($rH + rC = 2.90$ and $rI + rC = 3.68 \text{ \AA}$)^[22] and these values correspond to a reduction ratio, defined as $rr = dX\cdots Y / (RvdW(X) + RvdW(Y))$, which ranges in the hydrogen bond from 0.89 to 0.98 and in the halogen bond from 0.87 to 0.95. It can be observed that the halogen bond angles are more linear than the hydrogen bond angles, as mentioned in a previous section. The $C_{sp}-I\cdots\pi_{alk}$ angles range from 165.7° to 176.8° and they are more linear, as indicated by the reduction ratio. The CSD search was performed on the fragment $C_{sp}-I\cdots\pi_{alk}$. Seven hits were found and the average $I\cdots\pi$ distance was 3.466 \AA and the $C_{sp}-I\cdots C$ had an average value of 165.6° . The distances and angles are listed in Table 2.2.

Table 2.2 $C_{sp}-H\cdots\pi$ and $C_{sp}-I\cdots\pi$ interaction distances, angles and reduction ratios in pDEB, 1,3,5-TEB, 1,3,5-TIPCB, PBPT, pBIEB, mBIEB, 1,3,5-TIEB, 1,3,5-TIPCB and pBIPT crystal structures.

Compound		$d(C-D) \text{ \AA}$	$C-D\cdots Y \text{ \AA}$	$\angle(CDY)^\circ$	rr	ref
pBEB	$C_{sp}-H\cdots\pi_{alk}$	1.08	2.596	174.8	0.89	[2]
1,3,5-TEB	$C_{sp}-H\cdots\pi_{alk}$	1.08	2.681	165.7	0.92	[2]
	$C_{sp}-H\cdots\pi_{alk}$	1.08	2.723	147.3	0.94	
	$C_{sp}-H\cdots\pi_{alk}$	1.08	2.814	140.1	0.97	
1,3,5-TPCB	$C_{sp}-H\cdots\pi_{alk}$	1.08	2.84	144.0	0.98	
pBPT	$C_{sp}-H\cdots\pi_{alk}$	1.08	2.751	158.8	0.95	
pBIEB	$C_{sp}-I\cdots\pi_{alk}$	1.98	3.344	167.4	0.91	
mBIEB	$C_{sp}-I\cdots\pi_{alk}$	2.00	3.34	175.5	0.91	
1,3,5-TIEB	$C_{sp}-I\cdots\pi_{alk}$	1.997	3.293	169.3	0.89	
	$C_{sp}-I\cdots\pi_{alk}$	1.998	3.657	165.7	0.99	
1,3,5-TIPCB	$C_{sp}-I\cdots\pi_{alk}$	2.00	3.218	176.8	0.87	
pBIPT	$C_{sp}-I\cdots\pi_{alk}$	2.005	3.499	171.3	0.95	

Iodoethynyl halogen bond donors

The energy difference between the $C_{sp}-H \cdots \pi_{alk}$ hydrogen bond and the $C_{sp}-I \cdots \pi_{alk}$ halogen bond was evaluated by carrying out theoretical calculations on the stability energy of the T form ($C_{sp}-I \cdots \pi_{alk}$) interaction in the **pBIEB** structure. A value of 5.1 kcal/mol was obtained and this is approximately four times higher than the stabilization energy described previously (1.23 kcal/mol) for **pBEB**.^[21a] This result is significantly different from the effect of alkyne and iodoalkyne groups. For example, terminal alkynes behave as weak acids ($pK_a \approx 25$) and are poor hydrogen bond donors, whereas iodoalkynes are very good halogen bond donors.

In the following sections, the crystal structures of iodoethynyl derivative as halogen bond donors are compared with the precursor alkynes and the spatial arrangements of each pair will be discussed.

2.5.1 1,4-Bis(iodoethynyl)benzene (**pBIEB**) vs 1,4-bis(ethynyl)benzene (**pBEB**)

The structures from the first pair **pBEB**^[2] and **pBIEB**^[23] were solved in the different spatial groups $P2_1/c$ and $P2_1/n$, respectively. The spatial arrangements of the rigid planar pairs 1,4-bis(ethynyl)benzene (**pBEB**)/1,4-bis(iodoethynyl)benzene and 1,3,5-triethynylbenzene/1,3,5-tris(iodoethynyl-benzene) are isostructural. The molecules in **pBEB**^[2] and **pBIEB** crystal structures are connected by $C-H \cdots \pi$ hydrogen bonds and $C-I \cdots \pi$ halogen bonds, respectively, in a zig-zag pattern. Each molecule is fixed by two hydrogen/halogen bonds and this gives rise to parquet-like ordered layers as shown in Figure 2.4a. The aromatic rings are inclined from the midplane of the layer by 31.2° in **pBEB** and 46.5° in **pBIEB**. The inclination of aromatic rings in **pBIEB** leads to ribbons formed by $C_{sp2}-H \cdots I$ and $C_{sp2}-H \cdots \pi_{alk}$ hydrogen bonds. As mentioned before, the charge distribution in iodoethynyl has two zones that lead to weak hydrogen bonds from hydrogen atoms of the aromatic ring to the triple bond and the equatorial atom part of iodine (Figure 2.4b).

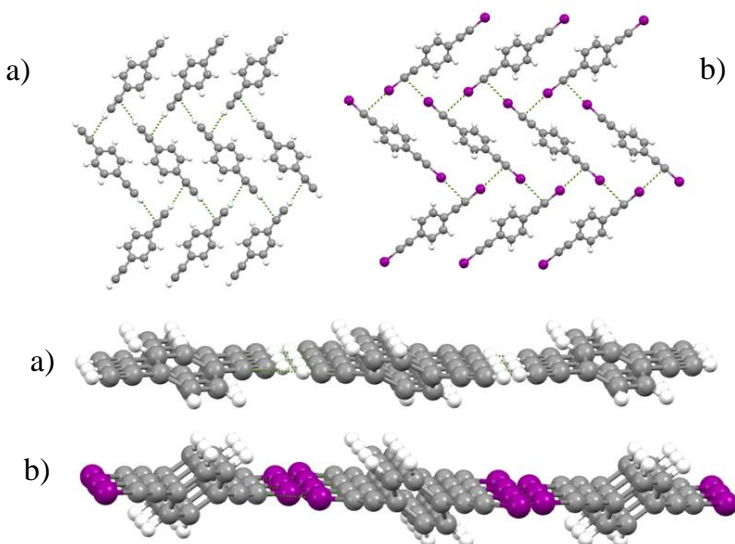


Figure 2.4- Comparison of halogen–hydrogen structures in a) pBEB and b) pBIEB.

The stability energy calculated for the supramolecular synthon due to hydrogen bonds (Figure 2.5) when compared to the isolated molecule is 5 KJ/mol. This energy is very similar to the $C_{sp}-I \cdots \pi_{alk}$ halogen bond energy and although this stability energy is weak it plays an important role in crystal structures that contain iodoalkyne derivatives.

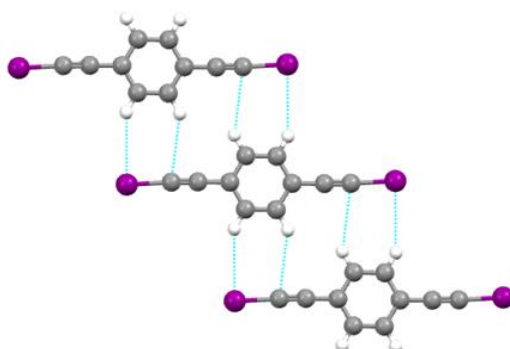


Figure 2.5 Section of the layer structure of pBIEB and the weak interactions.

Iodoethynyl halogen bond donors

Table 2.3 Hydrogen bond distances and angles in pBEB and pBIEB

Compound	D-H···A	Sym. equivalence	d(H···A) Å	d(D···A) Å	\angle (DHA) °
pBEB	$C_{sp^2}-H \cdots \pi_{alk}$	1-x, -y, 1-z	2.903	3.800	139.7
pBIEB	$C_{sp^2}-H \cdots I(1)$	x, y, -1+z	3.170	4.149	149.5
	$C_{sp^2}-H \cdots \pi_{alk}$	1-x, -y, 1-z	3.059	3.990	143.7

The distances and angles of the weak hydrogen bonds that play an important role in the pBIEB and pBIEB supramolecular structures are provided in Table 2.3. These comparative interactions confirm that halogenated alkyne derivatives have two partial negative charges, as outlined above.

The halogen bond length is strongly dependent on temperature^[8i, 24] and pressure.^[25] For example, the morpholine-*p*-iodophenylacetylene complex at 150 K has an N···I interaction distance of 2.7 vs 2.9 Å at room temperature.^[26]

In the CSD there is only one structure that contains and iodoethynyl moiety that has been studied at different temperatures. The $C_{sp}-I \cdots \pi_{alk}$ interaction distances were measured for 1,4-bis(iodoethynyl)bicyclo[2.2.2]octane at 295 K and 130 K and $C_{sp}-I \cdots \pi_{alk}$ interaction distances of 3.456 and 3.348 Å were determined, respectively.^[1d] In this case the distance decreased as the temperature decreased.

In order to study the temperature behavior of the $C_{sp}-I \cdots \pi_{alk}$ interaction in the crystal structure of **pBIEB** the same diffractometer and parameters were employed for data collection. The unit cell parameters are gathered at Table 2.4. The main difference observed is the volume parameter, which is significantly lower (3.5%) in the structure at low temperature (150 K). This volume reduction is similar to that observed in the structure of 1,4-bis(iodoethynyl)bicyclo[2.2.2]octane (3%).

Table 2.4 Unit cell parameters measured for the pBIEB structure at different temperatures.

Temperature, K	293	150
Crystal System	Monoclinic	Monoclinic
a, Å	4.23910(10)	4.1533(3)
b, Å	17.3031(5)	17.1541(16)
c, Å	7.1008(2)	7.0511(5)
β , deg	95.775(2)	95.332(7)
V, Å ³	518.20(2)	500.19(7)
Space group	P2 ₁ /n	P2 ₁ /n

The increase in the C_{sp}–I···π_{alk} distance in **pBIEB** between 150 and 293 K is 0.076 Å, Table 2.5, and this is lower than that observed in 1,4-bis(iodoethynyl)bicyclo[2.2.2]octane (0.108 Å). This finding may be due to the fact that the C_{sp}–I···π_{alk} distance in the latter structure is affected by the disorder observed in the structure at room temperature.

Table 2.5 Packing variations with temperature for pBIEB.

Temperature, K	293	150
C _{sp} –I···π _{alk} (Å)	3.420	3.344
C _{sp2} –H···I (Å)	3.176	3.115
C _{sp2} –H···π _{alk} (Å)	3.094	3.017
Inter layer distance (Å)	3.552	3.478

The best way to understand small differences between crystal structures is through Hirshfeld surface analysis. This analysis is accessible due to the implementation of Crystal Explorer software.^[27] This software allows different properties to be encoded on the Hirshfeld surface, such as shape index, curvedness, and internal (d_i) and external (d_e) distance. Internal and external distances are defined as the

Iodoethynyl halogen bond donors

distance from a point on the surface to the nearest internal or external atom on the Hirshfeld surface as shown in Figure 2.6. The representation of the Hirshfeld surface is a colored 2D graphic (d_i , d_e) that facilitates comparison between different crystal structures because it allows the visualization of their major features as a whole in a two-dimensional plot. In the 2D plots the points are colored from blue through green to red on changing from a low to high fraction of surface that is represented.

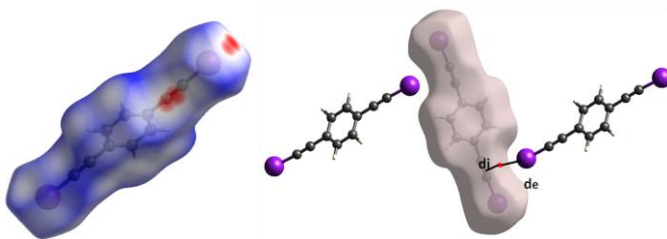


Figure 2.6 Hirshfeld surface of pBIEB (150 K), d_{norm} left and $d_{\text{e-di}}$ right.

Throughout this thesis we will consider the Hirshfeld surface analysis using the most appropriate tool of Crystal Explorer software in each case.

Despite the similarity of the 2D fingerprints of **pBIEB** structures collected at 293 K and 150 K (Figure 2.7) some differences can be observed.

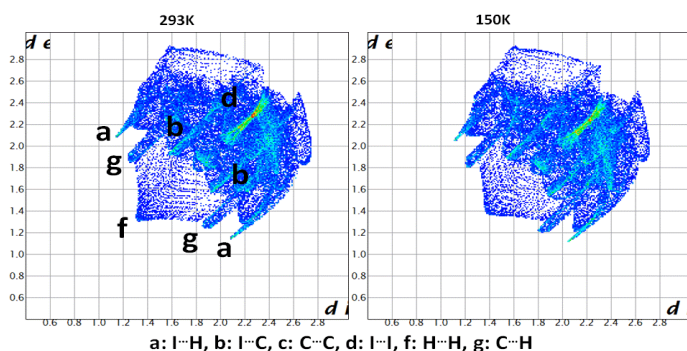


Figure 2.7 Fingerprints from Hirshfeld surface of pBIEB structures at 293 K and 150 K.

A slight displacement of the 2D plot towards the origin of the structure collected at 150 K can be observed due to the shortening of the distances between the molecules caused by the decrease in temperature. There is also a change in the intensity and width of green areas due to the change in the percentage of the Hirshfeld surface occupied by each contact. With decreasing temperature the contacts I···H and C···C increase while I···I and C···H decrease (Figure 2.8).

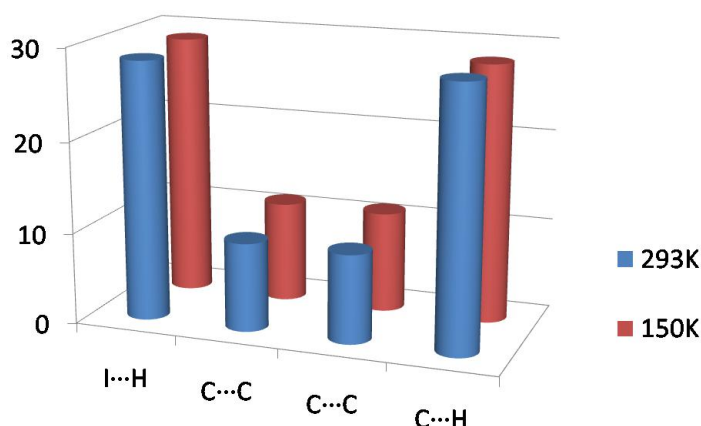


Figure 2.8 Comparison of main interactions from both structures at different temperatures.

However, the most obvious change is that corresponding to the H···H contact, denoted as **f** in Figure 2.7 and Figure 2.9, since in the first of the graphics this contact is more pointed, thus indicating a closer contact. The nearest H···H contact is between hydrogen atoms of the aromatic rings of two coplanar **pBIEB** molecules with distances of 2.60 and 2.72 Å at 293 and 150 K, respectively. At low temperature the **pBIEB** molecules are displaced to favor the C_{sp}²-H···I and C_{sp}²-H···π_{alk} interactions, as shown by the interaction distances in Table 2.2..

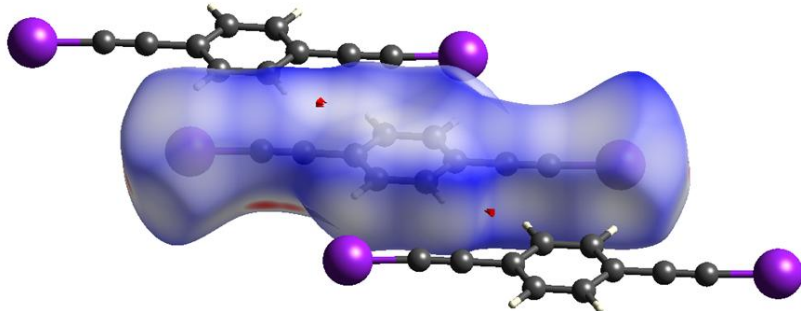


Figure 2.9 Shortest H···H contacts that cause a peak (f from Figure 2.7) from the fingerprint of pBIEB collected at 293 K.

2.5.2 1,3,5-Tris(iodoethynyl)benzene (**1,3,5-TIEB**) vs 1,3,5-tris(ethynyl)benzene

1,3,5-TEB^[2] and **1,3,5-TIEB** crystallize in the monoclinic C2/c space group. The asymmetric unit consists of one molecule in general position. The molecules are planar with a maximum distance to the midplane of 0.077 Å and 0.294 Å for **1,3,5-TEB** and **1,3,5-TIEB**, respectively.

The main attractive forces between **1,3,5-TEB** or **1,3,5-TIEB** are hydrogen or halogen bonds, respectively, with π -electrons of triple bonds. Each molecule acts three times as a donor and as an acceptor, thus making six contacts per molecule with three distinct distances. One of the ethynyl or iodoethynyl groups acts only as a donor, the second group acts as both a donor and an acceptor, and the third group acts as donor and double acceptor (Figure 2.10). The distances for all interactions and angles are listed in Table 2.6. It can be observed from the results in this table that all of the interactions are shorter than the sum of van der Waals radii and the angles range from 143.6° to 174.3° in **1,3,5-TEB** and 165.7° to 169.4° in **1,3,5-TIEB**.

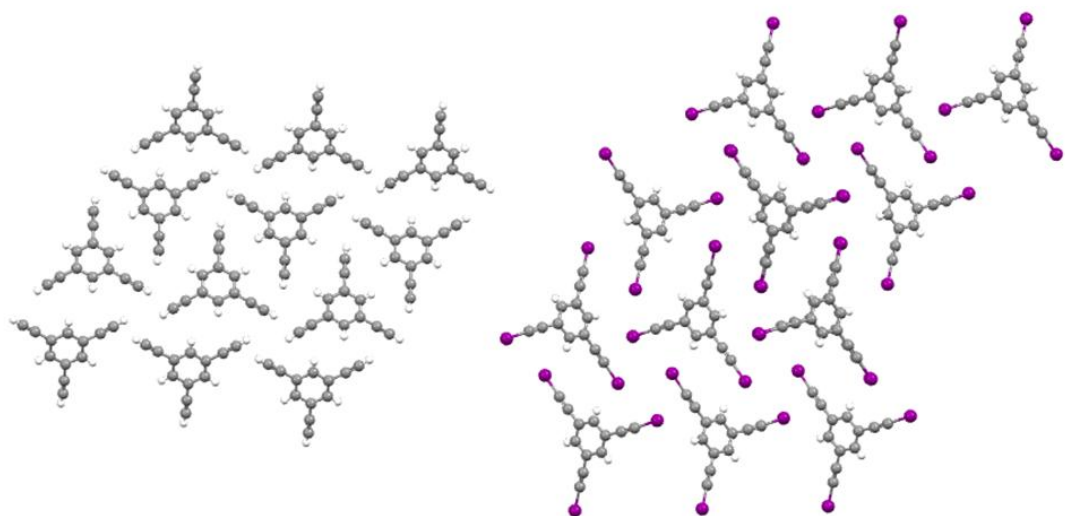


Figure 2.10 Packing in (left) 1,3,5-TEB and (right) 1,3,5-TIEB structures due to hydrogen and halogen bonding, respectively, with π -electrons of triple bonds.

Table 2.6 Interaction distances and angles in 1,3,5-TEB and 1,3,5-TIEB.

Compound	C–X…Y	d(C–X) Å	d(X…Y) Å	$\angle(CXY)^\circ$
1,3,5-TEB	$C_{sp}-H(1)\cdots C(9-10)$	-	2.602	143.6
	$C_{sp}-H(2)\cdots C(7-8)$	-	2.683	160.5
	$C_{sp}-H(3)\cdots C(9-10)$	-	2.577	174.3
1,3,5-TIEB	$C_{sp}-I(1)\cdots C(9-10)$	1.997(4)	3.293	169.3
	$C_{sp}-I(2)\cdots C(7-8)$	1.998(4)	3.657	165.7
	$C_{sp}-I(3)\cdots I(1)$	1.994(4)	3.772	169.4

Despite the fact that both crystals have similar packing structural features, there are some differences between them. **1,3,5-TEB** can be described as a folded layer structure, where layers are formed by connected ribbons from dimeric **1,3,5-TEB** synthons (Figure 2.11a). The dimer molecules are arranged in parallel planes with a distance of 1 Å between them (Figure 2.11b).

Iodoethynyl halogen bond donors

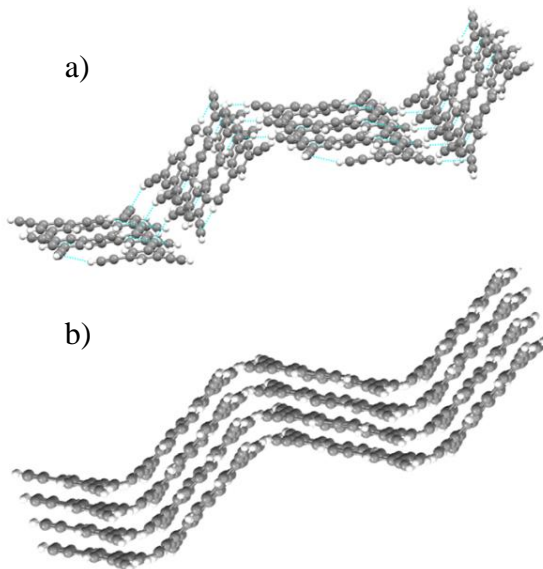


Figure 2.11 1,3,5-TEB spatial arrangement: a) layers are formed by connected ribbons from dimeric synthons and b) parallel planes with a distance of 1 Å between them.

Planes are not formed in the **1,3,5-TIEB** structure, probably due to the high volume of the iodine atom, which favors $C_{sp}-I \cdots \pi_{alk}$ interactions. Each molecule is tilted by 67.6° with respect to its neighbor. The $C_{sp}-I(2) \cdots \pi_{alk}$ interaction results in helices, along a two-fold axis, stabilized by $C_{sp2}-H \cdots I$ hydrogen bonds (Figure 2.12a and b). These helices are connected by $C_{sp}-I(1) \cdots \pi_{alk}$ interactions to two other enantiomeric helices and this gives rise to layers. These layers are joined through $C_{sp}-I(3) \cdots I(1)$ halogen bonds that are related through a two-fold screw axis (Figure 2.12c).

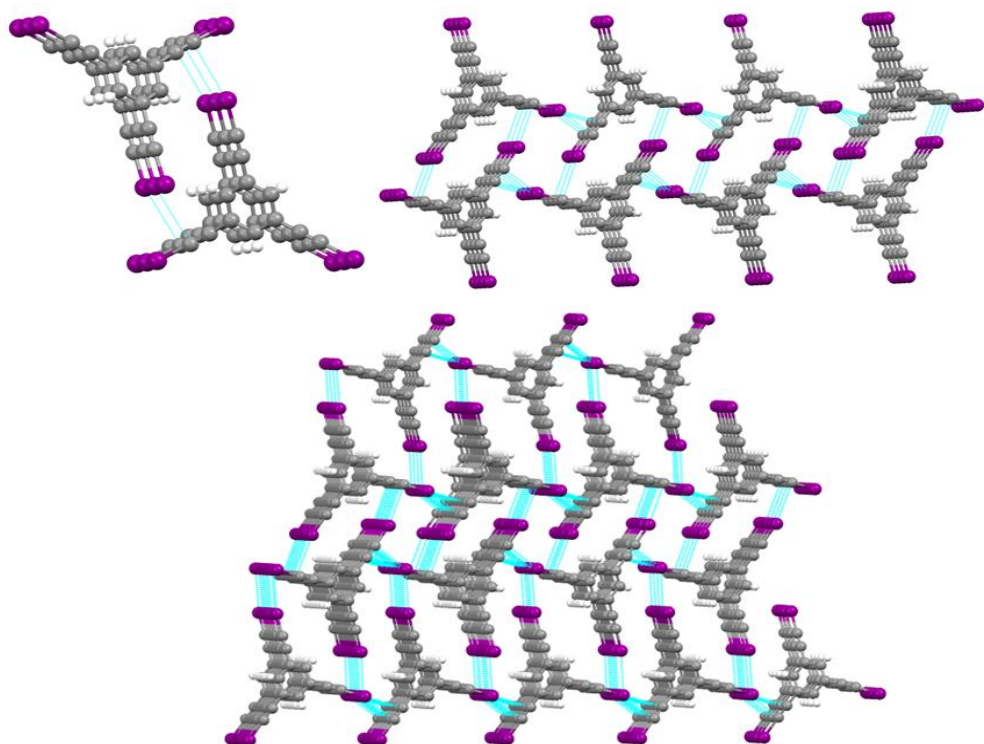


Figure 2.12 Representation of different interactions and arrangements in the 1,3,5-TIEB crystal structure: a) halogen bond interaction with π electron density represented for dimers, b) hydrogen bond interaction with a halogen to connect the dimers and c) halogen bond interaction with a halogen to connect the layers.

2.5.3 1,3-Bis(iodoethynyl)benzene (**mBIEB**)

The compound 1,3-bisethynylbenzene is liquid at room temperature and it was not possible to determine the crystal structure or, therefore, to compare it with 1,3-bis(iodoethynyl)benzene (**mBIEB**). **mBIEB** crystallizes in the monoclinic C2/c space group and the asymmetric unit consists of one molecule in general position.

The molecule is planar with a maximum distance to the midplane of 0.095 Å from one of the iodine atoms. The supramolecular organization of **mBIEB** is very similar to that of **1,3,5-TIEB** (Figure 2.14) and is characterized by $C_{sp}-I \cdots \pi_{alk}$ T-

Iodoethynyl halogen bond donors

shaped halogen bonds in which each iodine atom forms a $C_{sp}-I\cdots\pi$ interaction. This interaction results in the formation of helices along the b axis. The planes containing **mBIEB** related by a twofold axis form an angle of 57.4° (Figure 2.13).

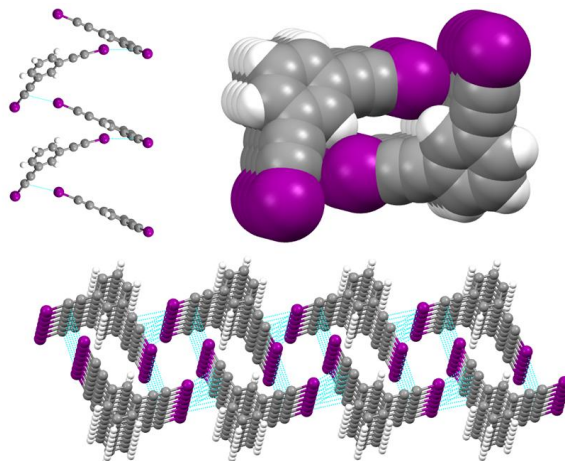


Figure 2.13 mBIEB spatial dispositions. Top left: helix formed by $C_{sp}-I(2)\cdots\pi$ interactions. Right: space fill molecules. Bottom: Interconnected helix formed by $C_{sp}-I(1)\cdots\pi$ interactions.

The helices are connected by $C_{sp}-I\cdots\pi_{alk}$ halogen bonds to two other enantiomeric helices and this gives rise to layers (Figure 2.14a). These layers are joined through $C_{sp2}-H\cdots\pi_{alk}$ and $C_{sp2}-H\cdots I$ weak hydrogen bonds (Figure 2.14b), instead of halogen bonds as in **1,3,5-TIEB**.

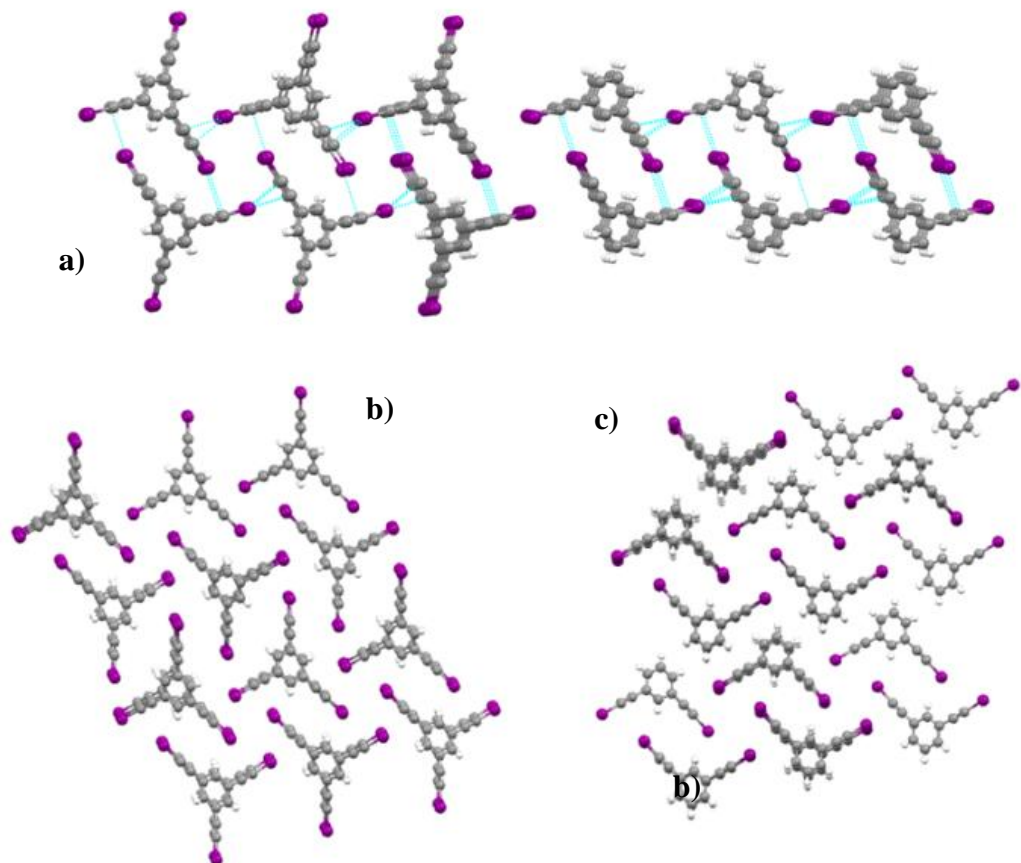


Figure 2.14- Comparison between 1,3,5-TIEB and mBIEB structures. a) Layers formed by intercrossing halogen bonds. b) Spatial arrangement (2D) formed by halogen bonding in 1,3,5-TIEB and c) hydrogen bonding in mBIEB.

Table 2.7 Interactions and angles in the mBIEB structure.

Compound	C-X···Y	d(C-X) Å	d(X···Y) Å	∠(CXY) °
mBIEB	C _{sp2} -H(3)···I	-	3.421	138.42
	C _{sp2} -H(2)···π	-	3.304	117.10
	C _{sp} -I···π	2.00	3.340	175.5

Iodoethynyl halogen bond donors

In the following sections the pairs dipropargyl terephthalate (**pBPT**)/bis(3-iodoprop-2-yn-1-yl) terephthalate (**pBIPT**) and tri(prop-2-yn-1-yl) benzene-1,3,5-tricarboxylate (**1,3,5-TPCB**)/tris(3-iodoprop-2-yn-1-yl) benzene-1,3,5-tricarboxylate (**1,3,5-TIPCB**) will be compared. These compounds have different properties such as conformational flexibility in the groups to which ethynyl or iodoethynyl groups are linked.

2.5.4 Bis(3-iodoprop-2-yn-1-yl) terephthalate (**pBIPT**) vs bispropargyl terephthalate (**pBPT**)

Bispropargylterephthalate (**pBPT**) – like **pBIPT** – crystallizes in the triclinic P-1 space group and the asymmetric units consists of two half molecules with an inversion center. Furthermore, in both structures the carbonyl groups have a *trans* conformation. Regarding the conformation, in the **pBIPT** molecule the iodopropoxycarbonyl group is tilted in relation to aromatic ring by *ca.* 6° and in **pBPT** the propynoxycarbonyl group is tilted by 10.7° (Figure 2.15).

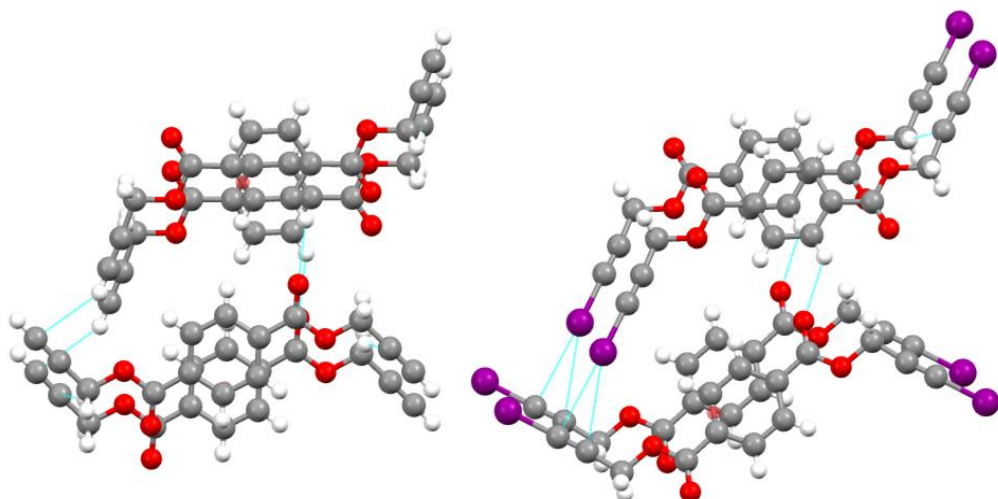


Figure 2.15- Left **pBPT** hydrogen bonding interaction and right **pBIPT** halogen bonding interaction between O_{sp2} and π electron density.

The main attractive forces in **pBPT** or **pBIPT** are T-shaped hydrogen or halogen bonds, respectively, involving π -electrons of the triple bonds or carbonyl groups. Each molecule acts twice as a donor and twice as an acceptor, thus making four contacts per molecule. The distances of all interactions, gathered in Table 2.8, are shorter than the sum of van der Waals radii and the angles are 140.6° for $C_{sp^2}-H \cdots O_{sp^2}$ **pBPT** and 171.2° for $C_{sp}-H \cdots O_{sp^2}$ in **PBPT** and 133.3° for $C_{sp^2}-H \cdots O_{sp^2}$ and 175.8° for $C_{sp}-I \cdots O_{sp^2}$ in **pBIPT**. In summary, a halogen bond is more linear than hydrogen bond (Figure 2.16).

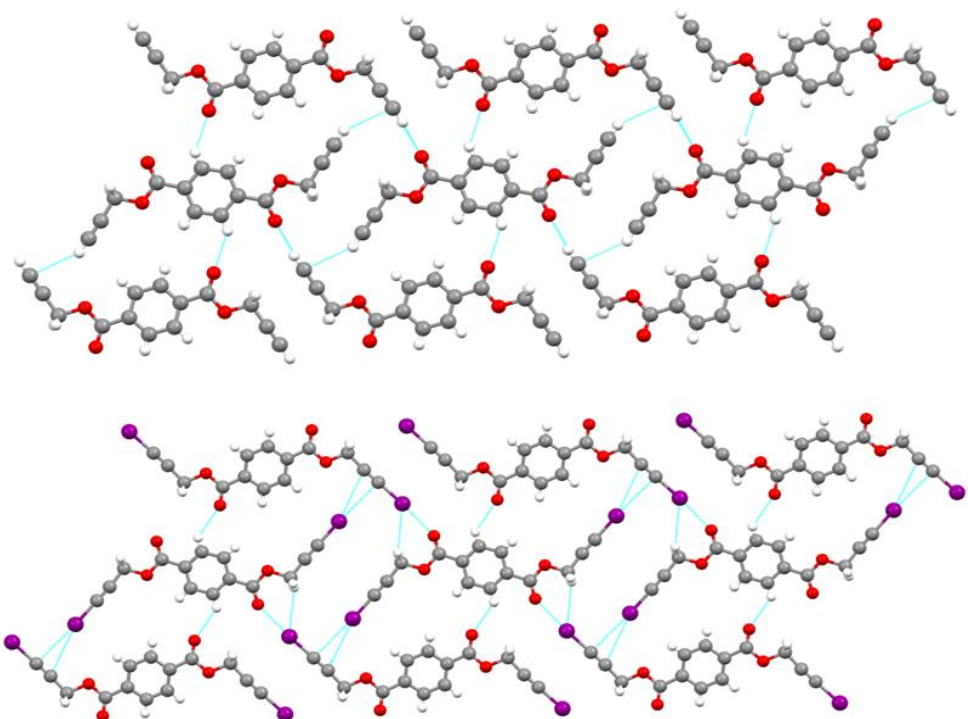


Figure 2.16- Top: **pBPT** intermolecular hydrogen bonding interaction.
Bottom: **pBIPT** intermolecular halogen bonding interaction. The halogen bond is more linear than the hydrogen bond.

The **pBPT** and **pBIPT** supramolecular organization may be described as a layer structure. The distance between the edge to edge $\pi-\pi$ stacked planes is 3.225 \AA and 3.258 \AA in **pBPT** and **pBIPT**, respectively. The planes are formed by hydrogen or

Iodoethynyl halogen bond donors

halogen bonding between ethynyl or iodoethynyl and the carbonyl group $C_{sp}-D\cdots O$ ($D = H, I$), with chains joined by hydrogen or halogen bonding $C_{sp}-D\cdots \pi_{alk}$ ($D = H, I$) (Figure 2.16).

Table 2.8 Interaction distances and angles in pBPT and pBIPT.

Compound	C-D…Y	d(C-D) Å	d(D…Y) Å	$\angle(CXY)^\circ$
pBPT	$C_{sp}-H\cdots O_{sp^2}$	0.930	2.180	171.2
	$C_{sp^2}-H\cdots O_{sp^2}$	0.930	2.450	140.6
pBIPT	$C_{sp}-I\cdots O_{sp^2}$	2.014	2.828	175.8
	$C_{sp^3}-H\cdots I$	0.970	3.1776	126.2
	$C_{sp^2}-H\cdots O_{sp^2}$	0.930	2.475	133.3
	$C_{sp^3}-H\cdots C_{sp}$	0.970	2.819	159.8

2.5.5 Tris(3-iodoprop-2-yn-1-yl) benzene-1,3,5-tricarboxylate (1,3,5-TIPCB) vs tris(prop-2-yn-1-yl) benzene-1,3,5-tricarboxylate (1,3,5-TPCB)

In the tris(prop-2-yn-1-yl) benzene-1,3,5-tricarboxylate (**1,3,5-TPCB**) and tris(3-iodoprop-2-yn-1-yl) benzene-1,3,5-tricarboxylate (**1,3,5-TIPCB**) structures, the supramolecular arrangements are very different, although in solid state the nature and number of interactions and conformations are similar. The three ethynyl groups act as hydrogen bond donors and the three iodoethynyl groups as halogen bond donors. The halogen and hydrogen bond acceptors are the same in both compounds. One of these is the π electron density of the triple bond and the other two are the sp^2 oxygen and sp^3 oxygen of the carboxylate groups.

As far as the conformation is concerned, both structures have 1,3,5-trimesylate as a core and this is practically plane with carboxylate angles in the range 6.2–17.7° in **1,3,5-TPCB** and 1.1–7.3° in **1,3,5-TIPCB**. However, the propargyl groups have different orientations in the two structures. In the **1,3,5-TIPCB** structure the three

propargyl groups are inclined to the same side of the aromatic ring plane, but in the case of **1,3,5-TPCB** two of them are inclined to one side and the other to the opposite side. This last propargyl group is practically coplanar with the aromatic ring while the other two groups have angles of 108° and 116° . The angles formed at the propargyl group in **1,3,5-TIPCB** are both 17° and the other is 107° (Figure 2.17).

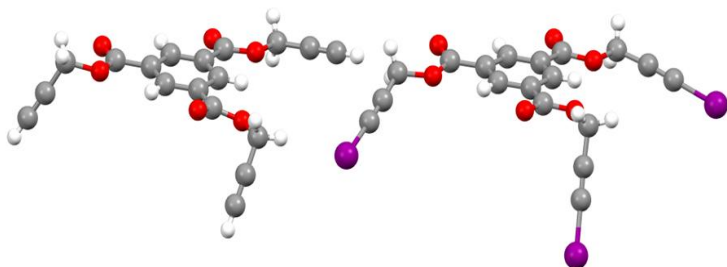


Figure 2.17 Conformations of 1,3,5-TPCB (left) and 1,3,5-TIPCB (right), showing the conformations of the propargyl groups.

The supramolecular arrangements in both structures are formed by π - π stacking, which is center to vertex in **1,3,5-TPCB** and edge to edge in **1,3,5-TIPCB** (Figure 2.18).

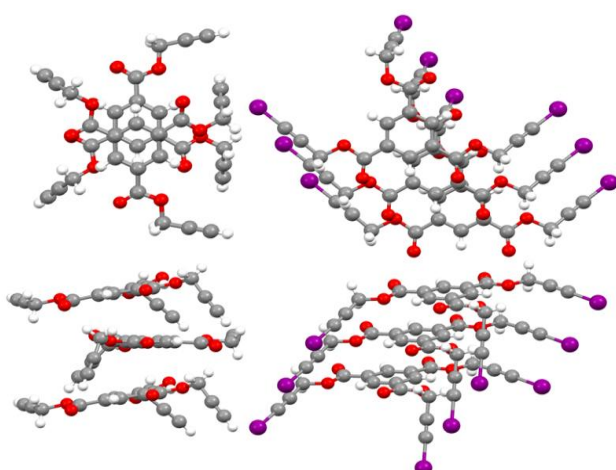


Figure 2.18 Comparison of π - π stacking in 1,3,5-TPCB and 1,3,5-TIPCB crystal structures.

Iodoethynyl halogen bond donors

The tris(prop-2-yn-1-yl) benzene-1,3,5-tricarboxylate (**1,3,5-TPCB**) crystallizes in the monoclinic P2₁/c space group. The core packing mentioned above grows along the *c* axis and molecules are not parallel, with an angle of 10.7° between them. The shortest distance measured between molecules is 3.31 Å (see Figure 2.18). The molecular packing is stabilized by C_{sp}-H···π_{alk} hydrogen bonds and the supramolecular organization is completed by the union of each column with another four hydrogen bonds. Two of these bonds are of the type C_{sp}-H···O_{sp2} and the other two are C_{sp}-H···O_{sp3}. (All the distance are gathered at Table 2.9)

Table 2.9- Interaction distances and angles in 1,3,5-TPCB and 1,3,5-TIPCB.

Compound	C-X···Y	d(C-X)Å	d(X···Y)Å	∠(CXY)°
1,3,5-TPCB	C _{sp} -H···O _{sp3}	-	2.70(2)	125(1)
	C _{sp} -H···π _{alk}	-	2.84(2)	144(2)
	C _{sp} -H···O _{sp2}	-	2.42(2)	147(2)
1,3,5-TIPCB	C _{sp} -I···O _{sp3}	2.02(2)	3.377(9)	162.2(6)
	C _{sp} -I···π _{alk}	2.00(1)	3.218	176.84
	C _{sp} -I···O _{sp2}	1.98(2)	2.890(1)	177.2(6)

Tris(3-iodoprop-2-yn-1-yl) benzene-1,3,5-tricarboxylate (**1,3,5-TIPCB**) stacks along the *a* axis and there is no intracolumnar halogen bond. Each column is bonded by C_{sp}-I···Y halogen bonds (Y = π_{alk}, O_{sp2} and O_{sp3}) to four adjacent columns. The C_{sp}-I···π_{alk} bonding forms chains perpendicular to the column stacks (Figure 2.19(a)). These organizations are interdigitated with other similar ones generated by an inversion center, thus leading to stabilized layers of C-I···O_{sp2} and C-I···O_{sp3} halogen bonds (Figure 2.19(b)). Finally, the layers are linked by C_{sp2}-H···O_{sp2} and C_{sp3}-H···O_{sp2} hydrogen bonds leading to a tridimensional organization (Figure 2.19(c)). (All the distance are gathered at tale 2.9)

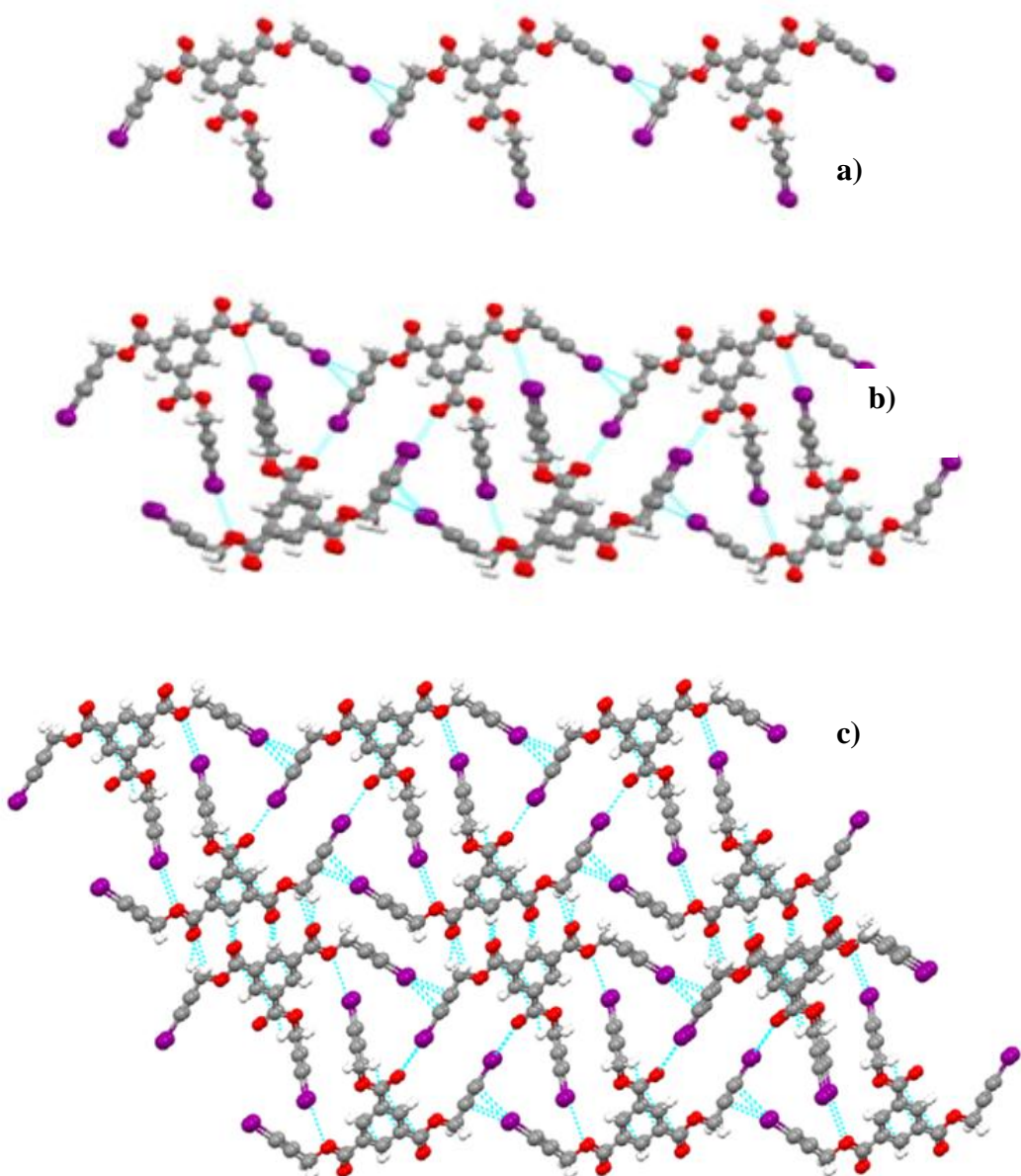


Figure 2.19 Interdigitated connection for 1,3,5-TIPCB: a) $\text{C}_{\text{sp}}-\text{I}\cdots\pi_{\text{alk}}$ halogen bonding interaction, b) stabilization of layers by $\text{C}_{\text{sp}}-\text{I}\cdots\text{O}_{\text{sp}2}$ and $\text{C}_{\text{sp}}-\text{I}\cdots\text{O}_{\text{sp}3}$ halogen bonds and c) tridimensional organization linked by $\text{C}_{\text{sp}2}-\text{H}\cdots\text{O}_{\text{sp}2}$ and $\text{C}_{\text{sp}3}-\text{H}\cdots\text{O}_{\text{sp}2}$ hydrogen bonds.

2.6 Conclusions

In this section it has been explained how alkynes and iodoalkynes, which are planar and rigid molecules, result in isostructural supramolecular arrangements. The differences between structures become more marked with the number of ethynyl groups and their proximity.

However, flexible molecules do not give rise to isostructuralism and the structure is not governed by the strongest interaction alone, e.g. halogen bond or hydrogen bond ($C_{sp}-I \cdots Y$ and $C_{sp}-H \cdots Y$). Other weak interactions, such as $C_{sp^2}-H \cdots Y$, are important for the final packing/crystal structure.

2.7 Experimental Section

2.7.1 Synthesis and characterization of halogenated derivatives and their precursors

1,3- and 1,4-bisethynylbenzene, 1,3,5-triethynylbenzene, 1,4-benzenedicarbonyl dichloride, 1,3,5-benzenetricarbonyl trichloride, N-iodosuccinimide, 2-propyn-1-ol and silver nitrate were used as received from commercial sources.

^1H and ^{13}C NMR spectra were recorded on a Bruker Avance 400 spectrometer (400.13 MHz for ^1H , 100.62 MHz for ^{13}C) or a Bruker Avance 300 spectrometer (300 MHz for ^1H , 75 MHz for ^{13}C). Infrared (IR) spectra were recorded on an ATR-unit-upgraded (Golden Gate) Bruker FT-IR Vertex 70 spectrophotometer. Mass spectra were recorded on a VG Auto-spec instrument, with the ESI technique. C, H, and N analyses were carried out on a Perkin-Elmer 2400 microanalyzer.

Halogenation procedures for all of the halogen bonding donors synthesized were carried out in the same way, with slight modification as reported previously.^[28]

2.7.2 General method

N-Iodosuccinimide (NIS) and AgNO_3 in a Schlenk tube were put under vacuum for 10 minutes. Acetylene in DMF or acetone under an argon atmosphere was slowly added to the Schlenk tube at 0 °C (ice/water bath). After 5 hours the mixture was filtered and added to water. The product was extracted three times with diethyl ether and cooled until a precipitate formed. The solid was filtered off and the ether was evaporated from the filtrate to give the product. Yields: 80–88%.

2.7.3 Characterization of halogen derivatives

*1,4-Bis(iodoethynyl)benzene (**pBIEB**)*: ^1H NMR (300 MHz, CDCl_3) δ ppm: 7.36 (s, 4H). ^{13}C NMR (75 MHz, CDCl_3) δ ppm: 9.14 ($\text{C}_{\text{Alk}}-\text{I}$), 77.16 ($\text{C}_{\text{Alk}}-\text{Ar}$), 93.74 ($\text{C}_{\text{Ar}}-\text{Alk}$), 123.88, 132.27.

*1,3-Bis(iodoethynyl)benzene (**mBIEB**)*: ^1H NMR (300 MHz, CDCl_3) δ ppm: 7.49 (t, $J = 1.4$ Hz, 1H), 7.41–7.33 (m, 2H), 7.29–7.20 (m, 1H). ^{13}C NMR (75 MHz, CDCl_3) δ (ppm): 7.79 ($\text{C}_{\text{Alk}}-\text{I}$), 93.23 ($\text{C}_{\text{Alk}}-\text{Ar}$), 123.78 ($\text{C}_{\text{Ar}}-\text{Alk}$), 128.40, 132.65, 136.20, 212.26.

*1,3,5-Tris(iodoethynyl)benzene (**1,3,5-TIB**)*: ^1H NMR (300 MHz, CDCl_3) δ ppm: 7.44 (d, $J = 0.8$ Hz, 3H, 1, 3, 5). ^{13}C NMR (75 MHz, CDCl_3) δ ppm: 9.14 ($\text{C}_{\text{Alk}}-\text{I}$), 92.29 ($\text{C}_{\text{Alk}}-\text{Ar}$), 124.11 ($\text{C}_{\text{Ar}}-\text{Alk}$), 135.95.

*Bis(3-iodoprop-2-yn-1-yl) terephthalate (**pBIPT**)*: ^1H NMR (300 MHz, CDCl_3) δ ppm: 8.14 (s, 4H), 5.09 (s, 4H).

Tris(3-iodoprop-2-yn-1-yl) benzene-1,3,5-tricarboxylate (1,3,5-TIPCB): ^1H NMR (300 MHz, CDCl_3) δ ppm: 8.92 (s, 3H), 5.13 (s, 6H).

2.7.4 X-ray monocrystal diffraction

The crystals are air stable and were mounted on the tip of a glass fiber with epoxy cement. X-ray diffraction experiments were carried out on an Oxford-diffraction Xcalibur S diffractometer. Data were collected at 293 K and 150 K with Mo- or Cu-K α radiation. The software package CrysAlys was used to process data.

Final cell parameters were obtained by global refinement of reflections obtained from integration of all the frames data. The structures were solved by direct methods and refined by the full-matrix method based on F^2 using SHELXTL program. The non-hydrogen atoms of structures were refined anisotropically, the hydrogen atoms were observed in difference electro density maps and refined

isotropically. The crystal parameters and basic information relating data collection and structure refinement for the compounds are summarized in Table 2.10.

Table 2.10 Crystal information of all bisethynyl and bisiodoethynyl crystal structures.

Compound	mBIEB	1,3,5-TIEBb	1,3,5-TPCB	1,3,5-TIPCB	pBPT	pBIPT
Emp. formula	C ₁₀ H ₄ I ₂	C ₁₂ H ₃ I ₃	C ₁₈ H ₁₂ O ₆	C ₁₈ H ₉ I ₃ O ₆	C ₁₄ H ₁₀ O ₄	C ₁₄ H ₈ I ₂ O ₄
Formula weight	377.93	527.84	324.28	701.95	242.22	494.00
Crystal system	Monoclinic	Triclinic	Monoclinic	Triclinic	Triclinic	Triclinic
a, Å	26.391(2)	8.6958(3)	11.1986(2)	4.2720(4)	3.9232(15)	4.1912(2)
b, Å	4.2415(3)	17.5984(7)	20.6035(3)	15.6898(10)	11.954(3)	13.6263(6)
c, Å	19.9116(15)	18.9764(8)	6.89860(10)	16.4678(10)	13.796(2)	13.6994(5)
α, deg	90	74.068(4)	90	113.383(6)	113.394(19)	104.683(3)
β, deg	108.977(9)	89.992(3)	96.081(2)	94.355(6)	95.08(2)	92.070(4)
γ, deg	90	82.891(3)	90	95.533(7)	90.24(2)	95.855(4)
Volume, Å³	2107.7(3)	2769.25(19)	1582.76(4)	1000.50(13)	591.0(3)	751.32(6)
T, K	293(2)	293(2)	99.98(10)	100.01(10)	100(2)	100.00(10)
Space group	C2/c	P -1	P2 ₁ /c	P -1	P -1	P -1
Z	8	8	4	2	2	2
μ(X K_α), mm⁻¹	5.913	6.740	0.872 (Cu)	37.091(Cu)	0.840 (Cu)	32.977 (Cu)
θ range, deg	3.11 to 26.22	3.15 to 24.71	3.97 to 74.25	2.95 to 67.00	3.51 to 74.12	3.34 to 73.91
Refl. collected	5038	39854	12955	3763	3370	4988
Uniq reflect/ Rint	1777 / 0.0639	9429 / 0.0331	3172 / 0.0289	3763/0.0000	1814 / 0.0762	2913 / 0.0371
R1/wR2 [I>2σ]	0.0662 / 0.0978	0.0491 / 0.1417	0.0321/0.0831	0.1002/ 0.2770	0.0887 / 0.2590	0.0389 / 0.0970
R1/wR2 (all data)	0.1179 / 0.1168	0.0908 / 0.1740	0.0365 / 0.0861	0.1099/ 0.2894	0.1433 / 0.2883	0.0430 / 0.1010
Residual p/ e Å⁻³	0.651 / -0.655	1980 / -1.480	0.272 / -0.229	3.127/-3.432	0.432/ -0.414	2.809/- 1.233

2.7.5 Hirshfeld Surfaces

Hirshfeld surfaces and the associated fingerprint plots were calculated using CrystalExplorer,^[29] which accepts a structure input file in the CIF format. Bond lengths to hydrogen atoms were set to typical neutron values (C–H = 1.083 Å, N–H = 1.009 Å, O–H = 0.983 Å). The distance from the Hirshfeld surface to the nearest atoms outside and inside the surface are characterized by the quantities d_e and d_i ,

Iodoethynyl halogen bond donors

respectively, and the normalized contact distance based on these, $d_{norm} = (d_i - r_i^{vdW}) / r_i^{vdW} + (d_e - r_e^{vdW}) / r_e^{vdW}$, with r_i^{vdW} and r_e^{vdW} being the van der Waals radii of the atoms. The 2D histograms, fingerprints, plot distance external to the surface (d_e) versus distance internal to the surface (d_i): is the distance from the surface to the nearest atom in the molecule itself.

2.8 Final Remarks

In this first chapter the preparation of halogen bond donors derived from iodoethynyl has been introduced. All halogen derivatives described were synthesized from their corresponding alkynes. Differences between each halogen molecule are the number of halogen bond donors and the conformational flexibility of groups. Crystal structures of the precursors and halogen derivatives were determined and compared. In spite of the differences in atom size (hydrogen and iodine), the interaction energy leads to similar supramolecular organizations.

In the following chapters the design of new with the halogen bond donors will be discussed.

2.9 Bibliography

- [1] a) L. Turunen, N. K. Beyeh, F. Pan, A. Valkonen and K. Rissanen, *Chem. Commun.* **2014**, *50*, 15920-15923; b) O. Dumele, D. Wu, N. Trapp, N. Goroff and F. Diederich, *Org. Lett.* **2014**, *16*, 4722-4725; c) J. Lieffrig, O. Jeannin and M. Fourmigué, *J. Am. Chem. Soc.* **2013**, *135*, 6200; d) C. Lemouchi, C. S. Vogelsberg, L. Zorina, S. Simonov, P. Batail, S. Brown and M. A. Garcia-Garibay, *J. Am. Chem. Soc.* **2011**, *133*, 6371-6379.
- [2] H.-C. Weiss, D. Blaser, R. Boese, B. M. Doughan and M. M. Haley, *Chem. Commun.* **1997**, 1703-1704.
- [3] F. Guthrie, *J. Chem. Soc.* **1863**, *16*, 239.
- [4] B. Casper, H.-G. Mack, H. S. P. Mueller, H. Willner and H. Oberhammer, *J. Phys. Chem.* **1994**, *98*, 8339-8342.
- [5] H. A. Bent, *Chem. Rev.* **1968**, *68*, 587.
- [6] a) T. Brinck, J. S. Murray and P. Politzer, *Int. J. Quantum Chem.* **1992**, *44*, 57; b) T. Brinck, J. S. Murray and P. Politzer, *Int. J. Quantum Chem.* **1993**, *48*, 73-88; c) J. S. Murray, K. Paulsen and P. Politzer, *Proc.—Indian Acad. Sci., Chem. Sci.* **1994**, *106*, 267.
- [7] G. Valerio, G. Raos, S. V. Meille, P. Metrangolo and G. Resnati, *J. Phys. Chem. A* **2000**, *104*, 1617-1620.
- [8] a) V. Nefedov, *Russ. J. Org. Chem.* **2007**, *43*, 1163-1166; b) A. Takemura, L. J. McAllister, S. Hart, N. E. Pridmore, P. B. Karadakov, A. C. Whitwood and D. W. Bruce, *Chem. Eur. J.* **2014**, *20*, 6721-6732; c) A. Vargas Jentzsch and S. Matile, *J. Am. Chem. Soc.* **2013**, *135*, 5302; d) F. Zapata, A. Caballero, N. G. White, T. D. W. Claridge, P. J. Costa, V. Felix and P. D. Beer, *J. Am. Chem. Soc.* **2012**, *134*, 11533-11541; e) A. Mateo-Alonso, N. Kulisic, G. Valenti, M. Marcaccio, F. Paolucci and M. Prato, *Chem. Asian J.* **2010**, *5*, 482-485; f) P. Cardillo, E. Corradi, A. Lunghi, S. Meille, M. Messina, P. Metrangolo and G. Resnati, *Tetrahedron* **2000**, *56*, 5535-5550; g) X. Pang and W. J. Jin in *Halogen Bonding in the Design of Organic Phosphors*, Vol. Springer, **2014**, pp. 115-146; h) P. Metrangolo, H. Neukirch, T. Pilati and G. Resnati, *Acc. Chem. Res.* **2005**, *38*, 386-395; i) A. Forni, P. Metrangolo, T. Pilati and G. Resnati, *Cryst. Growth Des.* **2004**, *4*, 291.
- [9] H. M. Yamamoto, Y. Kosaka, R. Maeda, J.-i. Yamaura, A. Nakao, T. Nakamura and R. Kato, *Acs Nano* **2008**, *2*, 143-155.
- [10] C. Lemouchi, C. S. Vogelsberg, L. Zorina, S. Simonov, P. Batail, S. Brown and M. A. Garcia-Garibay, *J. Am. Chem. Soc.* **2011**, *133*, 6371-6379.
- [11] C. Perkins, S. Libri, H. Adams and L. Brammer, *CrystEngComm* **2012**, *14*, 3033-3038.
- [12] a) N. S. Goroff, S. M. Curtis, J. A. Webb, F. W. Fowler and J. W. Lauher, *Organic Letters* **2005**, *7*, 1891-1893; b) H. Jin, A. M. Plonka, J. B. Parise and N. S. Goroff, *CrystEngComm* **2013**, *15*, 3106.
- [13] C. B. Aakeröy, M. Baldridge, J. Desper, P. Metrangolo and G. Resnati, *Chemistry – A European Journal* **2013**, *19*, 16240-16247.
- [14] M. Baldridge, G. Cavallo, M. R. Chierotti, R. Gobetto, P. Metrangolo, T. Pilati, G. Resnati and G. Terraneo, *Mol. Pharmaceutics* **2013**, *10*, 1760-1772.
- [15] S. Cicchi, P. Fabbrizzi, G. Ghini, A. Brandi, P. Foggi, A. Marcelli, R. Righini and C. Botta, *Chem. Eur. J.* **2009**, *15*, 754-764.
- [16] G. Chen, J. Kumar, A. Gregory and M. H. Stenzel, *Chem. Commun.* **2009**, 6291-6293.
- [17] K. Bouchmella, B. Boury, S. G. Dutremez and A. van der Lee, *Chem. Eur. J.* **2007**, *13*, 6130-6138.
- [18] W. Z. Guo, E. Galoppini, R. Gilardi, G. I. Rydja and Y. H. Chen, *Cryst. Growth Des.* **2001**, *1*, 231-237.
- [19] D. Cincic, T. Friscic and W. Jones, *New J. Chem.* **2008**, *32*, 1776-1781.
- [20] D. Cincic, T. Friscic and W. Jones, *J. Am. Chem. Soc.* **2008**, *130*, 7524-7525.
- [21] a) J. J. Novoa and F. Mota, *Chem. Phys. Lett.* **2000**, *318*, 345-354; b) O. V. Shishkin, *Chem. Phys. Lett.* **2008**, *458*, 96-100.
- [22] A. Bondi, *J. Phys. Chem.* **1964**, *68*, 441-451.

- [23] A. L. Barres, A. El-Ghayoury, L. V. Zorina, E. Canadell, P. Auban-Senzier and P. Batail, *Chem. Commun.* **2008**, 2194-2196.
- [24] V. G. Saraswatula and B. K. Saha, *New J. Chem.* **2014**, *38*, 897-901.
- [25] K. Wang, D. Duan, M. Zhou, S. Li, T. Cui, B. Liu, J. Liu, B. Zou and G. Zou, *J Phys. Chem. B* **2011**, *115*, 4639-4644.
- [26] a) R. H. Baughman, *J. Org. Chem.* **1964**, *29*, 964-&; b) A. S. Batsanov and J. A. K. Howard, *Acta Crystallogr.* **2000**, *C56*, 252-253.
- [27] G. Drefahl and E. Keil, *J. Prakt. Chem.* **1958**, *6*, 80-80.
- [28] L. Gonzalez, N. Gimeno, R. Maria Tejedor, V. Polo, M. Blanca Ros, S. Uriel and J. Luis Serrano, *Chem. Mat.* **2013**, *25*, 4503-4510.
- [29] M. A. Spackman and D. Jayatilaka, *CrystEngComm* **2009**, *11*, 19-32.

Chapter 3 Iodo Tröger's Base derivatives: Towards halogen bonded porous organic crystalline materials

3.1 Introduction

The preparation of porous materials has become an important challenge in Materials Science due the applications of such systems in fields as diverse as petrochemistry,^[1] water purification,^[2] and fuel cells,^[3] amongst others. The unique geometry and complementarity of Tröger's base makes it especially useful for this purpose. Taking into account the general objective of the PhD work described here, this chapter is devoted to the design, synthesis and crystal structure characterization of some diiodo Tröger's base derivatives with the aim of obtaining stable porous crystalline materials.

Iodo Tröger's Base derivatives: Towards halogen bonded porous organic crystalline materials

3.2 Previous work

The most important goal in this research field is to obtain materials with well-defined molecular topologies in order to optimize the physical properties inherent to their structures.^[4] Amongst other approaches, Supramolecular Chemistry, and more specifically crystal engineering, has proven to be very useful to control the molecular topology.^[5] In this context, porous organic polymers^[6] and crystalline materials (POCMs),^[7] which are less dense than other porous materials such as zeolites^[8] and metal-organic frameworks (MOFs),^[9] have attracted increasing interest in recent years. In order to obtain this type of material there are two fundamental points that need to be considered: the geometry of the molecules and the interactions promoted by their active groups.

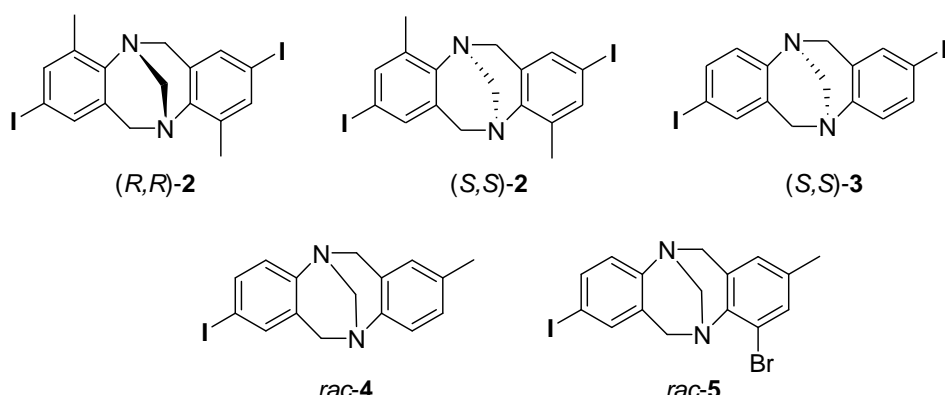
The bicovalently bonded Tröger's base (TB) analogs have been used as building blocks to obtain organic nanoporous polymers with a high BET surface.^[10]

These compounds are chiral diamines with a C_2 -symmetry, a V-shaped structure and a rigid conformation that provides a hydrophobic cavity. The methylene bridge precludes pyramidal inversion of the two nitrogen atoms and this means that only the enantiomers of *R,R* or *S,S* configuration are possible.^[11] In recent years, among the weak intermolecular interactions that have been exploited in supramolecular chemistry, halogen bonding has proven to be a very powerful tool for the preparation of new materials. Indeed, several POCMs based on halogen bonding have been described.^[12]

In the CSD there are thirty-four entries for Tröger's base derivatives that contain at least one halogen atom on one of the benzene rings. Of these structures only five have at least one iodo-substituent.

It can be seen from Scheme 3.1 that three of these five structures correspond to a pure enantiomer and the other two to a racemic mixture. Thus, (5*R*,11*R*)-2,8-

diiodo-4,10-dimethyl-6H,12H-5,11-methanedibenzo[b,f][1,5]diazocine ((**R,R**)-**2**), (5S,11S)-2,8-diiodo-4,10-dimethyl-6H,12H-5,11-methanedibenzo[b,f][1,5]diazocine ((**S,S**)-**2**) and (5S,11S)-2,8-diiodo-6H,12H-5,11-methanedibenzo[b,f][1,5] diazocine ((**S,S**)-**3**) are formed by pure enantiomers that contain two iodo-substituents. On the other hand, 2-iodo-8-methyl-6H,12H-5,11-methanedibenzo[b,f][1,5]diazocine (**rac-4**) and 4-bromo-8-ido-2-methyl-6H,12H-5,11-methanedibenzo[b,f][1,5]diazocine (**rac-5**) are formed by a racemic mixture and the enantiomers bear only one iodo-substituent.



Scheme 3.1 Iodo Tröger's base derivatives for which crystal structures have been deposited in the CSD.

The crystal structures described show only halogen bonds between the iodine atom and the electron density of the benzene rings. The crystal structure of the compound **(S,S)-2** is shown in Figure 3.1.

Iodo Tröger's Base derivatives: Towards halogen bonded porous organic crystalline materials

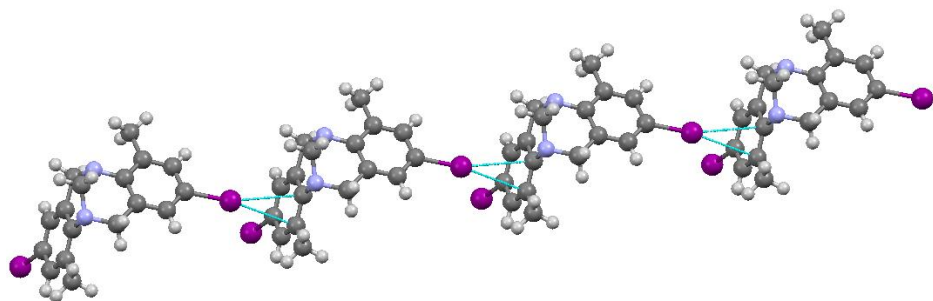


Figure 3.1 Polymer chain of the structure of (S,S)-2 formed by halogen bonds between the iodine atom and the benzene ring.

The crystal structure of the compound (S,S)-3,^[13] which contains two iodine atoms, has halogen bonds (3.52 Å and 170.2°, see Figure 3.2 (a)). These give rise to the formation of planes that are approximately perpendicular to one another and, when these are cross-linked, they give rise to channels along the *c* axis that represent 21.3% of the volume and in which the solvent molecules (hexane) are located (Figure 3.2 (b)).

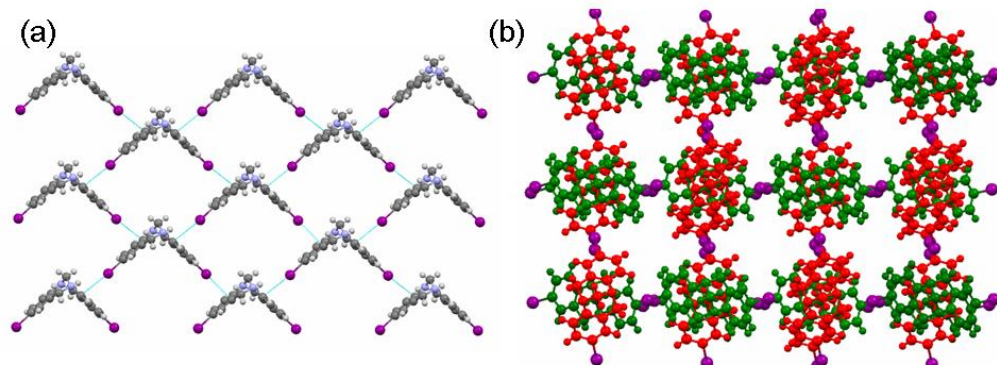


Figure 3.2 Crystal structure of compound (S,S)-3. a) Structural planes formed by the halogen bonds between the iodine atom and the benzene ring of neighboring molecules. b) Porous crystalline structure containing solvent molecules in the channel.

The crystal structures of the two racemic mixtures of Tröger's base derivatives bearing one iodine atom (**rac-4** and **rac-5**) have halogen bonds between the iodine atom and a nitrogen atom of the neighboring molecule (Figure 3.3).

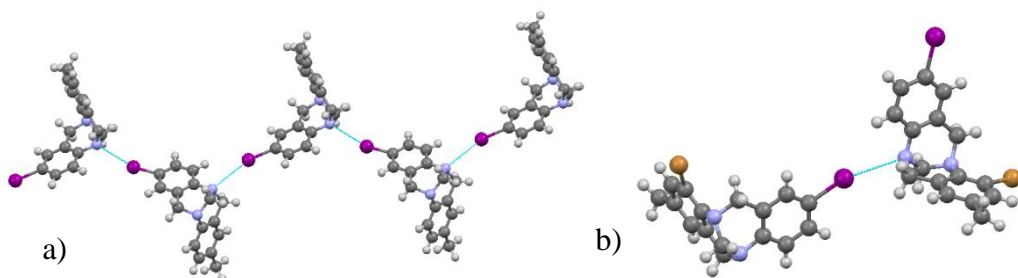


Figure 3.3 a) Crystal structure of the racemic mixture **rac-4** with chains and **b)** crystal structure of the racemic mixture **rac-5** forming dimers. In both cases the intermolecular interactions are formed by C-I...N halogen bonding.

Analysis of the crystal structures derived from the Tröger's base containing iodine shows that the halogen atoms favor intermolecular interactions and that the presence of a pure enantiomer or a racemic mixture has a decisive influence on the molecular organization in the crystal. The compound **(S,S)-3**, which contains two iodine atoms, forms a porous structure and this is one of our objectives.

3.3 Objectives and planning

3.3.1 Objectives

The main objective of this work was to obtain porous crystalline materials using diiodo Tröger's base derivatives as molecular units.

In the design of these compounds our idea was to use the halogen bonding interactions in order to favor the formation of porous structures.

Taking into account the chirality of Tröger's bases and the complementary nature of the structural packing of the enantiomers, a comparative study between the crystalline structures of the racemic mixture and a single pure enantiomer was carried out.

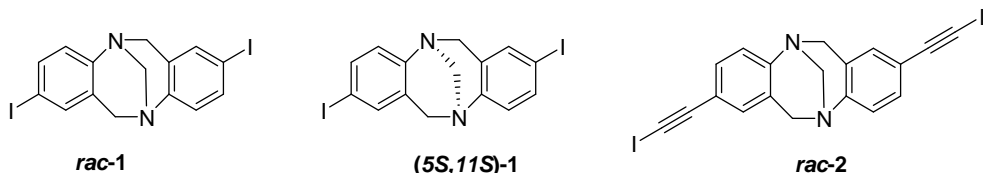
3.3.2 Planning

In order to achieve these objectives and taking into account the literature review, we decided to combine Tröger's base analogs and halogen bonding to obtain porous crystalline materials by taking advantage of the geometry and complementary nature of iodo Tröger's base derivatives. We prepared and characterized the crystalline structures of three iodo-containing Tröger's base derivatives functionalized in positions 2 and 8.

A racemic mixture of a derivative containing two iodo-substituents (2,8-diido-6*H*,12*H*-5,11-methanodibenzo[*b,f*][1,5]diazocine (**rac-1**), the pure enantiomer (2,8-diido-6*H*,12*H*-5,11-methano-dibenzo[*b,f*][1,5]diazocine (**5S,11S-1**) and a racemic mixture containing two ethynyl groups (2,8-bis(iodoethynyl)-6*H*,12*H*-5,11-methanodibenzo[*b,f*][1,5]diazocine, **rac-2**). The structures are shown in Scheme 3.2.

The racemic (**rac-1**) and the enantiopure (**5S,11S-1**) compounds were selected to compare their ability to form porous crystalline structures. The classical Wallach's

rule states that racemic crystals tend to be denser than their chiral counterparts,^[14] and consequently the enantiopure compounds favor the formation of porous crystalline structures.



Scheme 3.2 Tröger's base structures described in this chapter, from left to right: **rac-1**, **(5S,11S)-1** and **rac-2**.

The covalently bonded halogen atoms, as present in the compounds **rac-1** and **(5S,11S)-1**, show a positive electrostatic potential region (σ -hole) along the covalent bond, as shown Figure 3.4. Thus, the electron density map of the 2,8-diido Tröger's base analog shows two electron density donor groups (nitrogen atoms) and two electron density acceptors (iodine atoms) with a pseudo-tetrahedral distribution (Figure 3.4). It is noteworthy that in crystal structures of single-enantiomer iodo Tröger's base derivatives collected in the Cambridge Structure Database the halogen bond has as an acceptor the electron density of the aromatic rings,^[15] whereas in examples that contain the pair of enantiomers the nitrogen atoms act as halogen bond acceptors.^[16] To date, very few structures have been described for heterotopic AX_2Y_2 tectons that can bind through halogen bonds with a tetrahedral arrangement of functional groups. Only two examples appear in the literature: (i) the crystal structure of the 5*S*,11*S* enantiomer of 2,8-diido Tröger's base derivative **(5S,11S)-1** described by Wärnmark and co-workers,^[17] which contains channels – in which the solvent is located – formed by halogen bonding and (ii) 4,4-dinitro-4',4"-diiodotetraphenylmethane.^[18]

Iodo Tröger's Base derivatives: Towards halogen bonded porous organic crystalline materials

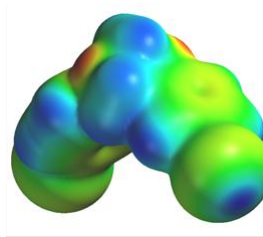


Figure 3.4 Electrostatic potential region of **rac-1**

We describe herein the wholly organic architectures of a dichloromethane solvate of 2,8-diido-4,10-dimethyl-6H,12H-5,11-methanodibenzodiazocine (**rac-1·CH₂Cl₂**) and compact structures of **rac-1** and (**5S,11S**)-**1**, with particular attention focused on the role played by each of the halogen bond donors and acceptors.

Based on the results obtained for these structures we prepared 2,8-diidoethynyl-4,10-dimethyl-6H,12H-5,11-methanodibenzodiazocine (**rac-2**) in order to increase the magnitude of the iodine σ -hole. Theoretical, statistical, and crystallographic studies demonstrated that the sp hybridization of the carbon atom adjacent to the halogen allows the ethynyl-based halogen to display a polar σ -hole of comparable magnitude to those in fluoro-substituted iodocarbons, which are the most commonly used halogen bonding donors.^[19] Furthermore, the extended linear nature of C–C≡C–I improves accessibility and makes the iodoethynyl group very interesting for crystal engineering. Haloalkynes have a well-established role in synthetic organic chemistry^[20] but their application in supramolecular chemistry is less well developed despite their long history.^[21]

3.4 Results and discussion

3.4.1 Preparation of the Tröger's base derivatives

The synthesis of Tröger's base analogs is often accomplished by the acid-promoted condensation of anilines with formaldehyde or another methylene synthon. The 2,8-diido TB derivative (**rac-1**) was synthesized according to the protocol described by Wärnmark *et al.*, which involves a condensation reaction between 4-iodoaniline and paraformaldehyde in trifluoroacetic acid (TFA).^[22] The two enantiomers of **rac-1** were resolved, as described by Arribas *et al.*,^[15a] on a preparative chiral phase HPLC column (CHIRALPAK[®]) using 4:1 hexane:EtOH as eluent.

As explained above, the racemic Tröger's base derivative 2,8-bis(iodoethynyl)-6H,12H-5,11-methanodibenzo[b,f][1,5]diazocine (**rac-2**) was prepared in order to make the halogen bond stronger and to obtain larger pores. Racemic **1** is transformed into racemic 2,8-diidoethynyl Tröger's base (**rac-2**) in two steps. The first step consists of a Sonogashira coupling with trimethylsilylacetylene^[23] and the second step is treatment with N-iodosuccinimide and silver nitrate in dimethylformamide.

3.4.2 X-ray monocrystal structures of iodo Tröger's base derivatives

Crystallization of **rac-1** from a dichloromethane solution gave rise to a clathrate (**rac-1·CH₂Cl₂**) that crystallizes in an orthorhombic system and was solved in the non-centrosymmetric Iba2 space group. The asymmetric unit of **rac-1·CH₂Cl₂** consists of two half molecules of **1** and a dichloromethane solvent molecule. The 2,8-diido Tröger's base analog acts a heterotopic tetradentate building block through C(1)–I(1)…N(2) (3.129 Å, 172.2°) and C(10)–I(2)…N(1) (3.217 Å, 159.5°) halogen bonding (Table 3.1). The halogen bonding distances are 11% and 9% shorter than the sum of I and N van der Waals radii (3.53 Å).^[24]

Iodo Tröger's Base derivatives: Towards halogen bonded porous organic crystalline materials

Table 3.1 Geometrical features of the halogen bond interactions in rac-1•CH₂Cl₂, rac-1, (5S,11S)-1 and rac-2

Compound	C-X···Y	Sym. equivalence	d(C–X) Å	d(I···Y) Å	<(CXY)°	rr ^a
<i>rac-1•CH₂Cl₂</i>	C(1)–I(1)···N(2)	-1/2+x, -1/2+y, -1/2+z	2.12(1)	3.129(8)	172.2(3)	0.89
<i>rac-1</i>	C(10)–I(2)···N(1)	x, 1-y, -1/2+z	2.09(1)	3.217(1)	159.5(4)	0.91
	C(8)–I(2)···N(11)	1+x, 1/2-y, 1/2+z	2.132(5)	3.159(4)	163.2(2)	0.89
<i>(5S,11S)-1</i>	C(28)–I(4)···I(2)	x, 1/2-y, 1/2+z	2.113(5)	3.8578(6)	172.9(1)	0.97
	C(11)–I(1)···I(3)	-1+x, 1+y, z	2.098(5)	3.8774(4)	162.4(1)	0.98
<i>rac-2</i>	C(17)–I(2)···π(Ar)	1-x, 1-y, 2-z	1.988(6)	3.469	170.38	0.94
	C(1)–I(1)···N(1)	-x, 1/2+y, 1/2-z	2.018(7)	2.800(5)	172.8(2)	0.79

a) Reduction ratio, rr = dI···(Halogen bond acceptor)/(R_{vdW}(I) + R_{vdW}(Halogen bond acceptor));
 $R_{vdW}(I) = 1.98 \text{ \AA}$, $R_{vdW}(N) = 1.55 \text{ \AA}$ [24]

Each molecule is surrounded by four molecules in a distorted tetrahedral environment (Figure 3.5(a)) and this gives rise to a diamond-like structure. Overall, the structure contains two interpenetrated diamondoid structures (red and green in Figure 3.4(b)) that form channels along the *c* axis, in which are located dichloromethane molecules.

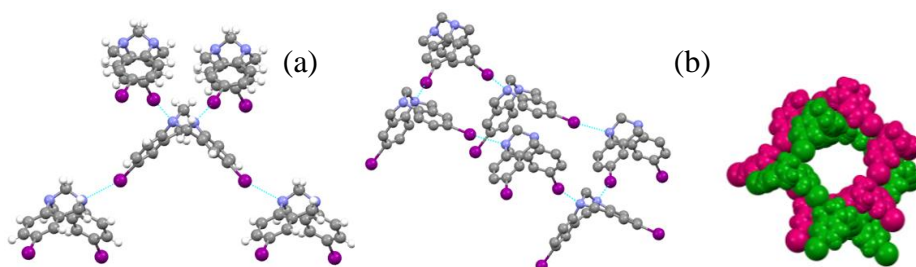


Figure 3.5 (a) Crystal structure of solvate rac-1•CH₂Cl₂. Diamondoid arrangement and (b) pseudo-tetrahedral environment of the 2,8-diiodo Tröger's base analog.

Each of these virtual channels, regardless of dichloromethane, has a volume of 209 Å³ per unit cell and this represents 23.7% of the total volume. The structure can also be described (Figure 3.6) as channels formed by a pseudo-helical arrangement

of the two enantiomers through halogen and C–H···I hydrogen bonds (Table 3.2) with four associated molecules in one helical turn.

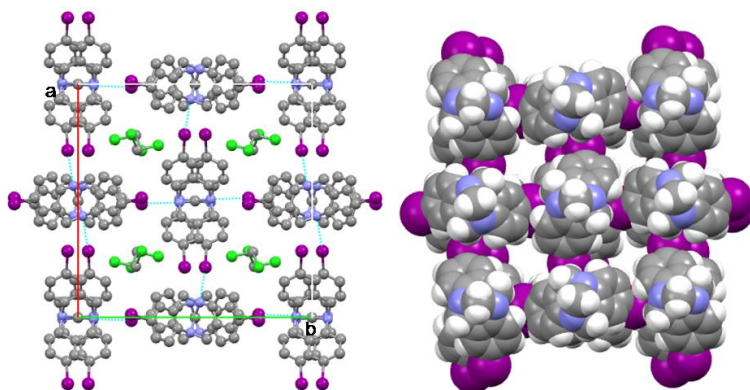


Figure 3.6 Crystal structure of solvate **rac-1·CH₂Cl₂**. (a) Channel along the *c* axis with CH₂Cl₂ molecules. (b) Spacefill view of the channels (solvent molecules have been omitted).

Table 3.2 Hydrogen bond distances and angles in **rac-1·CH₂Cl₂**, **rac-1**, **(5S,11S)-1** and **rac-2**

Compound	D–H···A	Sym. equivalence	d(D–H) Å	d(H···A) Å	d(D···A) Å	<(DHA) °
rac-1·CH₂Cl₂	C(17)-H···I(1)	1/2+x, 1.5-y, z	0.97	3.1187	4.04(1)	158.1
rac-1	C(13)-H···I(2)	-1+x, y, z	0.970	3.1262	4.049(6)	155.4
	C(9)-H···I(2)	x, 1/2-y, -1/2+z	0.931	3.1011	3.964(6)	155.0
(5S,11S)-1	C(15)-H···N(3)	-1+x, y, -1+z	1.04(5)	2.65(6)	3.641(6)	159(3)
	C(44)-H···π(Ar)	1+x, y, z	0.92(6)	2.78(6)	3.683(7)	167(4)
	C(14)-H···I(4)	-1+x, -1+y, -1+z	1.00(5)	3.19(3)	3.749(3)	117(3)
	C(12)-H···I(1)	x, -1+y, z	0.930	3.2210	4.143(3)	171.7
rac-2	C(19)- H···π(Alk)	-x, 1-y, -z	0.970	2.613	3.579	174.65
	C(12)-H···N(2)	x, y, 1+z	0.930	2.456	3.36(1)	164.7(1)

Crystals of **rac-1·CH₂Cl₂** lose crystallinity quickly when they are removed from the mother liquor. This change could be due to one or more of the following factors: the inherent instability of the clathrates with a diamond-like structure and the weakness, in this case, of halogen bonding. This weakness is manifested in the

Iodo Tröger's Base derivatives: Towards halogen bonded porous organic crystalline materials

small reduction in the I···N distance with respect to the sum of the van der Waals radii (*ca.* 10%) and it is due to low electron-deficiency of the iodine atom.^[25] The XRD pattern of **rac-1**·CH₂Cl₂ crystals taken out of the mother liquor resembled the calculated powder diffractogram for the more compact structure of **rac-1** obtained by crystallization from a toluene solution.

We also succeeded in crystallizing a condensed phase of the enantiomerically pure (5S,11S)-2,8-diiodo Tröger's base analog **(5S,11S)-1**. As mentioned in the introduction, the crystal structure of the **(5S,11S)-1**·hexane clathrate, which has channels containing disordered hexane molecules, has been described previously by Wärnmark *et al.*^[17] (CSD–REFCOD LUYZEL).^[26]

A first examination of **rac-1** and **(5S,11S)-1** compact structures revealed that the two crystals have the same density (1.522 g cm⁻³) and the R factor for the racemic crystals ($R_1 = 0.0387$ ($I > 2\sigma(I)$)) is higher than that of the homochiral partner ($R_1 = 0.0179$ ($I > 2\sigma(I)$)). The asymmetric unit of the two structures contains two molecules ($Z' = 2$) of the same enantiomer in the case of **(5S,11S)-1** and one of each enantiomer in the case of **rac-1**. These results contradict Wallach's rule, which states that racemic crystals tend to be denser than their chiral counterparts,^[14] and are more consistent with the conclusions of Gavezotti that racemic compounds are not necessarily more dense or stable than the homochiral ones.^[27]

Tröger's base has a rigid conformation despite the fact that the angle between the planes defining the chiral cleft may vary to suit the solid state packing. This angle is not significantly different in **rac-1** and **(5S,11S)-1**, with average values of 85.2[0.7]° and 87.4[1.1]°, respectively. Although **rac-1** and **(5S,11S)-1** crystallized in the monoclinic and triclinic systems, respectively, their supramolecular organizations show some similarities. In both cases the molecules stack along the *a* axis: in the case of **(5S,11S)-1** the stacks are formed in such a way that they result

in face-to-face offset dimers in which the molecules are rotated by 102.8° with respect to one another, while in ***rac-1*** they are formed by two interdigitated homochiral strings rotated with respect to each other by 45.6° (Figure 3.7).

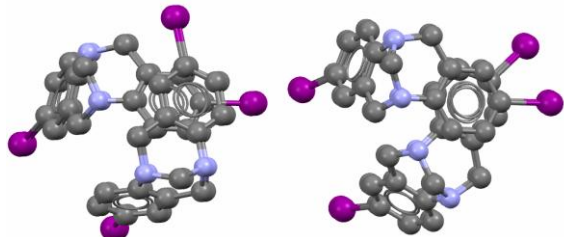


Figure 3.7 Detail of the stack along the *a* axis in (5*S*, 11*S*)-1 and *rac-1* crystal structures.

Each stack in ***rac-1*** is stabilized by $\pi\text{-}\pi$ interactions and hydrogen bonding (C(13)–H \cdots I(2) 3.13 Å, 155.4°) and the stacks interact with two others by halogen and hydrogen bonding (Figure 3.8 (a)). Thus, one can distinguish three types of iodine atoms depending on the type of halogen bonding formed. One iodine atom of each crystallographic independent molecule (I(1) and I(3)) does not establish interactions, while I(4) acts as a halogen bonding donor in an I \cdots I interaction (3.86 Å, 172°) and, finally, I(2) acts as a halogen bonding donor (I(2) \cdots N(11) 3.16 Å, 163°) and acceptor, as depicted in Figure 3.8 (b).

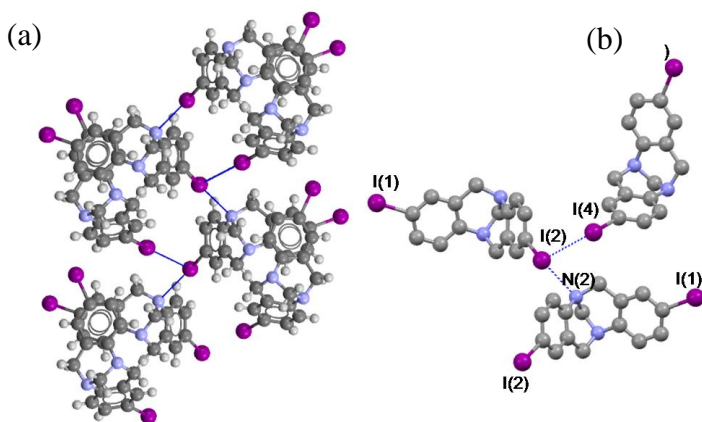


Figure 3.8 Halogen bond network in the crystal structure of 1, the cells are drawn with only two molecules for the sake of clarity. (b) Details of the N \cdots I and I \cdots I interactions in the structure

Iodo Tröger's Base derivatives: Towards halogen bonded porous organic crystalline materials

The supramolecular arrangement of ***rac-1*** is two-dimensional and is formed by *ac* planes. Iodine atoms I(1) and I(3) are located on the surface of these planes and they do not interact, thus isolating the planes from each other along the *b* axis (Figure 3.9).

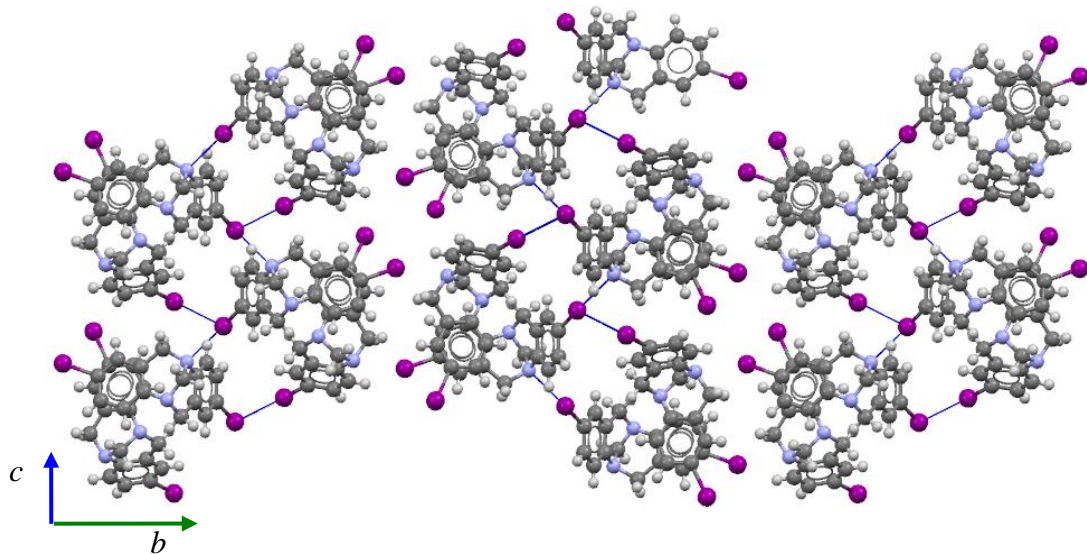


Figure 3.9 Supramolecular arrangement along the *a* axis of the ***rac-1*** crystal structure.

The stacks in **(5S,11S)-1** are stabilized by $\pi\cdots\pi$ interactions and weak $C_{sp^3}\text{--H}\cdots\pi$ interactions, while stacks are connected to each other along the *b* axis by $C\text{--I}\cdots\text{I}$ (3.88 Å and 162.4°) halogen bonding^[5] (purple in Figure 3.10) and along the *c* axis by hydrogen bonds ($C_{sp^3}\text{--H}\cdots\text{N}$ 2.65 Å and 159° and $C_{sp^3}\text{--H}\cdots\pi$) (blue in Figure 3.10). These interactions result in a compact three-dimensional network.

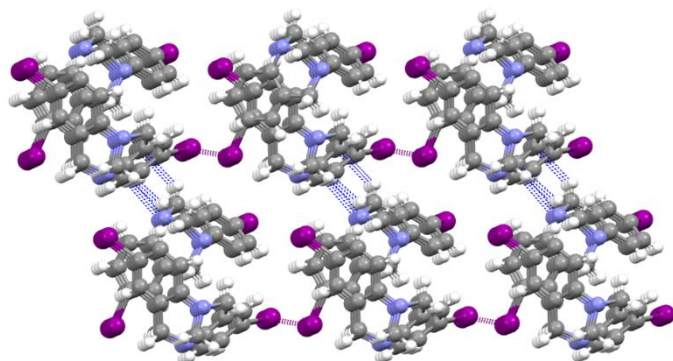


Figure 3.10 Halogen and hydrogen bonding 3D network along the *a* axis of the (5S,11S)-1 crystal structure.

It should be noted that both ***rac-1*** and **(5S,11S)-1** exhibit I···I halogen bonds and these are the first examples of such interactions in a Tröger's base and show the versatility of halogen bonding to form novel supramolecular organizations. These results are novel and interesting, but our objective to obtain nanoporous organic crystalline materials was not achieved. As explained above, in order to increase the magnitude of the iodine σ -hole we synthesized and obtained the crystal structure of the racemic mixture of 2,8-diiodoethynyl-4,10-dimethyl-6*H*,12*H*-5,11-methanodibenzodiazocine (***rac-2***).

Rac-2 crystallizes in the monoclinic $P2_1/c$ space group and its asymmetric unit consists of one molecule in a general position. The I···I distance is 13.28 Å and the cleft angle is 89.2°, with the average of these values in ***rac-1*·CH₂Cl₂**, ***rac-1*** and **(5S,11S)-1** being 9.95[0.42] Å and 86.6[1.3]°.

The ***rac-2*** supramolecular organization can be described starting from a two-enantiomer dimer through halogen bonding C—I···π_(Ar) (Figure 3.11(a)). These dimers are joined by C_{sp}—I···N halogen bonds (2.80 Å, 172.8°). The halogen bond distance is significantly shorter than those in the structures ***rac-1*·CH₂Cl₂** (3.129 and 3.22 Å) and ***rac-1*** (3.159 Å) due to the stronger electron-withdrawing effect of the sp iodo-carbon hybridization and the lower temperature employed for data collection in the case of ***rac-2***. The halogen bonded dimers result in distorted

Iodo Tröger's Base derivatives: Towards halogen bonded porous organic crystalline materials

hexagonal nets with distances between opposite sides of 15.1 and 19.0 Å (Figure 3.11(b)).

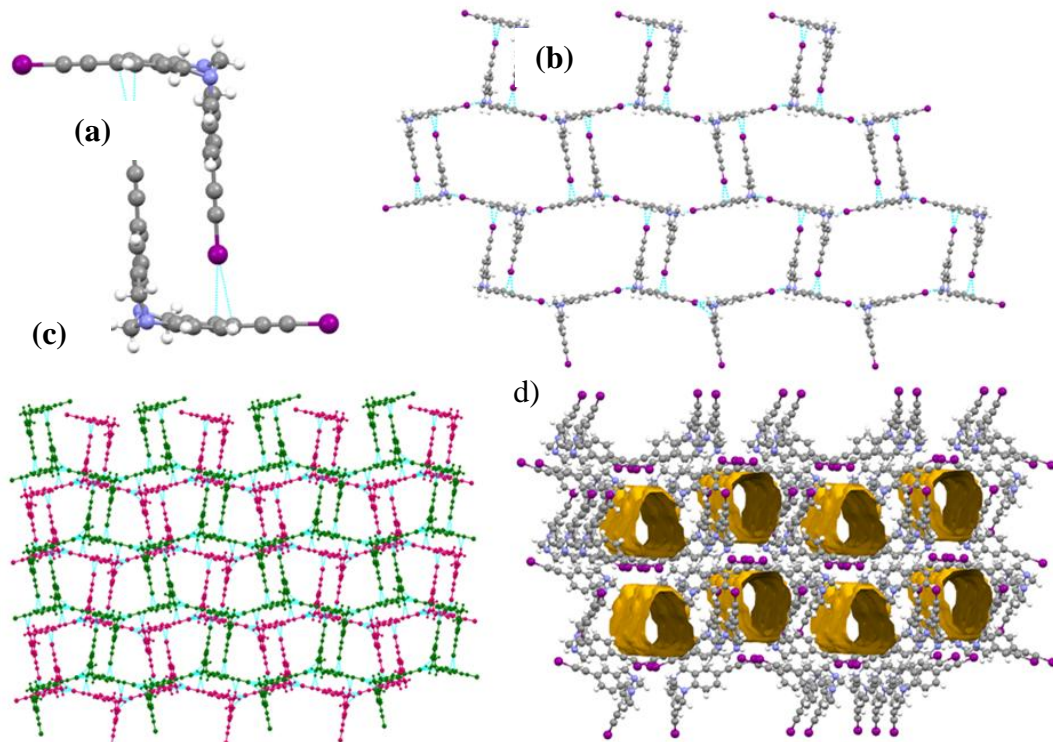


Figure 3.11 Crystal structure of rac-2: (a) Halogen bonded dimer; (b) planes forms by dimers; (c) voids in the halogen and hydrogen bonded 3D network along the *a* axis.

The planes are assembled with others, related by an inversion center, by weak C_{sp³}–H···π_{alk} hydrogen bonding and π···π stacking between dimers (Figure 3.11(c)). These two-dimensional aggregates are stacked, which leads to channels that represent 20% (417.51 Å³) of the unit cell volume, along the *c* axis (Figure 3.11(d)). Residual electron density peaks observed inside the channels were refined as 0.4 molecules of dichloromethane per 2,8-diiodoethyl Tröger's base molecule as a rigid group that pivots around one of the chlorine atoms.

3.5 Conclusions

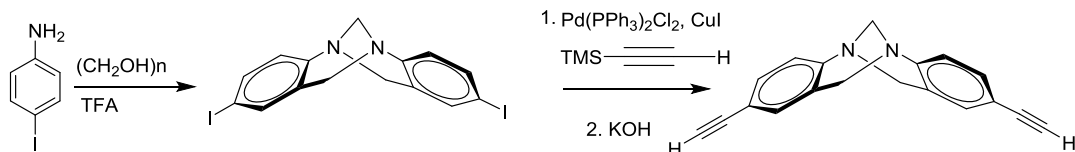
The iodo Tröger's base derivatives 2,8-diiodo-4,10-dimethyl-6*H*,12*H*-5,11-methano-dibenzodiazocine ***rac*-1** and **(5*S*,11*S*)-1** are suitable building blocks to obtain clathrate suprastructures and compact crystalline materials. Thus, we obtained a porous diamondoid-type structure, based on I···N halogen bonds, when ***rac*-1** was crystallized from dichloromethane. The supramolecular architectures of compact structures of ***rac*-1** and **(5*S*,11*S*)-1** have some similarities but the halogen bond plays a different role in each case. In ***rac*-1** N···I and I···I halogen bonds are observed, whereas in **(5*S*,11*S*)-1** only I···I is present. These are the first structures of iodo Tröger's base derivatives that have iodine···iodine interactions.

In contrast to the above, Tröger's base derivative 2,8-diiodoethynyl-4,10-dimethyl-6*H*,12*H*-5,11-methanodibenzodiazocine (***rac*-2**) crystallizes in the monoclinic P2₁/c space group and has nanometric channels that represent 20% of the cell volume and these are occupied by disordered solvent molecules. The two iodoethynyl groups behave as strong halogen bond donors, as evidenced by the I···N and I···π_(Ar) interaction distances. These interactions give rise to a dimeric unit formed by the two enantiomers **(5*S*,11*S*)-2** and **(5*R*,11*R*)-2**, which play a fundamental role in the formation of a nanoporous crystalline organization.

3.6 Experimental Section

3.6.1 Synthesis and chemical characterization

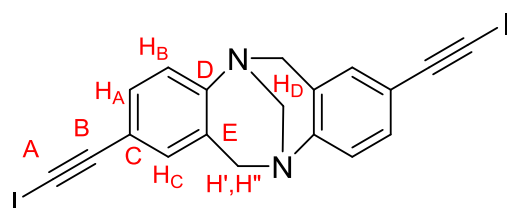
2,8-Diiodo-6H,12H-5,11-methanodibenzo[*b,f*][1,5]diazocine^[22a] was synthesized as previously described. The synthesis of 2,8-bisethynyl-6H,12H-5,11-methanodibenzo[*b,f*][1,5]diazocine, a Tröger's base derivative, was previously described^[23a] and carried out by the procedure published by Bew *et al.*^[26] as shown in Scheme 3.3 Synthesis of Tröger's base derivatives.



Scheme 3.3 Synthesis of Tröger's base derivatives.

All reagents and solvents employed were commercially available and were used as received without further purification. FT-IR spectra were recorded on a Nicolet Avatar FTIR spectrophotometer using KBr pellets. ^1H , ^{13}C , NMR spectra were recorded on a Bruker Avance 400 spectrometer (9.4T, 400.13 MHz for ^1H , 100.62 MHz for ^{13}C) on samples in CDCl_3 . Melting points were measured with a Stuart melting point apparatus. Elemental analyses were performed on a Perkin-Elmer 240 analyzer.

- **2,8-bis(iodoethynyl)-6H,12H-5,11-methanodibenzo[*b,f*][1,5]diazocine (*rac*-2)**



To a stirred solution of 2,8-bis(trimethylsilyl ethynyl)-6H,12H-5,11-methanodibenzo[b,f][1,5]diazocene (415 mg, 1 mmol) in DMF (30 mL) was added silver(I) nitrate (3.9 mg, 0.023 mmol). The mixture was stirred for 30 min. Under an argon atmosphere and at 0 °C, N-iodosuccinimide was slowly added (517.3 mg, 2.3 mmol). The mixture was stirred for 5 hours, protected from light, and the mixture was then filtered and added over water. The product was extracted 3 times with diethyl ether and cooled until a precipitate formed. The solid was filtered off and the ether was evaporated. Yield: 434 mg, 83%.

NMR (400 MHz, CDCl₃) δ ppm: 7.22 (dd, *J* = 8.3, 1.9 Hz, 1H, H_A), 7.04 (d, *J* = 8.3 Hz, 1H, H_B), 7.00 (d, *J* = 1.9 Hz, 1H, H_C), 4.62 (d, *J* = 16.7 Hz, 1H, H[']), 4.26 (s, 1H, H_D), 4.10 (d, *J* = 16.7 Hz, 1H, H^{''}). ¹³C NMR (101 MHz, CDCl₃) δ ppm: 29.86 (A), 58.55 (CH^{', H^{''}), 66.83 (CH_D), 93.85 (B), 119.11 (C), 125.05 (CH_B), 127.84 (E), 131.20 (CH_A), 131.57 (CH_C), 148.68 (D).}

3.6.2 X-ray monocrystal diffraction

X-ray diffraction intensity data were collected on an Oxford-diffraction Xcalibur S diffractometer. Data were collected with Mo-Kα (λ = 0.71069 Å) radiation. The software package CrysAlys were used to process data.^[28]

Final cell parameters were obtained by global refinement of reflections obtained from integration of all the frames data. The structures were solved by direct methods and refined by the full-matrix method based on F² using the program SHELXTL.^[29] The non-hydrogen atoms of structures were refined anisotropically, the hydrogen atoms were observed in difference electro density maps and refined isotropically or placed in idealized positions and refined as riding atoms. Solvent molecules were modelled as isotropic dichloromethane and finally SQUEEZE^[30] was applied. The crystal parameters and basic information relating data collection and structure refinement for the compounds are summarized in Table 3..

Iodo Tröger's Base derivatives: Towards halogen bonded porous organic crystalline materials

Table 3.3. General and crystallographic parameters for **rac-1·CH₂Cl₂**, **rac-1**, **(5S,11S)-1** and **rac-2**.

Compound	<i>rac-1·CH₂Cl₂</i>	<i>rac-1</i>	(5S,11S)-1	rac-2
Emp. formula	C ₁₆ H ₁₄ Cl ₂ I ₂ N ₂	C ₁₅ H ₁₂ I ₂ N ₂	C ₁₅ H ₁₂ I ₂ N ₂	C ₁₉ H ₁₂ I ₂ N ₂
Formula weight	558.99	474.07	474.07	522.11
Crystal system	Orthorhombic	Monoclinic	Triclinic	Monoclinic
a, Å	17.8602(6)	7.7955(5)	8.3611(2)	11.6765(2)
b, Å	17.9174(6)	36.484(7)	10.3462(2)	22.8696(4)
c, Å	11.0199(4)	10.5534(11)	10.3808(3))	8.36359(15)
α, deg			106.747(3)	
β, deg		105.088(7)	113.735(3)	110.549(2)
γ, deg			103.091(3)	
Volume, Å³	3526.5(2)	2898.0(7)	724.61(3)	2091.28(7)
T, K	293(2)	150(2)	150(2)	100.00(10)
Space group	Iba2	P2(1)/c	P1	P2 ₁ /c
Z	8	8	2	4
μ(X Kα), mm⁻¹	3.867	4.328	4.328	23.615
θ range, deg	3.14 to 24.75	2.61 to 26.38	2.66 to 26.44	3.87 to 74.04
Refl. collected	8976	56522	12928	15502
Uniq reflect/ Rint	2614 / 0.1321	5940 / 0.0427	5374 / 0.0192	4184 / 0.0382
R1/wR2 [I>2σ]	0.0654 / 0.1682	0.0387 / 0.0721	0.0171 / 0.0400	0.0488 / 0.1583
R1/wR2 (all data)	0.0660 / 0.1698	0.0521 / 0.0744	0.0181 / 0.0403	0.0523 / 0.1618
Residual ρ/ e Å⁻³	2.796 / -2.311	1.102 / -1.036	0.374 / -0.976	5.564 / -1.292

3.7 Bibliography

- [1] Z. Wang and Y. Wang, *Macromolecules* **2016**, *49*, 182-191.
- [2] W. Li, Y. Yang, J. K. Weber, G. Zhang and R. Zhou, *ACS Nano* **2016**, *10*, 1829-1835.
- [3] Z. Yang, I. Moriguchi and N. Nakashima, *ACS Appl Mater Interfaces* **2016**, *8*, 9030-9036.
- [4] L. F. Lai, J. A. Love, A. Sharenko, J. E. Coughlin, V. Gupta, S. Tretiak, T.-Q. Nguyen, W.-Y. Wong and G. C. Bazan, *J Am Chem Soc* **2014**, *136*, 5591-5594.
- [5] G. R. Desiraju, *J Am Chem Soc* **2013**, *135*, 9952-9967.
- [6] R. Dawson, A. I. Cooper and D. J. Adams, *Prog. Polym. Sci.* **2012**, *37*, 530-563.
- [7] S. Das, P. Heasman, T. Ben and S. Qiu, *Chem Rev* **2017**, *117*, 1515-1563.
- [8] M. E. Davis, *Chemistry of Materials* **2014**, *26*, 239-245.
- [9] L. Sun, M. G. Campbell and M. Dincă, *Angew. Chem., Int. Ed.* **2016**, *55*, 3566-3579.
- [10] a) X. Du, Y. L. Sun, B. E. Tan, Q. F. Teng, X. J. Yao, C. Y. Su and W. Wang, *Chem. Commun.* **2010**, *46*, 970-972; b) M. Carta, M. Croad, R. Malpass-Evans, J. C. Jansen, P. Bernardo, G. Clarizia, K. Friess, M. Lanc and N. B. McKeown, *Adv. Mat.* **2014**, *26*, 3526-3531; c) M. Carta, R. Malpass-Evans, M. Croad, Y. Rogan, J. C. Jansen, P. Bernardo, F. Bazzarelli and N. B. McKeown, *Science* **2013**, *339*, 303-307; d) A. Del Regno, A. Gonciaruk, L. Leay, M. Carta, M. Croad, R. Malpass-Evans, N. B. McKeown and F. R. Siperstein, *Ind. Eng. Chem. Res.* **2013**, *52*, 16939-16950; e) Z.-Z. Yang, H. Zhang, B. Yu, Y. Zhao, G. Ji and Z. Liu, *Chem. Commun.* **2015**, *51*, 1271-1274.
- [11] a) B. Dolensky, J. Elguero, V. Kral, C. Pardo and M. Valik in *Current Tröger's base chemistry*, Vol. 93 (Ed. A. R. Katritzky), Academic Press, **2007**, pp. 1-56; b) S. Sergeyev, *Helv. Chim. Acta* **2009**, *92*, 415-444; c) O. V. Runarsson, J. Artacho and K. Warnmark, *European J. Org. Chem.* **2012**, 7015-7041.
- [12] a) K. Raatikainen, J. Huuskonen, M. Lahtinen, P. Metrangolo and K. Rissanen, *Chem. Commun.* **2009**, 2160-2162; b) K. Raatikainen and K. Rissanen, *Cryst. Growth Des.* **2010**, *10*, 3638-3646; c) K. Raatikainen and K. Rissanen, *CrystEngComm* **2011**, *13*, 6972-6977; d) K. Raatikainen and K. Rissanen, *Chem. Sci.* **2012**, *3*, 1235-1239.
- [13] C. S. Arribas, O. F. Wendt, A. P. Sundin, C. J. Carling, R. Wang, R. P. Lemieux and K. Warnmark, *Chem Commun* **2010**, *46*, 4381-4383.
- [14] O. Wallach, *Justus Liebigs Annalen der Chemie* **1895**, 286, 90-118.
- [15] a) C. S. Arribas, O. F. Wendt, A. P. Sundin, C. J. Carling, R. Y. Wang, R. P. Lemieux and K. Warnmark, *Chem. Commun.* **2010**, *46*, 4381-4383; b) C. Benkhäuser-Schunk, B. Wezisla, K. Urbahn, U. Kiehne, J. Daniels, G. Schnakenburg, F. Neese and A. Lützen, *ChemPlusChem* **2012**, *77*, 396-403.
- [16] M. Faroughi, K.-X. Zhu, P. Jensen, D. C. Craig and A. C. Try, *Eur. J. Org. Chem.* **2009**, 2009, 4266-4272.
- [17] C. Solano, O. F. Wendt, A. P. Sundin, C. J. Carling, R. Y. Wang, R. P. Lemieux and K. Warnmark, *Chem. Commun.* **2010**, *46*, 4381-4383.
- [18] R. Thaimattam, C. V. K. Sharma, A. Clearfield and G. R. Desiraju, *Cryst. Growth Des.* **2001**, *1*, 103-106.
- [19] a) C. B. Aakeroey, M. Baldridge, J. Desper, P. Metrangolo and G. Resnati, *Chem. Eur. J.* **2013**, *19*, 16240-16247; b) J.-Y. Le Questel, C. Laurence and J. Graton, *CrystEngComm* **2013**, *15*, 3212-3221; c) E. Bosch, *Cryst. Growth Des.* **2014**, *14*, 126.
- [20] W. Wu and H. Jiang, *Acc. Chem. Res.* **2014**, *47*, 2483-2504.
- [21] a) H. M. Yamamoto, J. I. Yamaura and R. Kato, *J. Am. Chem. Soc.* **1998**, *120*, 5905-5913; b) H. M. Yamamoto, R. Maeda, J. I. Yamaura and R. Kato, *J. Mater. Chem.* **2001**, *11*, 1034; c) H. M. Yamamoto, Y. Kosaka, R. Maeda, J. Yamaura, A. Nakao, T. Nakamura and R. Kato, *ACS Nano* **2008**, *2*, 143-155; d) A. Sun, J. W. Lauher and N. S. Goroff, *Science* **2006**, *312*, 1030; e) L. Luo, C. Wilhelm, A. Sun, C. P. Grey, J. W. Lauher and N. S. Goroff, *J. Am. Chem. Soc.* **2008**, *130*, 7702; f) J. Lieffrig, O. Jeannin and M. Fourmigué, *J. Am. Chem. Soc.* **2013**, *135*, 6200; g) C. Perkins, S. Libri, H. Adams and L. Brammer, *CrystEngComm* **2012**, *14*, 3033-3038.

Iodo Tröger's Base derivatives: Towards halogen bonded porous organic crystalline materials

- [22] a) J. Jensen and K. Warnmark, *Synthesis* **2001**, 1873-1877; b) A. Hansson, J. Jensen, O. F. Wendt and K. Wärnmark, *Eur. J. Org. Chem.* **2003**, 3179 - 3188.
- [23] a) J. Jensen, M. Strozyk and K. Warnmark, *Synthesis* **2002**, 2761-2765; b) U. Kiehne and A. Lutzen, *Synthesis* **2004**, 1687-1695.
- [24] A. Bondi, *J. Phys. Chem.* **1964**, 68, 441.
- [25] T. Kitazawa, *Chem. Commun.* **1999**, 891-892.
- [26] S. P. Bew, L. Legentil, V. Scholier and S. V. Sharma, *Chem Commun* **2007**, 389-391.
- [27] A. Gavezzotti and S. Rizzato, *J. Org. Chem.* **2014**, 79, 4809-4816.
- [28] in *CrysAlis Vol.* **2006**.
- [29] G. M. Sheldrick in *SHELXTL*, Vol. Brucker Analytical X-ray Systems, Madison, WI, **1997**.
- [30] A. L. Spek, *Acta Crystallogr., Sect. D: Biol. Crystallogr.* **2009**, 65, 148-155.

Chapter 4 Supramolecular chemistry: Crystal engineering

4.1 Introduction

Crystal engineering mainly uses two strategies that involve the formation of homomeric or heteromeric networks to guide the arrangement adopted by the individual molecules in the solid state. This is the key for material performance in all molecular organic devices.^[1] The first approach requires the acceptor and donor sites to be present in the same molecule, which minimizes interference due to competition between different interactions.^[2] In chapters 2 and 3 we presented the homomeric networks formed by iodoethynyl derivatives. The second strategy consists of the cocrystallization of two or more components that interact by hydrogen bonding, halogen bonding, $\pi\cdots\pi$ stacking or a combination of such interactions. The advantage of this strategy is that it allows new architectures to be obtained in a versatile way using previously described compounds.^[3]

One of the objectives of crystal engineering is to control the dimensionality of the supramolecular architecture, ranging from isolated aggregates (0), chains, ribbons (1D), rosettes (2D) to three-dimensional (3D) crystal motifs. It is possible to construct by cocrystallization architectures of different dimensionalities by increasing the number of donor/acceptor sites and by orienting them in such a way that two or three synthetic vectors remain more or less orthogonal to each other. Different strategies to obtain 2D structures are shown in Figure 4.1.^[4] There is still a lack of 2D or 3D structures and this could be due to the synthetic challenges or problems with crystal growth.

Supramolecular chemistry: Crystal engineering

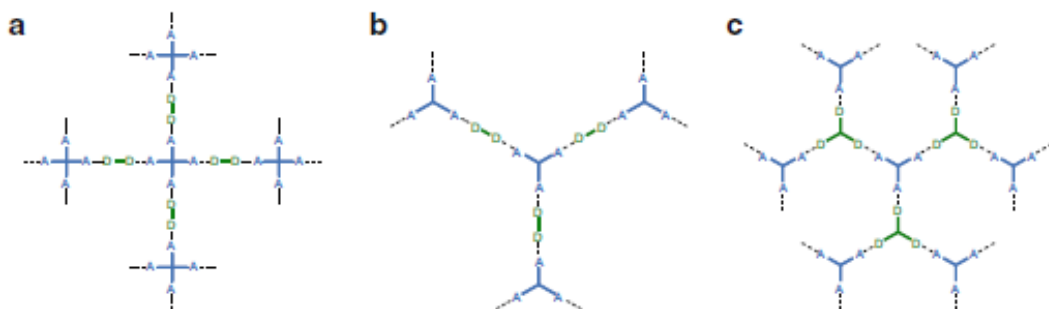


Figure 4.1 Examples of synthetic strategies for the assembly of 2D halogen bonded architectures. (a) Ditopic linear donor + planar fourfold acceptor. (b) Ditopic linear donor + planar threefold acceptor. (c) Planar threefold donor + planar threefold acceptor. Adapted from ref. [4]

One way to overcome such limitations may be to identify hierarchies of intermolecular interactions and then to develop supramolecular synthetic strategies that utilize synthons that can operate side-by-side without interfering with each other. In this context, we have explored the ability of the ditopic, rigid and conjugated halogen bonding donors, presented in Chapter 2, to form two-dimensional structures by combining halogen and hydrogen bonds with different halogen bond acceptors. Our hypothesis is that di(iodoethynyl)benzene derivatives are good ditopic halogen bonding donors, as we have shown in the previous chapters. These will give rise to chains (1D) with ditopic acceptors and, in addition, the electronic distribution of di(iodoethynyl) benzene derivatives will allow them to form edge-to-edge interactions through hydrogen bonds. These characteristics may give rise to two-dimensional structures with coplanar aromatic rings, as shown in Figure 4.2.

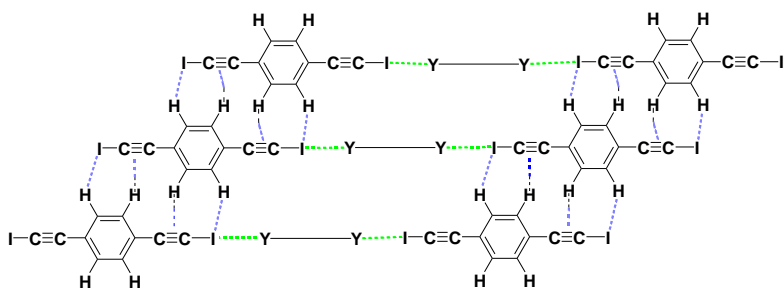


Figure 4.2 Two-dimensional structures with coplanar aromatic rings via hydrogen bonds

For instance, coplanar arrangements and stacking are required to obtain good electronic performance as this promotes effective electronic coupling between the π -systems of individual molecules.^[5] However, highly conjugated small molecules very often adopt herringbone packing motifs due to edge-to-face interactions, such as C–H \cdots π , which in many cases precludes effective electronic coupling between the π -systems of individual molecules.^[5-6] An important goal for the development of organic materials is therefore to overcome this tendency.^[7]

4.2 Objectives and work plan

In order to exemplify this strategy we employed as halogen bond donors 1,4-bis(iodoethynyl)benzene (**pBIEB**), 1,4-bis(bromoethynyl)benzene (**pBBrEB**), and 1,3-bis(iodoethynyl)benzene (**mBIEB**). We have divided this chapter into two sections. The first section concerns the studies with halogen bonding acceptors that contain nitrogen or oxygen atoms (halogen bonding cocrystals, section 4.3) and the second section covers the use of the bromide anion as an acceptor (halogen bonding salts, section 4.4).

4.3 Halogen bonding cocrystals

4.3.1 Previous works

The remarkable directionality of halogen bonding allows the structure and geometry of the resulting supramolecular architectures to be predicted, with a reasonably high degree of accuracy, from the structure and geometry of the self-assembling elements. There are numerous examples in the literature showing that when bidentate halogen bonding donors self-assemble with bidentate halogen bonding acceptors, infinite chains are formed in which the donor and acceptor alternate along the chains. The shape of these infinite chains predictably depends on the structure of the starting compounds. Thus, if donor and acceptor sites are colinear, linear copolymers are obtained (Figure 4.3a), e.g., 1,4-diiodotetrafluorobenzene·4,4'-bipyridine^[8] and 1,4-diiodotetrafluorobenzene·1,4-diazabicyclo(2.2.2)octane cocrystals.^[9] Staggered infinite chains are formed when the binding sites are parallel but not colinear (Figure 4.3b) and, when the binding sites form an angle, the resulting self-assembled chains adopt a zig-zag arrangement (Figure 4.3c).

Supramolecular chemistry: Crystal engineering

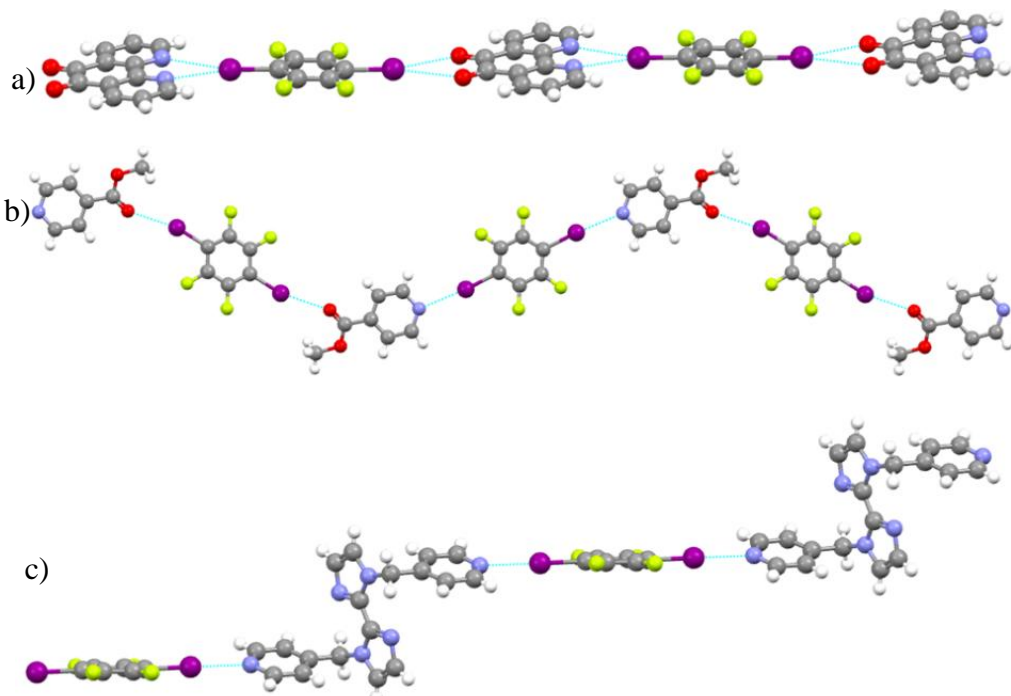


Figure 4.3 1,4-diiodotetrafluorobenzene·4,4'-bipyridine^[8] and 1,4-diido-tetrafluorobenzene·1,4-diazabicyclo(2.2.2)octane cocrystals.^[9] a) Linear copolymers when donor and acceptor sites are colinear. b) Staggered infinite chains are formed when the binding sites are parallel but not colinear

The angles along the chains correspond to the angles of binding site axes. For instance, this is the case when linear 4,4'-bipyridine interacts with *para*, *meta* or *ortho* dihalotetrafluorobenzene (halogen = Br, I), which form angles of 180, 120 and 60°, respectively,^[10] as shown in Figure 4.4.

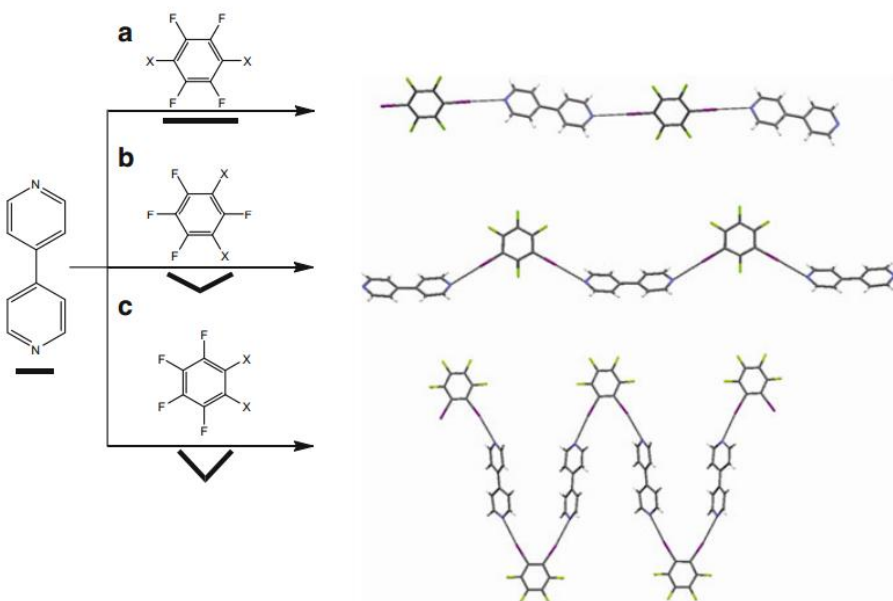


Figure 4.4 1D chain cocrystals of 4,4'-bipyridine with (a) 1,4-diiodotetrafluorobenzene, (b) 1,3-diiodotetrafluorobenzene, and (c) 1,2-diiodotetrafluorobenzene.^[10]

Halogen bonded adducts of 1-idoalkynes with Lewis bases were first reported many decades ago. However, few studies on halogen bonding have been undertaken for diiodoalkyne derivatives with ditopic neutral halogen bonding acceptors. Indeed, most of these materials have been reported by Goroff and co-workers, who described adducts of I-(C≡C)₂-I (8 structures) and I-(C≡C)₃-I (3 structures).^[11] Recently, halogen bonded complexes of bis- and tris(iodoethynyl)benzene derivatives with halogen bond acceptors other than halide anions have been described.^[12]

As mentioned before, one way to increase the dimensionality of supramolecular architectures is through the combination of different interactions. This type of approach has been employed successfully in the construction of ternary cocrystals, where hydrogen bonds of different strengths are responsible for organizing three molecular building blocks in a predictable manner.^[13] A combination of halogen and hydrogen bonds has been used recently for the effective assembly of ternary cocrystals containing desired one-dimensional architectures, as shown in Figure

Supramolecular chemistry: Crystal engineering

4.5.^[14] This result represents a particular synthetic challenge, which succeeded through a combination of hydrogen and halogen bonds supported by geometrical arguments based on the size and shape of molecules.

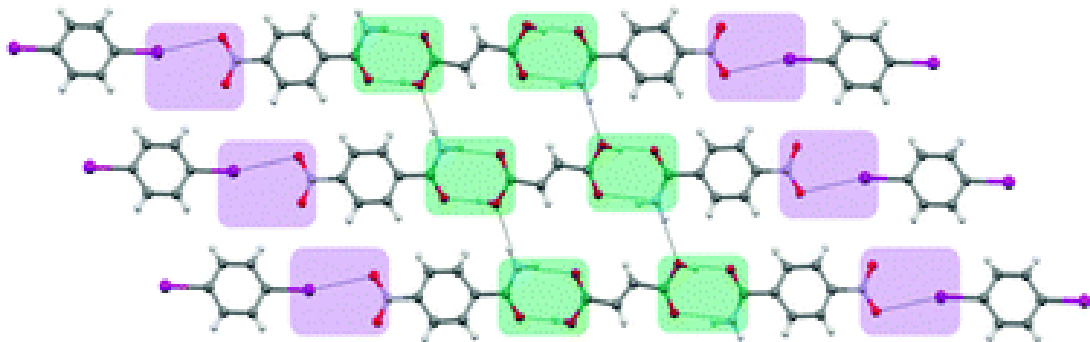


Figure 4.5 Ternary cocrystal of 4-nitrobenzamide : 1,4-diiodobenzene. Hydrogen bonds are highlighted in green and halogen bonds in pink.

This strategy has been successfully employed to promote two-component supramolecular gel formation. Thus, the halogen bond between 1,4-diiodotetrafluorobenzene and the pyridyl substituent on N,N"-butane-1,4-diylbis(3-(3-pyridinyl)urea) together with the hydrogen bonds between the ureas causes gelation, even in polar media such as aqueous methanol and aqueous dimethyl sulfoxide.^[15] The 2D network of halogen bonded adducts of 1,4-diiodotetrafluorobenzene·N,N"-butane-1,4-diylbis(3-(3-pyridinyl)urea) is shown in Figure 4.6.

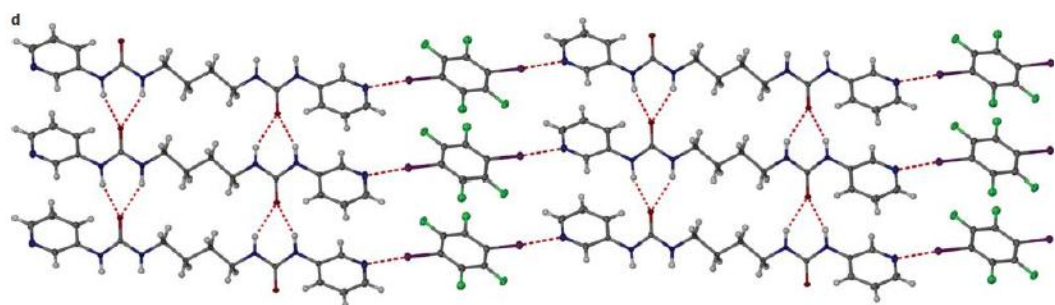


Figure 4.6 X-ray crystal structure of N,N"-butane-1,4-diylbis(3-(3-pyridinyl)urea) showing the urea-tape interaction and the halogen-bonding crosslinks involving the pyridyl groups.

Adapted from ^[15]

In the structures presented so far the halogen bond acceptor also acts as a hydrogen bonding donor and acceptor. In the case of the N-iodosuccinimide·hexamethylenetetramine cocrystal described by Rissanen et al., N-iodosuccinimide acts as a halogen bonding donor and hydrogen bond acceptor, as shown in Figure 4.7. This framework, which is obtained by a combination of halogen and hydrogen bonding, has channels with volumes up to 38.5% [1790 Å³] of the unit cell volume and with different solvent-dependent structural topologies.^[16]

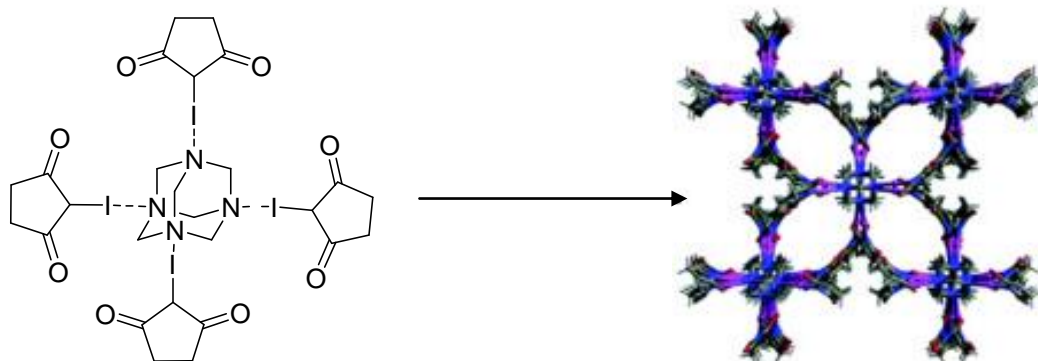


Figure 4.7 Left: molecular structures of the XB acceptor and donor. Right: crystal structures of the [N-iodosuccinimide]4·[hexamethylenetetramine] complexes obtained upon crystallization. Adapted from ref^[16]

In an effort to demonstrate the ability of bis(haloethynyl)benzene derivatives to prevent the formation of herringbone packing and promote the formation of two-dimensional organizations by combining halogen and hydrogen bonds, we cocrystallized ditopic 1,4- and 1,3-bis(haloethynyl)benzene derivatives, XB donors, with ditopic nitrogen bases (Figure 4.7). Having obtained the initial results for the model systems **1–3**, we introduced pyridazine (cocrystal **4**) and propanone (cocrystal **5**) as halogen bond acceptor coformers in order to expand the scope of application of our approach. Very few structures in which the carbonyl group acts as halogen bond acceptor have been reported to date, but the halogen bond has been employed for the molecular recognition of acetone^[17] and to activate carbonyl compounds.^[18] Finally, non-planar halogen bond acceptors

Supramolecular chemistry: Crystal engineering

(hexamethylenetetramine (**HTMA**) and 2,8-dimethyl-6*H*,12*H*-5,11-methanodibenzo[*b,f*][1,5]diazocine (**Tröger's base (TB)**) were used in which the nitrogen atoms have sp^3 hybridization, unlike the acceptors previously used, to study their effect on the supramolecular organization.

In the following sections, the supramolecular organization is interpreted through the analysis of morphological diversity, Hirshfeld surface analysis and DFT calculations in an effort to gain greater insights into the packing and energetic aspects of molecular crystal structures.

4.3.2 X-ray Crystal Structures

As mentioned in the antecedents, bidentate halogen-bonding donors self-assemble with ditopic halogen-bonding acceptors to form infinite chains in which the donor and acceptor alternate along the chains, thus linear building blocks afford linear infinite chains while angular modules afford zig-zag chains.^[8, 11b, 19] This is also the case when employing linear or angular bis(haloethynyl)benzene derivatives with linear or angular halogen bond acceptors, as shown in Figure 4.8.

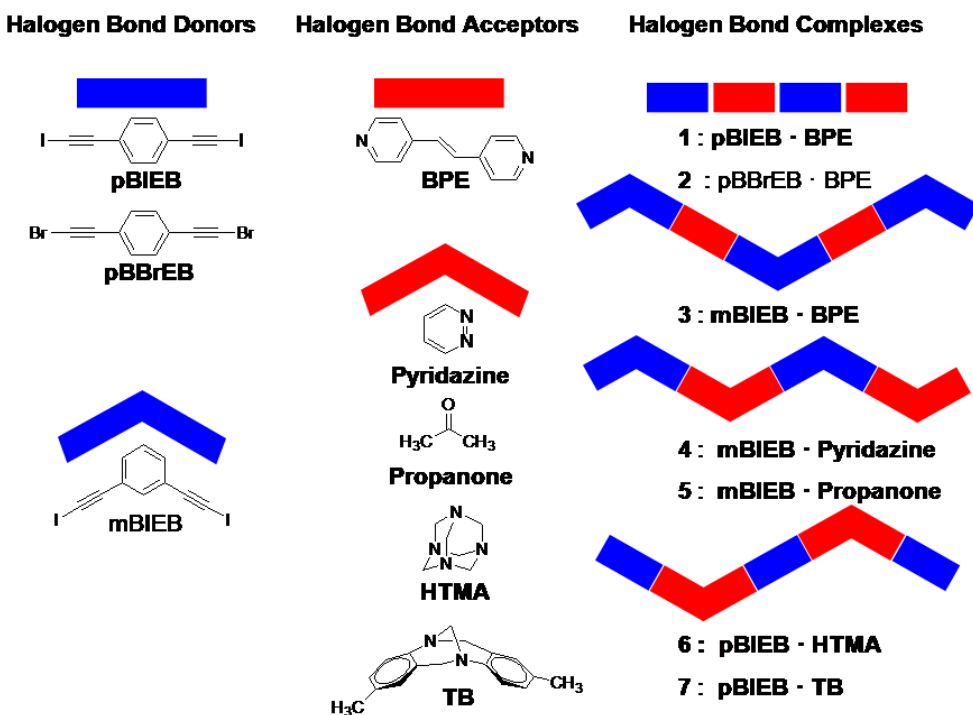


Figure 4.8 Representation of the different cocrystals studied.

In halogen-bonded complexes **1** to **7** all XB donors and acceptors behave as ditopic systems, despite the fact that propanone has only one acceptor atom and HTMA has four. Halogen bond distances, angles and reduction ratios, defined as $rr = d_{X \cdots Y} / R_{vdW}(X) + R_{vdW}(Y)$, in these complexes are gathered in Table 4.1

Table 4.1 Description of halogen bond acceptors

Name	Abbreviated name	Electronic parameter	Geometry	Rigidity
2-bis(4-pyridyl)ethylene	BPE	Conjugated	Linear	Rigid
pyridazine	-	Conjugated	Angular	Rigid
propanone	-	Conjugated	Angular	Rigid
hexamethylenetetramine	HTMA	Non conjugated	Angular	Rigid
2,8-dimethyl-6H,12H-5,11-methanodibenzo[b,f][1,5]diazocine	TB	Conjugated	Angular	Rigid

Supramolecular chemistry: Crystal engineering

BPE has previously been employed by other researchers for halogen bonding in solid state reactions^[20] and also to try to understand the halogen/hydrogen bond collaboration^[21] in relation to the (E)-1,2-bis(4-pyridyl)ethylene1,4-diiodotetrafluorobenzene complex ($bpeC_6\text{-}F_4I_2$)^[22] and the (E)-1,2-bis(4-pyridyl)ethylene1,4-dibromotetrafluorobenzene ($bpeC_6F_4I_2$). HTMA was also studied in the same way as reported for NIS.

Furthermore, the shape of the molecules selected is an important tool to obtain 3D supramolecular arrangements. This aspect will be discussed in this section and all of the halogen bond donor/acceptors and complexes are represented in Figure 4.8.

In terms of the present study, complexes **1–7** are deemed to produce 2D and 3D architectures by a combination of strong halogen bonds and weak hydrogen-bonded synthons displaying interesting topologies. Iodoethynylbenzenes exhibit a lateral complimentarity through weak $C_{sp^2}\text{-H}\cdots\pi_{alk}$ and $C_{sp^2}\text{-H}\cdots I$ hydrogen bonds due to their electron density distribution. Weak noncovalent forces such as $C_{sp^2}\text{-H}\cdots X$ ($X = \text{Hal, O, N}$) and $\pi\cdots\pi$ stacking ($C\text{-H}\cdots\pi$)^[23] ^[24] ^[25] with energies in the range 2–20 kJ mol⁻¹ have attracted attention in view of the stabilization and directionality that they impart on the final morphology, thus making their prediction and manipulation one of the most ambitious endeavors in modern crystal engineering and the design of solids with specific properties (Figure 4.9).

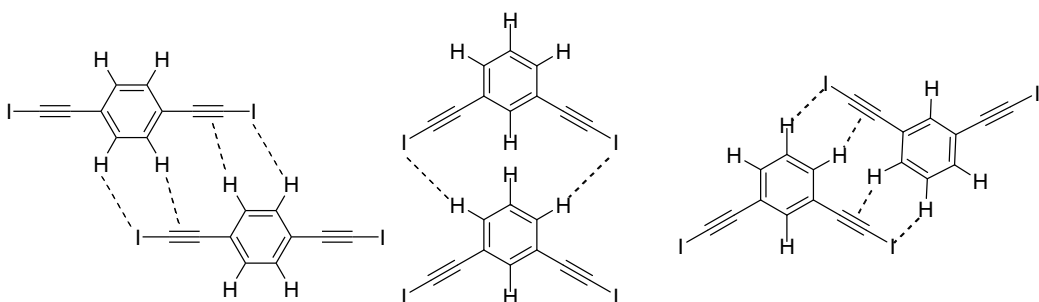


Figure 4.9 Representation of weak hydrogen bonds.

We attempted to exemplify our hypothesis by systematically investigating the different intermolecular contacts in the arrays beyond the sum of the van der Waals radii, since it has been noted that the sum of van der Waals radii as a cut-off parameter to assess and evaluate weak $C_{sp^2}-H\cdots X$ hydrogen bonds is not recommended and should not be taken into account.^[26]

The crystal structures of the seven halogen bonded complexes have $C_{sp^2}-X\cdots Y$ ($X = I, Br; Y = N, O$) distances shorter than the sum of the van der Waals radii and six of them have edge-to-edge $C-H\cdots X$ ($X = I, Br$) supramolecular hydrogen bond synthons. The stabilization energy of hydrogen bond synthons is in the range 2.9 to 5.7 kcal mol⁻¹, as determined by DFT calculations. The halogen bond distances, angles and reduction ratios, defined as $rr = d_{X\cdots Y} / R_{vdW}(X) + R_{vdW}(Y)$, in these complexes are gathered in Table 4.2.

Table 4.2 Distances and angles between $C_{sp^2}-X$ ($X = Br, I$) and halogen bond acceptors A ($A = N, O$).

Compound	$C-X\cdots Y$	Sym. equivalence	$d(C-X)\text{\AA}$	$d(I\cdots Y)\text{\AA}$	$\angle(CXY)^\circ$	rr
1	$C_{sp^2}-I(1)\cdots N(1)$	-1+x, y, -1+z	2.035(3)	2.729(3)	178.4	0.77
2	$C_{sp^2}-Br(1)\cdots N(1)$	x, y, z	1.810(2)	2.747(2)	178.54	0.81
3	$C_{sp^2}-I(1)\cdots N(1)$	1/2-x, -1/2-y, 1-z	2.024(2)	2.722(2)	177.48	0.77
4	$C_{sp^2}-I(1)\cdots N(1)$	1-x, 1/2+y, 1-z	2.27(3)	2.785(2)	172.9	0.79
5	$C_{sp^2}-I(1)\cdots O(1)$	2-x, 1/2+y, 2-z	2.011(4)	2.929	177.9	0.84
6	$C_{sp^2}-I(1)\cdots N(1)$	-1/2+x, -1/2+y, z	2.026	2.853	169.2	0.81
7	$C_{sp^2}-I(1)\cdots N(2)$	2-x, 1-y, 1-z	2.027(5)	2.841(4)	168.8	0.80
	$C_{sp^2}-I(2)\cdots N(1)$	1/2-x, -1/2+y, 1/2-z	2.019(5)	2.815(4)	175.0	0.80

As can be seen from the results in Table 4.2, the halogen bond distances are as follows: $C-Br\cdots N$, 2.747 Å, $C-I\cdots O$ 2.929 Å and $C-I\cdots N$ ranging from 2.722 to 2.853 Å. All of these distances are shorter than the sum of the van der Waals radii and correspond to a reduction ratio ranging from 0.77 to 0.84. The $C_{sp^2}-X\cdots Y$ ($X =$

I, Br; Y = N, O) angles are in all cases almost linear, with values ranging from 168.8 to 178.5°.

The cocrystals **1** to **3** are formed by the same XB acceptor (**BPE**). Cocrystals **1** and **2** were prepared with two different linear halogen donors, namely an iodo-derivative (**pBIEB**) in **1** and a bromo-derivative (**pBBrEB**) in **2**. The halogen donors in cocrystals **1** and **3** are both iodo-derivatives but with different geometries, i.e., linear for **pBIEB** (**1**) and angular for **mBIEB** (**3**). Comparison of the halogen bonding in **1** (C_{sp} –I···N), **2** (C_{sp} –Br···N) and **3** (C_{sp} –I···N) shows the same reduction ratio (0.77) in the case of linear (**pBIEB**, **1**) and angular (**mBIEB**, **3**) iodo-based XB donors and a higher ratio in **2** (0.81), where the halogen atom is bromine (**pBBrEB**). This latter finding is consistent with halogen bonding reduction ratios described previously for 1,4-diiodotetrafluorobenzene·BPE (0.78)^[27] and 1,4-dibromotetrafluorobenzene·BPE (0.84) cocrystals^[28] and also with the V(r) maximum positive value calculated for the iodo-substituent (172.4 kJ mol⁻¹) in 1-idoethynyl-4-iodobenzene and the less polarizable bromo-substituent (147.1 kJ mol⁻¹) in 1-bromoethynyl-4-iodobenzene.^[29] Furthermore, comparison of the halogen bond distances in the aforementioned BPE cocrystals with the iodo-XB donors **pBIEB** and 1,4-diiodotetrafluorobenzene^[27] shows that in both cases the distances are similar, with values of 2.729 and 2.768 Å, respectively. However, in the case of bromo-XB donors, the halogen bonding distance is significantly shorter in cocrystal **2**, which contains **pBBrEB** as the coformer (2.747 Å), than in the 1,4-dibromotetrafluorobenzene·BPE (2.814 Å) cocrystal. As a consequence, the bromo-substituent is more strongly affected by a triple bond unit than it is by the proximity of a perfluorinated benzene ring, thus making the bromoethynyl moiety a useful XB donor in crystal engineering.^[29-30]

Cocrystals **4** and **5** are formed with the angular **mBIEB** iodo-donor and two angular ditopic XB acceptors, namely pyridazine and propanone (with sp^2 hybridized nitrogen and oxygen, respectively). The halogen bond distance in **4**

shows a reduction ratio of 0.79, which is slightly higher than those observed in **1** and **3** – a finding that could be attributed to the low acceptor ability of the pyridazine due to the effect of the neighboring nitrogen. Cocrystal **5** has a longer halogen bond distance (C_{sp} –I \cdots O) (2.929 Å) with a reduction ratio of 0.84. This distance is slightly longer than those previously described for the C_{sp} –I \cdots O sp^2 2.877 Å interaction in the 1-[4-(iodoethynyl)phenyl]ethanone structure.^[31] This fact may be due to oxygen forming a bifurcated halogen bond in an analogous way to that described for 4,4'-bis(dimethylamino)benzophenone and dimethylformamide in halogen-bonding cocrystal structures with 1,4-diido-2,3,5,6-tetrafluorobenzene^[32] and diidoacetylene,^[33] respectively.

Finally, cocrystals **6** and **7** allowed us to analyze the influence that the nitrogen atom hybridization has on the XB distance. The halogen bond distances (C_{sp} –I \cdots N) in these structures, in which the nitrogen atom has sp^3 hybridization, are 2.853 Å (**6**) and 2.841 Å (**7**), respectively. Comparison of these distances with those in compounds **1** (2.729 Å), **3** (2.722 Å) and **4** (2.785 Å) – in which the hybridization is sp^2 – and with the distance in the previously described **pBIEB**·*p*-decyloxybenzonitrile structure^[34] (2.946 Å) and 4-(iodoethynyl)benzonitrile structure^[31] (2.962 Å), with sp hybridization, shows an increasing trend in this parameter from sp^2 to sp^3 to sp . This change may be due to steric effects, considering that in the states of higher hybridization the local environment of electronegative atoms is generally tighter, so the halogen atom is less accessible.

4.3.3 Halogen bonded complexes **1** and **2**: Linear XB donor and acceptor

The halogen bond acceptor used for the two structures described in this section is the same, namely 1,2-bis(4-pyridyl)ethylene (**BPE**). **BPE** forms isostructural 1:1 complexes with 1,4-bis(iodoethynyl)benzene (**pBIEB**) and 4-bis(bromoethynyl)benzene (**pBBrEB**), with the two complexes crystallizing in the triclinic P-1 space group. The asymmetric unit consists of half a molecule of **pBIEB** or **pBBrEB** and a **BPE** half molecule situated at an inversion center. Combination of the linear ditopic halogen bond donor (**pBIEB** or **pBBrEB**) and acceptor results in parallel linear assemblies propagated by $C_{sp}-\text{Hal}\cdots N$ ($X = I, \text{Br}$) halogen bonds (see Figure 4.10). The two aromatic rings of **BPE** are almost coplanar and the planes that contain **BPE** and **pBXB** ($X = I$ or Br) are tilted with respect to one another by 26.2° and 31.9° in **1** and **2**, respectively. Similar chains have been described in structures with BPE and ditopic halogen bonding donors such as 1,4-diiodotetrafluorobenzene^[35] and 1,4-dibromotetrafluorobenzene.^[36]

These chains in **1** and **2** are joined by weak $C_{sp}-\text{H}\cdots X$ ($X = I, \text{Br}$) and $C_{sp^2}-\text{H}\cdots\pi_{(\text{alkyne})}$ hydrogen bonds (Table 4.3) and this results in planes as shown in Figure 4.10, which stack donor over donor and acceptor over acceptor. This finding proves the validity of our approach to achieve two-dimensional organizations by edge-to-edge interactions between haloethynylbenzene derivatives.

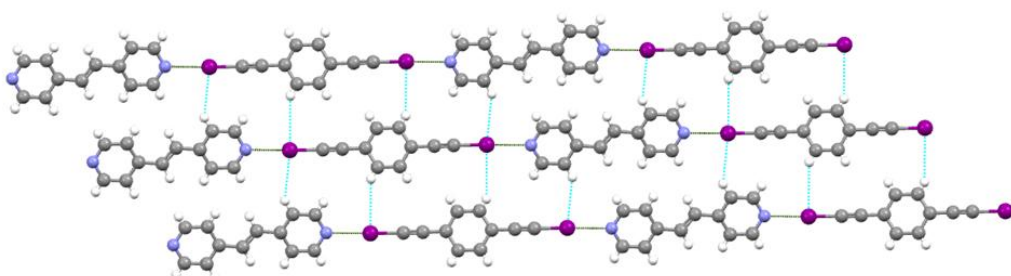


Figure 4.10 Layers in structure **1** formed by a combination of halogen bonds (green) and hydrogen bonds (blue)

Table 4.3 Hydrogen bond distances and angles in structures 1 and 2.

Compound	D–H…A	Sym. equivalence	d(D–H) Å	d(H…A) Å	d(D…A) Å	\angle (DHA) °
1	C_{sp^2} –H…I(1)	1+x, y, z	0.83	3.33	4.083	151
	C_{sp^2} –H… $\pi_{(alkyne)}$	-x, -y, 1-z	0.88	3.35	4.076	142
2	C_{sp^2} –H…I(1)	-x, -y, 1-z	0.92	3.44	4.171	138
	C_{sp^2} –H…Br(1)	-1+x, y, z	0.81	3.18	3.892	147
	C_{sp^2} –H… $\pi_{(alkyne)}$	-x, 2-y, -z	0.81	3.20	3.910	135

The hydrogen bonds described here help to stabilize the structures, with a short distance in the structure of **2** but, conversely, a long packing distance. This can be explained by the fact that the iodine atom is larger than bromine and this leads to a longer hydrogen bond distance.

4.3.4 Angular polymers

It is possible to obtain angular polymers if one or both coformers from the cocrystals are angular. In the following sections angular polymers obtained with different combinations of the geometries of halogen bond donor and acceptor will be described. The discussion begins with cocrystals formed by an angular donor and linear acceptor (**3**), followed by systems with an angular donor and acceptor (**4** and **5**) and finally those formed by a linear donor and angular acceptor (**6** and **7**).

4.3.4.1 Angular Structures 3: halogen bond angular donor and linear acceptor

The angular ditopic halogen bonding acceptor **mBIEB** forms 1:1 complexes with the linear ditopic halogen acceptor 1,2-bis(4-pyridyl)ethylene (**BPE**) (**3**). This complex crystallizes in the monoclinic C2/c space group and the asymmetric unit consists of a **BPE** half molecule on an inversion center and an **mBIEB** half molecule on a twofold axis.

Supramolecular chemistry: Crystal engineering

A displaced halogen bonding zig-zag polymer along the *b* axis in **3** is joined by weak $C_{sp^2}-H \cdots I-C_{sp}$ hydrogen bonds between the XB donors (Table 4.4), thus resulting in planes as shown in Figure 4.11a. The coplanar arrangement of **mBIEB** molecules in **3** leads to the proximity of the hydrogen atoms of the aromatic rings, which in turn leads to a very weak $C_{sp^2}-H \cdots I-C_{sp}$ hydrogen bond between the **mBIEB** molecules (3.88 \AA , 166°). Finally, the planes are stacked (3.2 \AA) and displaced by 8.6 \AA with respect to one another (Figure 4.11 b).

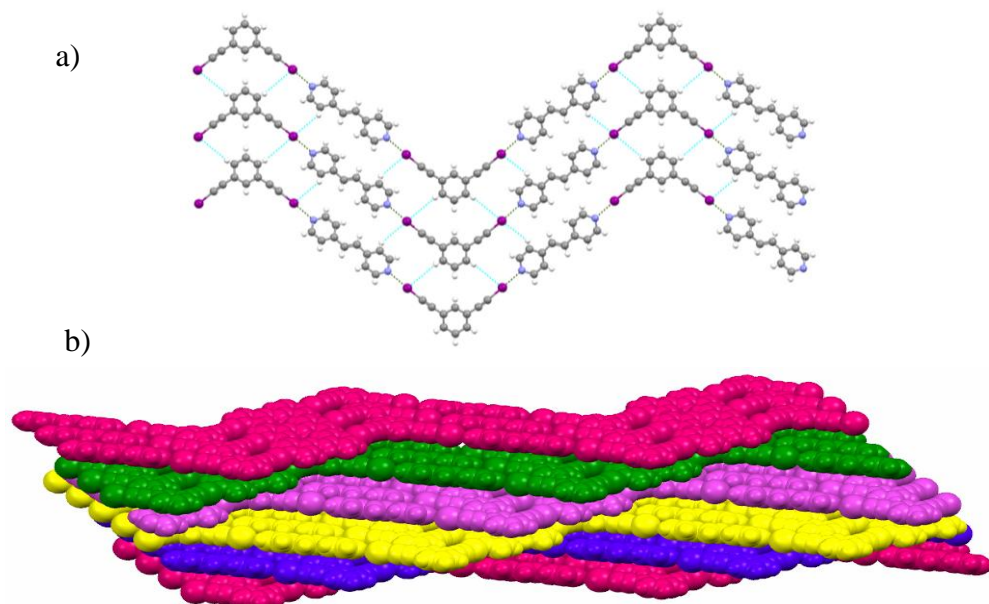


Figure 4.11 (a) Layers in structure **3** built by a combination of halogen bonds (green) and hydrogen bonds (blue); (b) displaced stacking planes

Table 4.4 Hydrogen bond distances and angles in **3**

Compound	D–H \cdots A	Sym. equivalence	d(D–H) \AA	d(H \cdots A) \AA	d(D \cdots A) \AA	$\angle(DHA)^\circ$
3	$C_{sp^2}-H(5) \cdots I(1)$	x, 1+y, z	0.87	3.88	4.731	166
	$C_{sp^2}-H(11) \cdots I(1)$	x, y, z	0.84	3.42	4.120	143

4.3.4.2 Angular Structures 4, 5: Angular halogen bond donor and acceptor.

Angular **mBIEB** forms 1:1 XB complexes with pyridazine and propanone and these crystallize in the orthorhombic Pnma space group (**4**) and in the monoclinic P2₁/n space group (**5**), respectively. The two asymmetric units consist of a half molecule of **mBIEB** and half a molecule of the acceptor, i.e., pyrazine or propanone.

The crystal structures **4** and **5** comprise zig-zag chains in which pyridazine (Figure 4.12a) and propanone act as ditopic halogen bond acceptors, in an analogous way to that described for 4,4'-bis(dimethylamino)benzophenone and dimethylformamide in halogen bonding cocrystal structures with 1,4-diiodo-2,3,5,6-tetrafluorobenzene^[32] and di-iodoacetylene,^[33] respectively.

The halogen-bonded chains in **4** are dimerized by $\pi\cdots\pi$ stacking between pyridazine and **mBIEB** rings that are tilted at an angle of 4.0°. The shortest distance between rings is 3.38 Å and between centroids it is 3.50 Å. The parallel dimerized chains are aligned along the *c* axis but these are shifted by 2.23 Å from one another, which prevents $\pi\cdots\pi$ interactions. These alignments are arranged in a parallel fashion as shown in Figure 4.12 b and this organization is criss-crossed with a similar one at an angle of 53.3° to give rise to a 3D supramolecular network (Figure 4.13 c). The structure is stabilized by a supramolecular synthon similar to that described for structure **3** but this is not coplanar (Figure 4.12 d). This arrangement allows a closer tie between the **mBIEB** molecules and, consequently, the C_{sp}2—H···I (3.79 Å, 133°) hydrogen bond is shorter than that in **3**. The hydrogen bond distances and angles in **4** and **5** are gathered in Table 4.5.

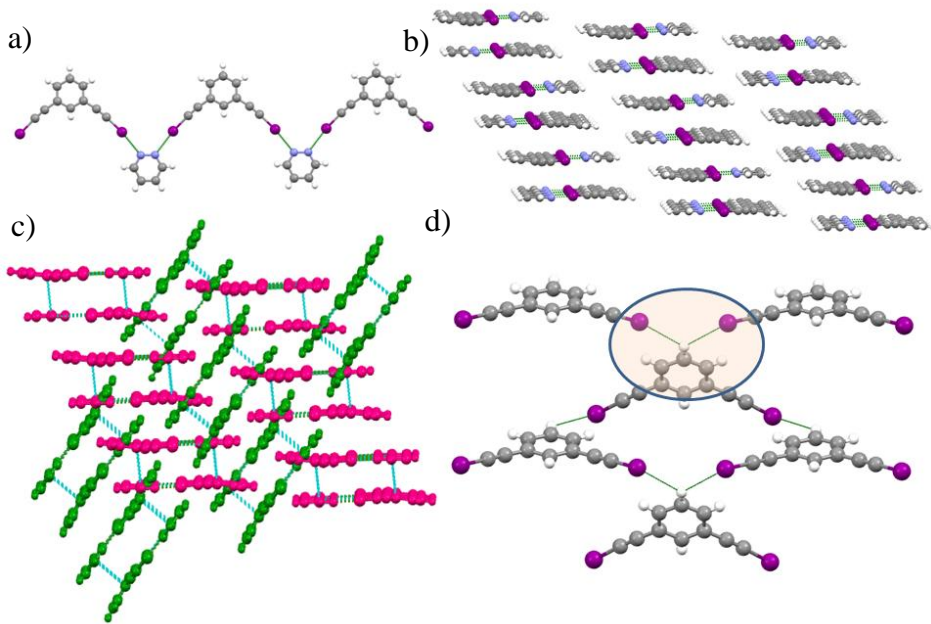


Figure 4.12 a) XB Chains; b) parallel alignments of dimerized halogen bonded chains; c) criss-cross packing diagram with halogen bonds in green and $\pi\cdots\pi$ interactions in blue; d) detail of the C–H \cdots I supramolecular synthon in 4.

Table 4.5. Hydrogen bond distances and angles in 4 and 5.

Compound	D–H \cdots A	Sym. equivalence	d(D–H) \AA	d(H \cdots A) \AA	d(D \cdots A) \AA	\angle (DHA) $^\circ$
4	$\text{C}_{\text{sp}2}\text{--H}\cdots\pi_{(\text{alkyne})}$	-1/2+x, 1/2-y,	0.92	2.903	3.83	177.5
	$\text{C}_{\text{sp}2}\text{--H}\cdots\text{I}(1)^{\text{(a)}}$	1/2-x, 1-y,	0.97	3.28	4.00	133
	$\text{C}_{\text{sp}2}\text{--H}\cdots\text{I}(1)$	-1/2+x, y,	0.98	3.79	4.512	133
5	$\text{C}_{\text{sp}2}\text{--H}\cdots\text{I}(1)^{\text{(a)}}$	1-x, 1-y, 1-z	0.88	3.51	4.247	142
	$\text{C}_{\text{sp}2}\text{--H}\cdots\pi_{(\text{alkyne})}$	1-x, 1-y, 1-z	0.96	3.022	3.949	162.3

(a) bifurcated

In the structure of **5** halogen bonded strands related by an inversion center give rise to ribbons through $\text{C}_{\text{sp}2}\text{--H}\cdots\text{I--C}$ (3.51 \AA , 142°) and $\text{C}_{\text{sp}2}\text{--H}\cdots\pi_{\text{alk}}$ (3.02 \AA , 162°) hydrogen bonds between the *m*-BIB molecule, as shown in Figure 4.13 and Table 4.5. A similar supramolecular synthon is present, although it was not described, in the structure of the 1,2-bis(iodoethynyl)benzene·4-(N,N-dimethylamino)pyridine

cocrystal^[37] and this shows that the halogen bond acceptors with oxygen atoms are also suitable for the formation of bidimensional arrangements through edge-to-edge interactions. Finally, ribbons are arranged in 2D arrays that stack along the *a* axis. These arrays are shifted by 2.1 Å from one another and this limits $\pi\cdots\pi$ stacking.

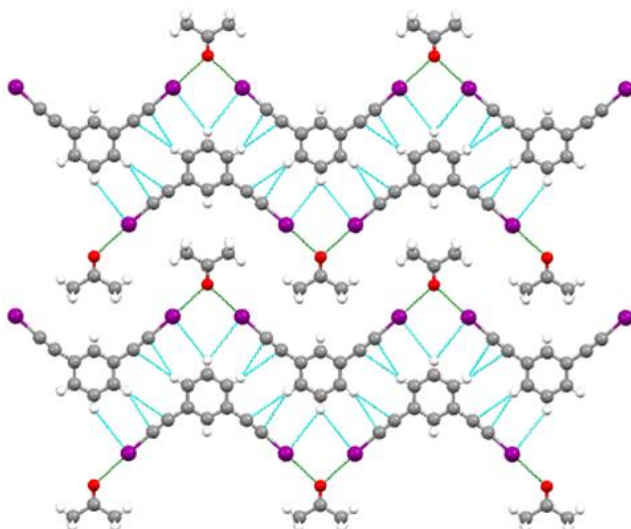


Figure 4.13 2D arrangement in **5**, stabilized by halogen bonds (in green) and hydrogen bonds (in blue).

4.3.4.3 Angular Structures **6**, **7**: Linear halogen bond donor and angular acceptor

The angular halogen-bond acceptors crystallized with **pBIEB** include hexamethylenetetramine (**HTMA**), which behaves as a ditopic system although it has four acceptor groups, and racemic 2,8-dimethyl-6*H*,12*H*-5,11-methanodibenzo[*b,f*]-[1,5]diazocene, Tröger's base (**TB**). In contrast to the halogen-bond acceptors described in previous sections, both **HTMA** and **TB** are not planar and their nitrogen atoms have sp^3 hybridization. **HTMA** and Tröger's base form 1:1 complexes with **pBIEB** and these crystallize in the orthorhombic Cmcm and the monoclinic P2₁/n space groups, respectively. The asymmetric unit of **6** consists

Supramolecular chemistry: Crystal engineering

of a half molecule of **HMTA** and **pBIEB** and that of **7** consists of a **TB** and a **pBIEB** molecule.

The size and geometry of **TB** and **HMTA** determine the dimensional characteristics of halogen bonding zig-zag polymers. Accordingly, the distances between two adjacent iodine atoms are 6.06 Å and 6.46 Å, between two nitrogen atoms 21.47 Å and 25.42 Å and the angles formed by the planes containing two contiguous *p*-BIB are 59° and 74° in **6** and **7**, respectively.

The halogen bond donors **pBIEB** in **6** are arranged in a herringbone-type fashion (along the *c* axis) separated by layers of **HMTA** molecules. These layers are related by $\text{C}_{\text{sp}^3}\text{-H}\cdots\text{N}(2)$ hydrogen bonds (3.690 Å, 162°) (Figure 4.14). In addition, **pBIEB** molecules interact edge-to-edge to form the supramolecular synthon, highlighted in Figure 4.14, as described for structure **1**. The hydrogen bond distances and angles for structures **6** and **7** are gathered in Table 4.6.

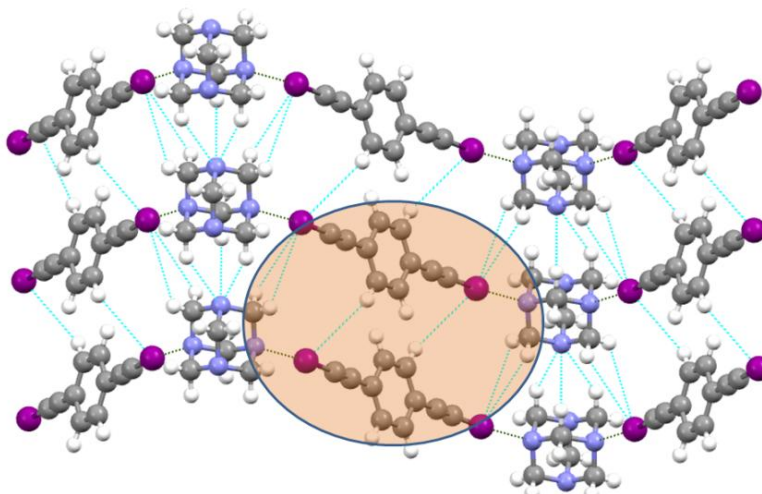


Figure 4.14 Packing diagram of *p*BIEBHMTA (**6**) complex by combining halogen bonds (green) and hydrogen bonds (blue).

Table 4.6. Hydrogen bonds in structures **6** and **7**.

Compound	D–H…A	Sym. equivalence	d(D–H) Å	d(H…A) Å	d(D…A) Å	\angle (DHA) °
6	C_{sp^2} –H…I(1)	1/2+x, 1/2+y, z	1.00	3.45	4.352	151
	C_{sp^2} –H…N(2)	1.5-x, 1/2+y, 1.07 1/2-z		3.04	3.968	146
	C_{sp^2} –H…N(2)	1.5-x, 1/2+y, 1/2-z	1.08	2.64	3.69	162
7	C_{sp^2} –H…I(1)	1+x, y, z	1.07	3.48	3.911	111
	C_{sp^2} –H… π (alkyne)	x, y, z	0.970	2.730	3.668	162.6
	C_{sp^2} –H… π (arene)	1-x, 1-y, 1-z	0.970	2.780	3.747	174.9
	C_{sp^2} –H… π (arene)	x, y, z	0.97(6)	2.699	3.665	171.9
	C_{sp^2} –H…I(1)	-1+x, y, -1+z	0.970	3.405	4.230	142.2
	C_{sp^2} –H…I(1)	-1+x, y, z	0.961	3.123	3.964	147.1
	C_{sp^2} –H…I(2)	1/2+x, 1/2-y, 1/2+z	0.930	3.351	4.124	142.0

TB core 1,5-diazabicyclo[1.3.3]nonane and the two attached aryl groups produce a rigid V-shaped molecule with a cleft angle of *ca.* 99° and an inherent chiral C₂-symmetry. The high framework stability, along with the relative ease of preparation and derivatization, offers an attractive starting point for a variety of functional materials.^{[36, 38] [39]} Despite this potential, only two **TB** cocrystal structures have been described to date and these were based on (–)-dibenzoyl-L-tartaric acid^[40] and **TB**.^[41]

In the structure of **7** the strength and directionality of XB translates the exo-face to exo-face **TB** dimers (Figure 4.15 (a)) stabilized by weak C_{sp^3} –H… π (arene) hydrogen bonds (2.78 Å and 175°) into 2D layers. These layers are built by rhombic units with a side length of 14 Å (Figure 4.15 (b)).

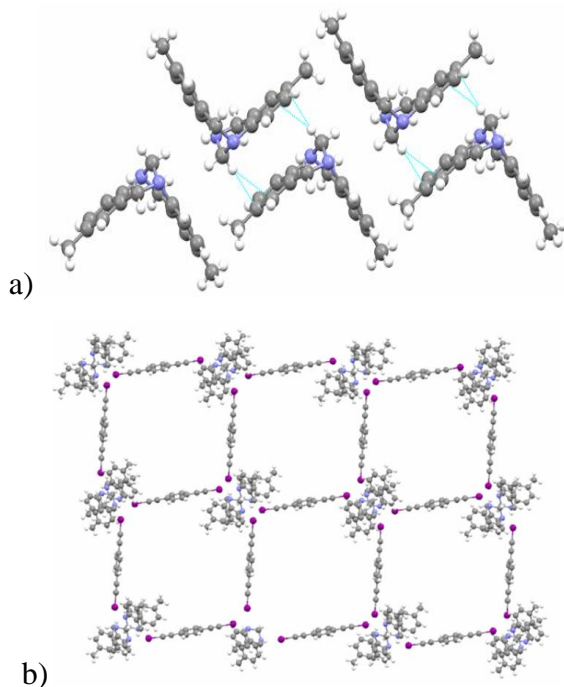


Figure 4.15 (a) Exo-face to exo-face TB dimers; (b) 2D rhombic layers with a (4,4) topology in complex 4.

Thus, the sheets have large cavities that allow the formation of an entangled system by interpenetration of three other rhombic frameworks, as shown in Figure 4.16. The overall lattice is stabilized by weak **TB** $\text{C}_{\text{sp}^3}\text{--H}\cdots\pi_{(\text{alkyne})}$ (2.73 Å and 162°) and **pBIEB** $\text{C}_{\text{sp}^2}\text{--H}\cdots\pi_{(\text{alkyne})}$ (2.89 Å and 155°) hydrogen bonds.

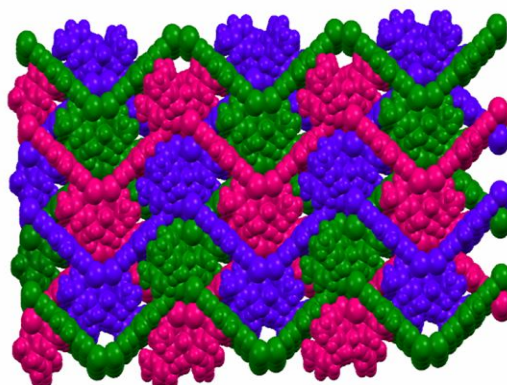


Figure 4.16 3-fold interpenetrated network of 7.

4.3.5 Hirshfeld Surface Analysis

The intermolecular contacts in the crystal structures of **1** to **7** were analyzed by Hirshfeld surface studies using the CrystalExplorer program.^[42] The sizes and shapes of the Hirshfeld surfaces reflect the intermolecular contacts between atoms in a crystal and, in addition, they may encode different properties in a three-dimensional picture, such as shape index or curvedness. This information can be summarized in a bidimensional fingerprint (d_i , d_e) graph.^[43]

As expected from the different environments of each crystallographically independent halogen bonding donor **pBIEB**, **pBBrEB** or **mBIEB** in structures **1** to **7**, the Hirshfeld surfaces and fingerprint plots are different. The main features of the fingerprint plots are related to stronger interactions. Consequently, $C_{sp}-X \cdots N$ ($X = I, Br$) halogen bonding appears as spikes denoted with the letter *a* in Figure 4.17(a) and (b) and $C_{sp}-I \cdots O$ spikes are denoted with the letter *b* in Figure 4.17(c). The presence of $C_{sp^2}-H \cdots X$ ($X = Br, I$) and $C_{sp^2}-H \cdots \pi_{(alkyne)}$ hydrogen bonds, which are characteristic of edge-to-edge supramolecular synthons that join halogen bond donors – as described in the crystal structures, is evidenced by the presence of peaks *c* and *d*, respectively. However, the presence of these peaks may be due to interactions between the halogen bond donor and acceptor, as in **4**. The fingerprint plot of **3** shows characteristic peak *e* (Figure 4.17a) due to the close proximity of two hydrogen atoms, which occurs when the supramolecular synthon shown in Figure 4.11(a) is formed.

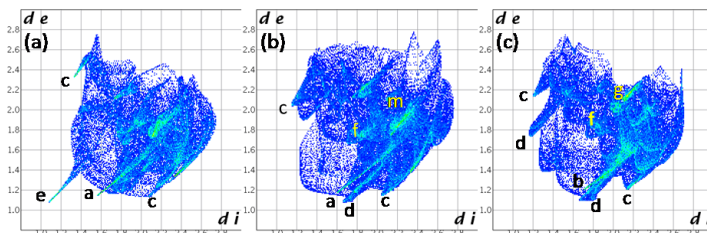


Figure 4.17 Fingerprint plots of halogen bonding donors in structures (a) **3**, (b) **4** and (c) **5**.

One of the objectives when studying the formation of planar arrangements by edge-to-edge interactions is to promote the overlap of π -orbitals. On the Hirshfeld surface $\pi \cdots \pi$ interactions are manifested as a large flat region across the molecule, which is most clearly visible on the ‘curvedness surfaces’ (Figure 4.18(a)), as a pattern of red and blue triangles on the same region of the shape index surface (Figure 4.18(b)) and in fingerprint plots they appear as clear areas in the vicinity of $(d_i, d_e) \approx 1.8\text{--}2.0 \text{ \AA}$, denoted by letter *f* in Figure 4.17.

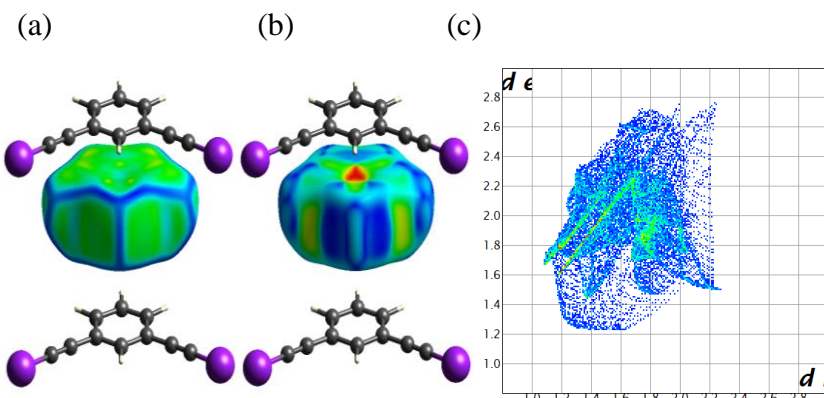


Figure 4.18. Curvedness (a), shape index (b) surfaces and (c) fingerprint plot of the pyridazine in 6 showing the $\pi \cdots \pi$ interaction between halogen bond donors and acceptors.

In the fingerprint graphics of the halogen bond donors an area around $(d_i, d_e) \approx 1.8\text{--}2.0 \text{ \AA}$ cannot be clearly observed. However, in the fingerprint graphics of flat halogen bond acceptors (BPE and pyridazine) this feature is more obvious (Figure 4.18(c)).

4.3.6 DFT Calculations.

The energetic features of $\text{C}_{\text{sp}^2}\text{--H} \cdots \text{Hal}$ and $\text{C}_{\text{sp}^2}\text{--H} \cdots \pi_{\text{alk}}$ non-covalent binding between the halogen bond donors in the assembly of supramolecular architectures **1** to **7** were studied by DFT calculations on fragments extracted from crystal structures.

Single point energy calculations for these complexes were performed using the B3LYP-D3 method combined with the DGDZVP basis set for iodine and the 6-311++G(d,p) for the other atoms. The uncorrected (ΔE) and corrected for BSSE (ΔE_{BSSE}) interaction energies of dimers are listed in Table 4.7. When the BSSE is not taken into account the interaction energies show a marked energy overestimation (about 13%), except for **2-D**. Even so, the interaction energies of the complex gave sufficiently negative values to indicate that these assemblies formed by non-covalent bonding are favorable. In most cases, the fragments comprise various nearly identical interactions related by symmetry elements in the crystal packing. These interactions cannot be separated when drawing fragments or ring patterns; hence, the energy values indicate the energy associated with the interplay of different interactions that cannot be calculated separately.

The interaction energies of supramolecular synthons between linear halogen bond donors, as depicted in Figure 4.19, are similar in all cases at around 5 kcal mol⁻¹ (Table 4.7), although differences are observed in the distances and the relative positions, with the halogen bond donors either coplanar or staggered (Figure 4.19).

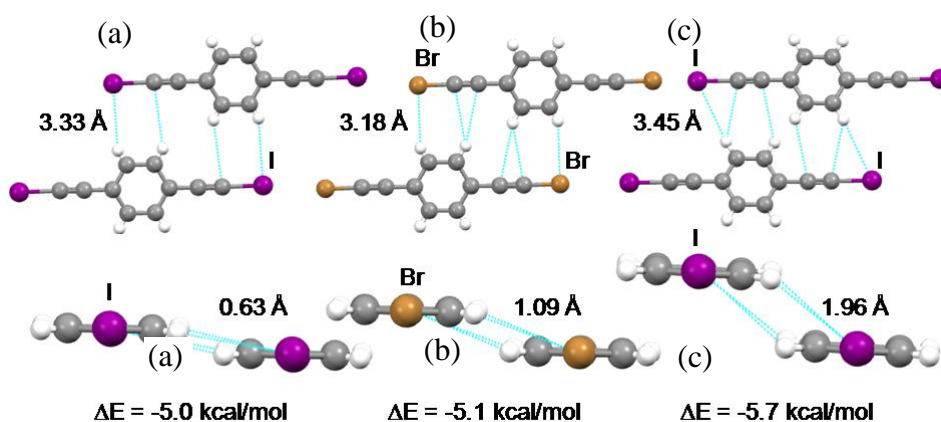


Figure 4.19 Hydrogen bond synthons and stabilization energies for p-BIB in structures **1** (1-D) (a) and **6** (6-D) (c) and p-BBrB in **2** (2-D) (b).

Supramolecular chemistry: Crystal engineering

Table 4.7 Uncorrected and corrected interaction energies of dimers (ΔE and ΔE_{BSSE} , respectively, kcal mol^{-1}) calculated using B3LYP-D3/6-311++(d,p)-DGDZVP (single point calculations).

Dimers ^(a)	$\Delta E \text{ kcal mol}^{-1}$	$\Delta E_{\text{BSSE}} \text{ kcal mol}^{-1}$
1-D	-5.7	-5.0
2-D	-5.1	-5.1
3-D	-3.4	-2.9
4-D	-4.1	-3.5
5-D	-5.5	-4.8
6-D	-6.5	-5.7

(a) D = Dimer (supramolecular synthon) in structures **1** to **6**, see Figure 4.19 and Figure 4.20

In compounds **3**, **4** and **5**, **mBIEB** forms three types of supramolecular synthon. These are shown in Figure 4.20, with two formed only by two $\text{C}_{\text{sp}2}-\text{H}\cdots\text{I}$ hydrogen bonds with a stabilization energy of about 3 kcal mol^{-1} , and the other formed by two $\text{C}_{\text{sp}2}-\text{H}\cdots\text{I}$ and two $\text{C}_{\text{sp}2}-\text{H}\cdots\pi_{(\text{alkyne})}$ hydrogen bonds with a stabilization energy of $4.8 \text{ kcal mol}^{-1}$. Despite the weak energies, it has been demonstrated that the effects of these interactions on the crystal structure and packing are relevant.

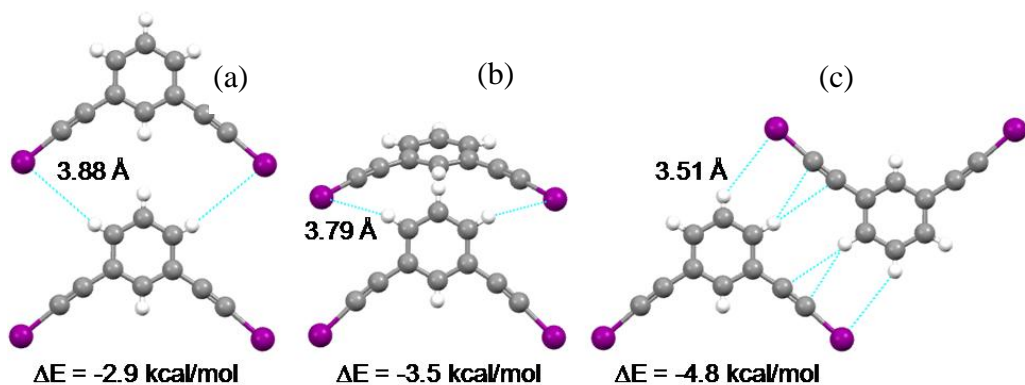


Figure 4.20 Supramolecular synthons and stabilization energies for m-BIB in structures **3 (**3-D**) (**a**), **4** (**4-D**) (**b**) and **5** (**5-D**) (**c**).**

With the aim of supporting our hypothesis, different intermolecular contacts in the arrays were systematically investigated beyond the sum of the van der Waals radii,

since it has been noted that the use of the sum of van der Waals radii as a cut-off parameter to assess and evaluate weak C–H \cdots X hydrogen bonds is not recommended and should not be taken into account.^[26]

To date, more attention has been paid to the halogen-bonding donor character of haloethynylbenzene derivatives. Thus, **pBIEB**, **pBBrEB** and **mBIEB** are strong ditopic XB donors that form linear or angular polymers with ditopic linear or angular halogen bond acceptors such as BPE, pyridazine, propanone, HTMA and Tröger's base.

As we proposed, the complementarity of the bis(haloethynyl)benzene derivatives by C_{sp²}–H \cdots X and C_{sp²}–H \cdots π _(alkyne) edge-to-edge hydrogen bonds that favor the formation of planar supramolecular synthons has been demonstrated. It was determined by means of DFT calculations that the negative interaction energies of such supramolecular synthons range from 2.9 to 5.7 kcal mol⁻¹. In spite of these weak energies, their effects on the crystal structure and packing are relevant and, in combination with strong halogen bonds, these interactions have proven to represent a useful strategy for the formation of two-dimensional arrangements in cocrystals with nitrogen and oxygen XB acceptors. Such materials are of great interest in the development of molecular organic materials.

4.4 Halogen bonding salts

As mentioned in the introduction of this chapter, this second section is devoted to the study of halogen bonding salts formed by **PBIEB** linear, rigid and ditopic halogen bond donors with four bromide salts of di(iodioethynyl)benzene derivatives to coordinate bromide anions as a function of the size and geometry of the counterions and how they influence the supramolecular architectures obtained. In addition, we established the thermodynamic features of the halogen bond interactions of such salts in solution by isothermal titration calorimetry (ITC).

4.4.1 Previous works

The study of the complexation of anions has moved from being an area of academic interest to a fundamental pillar of supramolecular chemistry with applications in many areas.^[3f] In recent years a large number of anion sensors,^[3f] anion-responsive materials, and organo catalytic processes involving anion complexation have been developed.^[44] Anions, such as transition metals, have a primary valence, i.e., a negative charge, and a secondary valence, i.e., the number of ligands that surround the anions and form their coordination sphere. This valence largely exceeds the requirements of the neutrality principle both in the solid state and in solution. The types of non-covalent interactions typically used to bind anionic guests include electrostatic interactions, coordination to metal ions, hydrogen bonding (HB) and, more recently, halogen bonding (XB).

Halogen bonding was shown to provide a highly efficient and directional interaction towards anion coordination.^[45] Anions, and particularly the smallest halide ones, act as very good halogen bond acceptors as their negative charge is concentrated on one single atom. Halide anions – like halogen bond acceptors – can adopt a variety of coordination numbers due to their spherical nature, with up to eight halogen bonds. Nevertheless, it has been shown that the halides have a moderate bias towards the formation of two or three X-bonds.^[45e] On the basis of

this interaction, numerous extended anionic networks have been described, including the cocrystallization of naked halide anions (i.e., with noncoordinating cations) together with polydentate halogen bond donors^[45e, 46] such as diiodoacetylene, 1,4-diiodotetrafluorobenzene, 1,4-bis(iodoethynyl)benzene.^[47] Depending on the number of iodine atoms in the neutral halogen bond donor and the nature and size of the cationic counterion, the dimensionality of the resulting networks can be engineered and numerous 1D (linear, angular or helical^[48] polymers), 2D and 3D structures^[45a] have been described. Thus, the cocrystallization of 1,4-diiodotetrafluorobenzene, a bidentate halogen bond donor, with halide salts results in linear, angular ($\text{C}-\text{Hal}\cdots\text{X}^-\cdots\text{Hal}-\text{C}$ angle from 180 to slightly more than 60°)^[45a] or helical polymers.^[48]

Halide anions as halogen bond acceptors can adopt a variety of coordination numbers due to their spherical nature, with up to eight halogen bonds, although it has been shown that the halides have a moderate bias towards the formation of two or three X-bonds.^[45a]

In cases where halides form three XB, 1D ribbons have been described for the cocrystal structure of 1,4-diiodotetrafluorobenzene : tetraphenylphosphonium halide (see Figure 4.21).^[49]

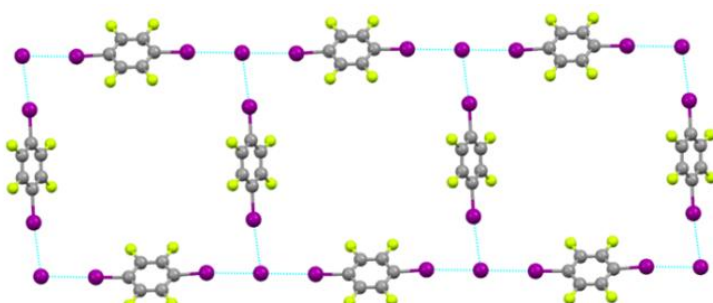


Figure 4.21 Ribbons formed when iodide anions self-assemble with 1,4-diiodotetrafluorobenzene in (1,4-diiodotetrafluorobenzene) (tetraphenylphosphonium) iodide cocrystal with a 3:2 stoichiometry. The cations have been removed for the sake of clarity

Supramolecular chemistry: Crystal engineering

Cocrystallization of a halogen bond donor with tetramethylphosphonium iodide (Figure 4.22 (a)) or tetraphenylphosphonium bromide (Figure 4.22 (b)) results in two-dimensional honeycomb structures that are corrugated to a greater or lesser degree – as shown in Figure 4.22, where the cations have been removed for the sake of clarity.^[28]

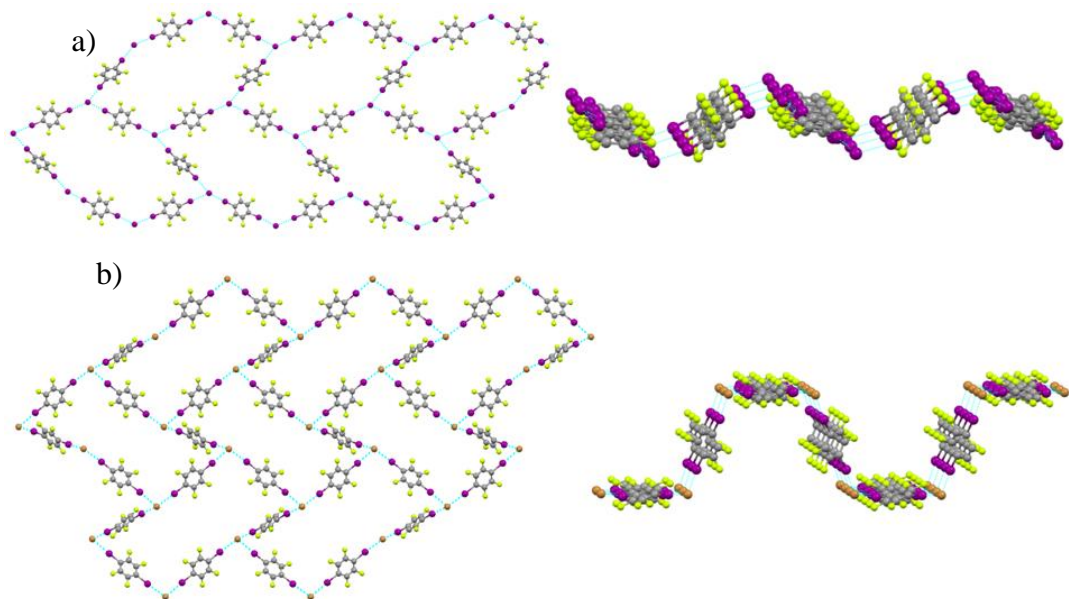


Figure 4.22 2D corrugated honeycomb arrangements in a) 1,4-diiodotetrafluorobenzene tetramethylphosphonium iodide and b) tetraphenylphosphonium bromide. The cations have been removed for the sake of clarity.

The tridentate halogen bond donor 1,3,5-triiodo-2,4,6-trifluorobenzene commonly affords 2D (6,3) networks when cocrystallized with halide salts of various counterions, with the smallest ones (Et_4N^+ , Et_4P^+) being able to stabilize the perfect honeycomb networks (Figure 4.23a),^[50] while larger cations ($n\text{Bu}_4\text{N}^+$, PPh_4^+) afford strongly corrugated (6,3) networks^[51] (see Figure 4.23b) (The cations have been removed for the sake of clarity).

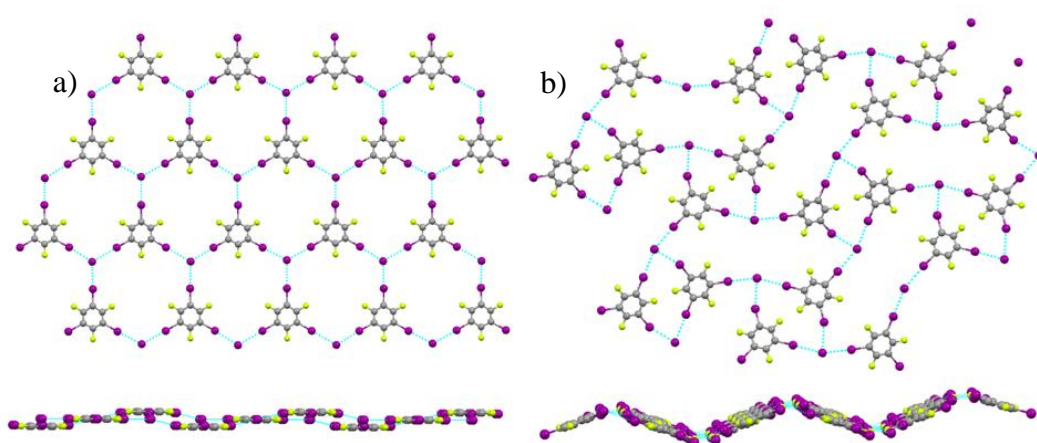


Figure 4.23 Honeycomb structures of 1,3,5-triodotri fluorobenzene with Et_4N^+ and nBu_4N^+ iodide.

Iodoethynyl derivatives were found to be very potent halogen bond donors. However, these compounds have not been studied in great detail as building blocks with halide salts. Primarily, 1,4-bis(iodoethynyl)benzene has been used to obtain electrical conductors or magnetic materials by electrocrystallization with tetrachalcogenfulvalene (chalcogen = S and Se) derivatives and halide salts. The 1D and 2D networks of 1,4-bis(iodoethynylbenzene) derivatives with tetrachalcogenfulvalenium halides are shown in Figure 4.24 (the cations have been removed for the sake of clarity).

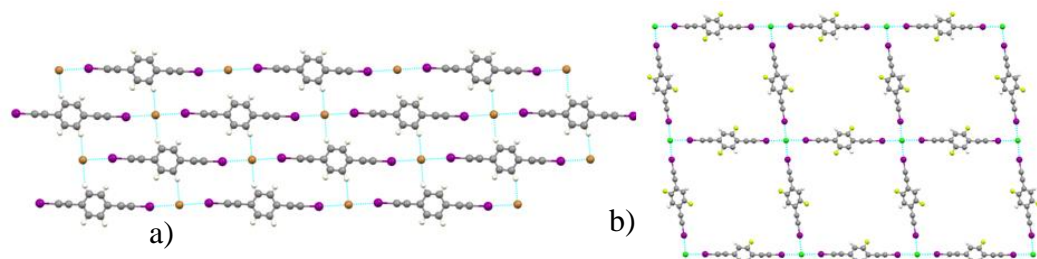


Figure 4.24 Different supramolecular architectures for 1,4-bis(iodoethynyl)benzene and tetrachalcogenfulvalenium halides

Recently, the cocrystallization of 1,3,5-tris(iodoethynyl)-2,4,6-trifluorobenzene with a variety of halide salts with organic cations afforded a range of structural motifs ranging from more or less corrugated 2D honeycomb lattices to 2-fold

interpenetrated, pyrite-type cubic lattices with an unprecedented octahedral coordination around the halide anion.^[52]

Despite the large amount of work published to date, a direct comparison of the binding properties of complexes formed by neutral, iodoethynyl-based multidentate XB donors with halides in the solid state, in solution, and in the gas phase has yet to be made. Only recently a similar study concerned neutral, iodoethynyl-based monodentate^[31] and iodopolyfluoroarene-based multidentate XB donors with neutral XB acceptors and halides, respectively.^[53] Studies of this kind would allow an evaluation of the predictive value of solid state structures and gas-phase calculations for the solution-phase binding of anions and would thus generate valuable information for the future design of XB-based anion receptors, catalysts, and materials.

In this context, we have undertaken the preparation of four halogen bonding adducts of pBIB with the bromide salts (DTMABr, TPABr, TBABr and Ph₄PBr) represented in Figure 4.25. The bromide anion was selected because it gives rise to strong halogen bonds and cations of different sizes and geometries. The aim was to study the influence of the salt on the supramolecular architectures and, in particular, on the edge-to-edge interactions. In addition, the solution-phase halogen bonding interactions were evaluated by isothermal titration calorimetry (ITC).

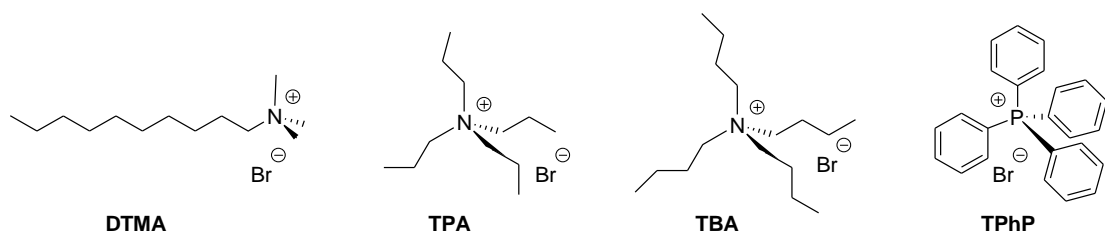


Figure 4.25. The bromide salts described in this section to form cocrystals.

4.4.2 X-ray Crystal Structures

Cocrystals of ditopic halogen bond donor **pBIEB** and several bromide salts, **pBIEB**·DTMABr (**8**), **pBIEB** TPABr (**9**), **pBIEB** TBABr (**10**) and **pBIEB** TPhPBr (**11**), were prepared by slow evaporation at room temperature of CH₂Cl₂ solutions of equimolecular quantities of **pBIEB** and the corresponding bromide salt. In the crystal structures of **8** to **10** the two iodine atoms of **pBIEB** form charge-transfer complexes with the bromide anion. The C_{sp}–I⋯Br[−] halogen bond distances range from 3.124 to 3.274 Å, i.e., as short as 0.82 to 0.85 times the sum of van der Waals radii for iodine (1.98 Å) and the Pauling ionic radius of bromine (1.95 Å). Very strong halogen bonds can have rr (rr = $d_{X\cdots Y}/R_{vdW}(X) + R_{vdW}(Y)$) values as low as 0.69.^[54] However, Nyburg proposed a value of 3.60 for C–I⋯Br, which is the value predicted by the anisotropic model for halogen bonding.^[55] The C–I⋯Br[−] interactions are approximately linear, with angles ranging from 173.9 to 177.3°. The much shorter distances observed here, combined with the linearity, demonstrate the strength of the halogen interactions in these salts. The relevant halogen bonding distances are provided in Table 4.8. Examination of these data indicates that the decreasing C_{sp}–I⋯Br[−]⋯I–C_{sp} angle is associated with an increase in the halogen bond distance C_{sp}–I⋯Br[−].

Table 4.8 Halogen bonding distances and angles, reduction ratio (rr = $d_{X\cdots Y}/R_{vdW}(X) + R_{vdW}(Y)$), where R_{vdW}(X) is the van der Waals radius of iodine (1.98 Å) and R_{vdW}(Y) is the radius of the halide anion (1.95 Å)

Comp	C–I (Å)	C–I⋯Br (Å)	C–I⋯Br [−] (°)	I⋯Br⋯I (°)	rr
pBIEB (293K)	2.024(8)				
pBIEB (150K)	1.980 (10)				
Structure 8	2.012(6)	3.1594(4)	174.36(20)	180.00(1)	0.80
Structure 9	2.024(8)	3.2091(6)	176.32(18)	138.98(4)	0.82
Structure 10	2.024(11)	3.2744(12)	173.96(25)	75.29(3)	0.83
Structure 11	2.01(1)	3.124(2)	177.3(3)	-----	0.79

Analysis of the four structures from the point of view of the halide anion provides a striking ‘coordination’ around the Br⁻ anion. The heteromeric three-component systems **8** to **10** are characterized by the presence of infinite, one-dimensional, X-bonded chains in which the **pBIEB** and the halide anions alternate and behave as ditopic XB donors and acceptors, respectively. The I···Br⁻···I angles range from straight in structure **8** to the acute angle 75.29° in structure **10**. Structure **9** shows an intermediate angle (138°). The coordination spheres of bromide anions and iodine atoms are completed by hydrogen bonds.

In the following sections we will describe each structure and compare the differences between them due to cation size and shape.

4.4.2.1 **pBIEB**•DTMABr complex, structure **8**.

Halogen bonded **pBIEB**•DTMABr in a 1:1 complex crystallizes in the monoclinic space group P2_{1/m}, where the asymmetric unit consists of a **pBIEB** half molecule located at an inversion center, one half DTMA on a mirror plane perpendicular to [0 1 0] and half a Br⁻ anion at an inversion center.

The bromide anion forms two halogen bonds (C—I···Br⁻ 3.159 Å and 174.3°) with **pBIEB** and two hydrogen bonds (C—H···Br⁻ 2.813 Å and 163.0 °) from the cation. The bromide coordination sphere is distorted square planar (I···Br⁻···I and H···Br⁻···H 180°, I···Br⁻···H 81.8° and 98.2°), leading to a three-dimensional supramolecular structure (Figure 4.26). The cation is also joined to the polymeric chain by a hydrogen bond to the iodine (C—H···I—C 3.115 Å and 79.3°).

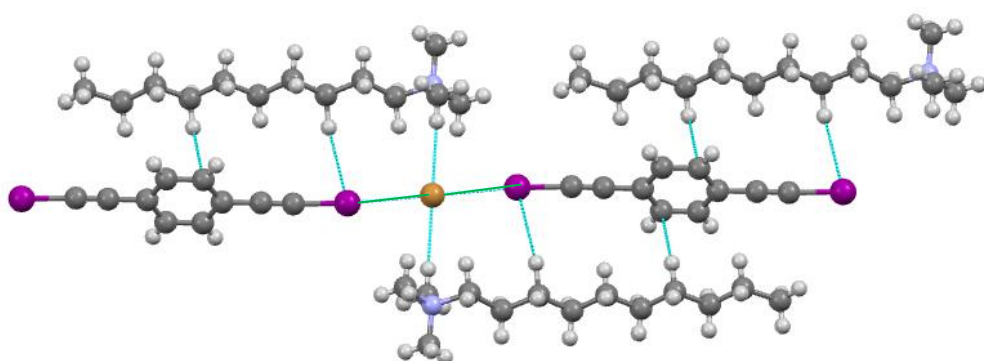


Figure 4.26. Detail of the bromide coordination sphere, with halogen bonds in green and hydrogen bonds in blue.

The halogen bonding donors form synthons via hydrogen bonds (Table 4.9) in a similar way to those described in the previous section of this chapter for the structures **pBXEB·BPE** ($X = \text{Br}, \text{I}$) and **pBIEB·HTMA**, thus resulting in planes, as shown in Figure 4.27.

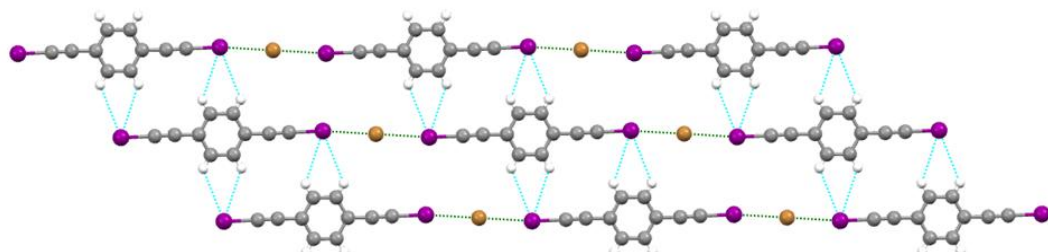


Figure 4.27 Layers in structure 8 built by a combination of halogen bonds (green) and hydrogen bonds (blue).

Table 4.9 Hydrogen bond distances and angles in 8.

Compound	D–H…A	Sym. equivalence	d(D–H) Å	d(H…A) Å	d(D…A) Å	$\angle(\text{DHA})^\circ$
8	$\text{C}_{\text{sp}^2}\text{--H}\cdots\text{I}(1)$	$1-x, -y, 1-z$	0.93	3.3284	3.977	128.8
	$\text{C}_{\text{sp}^2}\text{--H}\cdots\text{I}(1)$	$1-x, -y, 1-z$	0.93	3.2813	3.953	130.8
	$\text{C}_{\text{sp}^2}\text{--H}\cdots\text{Br}(1)$	$1+x, y, 1+z$	0.98	2.813	3.756	163

Supramolecular chemistry: Crystal engineering

The linear infinite chains formed by $\text{Br}^- \cdots \text{pBIEB} \cdots \text{Br}^-$ halogen bonds are arranged in almost perpendicular planes with respect to the *b* axis (Figure 4.28).

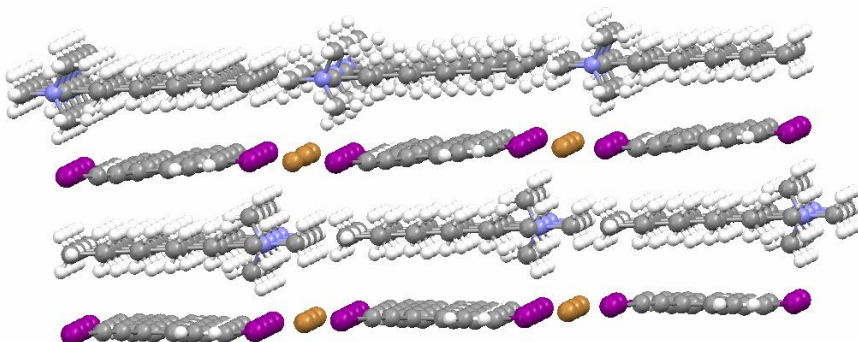


Figure 4.28 Projection of **pBIEB**·DTMABr showing the layered nature of the anionic and cationic networks.

This organization can be facilitated by the similarity in the length of the decyltrimethylammonium cation (15.479 \AA) and the bromide **pBIEB** assembly (15.220 \AA) (Figure 4.29). This situation is similar to that described previously by Yamamoto and Kato for structures of **pBIEB** and their derivatives with halogen anions and tetrathiafulvalene cations and by Metrangolo *et al.* in structures of α,ω -diiodoperfluoroalkane with bis(trimethylammonium)alkane diiodides.^[56]

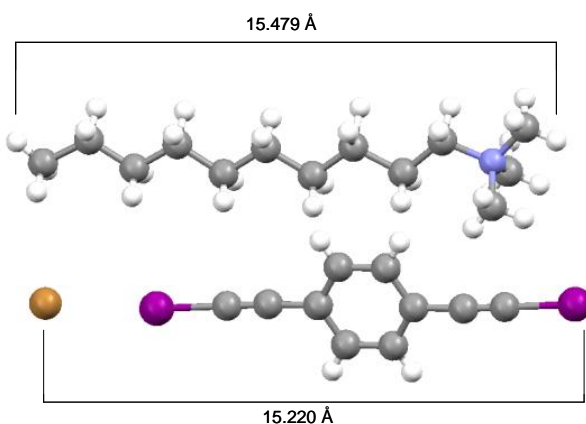


Figure 4.29 Comparison between the length of the DTMA cation and **pBIEB**· Br^- anionic assembly

On the other hand, structures **9** and **10** are characterized by the presence of zig-zag assemblies of halogen bonds; **pBIEB** and bromide anions give rise to infinite polymers by halogen bonding.

4.4.3 pBIEB·TPA_{Br} complex, Structure **9**.

The ditopic **pBIEB** halogen bond donor forms with TPA_{Br} a 1:1 XB complex (structure **9**) that crystallizes in the monoclinic space group P2/n. The asymmetric unit of **9** consists of one **pBIEB** half molecule situated at an inversion center and a half TPA cation and a Br⁻ anion centered on a twofold axis.

The halogen bond donor and bromide anion give rise to an infinite polymer by halogen bonding. Each bromide is also linked to two **pBIEB** molecules ($C_{sp^2}-H \cdots I$ 3.137 Å and 173.7°) and to two cations (TPA) via a hydrogen bond ($C_{sp^3}-H \cdots Br^-$ 3.062 Å and 155.8°), as shown in Figure 4.30. As a consequence, the bromide coordination sphere is distorted trigonal prismatic.

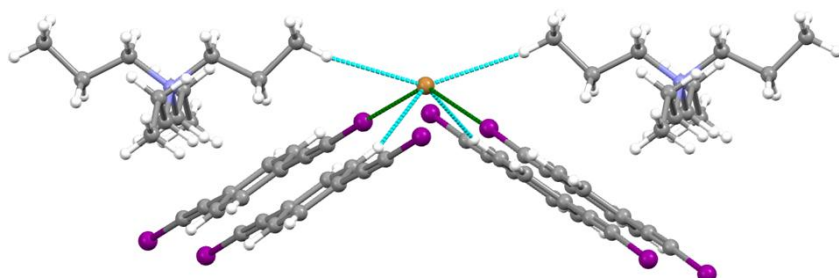
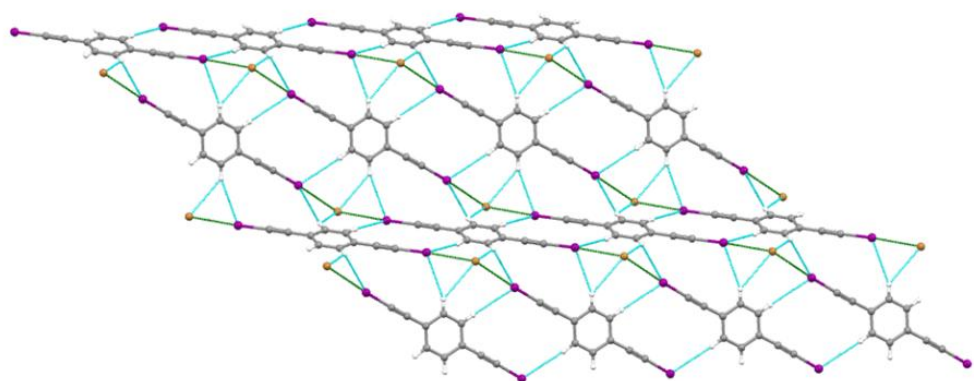


Figure 4.30 Bromine coordination showing halogen (green) and hydrogen (blue) bond interactions.

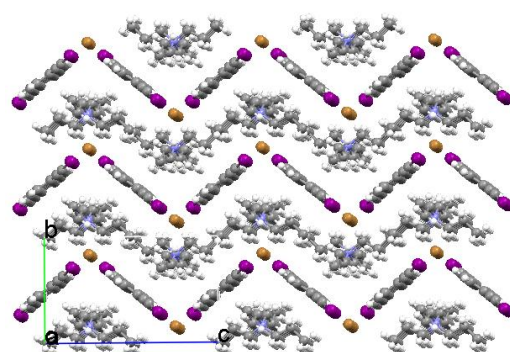
The polymeric halogen bonded chains are joined by two types of edge-to-edge $C_{sp^2}-H \cdots I$ hydrogen bonds (Table 4.10). The first, a coplanar edge-to-edge interaction similar to that described for structure 8, gives rise to ribbons. The second interaction joins the ribbons, which are tilted with respect to one another by ca. 135°. This arrangement results in corrugated planes along the *ac* axis, as shown in Figure 4.31.

Table 4.10 Hydrogen bond distances and angles in 9.

Compound	D–H···A	Sym. equivalence	d(D–H) Å	d(H···A) Å	d(D···A) Å	\angle (DHA) °
9	C _{sp²} –H···I(1)	2–x, 1–y, -z	0.93	3.1776	4.103	173.6
	C _{sp²} –H···I(2)	2.5–x, y, -1/2–z	0.93	3.2171	4.063	152.1
	C _{sp²} –H···Br(1)	1+x, y, z	0.93	3.1371	3.876	137.7
	C _{sp³} –H···Br(1)	2–x, -y, -z	0.96	3.0620	3.957	155.8
	C _{sp³} –H···I(1)	x, y, z	0.97	3.0859	4.014	160.6

**Figure 4.31 Corrugated planes in the structure built by a combination of halogen bonds (green) and hydrogen bonds (blue).**

The corrugated planes are separated by 6.89 Å and the tetrapropylammonium cations are intercalated in this interplanar space (Figure 4.32).

**Figure 4.32. Structure of 9 with corrugated planes and intercalated TPA cations**

4.4.4 pBIEB ·TBA Br complex, Structure 10.

The **pBIEB** · TBABr halogen bonded 1:1 complex (structure **10**) crystallizes in the monoclinic space groups P2/c. The asymmetric unit of **10** contains two half molecules of **pBIEB** which are situated at an inversion center and one TBA and Br in a general position.

In addition to two halogen bonds, each bromide forms three hydrogen bonds with two TBA cations (Figure 4.33) The hydrogen bond distances and angles for **10** are gathered in Table 4.11. If we consider the two hydrogen bonds with the same TBA as one, the bromide environment can be described as distorted tetrahedral.

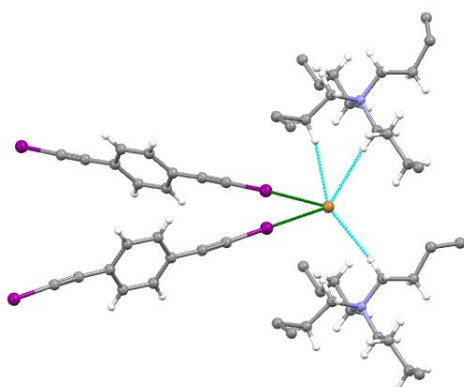


Figure 4.33. Detail of the bromide coordination sphere. Halogen and hydrogen bonds are shown in green and blue, respectively.

The **pBIEB** molecules form, by hydrogen bonding, only distorted ribbons (Figure 4.34) such as the second type of edge-to-edge interaction described for structure **9**. The C_{sp}²–H···I hydrogen bond distances in structure **10** are similar to those in **9**, but in **10** the interactions are less linear, as shown by the bond distances and angles gathered in Table 4.11.

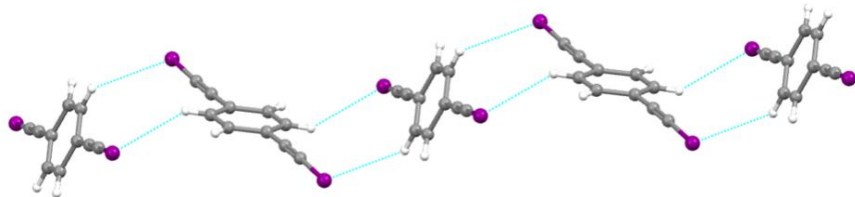


Figure 4.34 Ribbons along the *c* axis formed by hydrogen bonds between pBIEB molecules in the structure of 10.

Table 4.11 Hydrogen bond distances and angles in 10.

Compound	D–H···A	Sym. equivalence	d(D–H) Å	d(H···A) Å	d(D···A) Å	\angle (DHA) °
10	C_{sp^2} –H···I(1)	x, -y, $1/2+z$	0.93	3.1983	3.945	138.6
	C_{sp^2} –H···I(2)	$1-x, y, -1/2-z$	0.93	3.3543	3.973	126
	C_{sp^3} –H···Br(1)	x, y, z	0.97	2.904	3.82	157.6
	C_{sp^3} –H···Br(1)	x, $1+y, z$	0.97	2.886	3.79	155.8
	C_{sp^3} –H···Br(1)	x, y, z	0.97	2.867	3.79	158.5

Finally, the combination of the bromide coordination sphere, with an $I\cdots Br^- \cdots I$ angle of 75.29° , and distorted ribbons gives rise to a three-dimensional lattice. The tetrabutylammonium cations are located in the network channels shown in Figure 4.35 along the crystallographic axes.

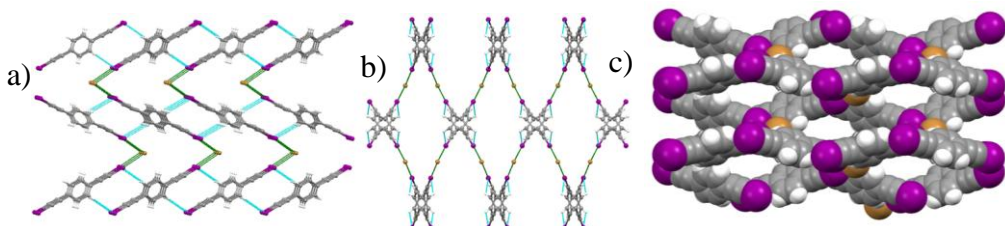


Figure 4.35. a) Projection view of the (pBIEB) Br^- anionic network along the *b* axis, b) along the *c* axis and c) along the axis as a space fill perpendicular view, which shows the formation of a 3D structure of anionic networks.

4.4.5 pBIEB ·[TPhPBr]₂ complex, Structure 11.

p-Bis(iodoethyl)benzene and TPhPBr form a 2:1 halogen bonded complex that crystallizes in the monoclinic space group $P2_1/c$. The asymmetric unit consists of a **pBIEB** half molecule situated at inversion center and one TPhP and one Br⁻ in general positions.

This structure is remarkable because the bromide anion forms only one halogen bond but completes its coordination sphere with hydrogen bonds from an atom of the tetraphenylphosphonium cations and **pBIEB**, as shown in Figure 4.36.

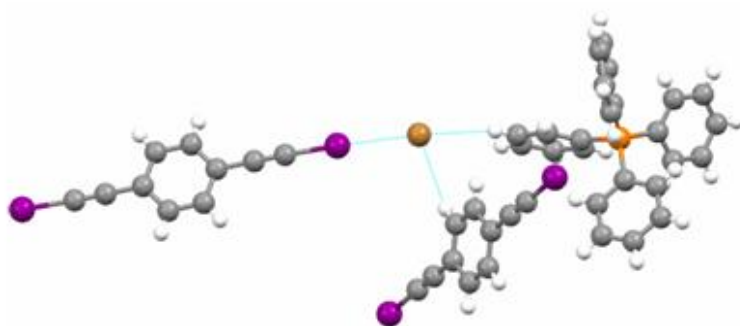


Figure 4.36 Perpendicular view of halogen interactions, which shows the formation of anionic structure networks.

Tetraphenylphosphonium cations dimerize (Figure 4.37 (a)) to give rise to chains formed by one molecule of **pBIEB** and two bromide anions separated by a dimer of tetraphenylphosphonium with an I···Br⁻···H-C_{Ph} angle of 172.5° (Figure 4.37 (b)).

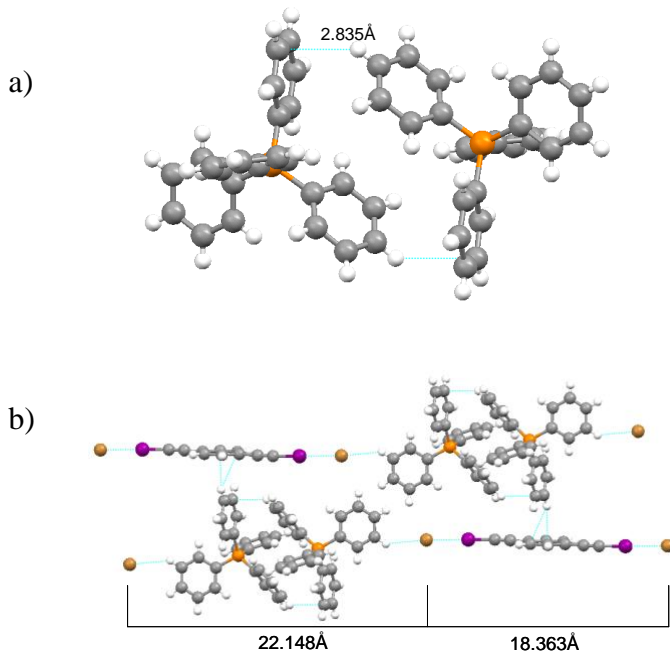


Figure 4.37 a) Projection view of the TPhP dimer in structure 11; **b)** ionic chains formed by combination of halogen and hydrogen bonds.

Parallel strings are attached by $\text{C}_{\text{Ar}}-\text{H}\cdots\pi$ hydrogen bonding (3.445 \AA and 155.1°) to give a lattice with rectangular holes from which protrude benzene rings directed in opposite senses and almost perpendicular to the plane (87.2°) (Figure 4.38). These planes are stacked along the c axis with the adjacent planes rotated by 43.3° .

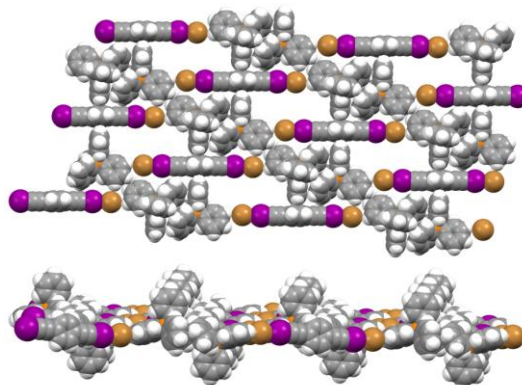


Figure 4.38 General view of structure 11.

4.4.6 Hirshfeld Surface.

In chapter 1 we described Hirshfeld surfaces and how this kind of analysis can contribute to a better understanding of each molecule in terms of its environment.

Each molecule in the asymmetric unit of a given crystal structure will have a unique Hirshfeld surface, and hence a direct comparison can be made between **pBIEB** molecules in different environments. The Hirshfeld surfaces generated for **pBIEB** itself and **pBIEB** cocrystal structures have distinctly different shapes, with the curvedness reflecting the very different packing modes. These surfaces show close contacts of hydrogen bond donors and acceptors, but other close contacts are also evident. Even though the $\text{I}\cdots\text{Br}^-$ interactions are the shortest and most likely the strongest, they cover at most 10% of the Hirshfeld surface of the **pBIEB** molecules, and hence other weaker interactions cannot be neglected (Figure 4.39). The relative contributions of the different interactions to the Hirshfeld surface were calculated for **pBIEB** itself and **pBIEB** cocrystal structures. Due to the varying compositions of crystals, the values are not directly comparable across the compounds, but they do offer an insight into the effect of different supramolecular organizations. Comparison of the **pBIEB** structures shows the variety of interactions of molecules that form the **pBIEB** and none of them exceed 35% of the Hirshfeld surface.

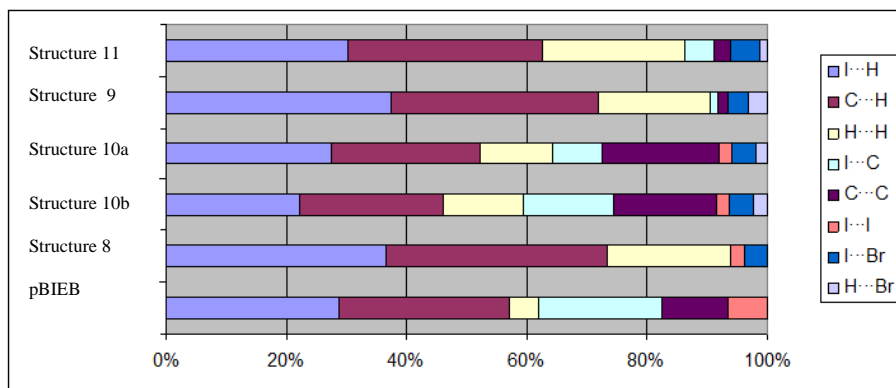


Figure 4.39. Relative contributions of various intermolecular contacts to the Hirshfeld surface of pBIEB in the structures of pBIEB and halogen bonded complexes 8 to 11.

Moreover, the shape index of **pBIEB** is characterized by adjacent red and blue triangles that are characteristic of $\pi\cdots\pi$ stacking interactions and the curvedness surface shows a planar zone in the aromatic region. In contrast to cocrystal structures, the main features are C–H··· π interactions, as shown by the curvedness surface with fewer flat areas and with a greater number of short contacts of the aromatic ring with hydrogen atoms, which are shown as red areas on the surface (Figure 4.40). In the fingerprint plots the features clearly show that the **pBIEB** structures are not symmetrical and lower symmetry is observed in the fingerprints of cocrystals. This is because in the co-crystal the interactions between one molecule of **pBIEB** and other **pBIEB** molecules are less marked than in the structure of **pBIEB** itself. In the case of adduct **11** the contacts between **pBIEB** and other **pBIEB** molecules are practically non-existent.

The halogen bonding interactions give rise to red lines centered at $di = 1.7 \text{ \AA}$ and $de = 1.9 \text{ \AA}$. The fingerprint of adduct **11** is characterized by a wing-shaped and pointy spike, with the first featuring C–H··· π interactions, as evidenced by the de surface.^[57]

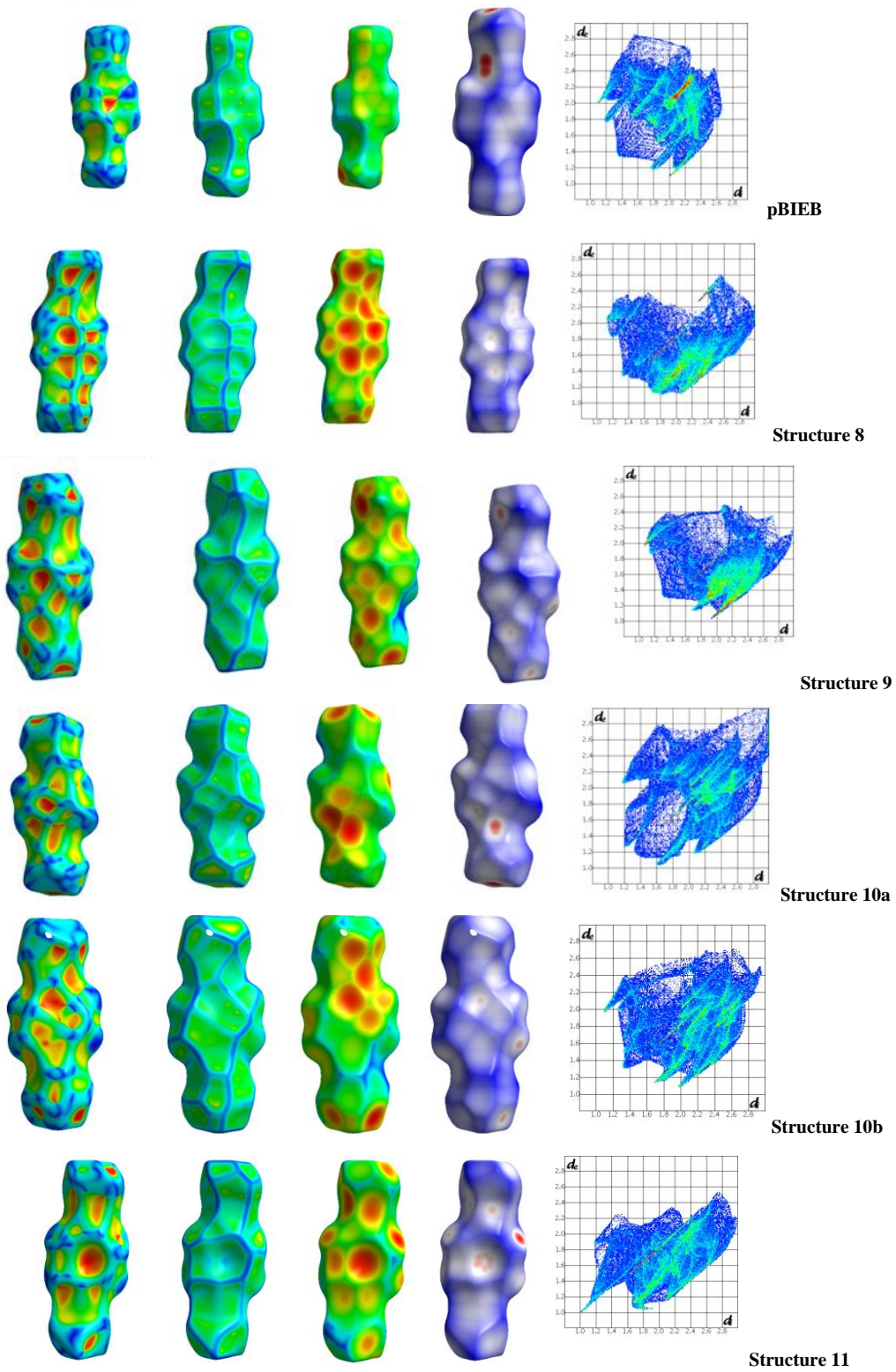
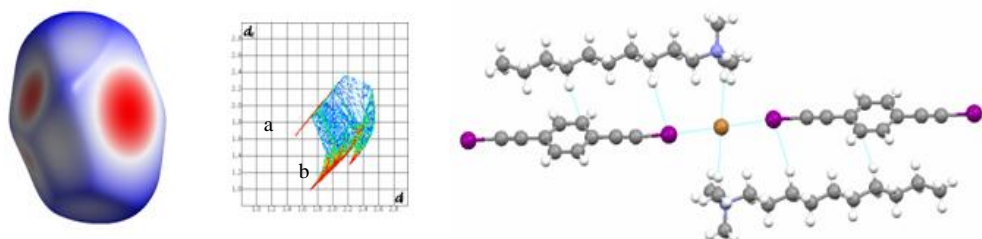
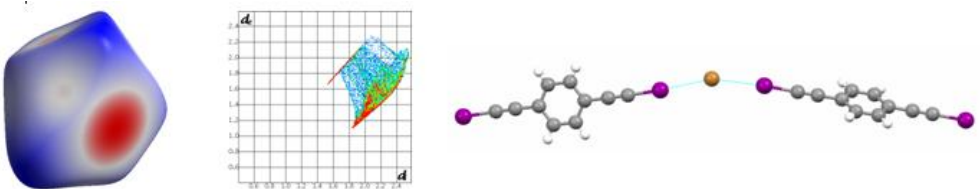


Figure 4.40 The shape index, Hirshfeld surface and fingerprint for all structures.

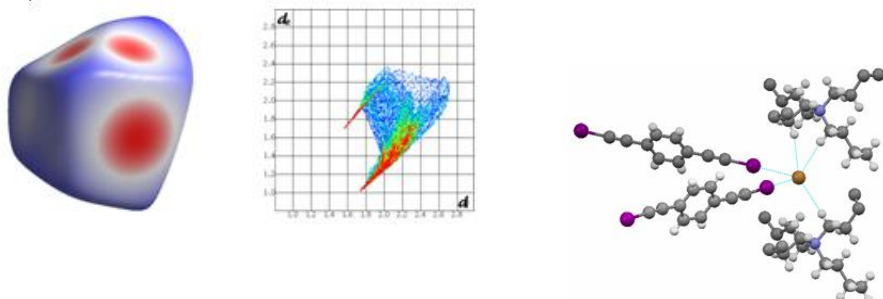
In the crystal structures of **8** to **11** the coordination sphere of the bromide anions is formed mainly by halogen and hydrogen bonds, with both the coordination number and geometry being very diverse (Figure 4.39). These latter two aspects are reflected in the Hirshfeld surfaces of the bromides, which are related to the volume occupied by the anion in the crystal structure and, although the volumes are similar in all the structures, their shapes are very different. The contribution to the Hirshfeld surface of each of these interactions is very different because, in all cases, hydrogen bonding exceeds 80% of the Hirshfeld surface and reaches 95% in the case of the adduct **11** as the bromide anion forms only one halogen bond. The fingerprint plots (Figure 4.41) are characterized by their lack of symmetry, by the appearance of a red line labeled as ‘a’ and a spike at the bottom of the graph labeled as ‘b’. The red line centred at $di = 1.7 \text{ \AA}$ $de = 1.9 \text{ \AA}$ is due to a $\text{C}_{\text{sp}}-\text{I}\cdots\text{Br}^-$ halogen bond, as discussed when describing the **pBIEB** fingerprint plots.



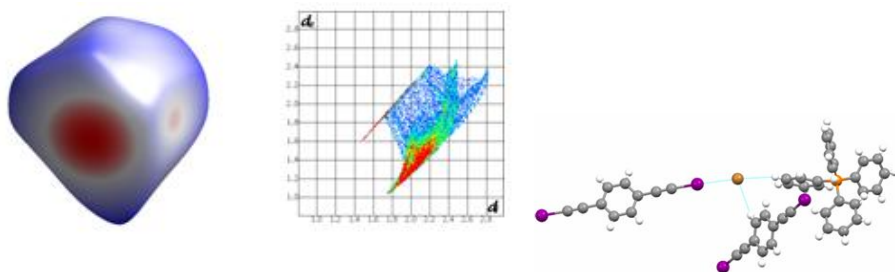
Structure 8



Structure 9



Structure 10



Structure 11

Figure 4.41 Bromide interaction view from Hirshfeld surfaces and fingerprint plots.

4.4.7 Isothermal Titration Calorimetry.

The aim of this section is to present the results of studies into the halogen bond in solution. This topic has not been discussed extensively in articles,^[58] despite its rich history and the unique types of insight that may be gained from solution phase experiments, such as thermodynamic data obtained from the determination of association constants (K_a).

A variety of spectroscopic techniques have been employed to investigate weak molecular forces in solutions. Optical spectroscopy was the first technique, but NMR spectroscopy has been by far the most widely used technique for solution studies of XB. NMR spectroscopy offers exceptionally detailed structural information and high versatility, but this approach suffers from comparably poor sensitivity, with a typical limit of detection in the nanomolar range for the most commonly detected ^1H and ^{19}F nuclei. Conversely, optical methods such as UV-VIS spectroscopy provide sensitivity in the femtomole range, yet they offer limited structural information. Hitherto scarcely utilized calorimetry allows the thermodynamic characterization of equilibrium processes; however, in a similar way to optical spectroscopy it is inherently weak in directly providing atomic level information. Isothermal titration calorimetry (ITC) is currently the most accurate, sensitive, fast and convenient technique to obtain thermodynamics data because it is the only method that yields enthalpies as direct experimental observables.^[59]

Supramolecular interactions by definition involve the reversible formation and rupture of weak bonds, not only between the molecular species under investigation but also the rearrangement of the solvation shell of all participating partners. The heat evolved or consumed due to the formation and breaking of bonds is the integral result of manifold simultaneous events in a global response. Calorimetry provides a reliable basis for experimental observables and leaves the connection to molecular behavior and structural detail open to interpretation.

The usual ITC procedure is to titrate a solution of compound A, placed in the calorimetric cell, with aliquots of a solution of compound B placed in an automated syringe. The exchanged heat is measured and this reveals quantitative information about the interaction between A and B.^[60] A typical output of an exothermic encapsulation is depicted in Figure 4.42.

The thermogram shown in Figure 4.42, top graph, shows upward or downward directed thermal power pulses (as a consequence of each injection) and these reflect the modulation of the feedback current required to maintain a zero temperature difference between the sample and the reference cell. The time integration of the heat pulses when plotted versus the nominal molar ratio of the injected compound over the one contained in the sample cell yields a titration curve or interaction isotherm, which is corrected by subtracting the results of a control experiment (dilution of compound from the syringe into solvent) if necessary. In the lower part of Figure 4.42 the sigmoidal form allows the determination of the molar enthalpy ΔH° from the extrapolated step height or deflection of the curve, the stoichiometry of the binding process from the position of the inflection point along the molar ratio axis and the affinity constant K_a from the slope at the inflection point.

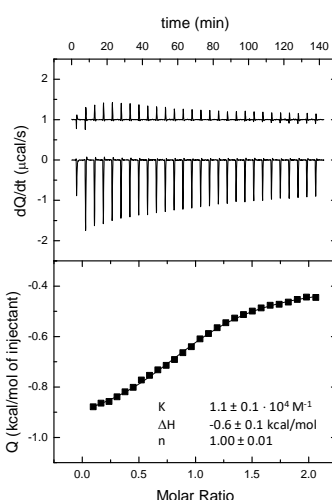


Figure 4.42 Thermogram from a typical Isothermal Titration Calorimetry experiment.

To date, the free energies of neutral XB interactions span a range from ~ 0 to 40 kJ mol $^{-1}$, with the strongest found to involve inorganic XB donors. While numerous association constant data with inorganic halogen-bond donors exist, there is a scarcity of quantitative data for organic halogen-bond donors such as haloalkynes and iodoperfluoro organics.^[3b] Of the few haloalkynes investigated, Laurence and co-workers proposed a soft basicity scale through the correlation of $\Delta v(C-I)$ values, i.e., changes in C–I stretching frequency by IR spectroscopy, with the formation enthalpy of the iodine complex ΔH_{I2} . Twenty years later, Goroff and co-workers studied the XB interactions of iodoalkynes in various Lewis basic solvents by ^{13}C NMR spectroscopy. Recently, binding constants between iodoethynylbenzene derivatives and 1-azabicyclo[2.2.2]octane were determined by 1H NMR titrations, with K_a values range from $6.3 \pm 0.6 \text{ M}^{-1}$ for the dimethylamino-substituted XB donor to $25 \pm 8 \text{ M}^{-1}$ for the nitro-substituted analog. A van't Hoff analysis of these data showed that the XB association is promoted by a favorable negative enthalpic term ΔH , which is partially compensated by an unfavorable negative entropic term $T\Delta S$.^[31]

Studies of halogen bond binding in solution by ITC of iodoethynyl derivatives have not been reported to date and most published studies employed cationic halogen bond donors such as 2-iodoimidazolium^[61] or iodo-1,2,3-triazoliums.^[62] We conducted isothermal calorimetric titrations in THF to investigate the halogen-bond strength of the bidentate *p*-bis(iodoethynyl)benzene halogen-bond donor toward the bromide anion in solution. In the three cases examined, the binding of **pBIEB** to bromide is always found to be entropically driven, which may indicate a significant desolvation process with the release of solvent molecules to the bulk solution. The binding affinities, which are gathered in Table 4.12, showed little dependency on the weakly coordinating counteranions of bromide salts, but became slightly stronger with a higher solubility salt (decytrimethylammonium ($8.3 \cdot 10^3 \text{ M}^{-1}$) > tetrabutylammonium ($7.9 \cdot 10^3 \text{ M}^{-1}$) > tetrapropylammonium ($2.8 \cdot 10^3 \text{ M}^{-1}$)). (See Figure 4.43)

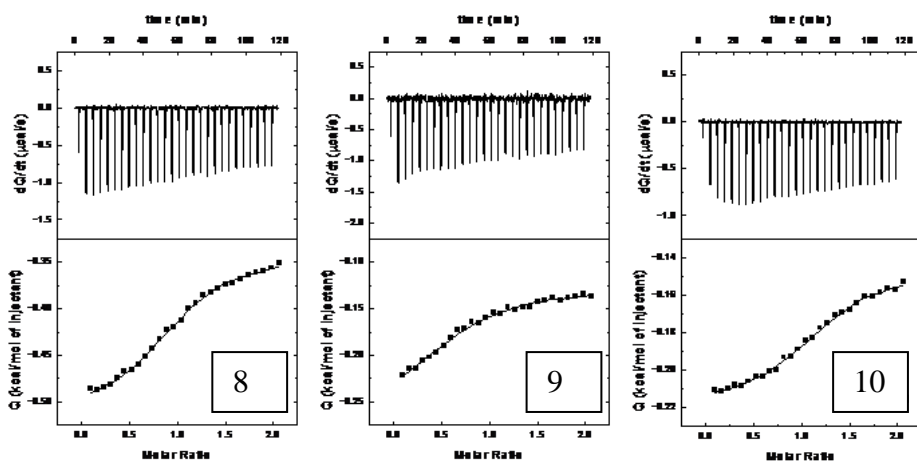
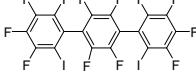
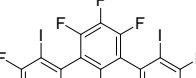
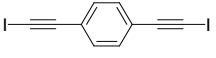


Figure 4.43 Thermograms of the interactions in structures 8, 9 and 10

The binding constants that were determined are one order of magnitude lower than that described for 2',3,3',3'',4,4'',5,5',5'',6'-decafluoro-2,2'',6,6''-tetraiodo-1,1':4',1"-terphenyl and bromide ($K_a = 6.6 \cdot 10^4$) in THF. In this case the entropic part of the binding makes only a minor contribution to the free energy (ΔG°) (see Table 4.12).^[53] In contrast, in the association of iodoimidazolium derivatives, cationic XB donors, with halides, the entropic contribution to the overall free energy of binding plays only a minor role for the neutral XB donors used in this study.^[61b]

The binding constants (translating to free energies ΔG°) and stoichiometric coefficient (N) are shown in Table 4.12 along with the ΔH° and ΔS° values. Remarkably, the entropic term accounts for more than 50% of the overall free energy of binding (ΔG°). The inclusion of the entropy term in these kinds of investigations is crucial, as data based solely on ΔH° values will neglect a substantial proportion of the overall interaction energy.

Table 4.12 ITC data for the interactions in the structures of 8, 9 and 10,

		K _a	ΔG (kJ/mol)	ΔH (kJ/mol)	TΔS (kJ/mol)	n	Ref
	TBABr T 30°	6.2 10 ⁴	-28.2	-33.0	5.2	0.99	[63]
	TOABr T 30°	6.6 10 ⁴	-28.0	-32.4	4.4	0.99	[63]
	TBABr T 30°	1.3 10 ⁴	-23.4	-27.21	3.8	1.33	[63]
	TOABr T 30°	1.9 10 ⁴	-24.8	-27.8	3.3	1.06	[63]
	TBABr	7.9 10 ³	-22.2	-0.8	-21.4	1.2	
	TPABr	2.8 10 ³	-19.7	-0.4	-19.3	1.1	
	DTMABr	8.3 10 ³	-22.2	-0.4	-21.8	1.1	

The titration of **pBIEB** with tetrabutylammonium bromide (TBAB) in THF at room temperature allowed an assessment of the nature and strength of the halogen bonds considered in this chapter.

4.5 Conclusions

In this chapter we have described eleven structures of bis(haloethynyl)benzene halogen bonded complexes with nitrogen, oxygen and halide bases. This information, together with the analysis of Hirshfeld surfaces and quantum chemical calculations, allowed us to establish that **pBIEB**, **pBBrEB** and **mBIEB** are strong ditopic XB donors and this makes them very useful in the supramolecular geometry based design.

The $C_{sp}-I \cdots N$ XB distance depends on the nitrogen atom hybridization and decreases following the trend from sp to sp^3 to sp^2 . In addition, the electronic distribution of the haloethynyl group shows cylindrical nucleophilic areas around the ethynyl and halogen atom and this allows the formation of edge-to-edge $C_{sp^2}-H \cdots X$ and $C_{sp^2}-H \cdots \pi_{(alkyne)}$ hydrogen bonds with a hydrogen of an aromatic ring. This possibility precludes the adoption of a herringbone type organization. The stabilization energy of these supramolecular structures ranges from 2.9 to 5.7 kcal mol⁻¹. In spite of these weak energies, their effects on the crystal structure and packing are relevant and, in combination with strong halogen bonds, they provide a useful strategy for the formation of two-dimensional arrangements in cocrystals with nitrogen and oxygen XB acceptors, which are of great interest in the development of molecular organic materials.

ITC is a useful tool to study halogen bond interactions and this helped us to understand the coordination sphere of, in this case, bromide.

4.6 Experimental

All of the general halogen bond acceptors were used as received from commercial sources. The molecule pBBrEB was synthesized in the same way as pBIEB: N-Bromosuccinimide (4.14 g, 36.2 mmol) and silver nitrate (0.62 g, 3.62 mmol) were added successively to a solution of 1,4-diethynylbenzene (2.28 g 18.1 mmol). The reaction mixture was stirred at 0 °C for 5 h. The crude product was filtered off and washed with diethyl ether. The solvent was removed under reduced pressure. The residue was dissolved in water (50 mL) and extracted with dichloromethane (3×50 mL). The organic layer was dried over Mg_2SO_4 and the solvent was evaporated. The pure product was recovered as yellow solid (5.13 g, 75%).

^1H NMR (300 MHz, CDCl_3): δ 7.38 (s, 4H).

4.6.1 Crystal synthesis and characterization

All crystal syntheses were carried out at ambient temperature in chloroform/dichloromethane in a 1:1 molar ratio.

4.6.2 X-ray monocrystal diffraction.

The crystals are air stable and were mounted on the tip of a glass fiber with epoxy cement. X-ray diffraction experiments were carried out on an Oxford-diffraction Xcalibur S diffractometer. Data were collected at 293 K and 150 K with Mo $\text{K}\alpha$ radiation. The software package CrysAlys was used to process data.

Final cell parameters were obtained by global refinement of reflections obtained from integration of all frames data. The structures were solved by direct methods and refined by the full-matrix method based on F^2 using the SHELXTL program. The non-hydrogen atoms of structures were refined anisotropically, the hydrogen atoms were observed in difference electron density maps and refined isotropically. The crystal parameters and basic information relating data collection and structure refinement for the compounds are summarized in Table 4.13 and Table 4.14.

Table 4.13 Crystal Structure Information section 4.4.

Compound	1	2	3	4	5	6	7	
Emp. formula	C ₂₂ H ₁₄ I ₂ N ₂	C ₂₂ H ₁₄ Br ₂ N ₂	C ₂₂ H ₁₄ I ₂ N ₄	C ₂₇ H ₂₂ I ₂ N ₂	C ₁₆ H ₁₆ I ₂ N ₄	C ₁₄ H ₈ I ₂ N ₂	C ₁₃ H ₁₀ I ₂ O	
Formula weight	560.15	466.17	588.17	628.27	518.13	458.02	436.01	
Crystal system	Triclinic	Triclinic	Monoclinic	Monoclinic	Orthorhombic	Orthorhombic	Monoclinic	
a, Å	7.1304(8)	6.905(3)	19.450(4)	9.9879(4)	9.2510(6)	12.56832(18)	4.2101(2)	
b, Å	8.3566(9)	8.325(4)	20.200(4)	23.8828(7)	7.8618(4)	14.3151(2)	14.0293(7)	
c, Å	8.9642(10)	8.847(4)	17.400(4)	10.9064(4)	23.920(11)	7.96899(12)	11.6962(6)	
α, deg	94.384(2)	93.931(8)	90.0	90.0	90.0	90.0	90.0	
β, deg	108.595(2)	108.073(7)	113.10(3)	111.637(4)	90.0	90.0	90.593(5)	
γ, deg	106.701(2)	106.888(8)	90.0	90.0	90.0	90.0	90.0	
Volume, Å³	476.52(9)	455.5(4)	6288(2)	2418.29(15)	1739.7(8)	1433.76(4)	690.80(6)	
T, K	100(2)	100(2)	100(2)	150(2)	298(2)	100(2)	293(2)	
Space group	P-1	P-1	Cc	P2 ₁ /n	Cmcm	Pnma	P2 ₁ /m	
Z	1	1	12	4	4	4	2	
μ(X Kα), mm⁻¹	3.308	4.456	3.015	2.617	3.617	34.318	4.530	
θ range, deg	2.44 27.55	to 27.53	2.46 26.37	to 26.37	2.92 9485	to 5351	3.40 to 26.37 6.18 to 74.15	2.90 27.16
Refl.	6153	5915	119497			9800		2330
collected Uniq reflect/Rint	2189/0.032 2	2081/0.032 7	12721/0.07 4	4947/0.027 9	968/0.0351	1509/0.0415	1322/ 0.0287	
R1/wR2 [I>2σ]	0.025/0.060	0.025/0.064	0.022/0.042	0.037/0.074	0.024/0.054	0.027/0.067	0.027/0.056	
R1/wR2 (all data)	0.027/0.061	0.027/0.066	0.028/0.043	0.058/0.083	0.039/0.057	0.0284/0.068	0.0350/0.060	
	0.001	0.001	0.003	0.001	0.001	0.001	0.001	
Residual ρ / e Å⁻³			1.110 and - 0.542	0.592 and - 0.599	0.512 and - 0.407	0.853 and - 1.968	0.785 and - 0.799	

Supramolecular chemistry: Crystal engineering

Table 4.14 Crystal Structure information section 4.5.

Compound	8	9	10	11
Emp. formula	C ₂₄ H ₃₄ BrI ₂ N	C ₂₂ H ₃₂ BrI ₂ N	C ₂₆ H ₄₀ BrI ₂ N	C ₃₄ H ₂₄ BrI ₂ P
Formula weight	658.22	644.20	700.30	608.25
Crystal system	Monoclinic	Monoclinic	Monoclinic	Monoclinic
a, Å	7.8843(4)	9.9332(4)	17.9505(8)	9.9983(6)
b, Å	14.5796(6)	8.8016(4)	8.6914(4)	18.5856(12)
c, Å	11.5600(4)	14.5701(7)	18.8483(7)	13.7234(11)
α, deg				
β, deg	97.065(3)	98.374(4)	90.616(4)	97.120(7)
γ, deg				
Volume, Å³	1318.73(10)	1260.25(10)	2940.4(2)	2530.5(3)
T, K	150(2)	150(2)	150(2)	
Space group	P2 ₁ /m	P2/n	P2/c	P2 ₁ /c
z	2	2	4	4
μ(X Kα), mm⁻¹	3.908	4.087	3.510	2.922
θ range, deg	2.95 to 26.37	2.71 to 25.68	2.81 to 24.71	2.90 to 24.71
Refl. collected	5627	6307	42018	8838
Uniq reflect/ Rint	2803 / 0.0410	2394 / 0.0769	5007 / 0.0403	4305 / 0.1055
R1/wR2 [I>2σ]	0.0480 / 0.0937	0.0431 / 0.0628	0.0553 / 0.1564	0.0760 / 0.0988
R1/wR2 (all data)	0.0712 / 0.1070 0.007	0.0943 / 0.0692 0.004	0.0785 / 0.1699 0.005	0.1545 / 0.11341 0.001
Residual ρ/ e Å⁻³	1.134 and -0.893	1.033 and -0.600	1.212 and -1.475	1.160 and -1.058

4.7 Hirshfeld Surfaces

Hirshfeld surfaces and the associated fingerprint plots were calculated using CrystalExplorer,^[43] which accepts a structure input file in the CIF format. Bond lengths to hydrogen atoms were set to typical values (C–H = 1.083 Å, N–H = 1.009 Å, O–H = 0.983 Å). The distance from the Hirshfeld surface to the nearest atoms outside and inside the surface are characterized by the quantities d_e and d_i , respectively, and the normalized contact distance based on these, $d_{norm} = (d_i - r_i^{\text{vdW}}) / r_i^{\text{vdW}} + (d_e - r_e^{\text{vdW}}) / r_e^{\text{vdW}}$, with r_i^{vdW} and r_e^{vdW} being the van der Waals radii of the atoms. The 2D histograms, fingerprint plot distance external to the surface (d_e) versus distance internal to the surface (d_i) is the distance from the surface to the nearest atom in the molecule itself.

4.8 Computational Methods.

Quantum chemical calculations were performed using the Gaussian 09^[64] suite of programs. Geometry optimizations were carried out in the gas phase with the B98^[65] method, employing the 6-311G+(d,p)^[66] basis set for all atoms except iodine, for which the DGDZVP^[67] basis set was used. Geometry optimizations were carried out without constraints, using the default convergence criteria for the Gaussian software. The natural bond orbital (NBO) analysis^[68] using the NBO module contained in the Gaussian 09 program were performed on the basis of the minimized structures in order to calculate the NBO charges. The resulting electronic energies of interaction were corrected for scale (0.9884),^[69] zero point differences and for basis set superposition errors.

4.9 Bibliography

- [1] a) C. B. Aakeröy and N. Schultheiss in *Assembly of Molecular Solids via Non-covalent Interactions, Vol. Making Crystals by Design* Eds.: D. Braga and F. Grepioni), Wiley-VCH verlag GmbH & Co. KGaA, Weinheim, **2007**, pp. 209-240; b) J. Chisholm, E. Pidcock, J. Van De Streek, L. Infantes, S. Motherwell and F. H. Allen, *Crystengcomm* **2006**, 8, 11-28; c) M. J. Zaworotko, *Crystal Growth & Design* **2007**, 7, 4-9; d) J. D. Wuest, *Chem. Comm.* **2005**, 5830-5837.
- [2] G. R. Desiraju, *Angew. Chem. Int. Ed.* **2007**, 46, 8342-8356.
- [3] a) R. W. Troff, T. Makela, F. Topic, A. Valkonen, K. Raatikainen and K. Rissanen, *Eur. J. Org. Chem.* **2013**, 1617-1637; b) L. C. Gilday, S. W. Robinson, T. A. Barendt, M. J. Langton, B. R. Mullaney and P. D. Beer, *Chem. Rev.* **2015**, 115, 7118-7195; c) P. Kratzer, B. Ramming, S. Roemisch and G. Maas, *Crystengcomm* **2015**, 17, 4486-4494; d) K. Bouchmella, B. Boury, S. G. Dutremez and A. van der Lee, *Chem. Eur. J.* **2007**, 13, 6130-6138; e) K. Rissanen, *Crystengcomm* **2008**, 10, 1107-1113; f) N. Busschaert, C. Caltagirone, W. Van Rossom and P. A. Gale, *Chem. Rev.* **2015**, 115, 8038-8155; g) C. B. Aakeroy, N. Schultheiss, J. Desper and C. Moore, *CrystEngComm* **2007**, 9, 421-426; h) A. C. B. Lucassen, M. Vartanian, G. Leitus and M. E. van der Boom, *Cryst. Growth Des.* **2005**, 5, 1671-1673.
- [4] T. Imakubo, T. Shirahata, K. Herve and L. Ouahab, *J. Mat. Chem.* **2006**, 16, 162-173.
- [5] J. E. Anthony in *Engineered Pentacenes, Vol.* Wiley-VCH Verlag GmbH & Co. KGaA, **2006**, pp. 58-74.
- [6] J.-H. Dou, Y.-Q. Zheng, Z.-F. Yao, Z.-A. Yu, T. Lei, X. Shen, X.-Y. Luo, J. Sun, S.-D. Zhang, Y.-F. Ding, G. Han, Y. Yi, J.-Y. Wang and J. Pei, *J. Am. Chem. Soc.* **2015**, 137, 15947-15956.
- [7] A. Putta, J. D. Mottishaw, Z. Wang and H. Sun, *Cryst. Growth Des.* **2014**, 14, 350-356.
- [8] R. B. Walsh, C. W. Padgett, P. Metrangolo, G. Resnati, T. W. Hanks and W. T. Pennington, *Cryst. Growth Des.* **2001**, 1, 165-175.
- [9] D. Cincic, T. Friscic and W. Jones, *Chem. Eur. J.* **2008**, 14, 747-753.
- [10] M. Fourmigue, P. Metrangolo and G. Resnati, *Halogen Bonding Fundamentals and Applications*, **2008**, p.
- [11] a) N. S. Goroff, S. M. Curtis, J. A. Webb, F. W. Fowler and J. W. Lauher, *Org. Lett.* **2005**, 7, 1891-1893; b) A. W. Sun, J. W. Lauher and N. S. Goroff, *Science* **2006**, 312, 1030-1034; c) L. Luo, C. Wilhelm, A. Sun, C. P. Grey, J. W. Lauher and N. S. Goroff, *J. Am. Chem. Soc.* **2008**, 130, 7702-7709; d) C. Wilhelm, S. A. Boyd, S. Chawda, F. W. Fowler, N. S. Goroff, G. P. Halada, C. P. Grey, J. W. Lauher, L. Luo, C. D. Martin, J. B. Parise, C. Tarabrella and J. A. Webb, *J. Am. Chem. Soc.* **2008**, 130, 4415-4420.
- [12] a) A. L. Barres, A. El-Ghayoury, L. V. Zorina, E. Canadell, P. Auban-Senzier and P. Batail, *Chem. Commun.* **2008**, 2194-2196; b) J. Lieffrig, O. Jeannin and M.

Supramolecular chemistry: Crystal engineering

- Fourmigue, *J. Am. Chem. Soc.* **2013**, *135*, 6200-6210; c) E. Bosch, *Cryst. Growth Des.* **2014**, *14*, 126-130; d) K. Eichstaedt, B. Wicher, M. Gdaniec and T. Polonski, *CrystEngComm* **2016**, *18*, 5807-5810.
- [13] C. B. Aakeroy, M. Fasulo, N. Schultheiss, J. Desper and C. Moore, *J. Am. Chem. Soc.* **2007**, *129*, 13772-13773.
- [14] S. Tothadi and G. R. Desiraju, *Chem. Commun.* **2013**, *49*, 7791-7793.
- [15] L. Meazza, J. A. Foster, K. Fucke, P. Metrangolo, G. Resnati and J. W. Steed, *Nature Chem.* **2013**, *5*, 42-47.
- [16] K. Raatikainen and K. Rissanen, *Chem. Sci.* **2012**, *3*, 1235-1239.
- [17] A. Linke, S. H. Jungbauer, S. M. Huber and S. R. Waldvogel, *Chem. Commun.* **2015**, *51*, 2040-2043.
- [18] S. H. Jungbauer, S. M. Walter, S. Schindler, L. Rout, F. Kniep and S. M. Huber, *Chem. Commun.* **2014**, *50*, 6281-6284.
- [19] a) J. L. Syssa-Magale, K. Boubekeur, P. Palvadeau, A. Meerschaut and B. Schollhorn, *CrystEngComm* **2005**, *7*, 302-308; b) C. B. Aakeroy, D. Welideniya, J. Desper and C. Moore, *CrystEngComm* **2014**, *16*, 10203-10209.
- [20] T. Caronna, R. Liantonio, T. A. Logothetis, P. Metrangolo, T. Pilati and G. Resnati, *J. Am. Chem. Soc.* **2004**, *126*, 4500.
- [21] M. Fourmigue, *Curr. Opin., Solid State Mater. Sci.* **2009**, *13*, 36-45.
- [22] R. Bianchi, A. Forni and T. Pilati, *Chemistry – A European Journal* **2003**, *9*, 1631-1638.
- [23] a) D. L. Reger, J. R. Gardnier, S. Bakbak, R. F. Semeniuc, U. H. F. Bunz and M. D. Smith, *New J. Chem.* **2005**, *29*, 1035-1043; b) T. Steiner and M. Tamm, *J. Organomet. Chem.* **1998**, *570*, 235-239.
- [24] a) W. Lu, M. C. W. Chan, N. Zhu, C. M. Che, Z. He and K. Y. Wong, *Chem. Eur. J.* **2003**, *9*, 6155 - 6166; b) A. Holme, K. J. Børve, L. J. Sæthre and T. D. Thomas, *J. Phys. Chem. A* **2013**, *117*, 2007–2019.
- [25] a) C. J. McAdam, S. A. Cameron, L. R. Hanton, A. R. Manning, S. C. Moratti and J. Simpson, *CrystEngComm* **2012**, *14*, 4369–4383; b) Y. Hu, Z. Li, Y. Zhao, Y. Yang, F. Liu and L. Wang, *RSC Adv.* **2015**, *5*, 10275–10289; c) E. Guzmán-Percástegui, J. G. Alvarado-Rodríguez, J. Cruz-Borbolla, N. Andrade-López, R. A. Vázquez-García, R. N. Nava-Galindo and T. Pandiyan, *Cryst. Growth Des.* **2014**, *14*, 3742–3757.
- [26] G. R. Desiraju, *Cryst. Growth Des.* **2011**, *11*, 896–898.
- [27] A. Forni, P. Metrangolo, T. Pilati and G. Resnati, *Cryst. Growth Des.* **2004**, *4*, 291-295.
- [28] A. De Santis, A. Forni, R. Liantonio, P. Metrangolo, T. Pilati and G. Resnati, *Chem. Eur. J.* **2003**, *9*, 3974-3983.
- [29] C. B. Aakeroy, M. Baldrihi, J. Desper, P. Metrangolo and G. Resnati, *Chem. Eur. J.* **2013**, *19*, 16240-16247.
- [30] C. B. Aakeroy, P. D. Chopade and J. Desper, *Cryst. Growth Des.* **2013**, *13*, 4145-4150.
- [31] O. Dumele, D. Wu, N. Trapp, N. Goroff and F. Diederich, *Org. Lett.* **2014**, *16*, 4722–4725.

- [32] J. L. Syssa-Magale, K. Boubeker and B. Schollhorn, *J. Mol. Struct.* **2005**, 737, 103-107.
- [33] C. Perkins, S. Libri, H. Adams and L. Brammer, *CrystEngComm* **2012**, 14, 3033-3038.
- [34] L. Gonzalez, N. Gimeno, R. Maria Tejedor, V. Polo, M. Blanca Ros, S. Uriel and J. Luis Serrano, *Chem. Mat.* **2013**, 25, 4503-4510.
- [35] R. B. Walsh, C. W. Padgett, P. Metrangolo, G. Resnati, T. W. Hanks and W. T. Pennington, *Cryst. Growth Des.* **2001**, 1, 165 - 175.
- [36] O. V. Runarsson, J. Artacho and K. Warnmark, *European J. Org. Chem.* **2012**, 7015-7041.
- [37] E. Bosch, *Cryst. Growth Des.* **2014**, 14, 126.
- [38] a) S. Sergeyev, *Helv. Chim. Acta* **2009**, 92, 415-444; b) B. Dolensky, M. Havlik and V. Kral, *Chem. Soc. Rev.* **2012**, 41, 3839-3858.
- [39] a) X. Du, Y. Sun, B. Tan, Q. Teng, X. Yao, C. Su and W. Wang, *Chem Commun* **2010**, 46, 970-972; b) M. Carta, R. Malpass-Evans, M. Croad, Y. Rogan, J. C. Jansen, P. Bernardo, F. Bazzarelli and N. B. McKeown, *Science* **2013**, 339, 303-307.
- [40] S. Satishkumar and M. Periasamy, *Tetrahedron: Asymmetry* **2006**, 17, 1116–1119.
- [41] J. T. Cross, N. A. Rossi, M. Serafin and K. A. Wheeler, *CrystEngComm* **2014**, 16, 7251.
- [42] S. K. Wolff, D. J. Grimwood, J. J. McKinnon, M. J. Turner, D. Jayatilaka and M. A. Spackman in *CrystalExplorer 3.0*, Vol. (Ed. C. 3.0), University of Western Australia, **2012**.
- [43] M. A. Spackman and D. Jayatilaka, *CrystEngComm* **2009**, 11, 19-32.
- [44] N. H. Evans and P. D. Beer, *Angew. Chem. Int. Ed.* **2014**, 53, 11716-11754.
- [45] a) G. Cavallo, P. Metrangolo, T. Pilati, G. Resnati, M. Sansotera and G. Terraneo, *Chem. Soc. Rev.* **2010**, 39, 3772-3783; b) A. Caballero, N. G. White and P. D. Beer, *Angew. Chem. Int. Ed.* **2011**, 50, 1845-1848; c) A. Caballero, F. Zapata, N. G. White, P. J. Costa, V. Felix and P. D. Beer, *Angew. Chem. Int. Ed.* **2012**, 51, 1876-1880; d) P. Metrangolo, T. Pilati, G. Terraneo, S. Biella and G. Resnati, *CrystEngComm* **2009**, 11, 1187-1196; e) G. Cavallo, S. Biella, J. A. Lu, P. Metrangolo, T. Pilati, G. Resnati and G. Terraneo, *J. Fluorine Chem.* **2010**, 131, 1165-1172.
- [46] A. Abate, S. Biella, G. Cavallo, F. Meyer, H. Neukirch, P. Metrangolo, T. Pilati, G. Resnati and G. Terraneo, *J. Fluorine Chem.* **2009**, 130, 1171-1177.
- [47] H. M. Yamamoto, Y. Kosaka, R. Maeda, J. Yamaura, A. Nakao, T. Nakamura and R. Kato, *ACS Nano* **2008**, 2, 143-155.
- [48] J. Lieffrig, A. G. Niassy, O. Jeannin and M. Fourmigue, *CrystEngComm* **2015**, 17, 50–57.
- [49] J. Grebe, G. Geiseler, K. Harms and K. Dehnicke, *Z. Naturforsch. B Chem. Sci.* **1999**, 54, 77-86.
- [50] A. Abate, J. Marti-Rujas, P. Metrangolo, T. Pilati, G. Resnati and G. Terraneo, *Cryst. Growth Des.* **2011**, 11, 4220-4226.

Supramolecular chemistry: Crystal engineering

- [51] S. Triguero, R. Llusar, V. Polo and M. Fourmigue, *Cryst. Growth Des.* **2008**, *8*, 2241-2247.
- [52] J. Lieffrig, O. Jeannin and M. Fourmigue, *J. Am. Chem. Soc.* **2013**, *135*, 6200.
- [53] S. H. Jungbauer, S. Schindler, E. Herdtweck, S. Keller and S. M. Huber, *Chemistry* **2015**, *21*, 13625-13636.
- [54] A. Abate, J. Marti-Rujas, P. Metrangolo, T. Pilati, G. Resnati and G. Terraneo, *Cryst. Growth Des.* **2011**, *11*, 4220-4226.
- [55] S. C. Nyburg and C. H. Faerman, *Acta Crystallogr., Sect. B: Struct. Commun.* **1985**, *41*, 274-279.
- [56] a) A. Abate, S. Biella, G. Cavallo, F. Meyer, H. Neukirch, P. Metrangolo, T. Pilati, G. Resnati and G. Terraneo, *J. Fluor. Chem.* **2009**, *130*, 1171-1177; b) P. Metrangolo, Y. Carcenac, M. Lahtinen, T. Pilati, K. Rissanen, A. Vij and G. Resnati, *Science* **2009**, *323*, 1461-1464.
- [57] J. J. McKinnon, M. A. Spackman and A. S. Mitchell, *Acta Crystallogr. B* **2004**, *60*, 627-668.
- [58] M. Erdelyi, *Chem. Soc. Rev.* **2012**, *41*, 3547-3557.
- [59] a) A. Velazquez-Campoy and E. Freire, *Nat. Protoc.* **2006**, *1*, 186-191; b) A. Velazquez-Campoy, S. A. Leavitt and E. Freire, *Methods Mol. Biol.* **2015**, *1278*, 183-204.
- [60] A. Arnaud and L. Bouteiller, *Langmuir* **2004**, *20*, 6858-6863.
- [61] a) S. M. Walter, F. Kniep, L. Rout, F. P. Schmidtchen, E. Herdtweck and S. M. Huber, *J. Am. Chem. Soc.* **2012**, *134*, 8507-8512; b) S. Chakraborty, R. Dutta and P. Ghosh, *Chem. Commun.* **2015**, *51*, 14793-14796; c) S. H. Jungbauer and S. M. Huber, *J. Am. Chem. Soc.* **2015**, *137*, 12110-12120.
- [62] R. Tepper, B. Schulze, M. Jager, C. Fribe, D. H. Scharf, H. Gorls and U. S. Schubert, *J. Org. Chem.* **2015**, *80*, 3139-3150.
- [63] S. H. Jungbauer, S. Schindler, E. Herdtweck, S. Keller and S. M. Huber, *Chem. Eur. J.* **2015**, *21*, 13625-13636.
- [64] G. W. T. J. Frisch, H. B. Schlegel, G. E. Scuseria, M. A. Robb, J. R. Cheeseman, G. Scalmani, V. Barone, G. A. Petersson, H. Nakatsuji, X. Li, M. Caricato, A. Marenich, J. Bloino, B. G. Janesko, R. Gomperts, B. Mennucci, H. P. Hratchian, J. V. Ortiz, A. F. Izmaylov, J. L. Sonnenberg, D. Williams-Young, F. Ding, F. Lipparini, F. Egidi, J. Goings, B. Peng, A. Petrone, T. Henderson, D. Ranasinghe, V. G. Zakrzewski, J. Gao, N. Rega, G. Zheng, W. Liang, M. Hada, M. Ehara, K. Toyota, R. Fukuda, J. Hasegawa, M. Ishida, T. Nakajima, Y. Honda, O. Kitao, H. Nakai, T. Vreven, K. Throssell, J. A. Montgomery, Jr., J. E. Peralta, F. Ogliaro, M. Bearpark, J. J. Heyd, E. Brothers, K. N. Kudin, V. N. Staroverov, T. Keith, R. Kobayashi, J. Normand, K. Raghavachari, A. Rendell, J. C. Burant, S. S. Iyengar, J. Tomasi, M. Cossi, J. M. Millam, M. Klene, C. Adamo, R. Cammi, J. W. Ochterski, R. L. Martin, K. Morokuma, O. Farkas, J. B. Foresman, and D. J. Fox, in *Gaussian 09*, Vol. Gaussian Inc., Wallingford CT, **2009**.
- [65] a) P. M. W. Gill, *Mol. Phys.* **1996**, *89*, 433-445; b) J. P. Perdew, K. Burke and M. Ernzerhof, *Phys. Rev. Lett.* **1996**, *77*, 3865-3868.

- [66] W. J. Hehre, L. Radom, S. P. V. R. and J. A. Pople in *Ab initio Molecular Orbital Theory*, Vol. Wiley, New York, **1986**.
- [67] N. Godbout, D. R. Salahub, J. Andzelm and E. Wimmer, *Can. J. Chem.* **1992**, *70*, 560-571.
- [68] A. E. Reed, L. A. Curtiss and F. Weinhold, *Chem. Rev.* **1988**, *88*, 899-926.
- [69] J. P. Merrick, D. Moran and L. Radom, *J. Phys. Chem. A* **2007**, *111*, 11683-11700.

Chapter 5 Liquid Crystals: Promesogenic Calamitic, Bent-core and Discotic Shapes by Halogen Bonding.

5.1 Introduction

Liquid Crystals is an interesting research field that involves both Materials and Life Sciences. The first document dealing with the liquid crystal state appeared in 1888 when F. Reinitzer sent a letter to Professor O. Lehmann describing the mesogenic properties of some cholesterol derivatives. Today this field remains of great interest in the scientific community due to the unique properties of these materials.^[1] Liquid Crystals are known as ‘The Fourth State of the Matter’ and their properties are related to their name. The concept of ‘liquid crystal’ does not seem to be logical. The term seems to suggest that a liquid crystal is an intermediate state between the liquid and the crystal. In fact, Liquid Crystals have some typical properties of a liquid – such as fluidity, inability to support shear, the formation and coalescence of droplets – as well some properties of crystals, such as anisotropy in optical, electrical, and magnetic properties, periodic arrangement of molecules in one spatial direction, etc.^[2] Today Liquid Crystals are ubiquitous and appear in fields as diverse as electrooptic displays, thermometry, optical imaging, nondestructive mechanical testing of materials under stress, bioinspired materials, biotic-abiotic interfaces, dynamic materials, interfacial protein assemblies, mesomorphic lipid assemblies, and polymeric multilayers, amongst others.^[3]

Liquid crystals are part of supramolecular chemistry and, in fact, they represent one example of self-organized structures obtained by spontaneous associations of molecules. In the mesomorphic state shown by these materials, the molecules have different organizations that are stabilized by non-covalent interactions, which are generally weaker forces than, for example, van der Waals forces, π - π interactions, dipolar interactions, H-bonds etc.^[4] Most of the tens of thousands of liquid crystalline compounds described to date are single molecules, but in recent years a growing number of papers dealing with ‘supermolecules’ that form liquid crystals have appeared in the literature. These supermolecules or complexes are formed by the self-assembly of different building blocks by means of weak

Liquid Crystals: Promesogenic Calamitic, Bent-core and Discotic Shapes by Halogen Bonding

interactions in a combination of the two different types of supramolecular approaches: Self-assembly & self-organization. Most of these supramolecular organizations are formed by ionic or H-bonding interactions.^[5]

Taking into account that one of the main objectives of the work described in this doctoral thesis is the study of supramolecular systems based on halogen bonding interactions, we decided to use halogen bonding as an alternative approach to hydrogen bonding to obtain liquid crystalline materials.

Prior to planning the synthesis of specific materials it was necessary to carry out an in-depth review of the literature in this area. A summary of this review is provided in the next section.

5.2 Previous works

Non-covalent interactions (hydrogen bonding, van der Waals forces, π - π interactions, ionic interactions, etc.) have become an extraordinary and versatile tool to generate numerous original and attractive supramolecular architectures and functionalities in different fields. Among them, it is worth highlighting the remarkable evolution of hydrogen bonding from being a curious intermolecular interaction between a hydrogen atom and an electron-rich partner to being a powerful tool for molecular control of protein and DNA chemistry, crystal engineering of solid-state materials and also in soft matter assemblies. Regarding soft materials, the use of hydrogen bonding is quite widespread in the field of liquid crystals, in which it has been successfully used to prepare functional materials with varied mesomorphic organizations.^[6] Although pioneering studies were focused on preparing calamitic and discotic hydrogen-bonded liquid crystals,^[7] bent-shaped liquid crystals have recently been obtained using this strategy.^[8]

An alternative approach to hydrogen bonding (HB) is halogen bonding (XB).^[9] Indeed, a great deal of research has recently been carried out with the aim of understanding and harnessing this type of non-covalent interaction, which involves pairing a halogen atom with an electron-rich partner. Although the halogen bond was described more than 150 years ago,^[10] it was not until the seventies that Hassel highlighted the ability of this interaction to manage self-assembly processes.^[11] During the past decade, many applications of halogen bonding in fields as diverse as crystal engineering, enantiomer separation, biology and supermolecular architectures have been reported and reviewed.^[12] This non-covalent interaction exhibits similar characteristics to HB in directionality and strength and may cooperate with, or prevail over, HB – as mentioned in previous chapters.^[13]

Liquid Crystals: Promesogenic Calamitic, Bent-core and Discotic Shapes by Halogen Bonding

5.2.1 Liquid crystals: Properties and classification

In a liquid crystal the crystallinity or the high order in the structure is reduced and this gives the molecule some degree of mobility. The order in the liquid crystal is dominated by the molecular orientation, i.e., the molecules align parallel to each other to minimize the excluded volume and maximize the attractive intermolecular interactions. In liquid crystalline materials the different properties are dependent on the direction in which they are measured (optical, electric, magnetic and mechanical). Moreover, the mobility of the molecules in the liquid crystal mesophase enables such assemblies to respond to different types of external stimuli and allows ‘self-healing’ of defects.^[6b] All of these properties are strongly related to the molecular structure, which controls the molecular interactions.

Liquid Crystals (LC) can be classified as being either thermotropic, where the liquid crystalline phases are achieved by varying the temperature of the system, or as lyotropic, where variation of the concentration of the constituents in a solvent leads to the liquid crystalline phases.

In thermotropic LCs (discussed in this chapter), on heating the material above its melting point (T_m) the thermal motion of the molecules has increased to such an extent that the material passes from the solid phase to the liquid crystal phase, which is also known as a mesophase. On increasing the temperature further the molecular mobility increases and either less ordered mesophases or the isotropic liquid may be formed.

Liquid crystalline compounds are commonly called ‘mesogenic’ materials and ‘mesomorphism’ describes their ability to form liquid crystal phases. In thermotropic liquid crystals the melting point is defined as the temperature of the transition between the last crystalline organization of the compounds and the first mesophase that appears in the heating process. In this process the transition temperature between the last mesophase observed and the isotropic liquid is known

as the ‘*clearing point*’. In cases where there are intermediate mesophases the transition temperature(s) between these phases are denoted by specifying the name of each phase. When a phase appears in both the heating and the cooling cycle it is named ‘*enantiotropic*’ whereas if the phase only appears in the cooling process due to the occurrence of hysteresis in the crystallization it is named ‘*monotropic*’.

Many factors can determine the mesophase shown by a particular liquid crystal, but one of the most important parameters is the molecular shape. This parameter is also fundamental in the mesophases obtained by supermolecules generated by non-covalent interactions. Depending on the strength of the intramolecular interaction and the intermolecular interaction, the weak interaction dissipates while the stronger interaction remains, but in many cases the liquid crystalline behavior disappears.

Liquid crystals have been classified into different types depending on the molecular shape that generates the liquid crystal mesophase. The most important shapes are calamitic (rod-like), discotic (disc-like) and bent-core liquid crystals.

5.2.1.1 Calamitic mesogens

The molecules have a rod-like shape and their mesophases are denoted as calamitic. The most common liquid crystalline phases observed for calamitic liquid crystals are nematic (N) and smectic (Sm) phases. In the N phase, the molecules have orientational order but are positionally disordered. The molecules are aligned in one common direction, known as the director (n). The smectic A (SmA) phase is formed by molecules that are loosely arranged in layers with no ordering within the layer; the director of the molecules is orthogonal to the layers. In the tilted Smectic phases, such as the smectic C (SmC) phase, the molecules are tilted with respect to the layers (see Figure 5.1).

Liquid Crystals: Promesogenic Calamitic, Bent-core and Discotic Shapes by Halogen Bonding

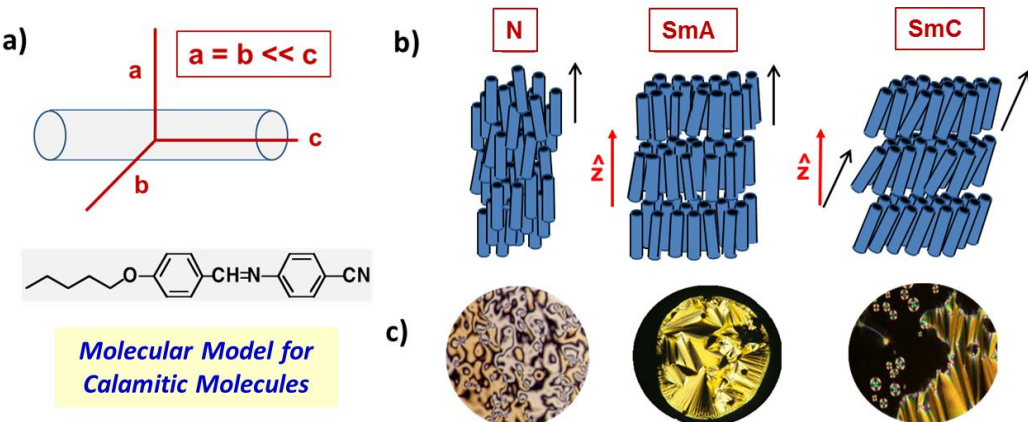


Figure 5.1- Thermotropic calamitic liquid crystal phases. a) Molecular model for a calamitic molecule, b) Molecular arrangements in a nematic, smectic A and smectic C mesophases and c) textures observed for these phases.

The introduction of chirality into mesogenic molecules produces significant changes in the molecular arrangements in the mesophase. This effect is especially remarkable in the nematic and in the tilted smectic phases, which show long range helical molecular order defined by a helical pitch. The chiral nematic phase is also known as the cholesteric phase and the chiral tilted nematic phases are denoted with an asterisk (Sm^*). Some highly ordered smectic phases are no longer considered to be genuine LC phases, but as soft or disordered crystal phases, or as anisotropic plastic crystal phases. These phases are also termed '*crystal smectic phases*' and are denoted by a letter code that refers to their historical classification as an LC smectic phase but without the prefix 'Sm'. In these phases there is long-range (intralayer and/or interlayer) positional order. However, the thermal rotational molecular motion is not completely frozen out, and the alkyl chains are not fully crystallized. The following phases are usually distinguished: crystal B (B and B^*), crystal J (J and J^*), crystal G (G and G^*) crystal E (E), crystal K (K and K^*), and crystal H (H and H^*).

5.2.1.2 Discotic or disc-like mesogens

Discotic mesogens have a disc-like molecular structure, as shown in Figure 5.2.

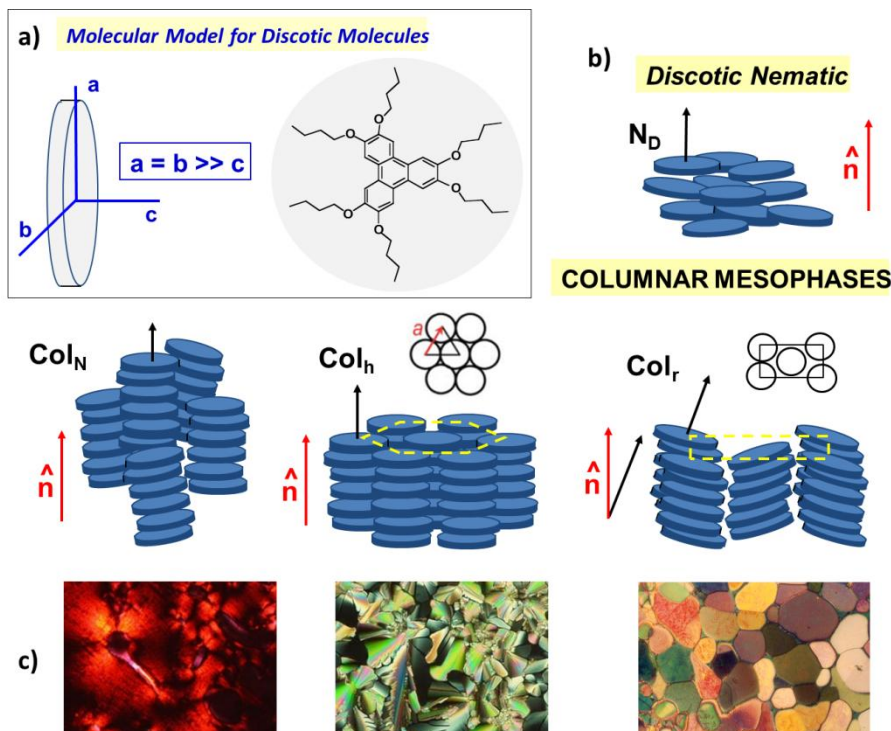


Figure 5.2- Thermotropic discotic liquid crystal phases. a) Molecular model for a discotic molecule, b) Molecular arrangements in a discotic nematic and a columnar nematic, hexagonal and rectangular mesophases and c) textures observed for these phases.

In the most typical cases, the molecules consist of a more or less rigid flat core (usually aromatic) surrounded by at least three flexible chains that make up the ‘soft’ region. The rigid core can also be bowl-like, cone-like, or pyramidal (it can even be a hollow ring). In many cases, individual molecules do not match these criteria, but they are capable of aggregating into units that do fulfill them.

The least ordered discotic phase is the discotic nematic phase. In this phase, the molecules move freely with their short axes in parallel to the director. However, the discotic liquid crystals typically form columnar phases, where the molecules

Liquid Crystals: Promesogenic Calamitic, Bent-core and Discotic Shapes by Halogen Bonding

arrange themselves into columns. Thus, the Columnar Nematic phase does not show long-range order and the columns are arranged in the same way as the molecules in a nematic phase. Other columnar phases with long-range order are classified by their two-dimensional lattices: hexagonal, tetragonal, rectangular, etc. In the columnar hexagonal phase the columns are ordered in a hexagonal lattice with six molecules in the vertex of a hexagon and the other in the center. The columnar rectangular mesophase consists of the stacking of the molecules in columns, which are in turn packed in a rectangular fashion. These phases could also be classified as orthogonal and tilted phases depending on whether the short axis of the disc is parallel or tilted with respect to the director of the phase (see Figure 5.2).

5.2.1.3 Bent-core mesogens

Bent-core mesogens, which are V-shaped or banana-shaped, have attracted interest because of their unique properties, such as the ability to form LC mesophases with super-structural chirality from constituent molecules that are achiral (see Figure 5.3).

The mesophases exhibited by bent-core compounds are similar in some cases to calamitic ones, i.e., nematic and smectic ordering, but new specific banana types can be observed in most cases. The occurrence of this mesophase type is strongly related on the angle between the two arms of the bent-core molecule.

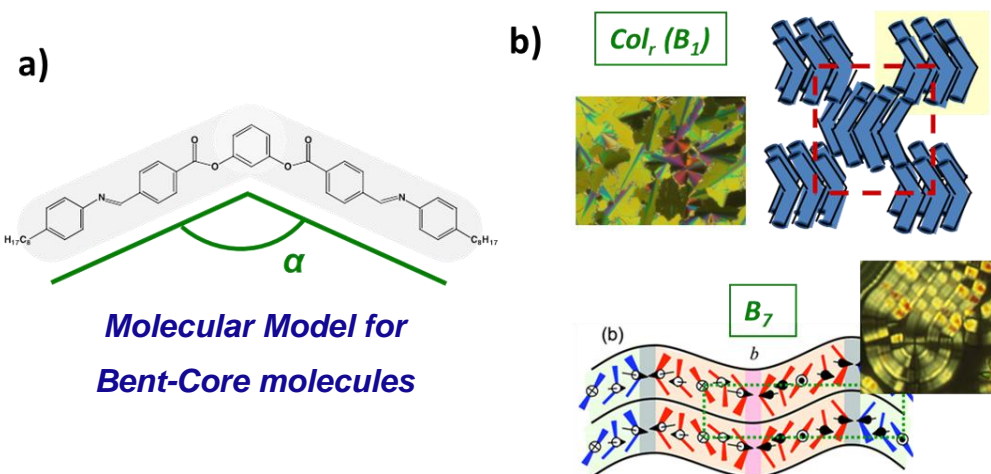


Figure 5.3- Thermotropic bent-core liquid crystal phases. a) Molecular model for a bent-core molecule, b) Molecular arrangements in phases B1 and B7 and textures observed in these phases.

5.2.2 Liquid Crystal Characterization

The characterization of thermotropic liquid crystals is usually carried out by means of Polarized Optical Microscopy (POM) on a microscope equipped with a heating stage, calorimetric studies by Differential Scanning Calorimetry (DSC) or Differential Thermal Analysis (DTA) and by X-ray Diffraction measurements. The characterization of the different mesophases is achieved by observing the microscopic images of the liquid crystals under polarized light, which show characteristic ‘textures’. Many of these textures, which generally arise due to defects that appear within the ordered microdomains that form the mesophases, are characteristic of the specific mesophases and allow their identification. X-ray studies allow the molecular order in the mesophase to be determined. Finally, calorimetric studies provide thermal and thermodynamic parameters and temperatures of the transitions between the phases.

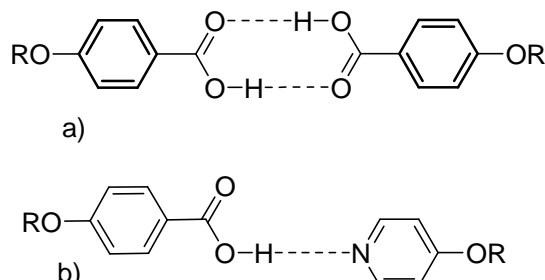
Liquid Crystals: Promesogenic Calamitic, Bent-core and Discotic Shapes by Halogen Bonding

5.2.3 Liquid crystals by hydrogen bonding

Liquids crystals formed by hydrogen bonding are materials that are not mesomorphic in their own right or cause phase behavior that is different to that of the constituents.

The first liquid crystals described as being formed by hydrogen bonding were benzoic acid derivatives. These compounds dimerize through the H-bonding intermolecular interactions as shown in Scheme 5.1a. The variety of mesogenic compounds obtained by hydrogen bonding is very wide and one of the most common supermolecules described involves carboxylic acids and N-pyridyl derivatives (Scheme 5.1b).

The strength of this interaction is evidenced by the fact that formation of the N···H interaction is favored over hydrogen bonds in the benzoic acid dimer. The stability of the hydrogen bond is an important consideration in the study of hydrogen-bonded liquid crystals, particularly in relation to the clearing temperature.^[6b, 7a, 14]



Scheme 5.1 a) Dimer formed by intermolecular hydrogen bonding between a) benzoic acids and b) pyridine derivatives.

Indeed, the formation of mesogenic molecules through HB interactions is favored due to the complementary nature of the interacting components and the directionality of this bond. In fact a large number of H-bonded complexes exhibit liquid crystalline behavior due to a single H-bond.^[15]

5.2.4 Liquid crystals by halogen bonding

In a similar way to the hydrogen bond, halogen bonds have been observed to induce mesomorphic behavior in materials that are not themselves mesomorphic. As occurs with the H-bond, the X-bond also shows high directionality and in order to obtain liquid crystalline behavior the complementary nature of the complex plays a fundamental role. Xu, Bruce and Metrangolo took advantage of the interaction between iodine atoms in perfluorinated benzenes or perfluoralkanes and basic amine/imine nitrogens to prepare mesomorphic species. These complexes, which were prepared as dimeric, trimeric or polymeric species, have an elongated shape that gives rise to calamitic liquid crystals.^[13, 16] Pioneering studies were carried out on halogen-bonded complexes formed by a pyridine-stilbene derivative and a perfluoroiodobenzene molecule. These compounds afforded nematic and smectic A mesophases in all cases. More complex structures were obtained by preparing trimeric materials.

Different flexible or rigid structures bearing two donor positions, i.e., two iodine atoms, have been bonded to two stilbene derivatives and in most cases nematic materials were obtained regardless of the rigidity and linearity of the central unit. Moreover, if ditopic donors and acceptors are employed, polymeric materials are obtained that show only a monotropic nematic phase. In these studies the fluorine atoms improve the electron acceptor ability of both diiodotetrafluorobenzene^[16b, 16g] and diiodoperfluoroalkane^[16d] derivatives. In most of the compounds described by these authors the iodotetrafluorobenzene was used as the XB donor moiety.^[16c]

The first reports on the use of alternative XB motifs were published in 2013 by Mcallister et al.^[17] and Gonzalez et al.^[18] Complexes between N-acceptor alkoxystilbazole derivatives and halogen molecules exhibited unusually large mesophase stability and clearing points above 200 °C. Liquid crystallinity was not observed when I₂ was replaced with Br₂, and the stilbazolium bromide in which one of the ethylenic hydrogens was replaced with bromine was formed.^[17] In

Liquid Crystals: Promesogenic Calamitic, Bent-core and Discotic Shapes by Halogen Bonding

another study,^[19] the alkoxy stilbazole was replaced with an azopyridine to yield photoresponsive liquid crystals. In this case, both I₂ and Br₂ XB donors gave rise to liquid crystalline complexes. This work demonstrated that not only can bromine-based XB donors be used in the successful design of supramolecular LCs but, more surprisingly, dibromine significantly stabilized the mesophase compared to diiodine.

A different approach to improve the complexation ability is to attach an iodine atom to an acetylene unit. Indeed, in the early eighties iodoacetylenes were among the first halogen-bond donors studied in solution in an investigation by Laurence et al.^[20] Despite the fact that iodoacetylenes behave as strong Lewis acids due to the I–C_{sp} bond, they have been largely ignored in supramolecular chemistry until recent applications in the design of conducting organic crystals^[21] and the synthesis of highly organized conjugated polymers^[22] and molecular rotors.^[23]

5.3 Objectives and planning work

5.3.1 Objectives

The **main objective** of the work described in this chapter was:

- To obtain new Liquid Crystals using ‘supermolecules’ formed by means of halogen bonding interactions.

Secondary objectives:

- The design and synthesis of halogen bond donors based on bis(iodoethynyl)benzene derivatives and halogen bond acceptors based on basic nitrogen-containing molecules. These compounds could act as building blocks in the preparation of the supermolecules.

Characterization of the liquid crystal properties and

- A study of the structure-activity relationships for the complexes obtained.

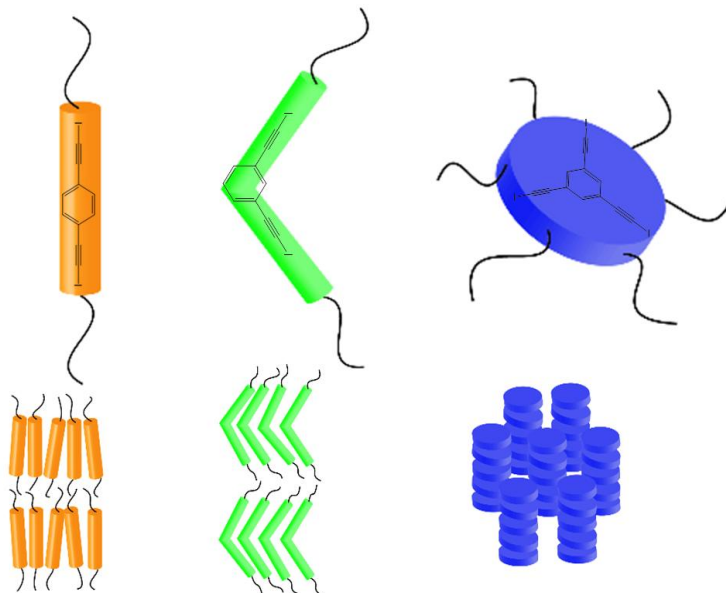
5.3.2 Planned work

In order to achieve the aforementioned aims the use of bis(iodoethynyl)benzene derivatives as XB-donors can favor liquid crystalline arrangements and give rise to mesophases that differ from those described to date for XB complexes.

Three of the five halogen bond donors described in Chapter 2 were selected (see Scheme 5.2 and Table 5.1), two of which were angular (**mBIEB** and **1,3,5-TIEB**) and the other one linear (**pBIEB**). Only the rigid ditopic synthons were selected because they form part of the molecular core and, in most liquid crystals, the rigidity and conjugation of this part favors mesomorphism. The shape of these

Liquid Crystals: Promesogenic Calamitic, Bent-core and Discotic Shapes by Halogen Bonding

iodoacetylene central cores could favor the formation of calamitic discotic and banana liquid crystals.



Scheme 5.2- Different halogen bonding donor mesogen shapes: orange pBIEB, green mBIEB and blue 1,3,5-TIEB.

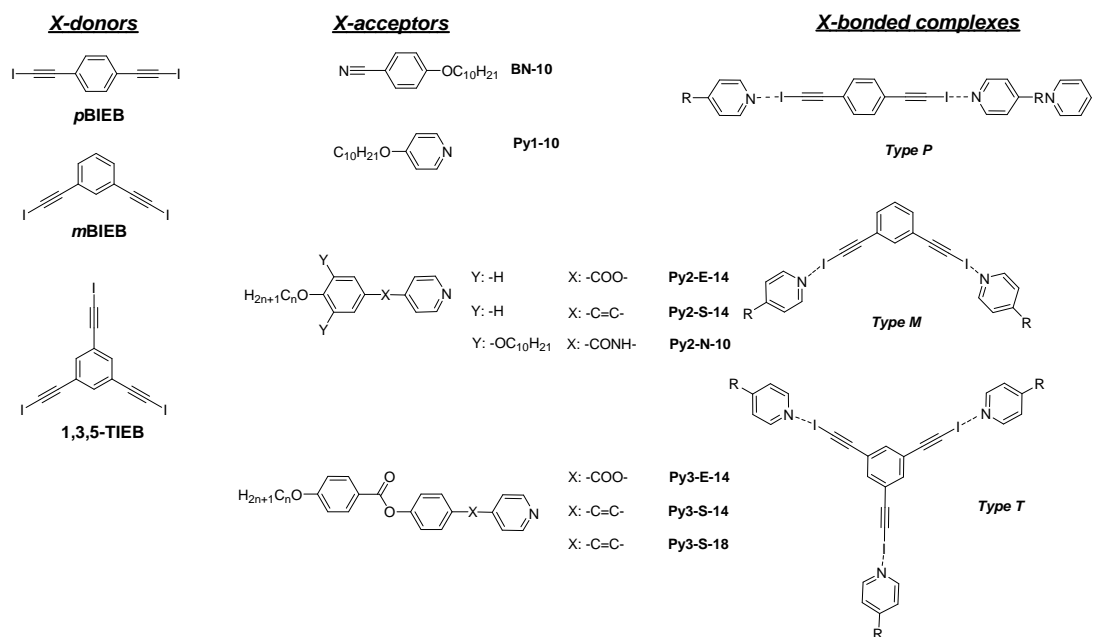
Table 0.1 Halogen bond donor mesogens

Name	Abbreviated name	Electronic parameter	Geometry	Rigidity
1,4-bis(iodoethynyl)benzene	pBIEB	Conjugated	Linear	Rigid
1,3-bis(iodoethynyl)benzene	mBIEB	Conjugated	Angular	Rigid
1,3,5-tris(iodoethynyl)benzene	1,3,5-TIEB	Conjugated	Angular	Rigid

As basic nitrogen-containing molecules that could act as halogen bond acceptors two different types of acceptors were assayed: A benzonitrile derivative with an

Nsp nitrogen atom of a nitrile group (**BN-10**) and seven pyridine derivatives with a Nsp² atom 4-(n-decyloxy)pyridine (**Py1-10**), 4-[2-[4-(n-tetradecyloxy)phenyl]ethenyl]pyridine (**Py2-S-14**), 4-pyridinyl-4-(n-tetradecyloxy)benzoate (**Py2-E-14**), 4-(2-(pyridin-4-yl)vinyl)phenyl-4-(n-tetradecyloxy)benzoate (**Py3-S-14**), 4-(2-(pyridin-4-yl)vinyl)phenyl 4-(n-octadecyloxy)benzoate (**Py3-S-18**), 4-pyridinyl-4-[(4-(n-tetradecyloxy)benzoyl)oxy]benzoate (**Py3-E-14**), 3,4,5-tris(decyloxy)-N-(pyridin-4-yl)benzamide (**Py2-N-10**).

As can be seen in Scheme 5.3, three new series of halogen-bonded complexes based on linear **p**-BIEB (series P), bent **m**-BIEB (series M) and **1,3,5-TIEB** (series T, showing a 3h symmetry) donors have been prepared.



Scheme 5.3- Chemical structures of halogen bonding donors and acceptors used in the promesogenic XB-complexes.

Liquid Crystals: Promesogenic Calamitic, Bent-core and Discotic Shapes by Halogen Bonding

In the series P, M and T trimeric complexes based on one bis-/tris-(iodoethynyl)benzene and two/three nitrile or pyridine derivatives were prepared. Depending on the positions of the iodoethynyl substituents in the donor ring, complexes with three different geometries are expected, i.e., rod-like complexes (for 1,4-substitution), bent-shaped complexes (for 1,3-substitution) and disc-like complexes (for 1,3,5-substitution). These complexes would be expected to give calamitic, bent core and discotic liquid crystalline behavior, respectively.

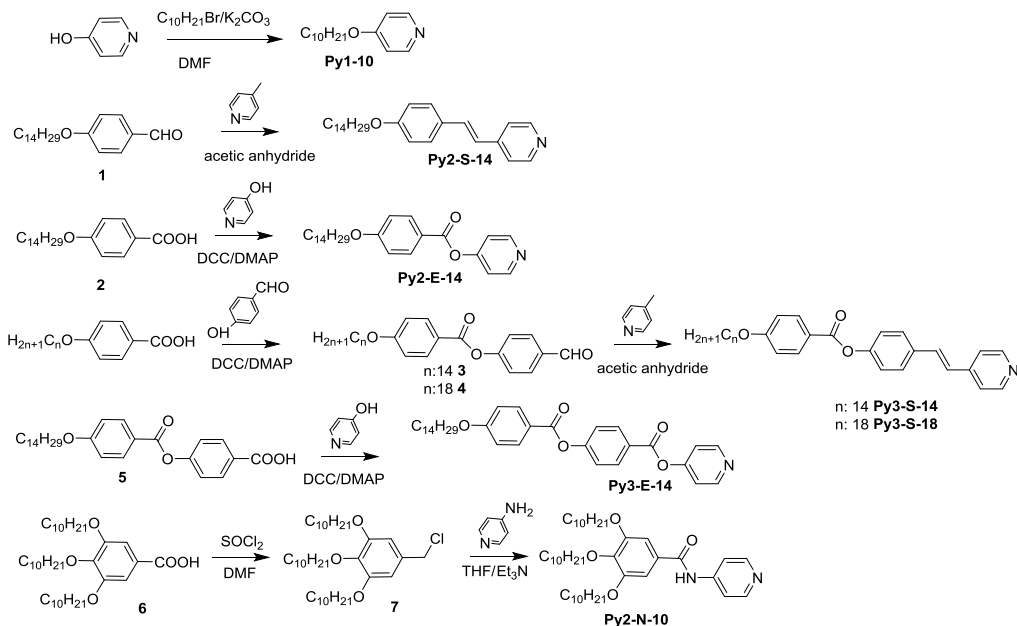
The new halogen-bonded complexes reported here are identified using a notation system that indicates first the XB-donor (P, M or T) and XB-acceptor as denoted in Scheme 5.3. Thus, P-Py3-E-14 is the complex of series P, formed from the XB-donor P and the XB-acceptor Py3-E-14.

5.4 Synthesis and Characterization of the precursors and the complexes

5.4.1 General Synthesis

The general synthetic procedures to prepare the three XB-donors were described in chapter 2.

The synthesis pathways used to prepare the different pyridine derivatives (**Py1-10**, **Py2-E-14**, **Py2-S-14**, **Py3-E-14**, **Py3-S-14**, **Py3-S-18** and **Py2-N-10**) are shown in Scheme 5.4. Compounds **1-7** have been described previously^{[24],[8c, d]} and our data are consistent with those reported.



Scheme 5.4 Synthesis of the XB-Acceptors.

The XB-complexes were obtained according to the method reported by Gimeno et al.^[8a] for the preparation of HB-complexes. XB-complexes were prepared by mixing the two components in a 1:2 or 1:3 stoichiometry in chloroform, followed

Liquid Crystals: Promesogenic Calamitic, Bent-core and Discotic Shapes by Halogen Bonding

by stirring the mixture at room temperature until the solvent had evaporated. The resulting solid was dried under vacuum for two hours at room temperature.

5.4.2 Characterization

Formation of halogen bonding in the complexes was confirmed by several techniques, such as Fourier transform infrared spectroscopy (FT-IR), X-ray photoelectron spectroscopy (XPS), Raman spectroscopy, Isothermal Titration Calorimetry (ITC) and single crystal X-ray diffraction (XRD). The strengths of the bonds were studied by ab initio molecular orbital calculations. Furthermore, the thermal properties of the complexes were studied by polarized optical microscopy (POM), differential scanning calorimetry (DSC), thermogravimetric analysis (TGA) and XRD. In most cases liquid crystalline materials were obtained even if the building blocks were not mesomorphs.

5.4.2.1 FT-IR, Raman and XPS spectroscopy

The formation and strength of halogen-bonding interactions in the neat materials were investigated by FT-IR, Raman and XPS spectroscopies. Intermolecular X-bond formation results in the perturbation of electron density at the associated atoms and subsequently induces a change in the infrared (IR) and Raman vibration frequency and the X-ray photoelectron spectroscopy (XPS) binding energy.

As reported in the case of the pyridine derivatives, up to three characteristic stretching bands appear in the IR spectra in the range $1540\text{--}1640\text{ cm}^{-1}$ and these are related to the pyridine skeleton. Among them, the band at *ca.* 1586 cm^{-1} is known to be the most sensitive, shifting to higher wavenumbers due to interactions, e.g., a large shift to *ca.* 1640 cm^{-1} due to protonation by strong acids, a smaller shift to *ca.* 1620 cm^{-1} due to metal coordination, a relatively small shift to *ca.* 1604 cm^{-1} due to phenolic hydrogen bonding^[25] and a very small shift to *ca.* 1593 cm^{-1} due to halogen bonding.^[16b]

Analysis of the IR spectra of the XB-acceptors and the complexes in the appropriate wavenumber range shows the three characteristic bands of the pyridine skeleton (see Table 5.2). The blue shift of some of these bands in the complexes (with respect to the unbonded XB-acceptors) confirms the formation of the halogen bond. However, some differences that depend on the groups linked to the pyridine ring should be highlighted.

Table 5.2 Infrared absorption of halogen bonding acceptors and complexes in ATR.

	Characteristic bands (cm^{-1})					
Py1-10	1593	Δ	1579	Δ	1569	Δ
P-Py1-10	1599	3	1587	8	1568	-1
M-Py1-10	1601	8	1589	10	1568	-1
Py2-S-14	1607		1588		1576	
P-Py2-S-14	1605	-2	1591	3	1575	-1
M-Py2-S-14	1605	-2	1593	5	1573	-3
Py2-E-14	1605		1583		1577	
P-Py2-E-14	1604	-1	1591	8	1576	-1
M-Py2-E-14	1604	-1	1589	6	1576	-1
Py2-N-10	1514		1501		1493	
P-Py2-N-10	1514	0	1502	-1	1493	0
T-Py2-N-10	1516	2	1504	3	1493	0

* Δ = Complex formed with the halogen bond acceptor

For the stilbene derivatives, only a small blue shift ($2\text{--}4 \text{ cm}^{-1}$) of the central band is observed, which is in accordance with data previously reported for the same type of compound.^[16f] A blue shift of up to $6\text{--}8 \text{ cm}^{-1}$ is observed for the pyridine ester complexes (e.g., from 1583 cm^{-1} in **Py2-E-14** to 1589 cm^{-1} in **M-Py2-E-14** or 1591 cm^{-1} in **P-Py2-E-14**, see Figure 5.4).

Liquid Crystals: Promesogenic Calamitic, Bent-core and Discotic Shapes by Halogen Bonding

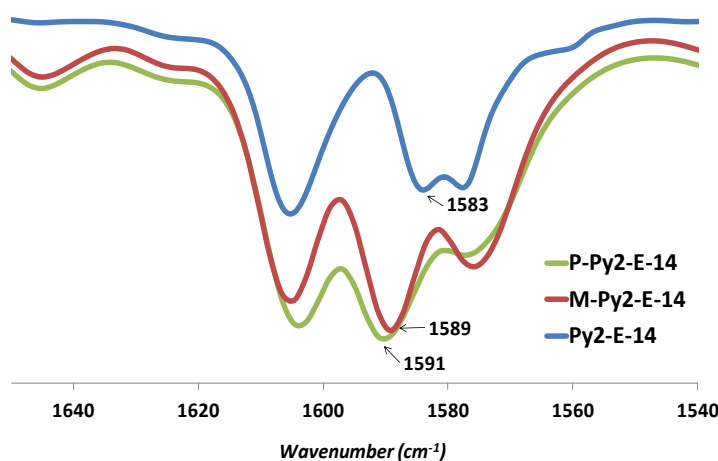


Figure 5.4 FT-IR spectra of Py2-E-14 (blue), P-Py2-E-14 (green) and M-Py2-E-14 (red).

Slightly different behavior was observed for **Py1-10**. In this case, the bands were initially red-shifted with respect to the other pyridine analogs (1593, 1579 and 1569 cm^{-1}) and upon complexation the two bands at higher wavenumber shifted by between 8 and 10 cm^{-1} . Thus, in the case of **M-Py1-10** the bands shifted from 1593 to 1601 cm^{-1} and from 1579 to 1589 cm^{-1} . The bands due to the amide connectors employed were shifted in the range 1480–1530 cm^{-1} . A blue shift of up to 2–3 cm^{-1} was observed for **T-Py2-N-10**. A correlation can be observed between the pyridine band wavenumber in unbonded XB-acceptors and the shift of the same band in the complexes. The band is shifted to a lower wavenumber in the unbonded XB-acceptor band and a larger shift is observed in the corresponding band of the complex. Despite these findings, **P-Py2-N-10** does not show an observable shift and this probably indicates that the interaction does not occur in this case.

Finally, for the complex based on **BN-10** a blue shift (of around 10 cm^{-1}) of the nitrile group stretching mode was observed and this is associated with the formation of halogen bonding between nitrogen and iodine atoms.

XPS is also an effective spectroscopic method to investigate intermolecular interactions, such as ionic and H-bonding interactions, due to changes in binding

energy.^[16b, 26] Thus, we examined and compared the XPS spectra of selected X-bonded complexes and their corresponding unbonded components. The XPS spectra of XB-complexes of series **P** and **M**, with XB-acceptors **Py2-S-14**, **Py3-S-14** and **Py3-S-18**, were compared. The binding energies for the I3d doublet and N1s are gathered in Table 5.3. It was decided to compare this complex because at ambient temperature the other complexes (ester and amide series) are waxy solids.

Table 5.3- Binding energies of N 1s and I 3d of unbonded pBIEB, mBIEB and P2-S-14 and XB-complexes of series P and M.

Complexes	N 1s (eV)	ΔBE_{N1s} (eV)	I 3d (eV)	ΔBE_{I3d} (eV)
<i>pBIEB</i>			618.06	
			629.51	
<i>mBIEB</i>			617.96	
			629.41	
Py2-S-14	394.56			
P-Py2-S-14	395.72	1.16	617.96	-0.10
			629.43	-0.08
P-Py3-S-14	395.69	1.13	617.97	-0.09
			629.43	-0.08
P-Py3-S-18	395.68	1.12	617.87	-0.19
			629.31	-0.20
M-Py2-S-14	395.29	0.73	617.60	-0.36
			629.00	-0.41
M-Py3-S-14	395.60	1.04	617.79	-0.17
			629.25	-0.16
M-Py3-S-18	395.70	1.14	617.75	-0.21
			629.24	-0.17
^a $\Delta BE_{N1s} = BE_{N1s}(\text{complex}) - BE_{N1s}(\text{Py2-S-14});$ $\Delta BE_{I3d} = BE_{I3d}(\text{complex}) - BE_{I3d}(\text{BIB})$				

In all complexes, a shift to lower energy is observed for the I3d doublet signal (from 0.08 to 0.41 eV) and to higher energy for N1s (from 0.73 to 1.16 eV) with respect to the values for the pure compound (See Figure 5.5). These changes are

Liquid Crystals: Promesogenic Calamitic, Bent-core and Discotic Shapes by Halogen Bonding

indicative of halogen bond formation between the constituents. The binding energy shifts of N1s are greater than those described in the literature for similar interactions.^[16b, 26b, 27] The I3d binding energy shifts for the complexes with respect to their corresponding unbonded species (*ca.* 0.14 eV) are smaller than those described in the literature (*ca.* 0.30 eV).^[16b] In order to explain this difference, we calculated the energy of the of halogen bonding between iodine and the carbon-carbon triple bond (-5.1 kcal/mol) present in unbonded pBIEB^[28] (Table 5.3).

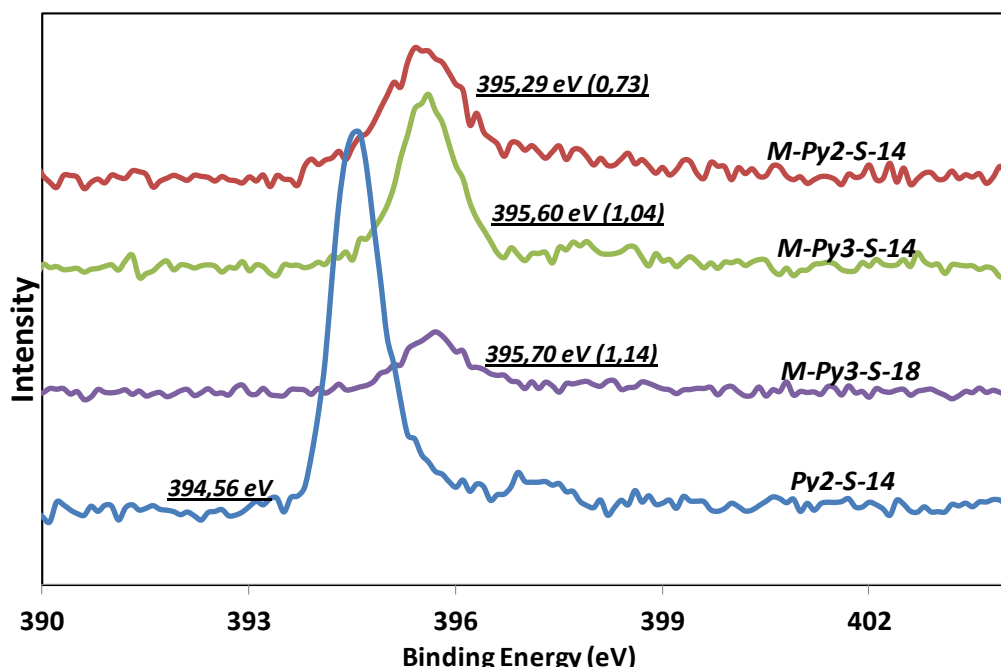


Figure 5.5- N1s core-level X-ray photoelectron spectra of pristine Py2-S-14 (blue) and M-type X-bonded complexes with Py2-S-14 (red), Py3-S-14 (green) and Py3-S-18 (purple).

This value is less than those calculated for the halogen bonded complexes but is similar to values for weaker halogen-bonding interactions. This may explain the differences in the I3d binding energy shifts as iodine in benzene derivatives is not involved in halogen bonding interactions.

The waxy complexes were also characterized by Raman spectroscopy. Unfortunately, although it was possible to carry out this study on each compound isolated, the occurrence of a fluorescence phenomenon in the complexes made Raman characterization difficult. Nevertheless, the appearance of fluorescence in the mixture provides an indirect way to probe the formation of the X-bond.^[29]

The Raman properties of the three halogen bond donors are quite similar (see Figure 5.6). The spectra are characterized by three signals at around 2160, 1600 and 1250 cm^{-1} . Others signals appeared depending on the molecular symmetry: D_{2h} **pBIEB**, C_{2v} **mBIEB** and D_{3h} **1,3,5-TIEB**.

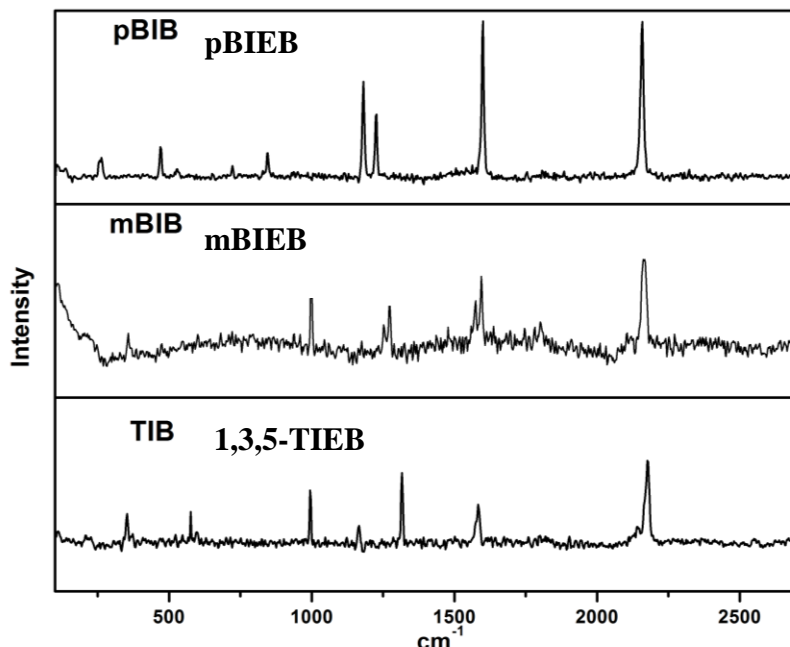


Figure 5.6- Raman spectra of isolated halogen compounds of pBIEB, mBIEB and 1,3,5-TIEB

In the Raman data for the isolated compounds the base line was processed because the spectra show fluorescence. Fluorescence could be induced because the powder forms of the compounds are microcrystalline and, as explained in the first chapter, the halogen bond is present as $\text{C}_{sp}-\text{I}\cdots\pi$.

Liquid Crystals: Promesogenic Calamitic, Bent-core and Discotic Shapes by Halogen Bonding

The Raman spectra of the halogen complexes show fluorescence and the signals are hidden. However, the isolated compounds did not present fluorescence or, in cases where they did, the signals were perceptible (see Figure 5.7).

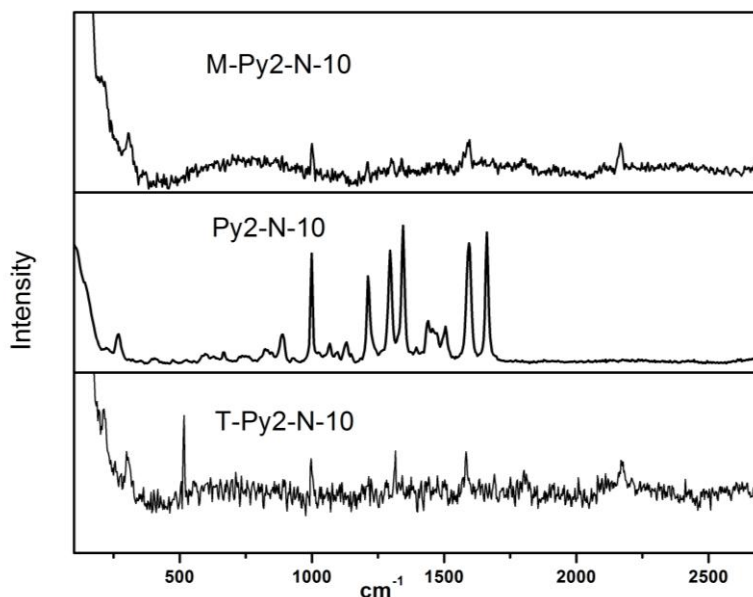


Figure 5.7- Raman spectra of mixtures of compounds and halogen bond acceptor with the base line corrected.

Some small signals can be observed for the mixtures, but these are not particularly meaningful because the fluorescence mitigate.

5.4.2.2 Isothermal titration calorimetry (ITC)

Isothermal titration calorimetry (ITC) measures directly the energy associated with the chemical reaction triggered by the mixing of two components. ITC has been used extensively to study the binding of small molecules to proteins,^[30] but nowadays it is widely employed to investigate the halogen-bond strength of cationic halogen-bond donors toward halides.^[31]

The Raman spectra are not consistent with the expected results and, for this reason, we studied the halogen bond interaction strength with pyridine derivatives by ITC. Measurements were performed as follows: Solutions of halogen bond donor in dry THF were prepared in the range 0.1–0.5 mM. These solutions were then individually titrated with the halogen bond acceptor at 25 °C. The original heat pulses were normalized using reference titrations carried out using the same acceptor solution but with pure solvent, as opposed to a solution containing the donor. The values are provided in Table 5.4, where the data for T-Py2-N-10 correspond to the titration of 1,3,5-TIEB with Py2-N-10 and M-Py2-N-10 to mBIEB with Py2-N-10.

Table 5.4 Association Constant (Kass) and Thermodynamic Parameters for the halogen bond interactions measured by ITC (Isothermal Titration Calorimetry) at 25 °C using the corresponding mixtures.

Data	Syringe XB acceptor	Cell XB donor	Kass (M ⁻¹)	T Kelvin	ΔH° (kJ/mol)	ΔG° (kJ/mol)	TΔS	Solvent	N
T-Py2-N-10	3 (3 mM)	1 (0.1 mM)	6.40E+04	298	2.94E+00	-2.74E+01	-3.04E+01	THF	2,8
M-Py2-N-10	2 (6 mM)	1 (0.3 mM)	2.62E+04	298	4.19E-01	-2.52E+01	-2.56E+01	THF	1,8

The entropy change was obtained by using the standard thermodynamic expression $\Delta G = \Delta H - T\Delta S$ in conjunction with the plots (Figure 5.8) and experimental enthalpy data (results Figure 5.8 below data). The enthalpy values obtained are positive – in contrast with those reported in other references on halogen bonding, mainly with organic salts. In this case, the positive experimental enthalpy may be due to a combination of factors. THF is a polar aprotic solvent and the ligand used is amphiphilic, i.e., it has both hydrophilic and hydrophobic (lipophilic) properties. The high binding affinity is due to the combination of an extremely large positive entropy of solvation (high hydrophobicity) and a minimal loss of conformational entropy (conformationally constrained molecules), which more than compensates for the unfavorable or only slightly favorable binding enthalpy. The ITC technique

Liquid Crystals: Promesogenic Calamitic, Bent-core and Discotic Shapes by Halogen Bonding

is useful to understand the interaction strength and the complex stoichiometry. As can be seen from the results in Table 5.4, N corresponds to the stoichiometry and it is consistent with the expected value.

However, for the sample P-Py2-N-10 it was not possible to find a stoichiometry by ITC. The experiments confirm that the reactants do not interact with one another and consequently the complex is not formed.

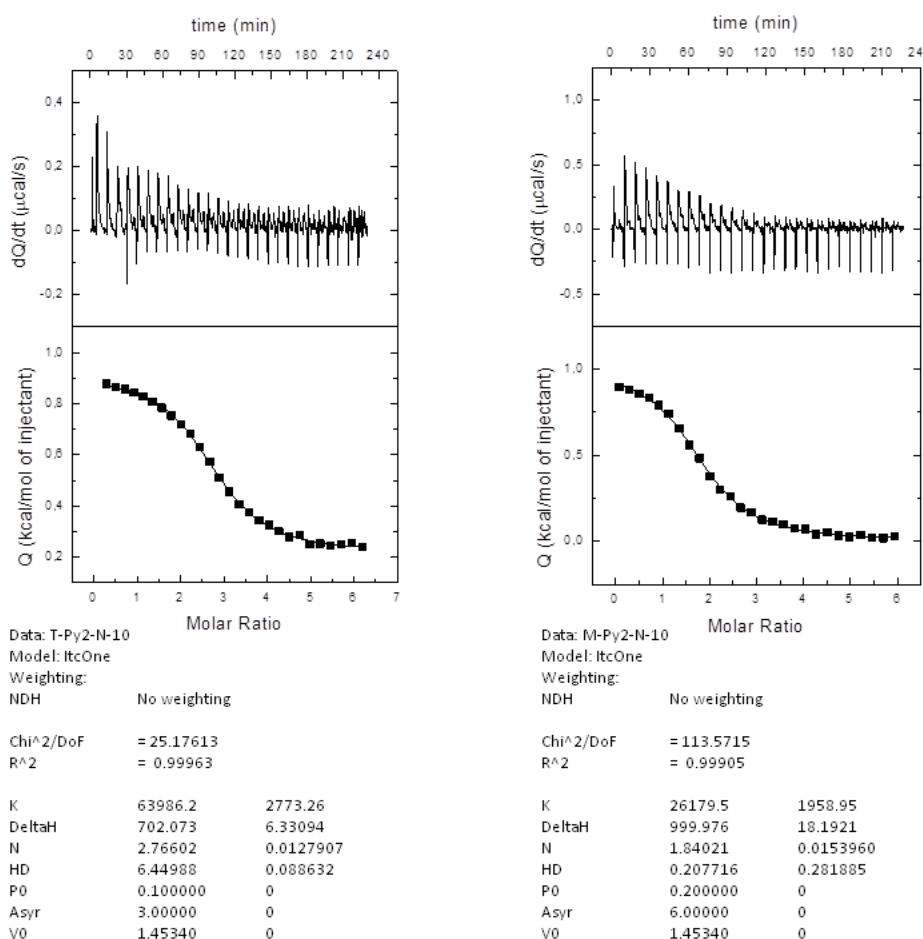


Figure 5.8 Monitored halogen bonding of complexes by Isothermal Titration Calorimetry at 25 °C.

5.5 Liquid crystal properties of the complexes

The thermal properties of the new materials were determined by polarizing optical microscopy (POM), differential scanning calorimetry (DSC), thermogravimetry (TGA) and X-ray diffraction (XRD) in the mesophase. The thermal properties of the XB-donors, XB-acceptors and complexes are gathered in Table 5.5.

Table 5.5 Thermal properties of halogen-bonding donors, acceptors and trimeric halogen-bonded complexes.

Compound / Complex	Phase transition temperature °C [Enthalpy, kJ mol ⁻¹] ^{a,b}
<i>p</i> BIEB	Cr 129 [7.6] I ^c
<i>m</i> BIEB	Cr 88 [12.8] I ^c
1,3,5-TIEB	Cr 141 ^{c,g}
BN-10	Cr 31 [38.2] I
Py1-10	I (rt)
Py2-E-14	Cr 75 [48.0] I
Py2-S-14	Cr 89 [60.9] I
Py2-N-10	Cr 61 [19.1] I
Py3-E-14	Cr 124 [65.8] SmA 139 [6.2] I
Py3-S-14	Cr 108 [44.2] SmA 172 [6.4] I
Py3-S-18	Cr 109 [49.8] SmA 168 [6.4] I
P-Py1-10	Cr 91 CrG 100 [81.7] ^d I
P-Py2-E-14	Cr 87 [18.9] SmB 109 ^e [50.5] I
P-Py2-S-14	Cr 84 [2.6] Cr' 105.3 [3.8] SmG 151.8 [77.9] dec. ^c
M-Py1-10	Cr 53 [52.5] I
M-Py2-E-14	Cr 68 [70.9] I
M-Py2-S-14	Cr 111 [87.5] I
M-Py3-E-14	Cr 120 [93.0] SmAP ^f 133 [5.4] I
M-Py3-S-14	Cr 107 [61.1] SmAP ^f 159 I. ^{c,g}
M-Py3-S-18	Cr 101 [100.2] SmAP ^f 164 [12.6] I
T-Py2-N-10	Cr -8 Colr

^a Onset values for transitions observed in the second scan at 10 °C min⁻¹. ^b Cr: crystalline phase, SmB: smectic B phase, CrG: crystal G phase, SmAP: smectic A polar-like phase, I: isotropic liquid. ^c First scan data as the sample decomposed on reaching the isotropic liquid. ^d Combined enthalpy of two transitions. ^e Maximum of a broad peak. ^f Lamellar orthogonal polar mesophase similar to liquid crystal phases reported for bent-core compounds. ^g Enthalpy could not be measured due to decomposition of the sample.

Liquid Crystals: Promesogenic Calamitic, Bent-core and Discotic Shapes by Halogen Bonding

All of the XB-complexes were first studied by POM. The solid samples should melt cleanly without the appearance of biphasic regions, which would indicate the presence of nonstoichiometric complexes. Unfortunately, all attempts to prepare suitable samples of complexes P-BN-10 and P-Py2-N-10 were unsuccessful and only inhomogeneous samples were obtained.

All of the building blocks – both XB-donors and XB-acceptors – are either liquids or crystalline solids, except for the pyridine derivatives containing three aromatic rings, which show a SmA mesophase. It can be seen that in all cases, i.e., the amide, ester and stilbene derivatives, at least three aromatic rings are needed to induce mesomorphism. The complex formed with promesogenic units bearing only two aromatic rings are not liquid crystals. On the other hand, if we compare three-ring systems, the stilbene derivatives promote stronger stabilization of the SmA mesophase in comparison with the ester or amide analogs. This may be due to the stilbene derivatives preferentially adopting a flat conformation, in contrast to the other derivatives.

Regarding the complexes, the mesomorphic behavior depends strongly on the type of XB-donor used. Complexes in series P preferentially showed calamitic mesophases. In this case, mesomorphism is already favored by short acceptors, either with one or two aromatic rings. All of the complexes with longer acceptors (three aromatic rings) were liquid crystalline materials that decomposed before reaching the isotropic liquid. However, for Type M materials, mesomorphism was only observed for the longest XB-acceptors, i.e. those bearing at least seven aromatic rings in the complex. For series T only amides were employed to form complexes, because it was expected that π -stacking would be favored. Some representative DSC curves are gathered in Figure 5.9.

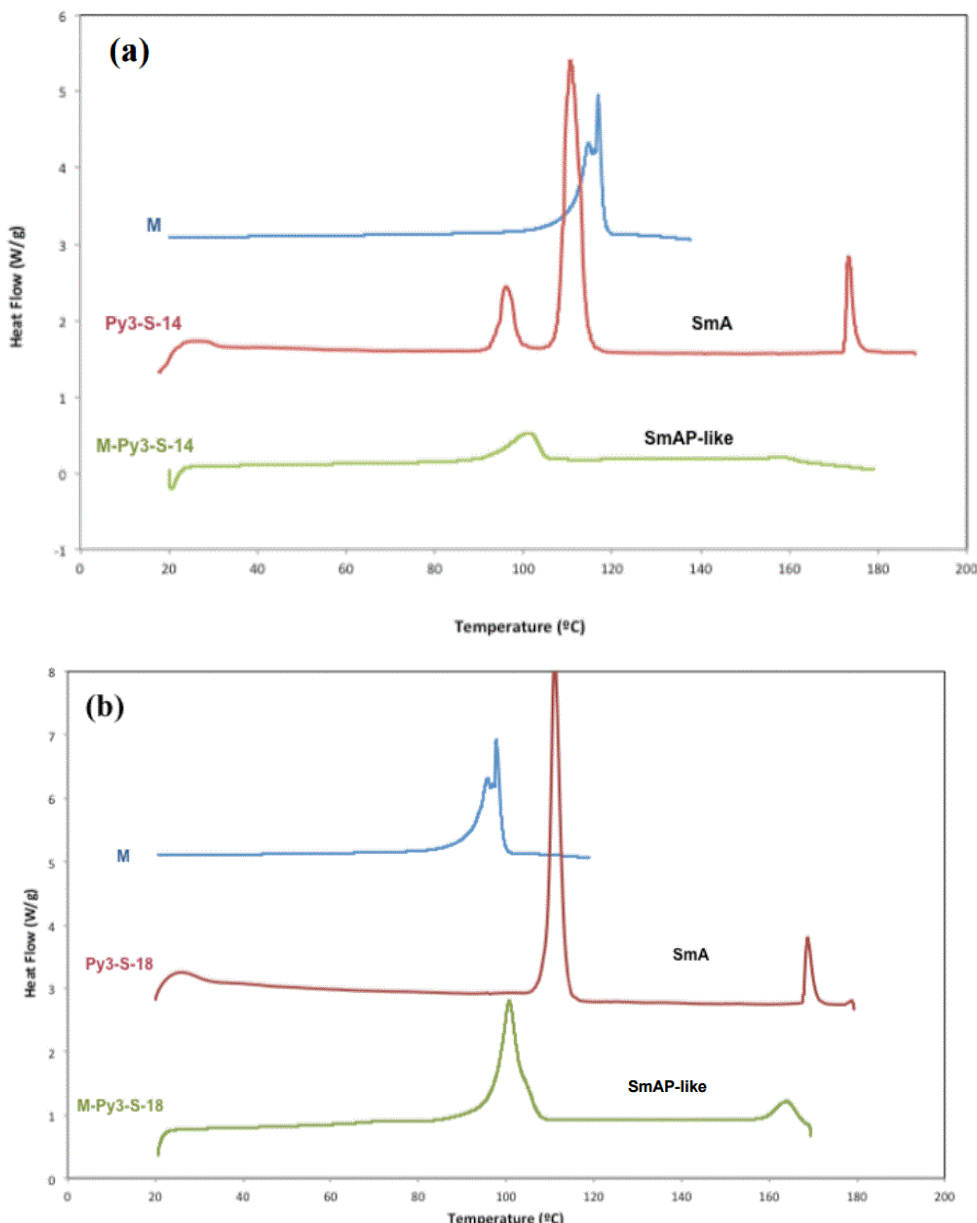


Figure 5.9- DSC Thermograms of first heating scans at 10 °C/min for (a) M, Py3-S-14 and M-Py3-S-14 and (b) M, Py3-S-18 and M-Py3-S-18.

In the next section a detailed explanation of the mesogenic behavior of the different series of complexes is provided.

5.5.1 Series P (rod-like structures)

The three complexes of this series are mesomorphs. Indeed, complexes **P-Py1-10**, **P-Py2-E-14** and **P-Py2-S-14**, with 3 or 5 aromatic rings, showed highly ordered mesophases. To date, most of the liquid crystals based on halogen bonds have only shown low order calamitic mesophases such as nematic and smectic A.^[16b, 16g]

The mesophase of the shortest compound, **P-Py1-10**, was assigned as crystal G as it showed the characteristic texture of this phase (dendritic growth of elongated platelets that are rectangular in shape) (Figure 5.10 (left)).^[28] This phase is highly viscous and showed an X-ray pattern with several sharp peaks that are characteristic of the high order of this phase. The same type of mesophase was assigned for complex **P-Py2-S-14** due to the similar textures observed by POM. In this case, a rapid cooling process from the isotropic liquid was carried out in order to minimize decomposition of the sample.

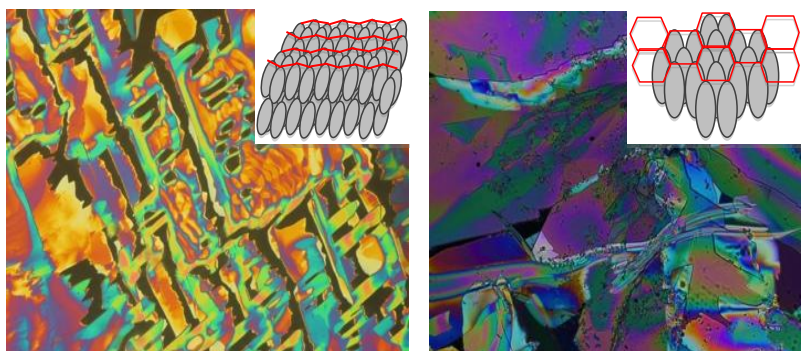


Figure 5.10- Optical textures of: (left) CrG phase of **P-Py1-10** at 86 °C, (right) SmB phase of **P-Py2-E-14** at 108 °C.

In contrast to the above, the other complex (**P-Py2-E-14**) showed a different mosaic texture, which in this case is assigned to a SmB mesophase (Figure 5.10 (right)).^[32] The crystalline nature of this phase was also confirmed by XRD, which showed two sharp reflections (Figure 5.11) and the absence of a diffuse halo.

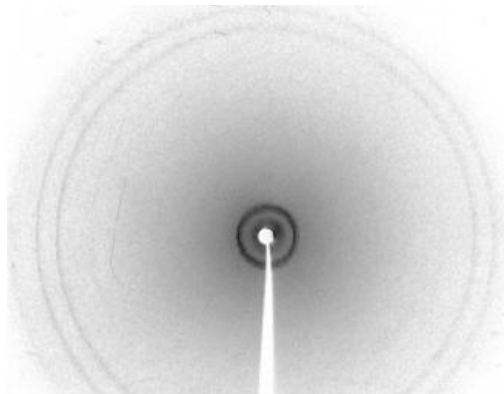


Figure 5.11-. X-ray diffractogram of the XB complex P-Py2-E-14 in the SmB phase at 95 °C.

Both SmB and crystal G are highly ordered phases that are more ordered than the SmA mesophase found in the XB-acceptors. In particular, in the SmB phase the molecules exhibit hexagonal ordering within the orthogonal layers. In contrast, the crystal G phase is one of the so-called tilted soft crystal phases. This phase is even more ordered and shows long-range positional order in three dimensions, with the molecules tilted within the layers. Such high order arrangements are quite common in rod-like hydrogen-bonded complexes.^[33] Furthermore, it has been claimed that these compounds have attractive optical applications,^[34] for example as hosts in highly ordered host-guest systems for polarizers.

5.5.2 Series M (bent-shaped structures)

Seven complexes bearing ***mBIEB*** as the XB-donor were prepared and characterized. However, only the longest compounds, which contain seven aromatic rings, afforded mesomorphic materials. The other materials, with either three (**M-Py1-10**) or five (**M-Py2-E-14** and **M-Py2-S-14**) aromatic rings, did not show any liquid crystalline phases. Regarding seven-ring systems, those based on stilbene receptors (**M-Py3-S-14** and **M-Py3-S-18**) showed wide mesophase ranges at relatively high temperatures. Even in cases where the textures observed in the heating process were not clear, XRD experiments allowed us to assign the type of

Liquid Crystals: Promesogenic Calamitic, Bent-core and Discotic Shapes by Halogen Bonding

mesophase. Up to two sharp reflections in the small-angle region and a diffuse halo in the wide-angle region were detected, thus confirming the mesomorphic nature of the phase. (See Figure 4.12)

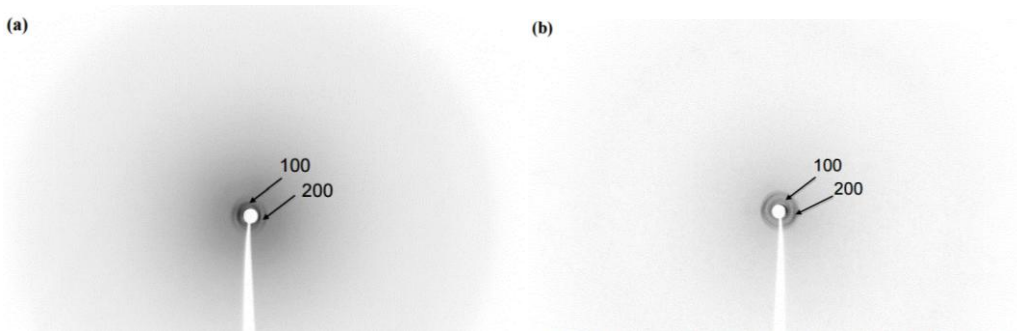


Figure 5.12- X-ray diffractograms of the XB complex M-Py3-S-18 in the SmAP-like mesophase (a) at 120 °C and (b) at room temperature after rapid cooling from the mesophase temperature. Two sharp reflections in the low angle region are observed.

The presence of two or more reflections is not common in classical SmA phases but is usually found in XRD diffractograms of the SmAP phase, which was recently found in bent-core liquid crystals (see Figure 5.12). Moreover, layer spacings of 79.2 Å and 89.6 Å were measured for **M-Py3-S-14** and **M-Py3-S-18**, respectively. These values are in the range of the molecular lengths calculated theoretically using Chemsketch (84 and 92 Å) for the trimeric complexes in all-trans conformations, indicating an orthogonal arrangement of the molecules within the mesophase and hence an orthogonal mesophase. In addition, these values are much higher than the layer spacings measured for the corresponding X-B acceptors **Py3-S-14** and **Py-3-S-18** in the SmA phase (38.5 Å and 44.6 Å, respectively) (Figure 5.13).

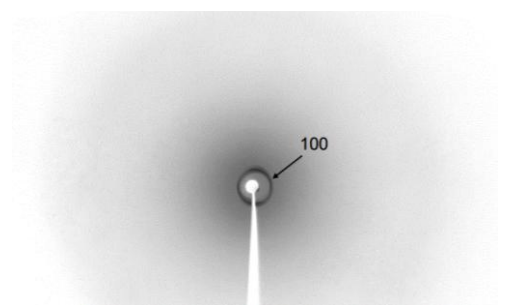


Figure 5.13- X-ray diffractogram of the XB donor Py3-S-18 at 140 °C in the SmA.

Decomposition of the material on reaching the isotropic state precluded further observation of the textures or study under an electric field. A higher stability was observed in the case of the complex **M-Py3-E-14**, which contains an ester linking unit. Interestingly, this structural change again induced significant destabilization of the mesophase and led to lower clearing temperatures and a narrow mesophase range. However, this characteristic did enable us to study the material in the cooling process, with a typical fan-shaped texture observed with homeotropic zones. This texture is characteristic of the SmA phase (Figure 5.14).

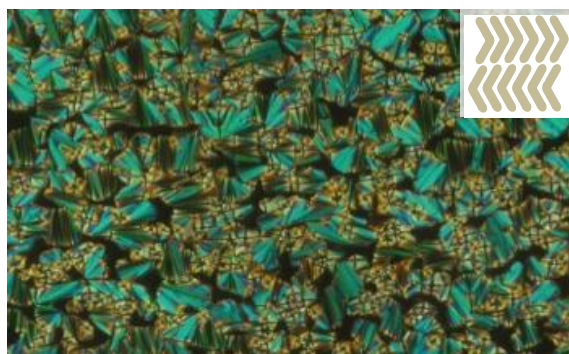


Figure 5.14- Fan-shaped optical texture and proposed orthogonal arrangement of the SmAP-like mesophase exhibited by complex M-Py2-E-14 at 131 °C. Black areas correspond to homeotropic regions of the sample.

It was possible to fill 5-μm ITO (indium tin oxide)-coated cells in order to study the behavior of the compounds under electric fields. Even when the material

Liquid Crystals: Promesogenic Calamitic, Bent-core and Discotic Shapes by Halogen Bonding

showed some instability under high electric fields, upon the application of moderate voltages, molecular switching could be detected, thus indicating polar organization in the material. A peak was not observed in the polarization current curve, probably due to the low stability of the sample. Nevertheless, based on these results and the XRD data, which suggest a compact packing, we identified the mesophase as a SmAP-like mesophase.^[35] The SmAP phase is a polar variation of the SmA phase. This polar orthogonal phase was first reported for a bent-shaped molecule in 2001.^[32] Several variations of this polar non-tilted phase have since been reported (SmAP_R, SmAP_{AR}, SmA_dP_A etc.)^[33-36] and they are still a topic of intensive study. The good alignment observed for SmAP mesophases together with the fast response of this phase under electric fields has confirmed them as promising candidates for display applications.

5.5.3 Series T (disc-like structures)

In the MOP studies the complex in the first heating cycle gives an amorphous texture (see Figure 5.15). Logically this texture disappears when the isotropic liquid state is reached and it is not observed again in successive scans. In the second heating scan the complex appears completely black (homeotropic texture) under the microscope, which may indicate that the columns are aligned parallel to the polarized plane of the light.

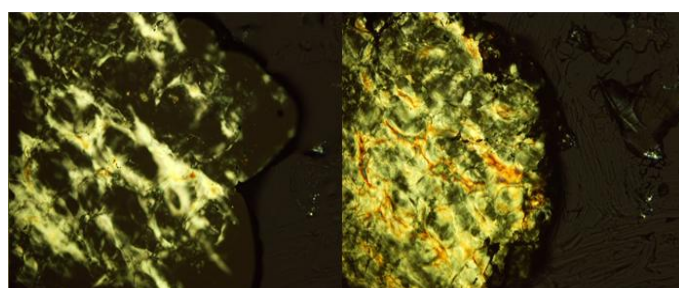


Figure 5.15- MOP textures observed before reaching the isotropic liquid (left) and the virgin mixture (right).

The DSC data confirmed that a new compound was formed. It can be seen from Figure 5.16 (the second heating cycle) that compound **Py2-N-10** presents a characteristic enthalpy peak that was not observed for the mixture. The mixture, **T-Py2-10**, nevertheless, has a Tg very close to 0 °C. This Tg was confirmed by two experiments carried out at different rates, 10 °C/min and 20 °C/min.

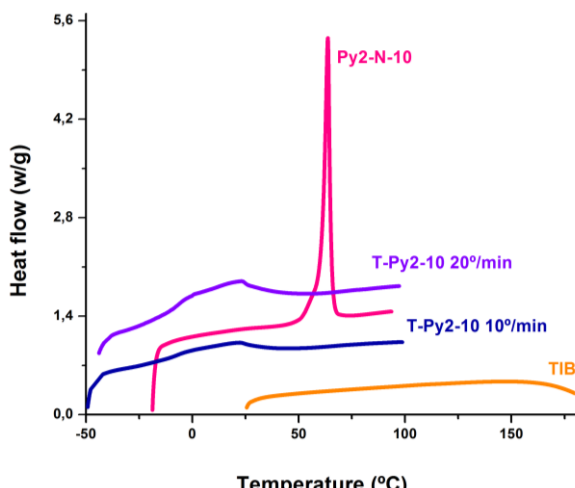


Figure 5.16- Thermogram for the second heating scan at 10 °C/min.

XRD experiments allowed us to assign the type of mesophase. Two sharp reflections were observed in the small-angle region (Figure 5.17) and three diffuse haloes in the wide-angle region were detected, thus confirming the Colr mesomorphic nature of the phase.

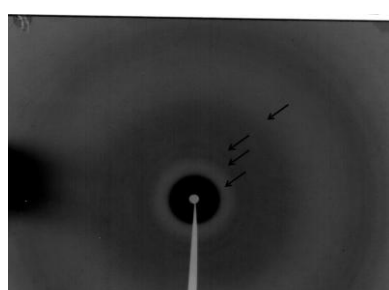


Figure 5.17. X-ray diffraction pattern at ambient temperature without previous treatment.

Liquid Crystals: Promesogenic Calamitic, Bent-core and Discotic Shapes by Halogen Bonding

Two strong peaks in the small angle region are characteristic of a rectangular columnar phase and the other three weak peaks observed in the small angle region can be indexed for a rectangular lattice. In this case the lattice parameters measured were $a = 82.10 \text{ \AA}$ and $b = 39.00 \text{ \AA}$ (Figure 5.18). A schematic model of a tilted columnar rectangular phase are represented in figure 5.19.

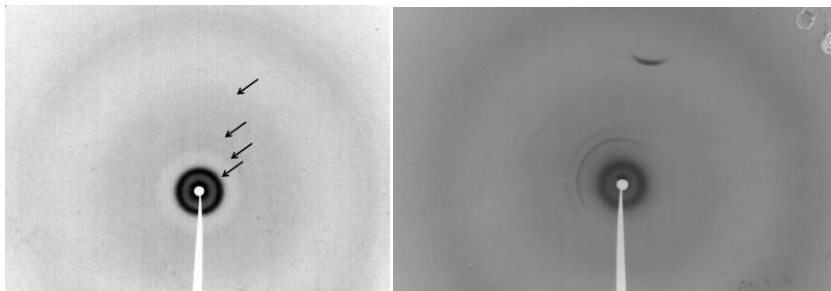


Figure 5.18. X-ray diffraction patterns at ambient temperature after heating to 80 °C and rapid cooling. 3 hours (left) and 8 hours (right).

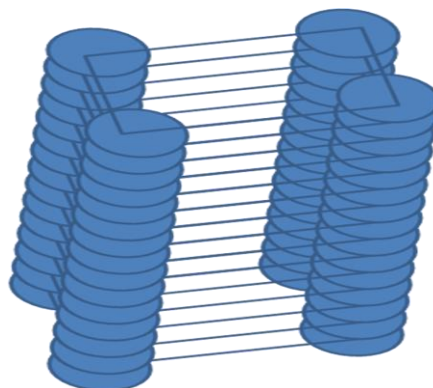


Figure 5.19. Columnar rectangular schematic example.

5.6 Crystal and Molecular Structure

In an effort to gain a better understanding of the different abilities of these series of complexes to form liquid crystal phases, further studies on some HB-complexes were carried out. The crystalline packing of **P-Py1-10** and **P-BN-10** was studied and modelling approaches were applied to simpler analogs (**P-Py1-1**, **M-Py1-1** and **P-BN-1**).

Complexes **P-Py1-10** and **P-BN-10** crystallize in a triclinic system and their structures were solved in the centrosymmetric space group P-1. Crystallographic data for complexes **P-Py1-10** and **P-BN-10** are gathered in Table 5.7 at the end of this chapter. The asymmetric unit contains a molecule of nitrogen base and a half-molecule of **pBIEB**, the center of which is located at an inversion center. The alkoxy chains adopt a perfect all-trans linear arrangement and are coplanar with the aromatic rings. The bond distances and angles of **pBIEB** are similar to those described for unbonded **pBIEB**^[28] and small differences will be discussed in terms of X bonds.

The **pBIEB** acts as a bidentate XB-donor and is pinned to its binding sites by two nitrogen bases, which in turn act as monodentate electron-donors (Figure 5.20). The distance between the nitrogen and the iodine is 2.757 Å in **P-Py1-10** and 2.946 Å in **P-BN-10**. These distances correspond to a reduction by approximately 22% and 16%, respectively, of the sum of the van der Waals' radii of N and I (3.53 Å). The N···I–C angles are almost linear (172.9 and 176.4°, respectively). These experimental values match very well with the calculated distances and angles (Table 5.6). The longest N···I distance in **P-BN-10** indicates a lower strength for the non-covalent interaction. The difference between halogen bonding angles may be attributed to the steric hindrance – the nitrile group is less hindered as it is easier to approach by the most favorable direction. Angles found in other crystal structures of diiodotetrafluorobenzene trimeric complexes are in the range 171.2–176.7°.^[16g]

Liquid Crystals: Promesogenic Calamitic, Bent-core and Discotic Shapes by Halogen Bonding

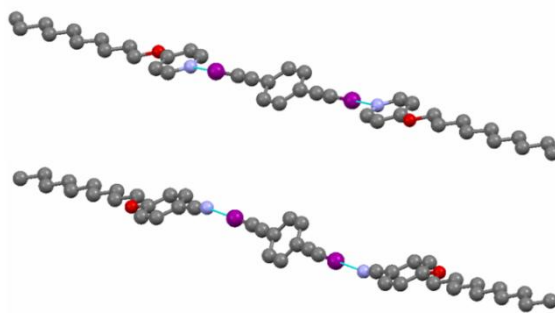


Figure 5.20- X-ray structures of trimeric **P-Py1-10** and **P-BN-10** halogen-bonded complexes. Hydrogen atoms have been omitted for clarity.

Table 5.6- Absolute energies of the XB-donors, XB-acceptors and complexes (E_{au}); interaction energies (ΔE_{int}), basis set superposition errors (BSSE), halogen bonding distances ($D_{I...N}$) and angles ($Z_{C-I...N}$) of the complexes.^a

Partner/Complex	ΔE_{int} kcal/mol	BSSE kcal/mol	$D_{I...N}$ Å	D_{C-I} Å	$Z_{C-I...N}$ deg	q_N e	q_I e	$V_{s,min}$ kcal/mol	$V_{s,max}$ kcal/mol
Py1-1						-0.468		-31.0	
BN-1						-0.317		-33.7	
p-BIB				1.999			0.352		24.6
m-BIB				2.000			0.350		24.7
P-Py1-1	-20.0	1.9	2.906	2.028	179.9	-0.517	0.346		
M-Py1-1	-20.0	1.7	2.890	2.029	178.6	-0.518	0.342		
P-BN-1	-15.0	1.1	3.095	2.012	179.2	-0.370	0.368		
Complex p-BIB	-5.1	1.7							

^aBond length of the C–I bond and NBO charges of N, q_N, and I, q_I, of the partners and complexes. Partners and complexes optimized at the B98/6-311+G(d,p)-DGDZVP level of theory.

In the structure of **P-Py1-10** the pyridine rings are coplanar and twisted with respect to the **pBIEB** plane by 20.6°. The trimers are held together in the plane of the pyridine rings by weak intermolecular C_{Ar}–H⋯H–C_{Alk} contacts (2.38 Å), which give rise to ribbons. The alkyl chains of ribbons interdigitate to form parallel planes that are 3.2 Å apart. The supramolecular arrangement in **P-BN-10** is quite similar to that described for **P-Py1-10**. In this case the benzonitrile rings that form the trimer are staggered (1.5 Å) and rotated (32.5°) with respect to the central **pBIEB** ring and, finally, the distance between parallel planes is 3.7 Å.

These data, and in particular the longer N···I distance for **P-BN-10** (2.946(1) Å versus 2.757(1) Å for **P-Py1-10**, showing weaker non-covalent interactions in the former) support the differences between these two types of complexes in terms of their mesomorphic properties.

5.7 Theoretical modeling

In order to verify theoretically the occurrence, nature and strength of the halogen-bonding interactions, the complexes **P-Py1-1**, **M-Py1-1** and **P-BN-1** were considered as model systems, with the decyloxy substituents replaced by methoxy groups. Complex **pBIEB** was also optimized in order to evaluate the interaction between the iodine and the π -electrons of the carbon-carbon triple bond. The calculations were carried out using the B98 exchange and correlation functional combined with the DGDZVP basis set for iodine and the 6-311+G (d,p) basis set for the other atoms. All structures were geometrically optimized in gas-phase conditions and characterized using frequency analysis. The electrostatic potential of the complex partners **4-methoxypyridine (Py1-1)** and **1,4-methoxybenzonitrile (BN-1)**, **pBIEB** and **mBIEB** are shown in Figure 5.21.

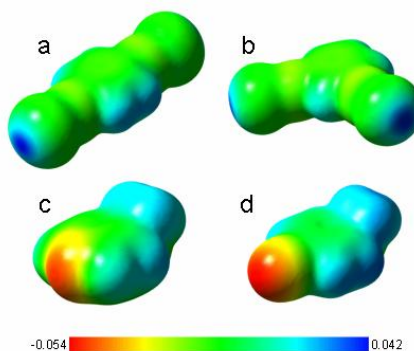


Figure 5.21- Computed electrostatic potential of the minimized halogen-bonding donors and acceptors, a) pBIEB, b) mBIEB, c) Py1-1 and d) BN-1.

The sigma-hole in the XB-donors, created by the anisotropic distribution of electronic density around the iodine atom, can be seen. Key features of the B98-calculated geometries and the interaction energies between the XB-donors and XB-acceptors are gathered in Table 5.6. The calculated non-covalent bonding angles $Z_{C-I \cdots N}$ are almost linear (179.9° in **P-Py1-1** and 179.2° in **P-BN-1**) and the

halogen-bonding distances $D_{I\cdots N}$ (2.906 Å in **P-Py1-1** and 3.095 Å in **P-BN-1**) are appreciably shorter than the sum of the van der Waals radii (3.53 Å). These data show good agreement with angles (172.95° in **P-Py1-10** and 176.45° in **P-BN-10**) and halogen-bonding distances (2.757 Å in **P-Py1-10** and 2.946 Å in **P-BN-10**) determined in the crystal structures of **P-Py1-10** and **P-BN-10**. The C–I bond distances increase upon halogen-bonding complex formation.

The interaction energies (ΔE_{int}) were determined using the equation:

$$\Delta E_{int} = E_{complex} - \sum E_{partner}$$

with values of –20.0 kcal/mol obtained for complexes **P-Py1-1**, **M-Py1-1** and –15.0 kcal/mol for the **P-BN-1**. These values are higher than those calculated for some analogous pyridine-halotetrafluorobenzene complexes^[16b, 27, 37] and are in the typical range for medium-to-strong hydrogen bonding.^[38] Furthermore, these energies depend on the halogen-bonding acceptor, with pyridine complexes showing higher interaction energies than the nitrile complex. In addition, the I···N distance of the trimers **P-Py1-1** and **M-Py1-1** is shorter than the analogous distance in the complex **P-BN-1**. This fact is consistent with the nitrogen of the pyridine derivative enhancing the halogen bonding appreciably.

The presence of a sufficiently strong positive region on the outer surface of an atom is an indication that an attractive interaction with a nucleophile is likely, although this is not the only factor.^[39] The values of the most positive electrostatic potentials on the molecular surfaces ($V_{s,max}$) for **pBIEB** and **mBIEB** (24.6 kcal/mol) are similar to that of 1,4-diiodotetrafluorobenzene (23.2 kcal/mol). Despite this, the interaction energies calculated for the complexes **P-Py1-1** and **M-Py1-1** ($\Delta E_{int} = -10$ kcal/mol) are higher than those described for 1,4-diiodotetrafluorobenzene with pyridine derivatives ($\Delta E_{int} = -5.59$ kcal/mol).^[37] This may be due to combination of a higher $V_{s,max}$ and the lower steric hindrance of bis(iodoethyl)benzene derivatives.

5.8 Conclusions

Iodoethynylbenzene derivatives have proven to be good halogen-bonding donors. The binding of an iodine atom to an sp hybridized carbon atom generates a deep σ -hole in the iodine atom and this, combined with the low steric hindrance of this system, leads to the formation of strong non-covalent interactions with pyridine derivatives ($\Delta E_{\text{int}} = -10$ kcal/mol) and somewhat weaker interactions with benzonitriles ($\Delta E_{\text{int}} = -7.5$ kcal/mol).

The linear **pBIEB** forms halogen-bonding complexes with pyridine-based acceptors bearing one or two aromatic rings to give complexes that show ordered calamitic phases (SmB and CrG) over wide temperature ranges. On the other hand, the bent **mBIEB** forms halogen-bonding complexes with pyridine derivatives that contain three aromatic rings. Furthermore, disc-like **1,3,5-TIEB** forms halogen-bonding complexes with pyridine derivatives with amines as connectors. These complexes show liquid crystal phases that are characteristic of bent-core compounds and they respond under electric fields. XRD, ITC, Raman and modeling studies support the experimental results and also explain the weaker interactions of these iodine donors with a benzonitrile-based acceptor. It was found experimentally that this weaker interaction prevents the formation of homogeneous halogen-bonding complexes on melting.

5.9 Experimental Section

All commercial reagents were used as purchased. FT-IR spectra were recorded on a Bruker Vertex spectrophotometer. ^1H and ^{13}C NMR spectra were recorded on a Bruker Avance 400 spectrometer (9.4 T, 400.13 MHz for ^1H , 100.62 MHz for ^{13}C) or a Bruker Avance 300 spectrometer (9.4 T, 400.13 MHz for ^1H , 100.62 MHz for ^{13}C). The mesophase identification was based on microscopic examination of the textures formed by samples between two glass slides. NIKON and OLYMPUS BH-2 polarizing microscopes equipped with a LINKAM THMS600 hot stage were used. The temperatures and enthalpies of the phase transitions were determined by calorimetric measurements performed with DSC TA Instruments Q-20 and Q-2000 systems. Thermogravimetric analysis (TGA) was performed using a TA Q5000IR instrument at a heating rate of 10 °C /min under a nitrogen atmosphere. The X-ray investigations on non-oriented samples were carried out in Lindemann capillary tubes (diameter: 0.9 or 1 mm) using a PINHOLE (ANTON-PAAR) film camera. The XPS instrument was a Kratos Aris Ultra DLD. The X-ray source was run at 12 kV and 10 mA. All core-level spectra were referenced to the C 1s neutral carbon peak at a binding energy of 285.0 eV in order to compensate for surface charge effects. The pressure in the analysis chamber was maintained under ultrahigh vacuum below 10^{-9} mbar.

5.9.1 Synthesis

4-(Decyloxy)benzonitrile BN-10. 4-Dihydroxybenzaldehyde (7.00 g, 52.63 mmol) and anhydrous potassium carbonate (21 g, 157.89 mmol) were stirred in dry DMF (95 mL). The mixture was heated to 100 °C under an inert atmosphere and then 1-bromodecane (14 g, 63.20 mmol) was added slowly. The mixture was stirred at 80 °C for 12 h. The reaction mixture was poured into ice-water and extracted with CH_2Cl_2 . The combined extracts were washed with water and brine, dried over anhyd Na_2SO_4 and concentrated. The crude product was recrystallised from ethanol to give the pure product. Yield 5.8 g (80%).

Liquid Crystals: Promesogenic Calamitic, Bent-core and Discotic Shapes by Halogen Bonding

¹H NMR (300 MHz, CDCl₃) δ (ppm): 7.57 (d, 2H, J = 6 Hz, Ar), 6.93 (d, 2H, J = 6 Hz, Ar), 3.99 (t, 2H, J = 6 Hz, 1 × OCH₂), 1.24–1.81 (m, 16H, 8 × CH₂), 0.88 (t, 3H, J = 6 Hz, 1 × CH₃); ¹³C NMR (CDCl₃, 100 MHz): 162.67, 134.16, 119.55, 115.37, 103.82, 68.63, 32.08, 29.73, 29.51, 29.18, 26.13, 22.88, 14.31; MS (ESI+-MS) m/z: 260.2 [M + H]⁺.

4-(Decyloxy)pyridine (Py1-10). 4-Hydroxypyridine (5.00 g, 52.63 mmol) and anhydrous potassium carbonate (21 g, 157.89 mmol) were stirred in dry DMF (95 mL). The mixture was heated to 100 °C under an inert atmosphere and then 1-bromodecane (14 g, 63.20 mmol) was added slowly. The mixture was stirred at 100 °C for 6 h. The mixture was allowed to cool to room temperature and extracted with a mixture of hexane/ethyl acetate (1:1). The organic solution was washed with NaOH (10%) and brine and then dried over MgSO₄, filtered and the solvent was evaporated. The resulting product was purified by column chromatography using hexane/dichloromethane (3:2) as eluent to give red oil. Yield 3.52 g (70%).

¹H NMR (300 MHz, CDCl₃) δ (ppm): 0.83–0.94 (t, J = 6.7 Hz, 3H), 1.18–1.39 (s, 8H), 1.39–1.52 (m, 2H), 1.61–1.71 (s, 1H), 1.73–1.87 (p, J = 6.6 Hz, 2H), 3.95–4.06 (t, J = 6.5 Hz, 2H), 6.76–6.82 (d, J = 4.9 Hz). ¹³C NMR (101 MHz, CDCl₃) δ (ppm): 14.03, 22.61, 25.86, 28.82, 29.25, 29.47, 31.82, 67.78, 76.84, 110.17, 150.89, 164.98. MS (ESI⁺-MS) m/z: 236 [M + H]⁺

4-[2-[4-(Tetradecyloxy)phenyl]ethenyl]pyridine (Py2-S-14). A mixture of compound **1** (1.35 g, 3.1 mmol) and picoline (0.287 g, 3.1 mmol) was heated under reflux in acetic anhydride for 48 h. The reaction mixture was cooled down to rt and the solid was filtered and recrystallized from ethyl acetate to yield a yellowish solid. Yield 3 g (30%).

¹H NMR (400 MHz, CDCl₃) δ (ppm): 0.88 (t, J = 6.0 Hz, 3H) 1.27–1.45 (m, 22H), 1.80 (m, 2H), 3.98 (t, J = 6.0 Hz, 2H), 6.86 (d, J = 16 Hz, 1H), 6.90 (d, J = 8 Hz, 2H), 7.24 (d, J = 16.0 Hz, 1H) 7.32 (d, J = 8.0 Hz, 2H), 7.46 (d, J = 8.0 Hz,

2H), 8.53 (d, J = 8.0 Hz, 2H). ^{13}C NMR (100 MHz, CDCl_3) δ (ppm): 14.1, 22.7, 26.0, 29.2, 29.3, 29.4, 29.5, 29.6, 29.7, 29.8, 31.9, 68.1, 114.8, 120.6, 123.5, 128.4, 128.7, 132.9, 145.1, 150.0, 159.8.

4-Pyridinyl-4-(tetradecyloxy)benzoate (Py2-E-14). Compound **2** (0.50 g, 1.4 mmol), 4-hydroxypyridine (0.134 g, 1.4 mmol) and DMAP (0.02 g, 0.14 mmol) were dissolved in dry dichloromethane (50 mL) in an ice bath. The reaction mixture was stirred under an argon atmosphere for 30 min. DCC (0.32 g, 1.5 mmol) was added and the mixture was stirred at room temperature for 24 h. The solid was filtered off and the solvent was evaporated. The crude product was purified by flash chromatography using dichloromethane as eluent to yield a white solid. Yield 0.25 g (43%).

^1H NMR (300 MHz, CDCl_3) δ (ppm): 0.89 (t, J = 6.0 Hz, 3H) 1.27–1.49 (m, 22H), 1.84 (m, 2H), 4.05 (t, J = 6.0 Hz, 2H), 6.99 (d, J = 8.9 Hz, 2H), 7.26 (d, J = 5.1 Hz, 2H) 8.13 (d, J = 9.0 Hz, 2H), 8.68 (d, J = 5.1 Hz, 2H). ^{13}C NMR (100 MHz, CDCl_3) δ (ppm): 14.1, 22.7, 26.0, 29.0, 29.3, 29.5, 29.6, 29.7, 31.9, 68.4, 114.5, 117.2, 120.6, 132.5, 151.3, 158.1, 163.8, 164.0.

4-(2-(Pyridin-4-yl)vinyl)phenyl-4-(tetradecyloxy)benzoate (Py3-S-14). A mixture of compound **3** (1.35 g, 3.1 mmol) and picoline (0.287 g, 3.1 mmol) was heated under reflux in acetic anhydride for 48 h. The reaction mixture was cooled down to room temperature and the solid was filtered and recrystallized from ethyl acetate to yield a yellowish solid. Yield 0.70 g (44%).

^1H NMR (300 MHz, CDCl_3) δ (ppm): 0.90 (t, J = 6.0 Hz, 3H) 1.27–1.60 (m, 30H), 1.83 (m, 2H), 4.07 (t, J = 6.0 Hz, 2H), 6.99–7.05 (m, 3H), 7.23 (m, 2H), 7.41 (m, 3H), 7.62 (d, J = 9.0 Hz, 2H), 8.18 (d, J = 9.0 Hz, 2H), 8.54 (d, J = 6.0 Hz, 2H). MS (FAB+-MS) m/z: 514 [M + H]⁺.

4-(2-(Pyridin-4-yl)vinyl)phenyl 4-(octadecyloxy)benzoate (Py3-S-18). A mixture of compound **4** (1.00 g, 2.0 mmol) and picoline (0.23 g, 2.4 mmol) was heated

Liquid Crystals: Promesogenic Calamitic, Bent-core and Discotic Shapes by Halogen Bonding

under reflux in acetic anhydride for 48 h. The reaction mixture was cooled down to rt and the solid was filtered off and recrystallized from ethyl acetate to yield a yellowish solid. Yield 0.50 g (43%).

¹H NMR (300 MHz, CDCl₃) δ (ppm): 0.90 (t, J = 6.0 Hz, 3H), 1.27–1.60 (m, 30H), 1.83 (m, 2H), 4.07 (t, J = 6.0 Hz, 2H), 6.99–7.05 (m, 3H), 7.23 (m, 2H), 7.41 (m, 3H), 7.62 (d, J = 9.0 Hz, 2H), 8.18 (d, J = 9.0 Hz, 2H), 8.54 (d, J = 6.0 Hz, 2H). MS (FAB⁺-MS) m/z: 570 [M + H]⁺.

4-Pyridinyl-4-[(4-(tetradecyloxy)benzoyl)oxy]benzoate (Py3-E-14). Compound 2 (0.50 g, 1.4 mmol), 4-hydroxypyridine (0.134 g, 1.4 mmol) and DMAP (0.02 g, 0.14 mmol) were dissolved in dry dichloromethane (50 mL) in an ice bath. The reaction mixture was stirred under an argon atmosphere for 30 min. DCC (0.32 g, 1.5 mmol) was added and the mixture was stirred at rt for 24 h. The solid was filtered off and the solvent was evaporated. The crude product was purified by flash chromatography using dichloromethane as eluent to yield a white solid. Yield: 0.25 g (43%).

¹H NMR (400 MHz, CDCl₃) δ (ppm): 0.90 (t, J = 6.0 Hz, 3H) 1.27–1.60 (m, 22H), 1.83 (m, 2H), 4.07 (t, J = 8.0 Hz, 2H), 7.00 (d, J = 8.0 Hz, 2H), 7.23 (d, J = 4 Hz, 2H), 7.41(d, J = 8.0 Hz, 2H), 8.16 (d, J = 8.0 Hz, 2H), 8.28 (d, J = 8.0 Hz, 2H), 8.70 (d, J = 4.0 Hz, 2H). ¹³C NMR (100 MHz, CDCl₃) δ (ppm): 14.1, 22.7, 26.0, 29.1, 29.3, 29.4, 29.5, 2.6, 29.7, 29.8, 31.9, 68.4, 114.4, 117.1, 120.8, 122.3, 126.0, 132.0, 132.5, 151.5, 155.8, 157.8, 163.1, 163.9, 164.2. MS (FAB⁺-MS) m/z: 570 [M + H]⁺.

5.9.2 Computational methods

Quantum chemical calculations were performed using the Gaussian 09^[40] suite of programs. Geometry optimizations were carried out in the gas phase with the B98^[41] method, employing the 6-311G+(d,p)^[42] basis set for all atoms except

iodine for which the DGDZVP^[43] basis set was used. Geometry optimizations were carried out without constraints, using the default convergence criteria for the Gaussian software. Vibrational frequency calculations were performed at the same level of theory as the geometry optimization and the frequency scale factor estimated by Radom *et al.*^[44] was used (0.9676). The basis set superposition error (BSSE) for noncovalent complexes was estimated using the counterpoise method of Boys and Bernardi.^[45] The natural bond orbital (NBO) analysis^[46] using the NBO module containing in Gaussian 09 program was performed on the basis of the minimized structures in order to calculate the NBO charges. The energies of interaction (ΔE_{int}) were calculated by subtracting the electronic energies of the optimized isolated partners ($E_{partner}$) of the electronic energy of the optimized noncovalent complex ($E_{complex}$), in accordance with the following equation:

$$\Delta E_{int} = E_{complex} - \sum E_{partner}$$

The obtained electronic energies of interaction were corrected for scale (0.9884)^[44] zero point differences and for basis set superposition errors.

5.9.3 X-ray monocrystal diffraction

X-ray quality single crystals were obtained by slow evaporation of solutions of complexes **P-Py1-10** and **P-BN-10** in CH₃CN. The crystals are air stable and were mounted on the tip of a glass fiber using epoxy cement. X-ray diffraction experiments were carried out on an Oxford-diffraction Xcalibur S diffractometer. Data were collected at 150(2) K with Mo-K α radiation. The software packages XSCANS^[47] and CrysAlis^[48] were used to process data.

Final cell parameters were obtained by global refinement of reflections obtained from integration of all the frames data. The structures were solved by direct methods and refined by the full-matrix method based on F² using the SHELXTL program.^[49] The non-hydrogen atoms of **P-Py1-10** and **P-BN-10** were refined

Liquid Crystals: Promesogenic Calamitic, Bent-core and Discotic Shapes by Halogen Bonding

anisotropically, the hydrogen atoms were observed in difference electron density maps and refined isotropically. The crystal parameters and basic information relating data collection and structure refinement are summarized in Table 5.7.

Table 5.7. Crystallographic data for complexes P-Py1-10 and P-BN-10

Compound	P-Py1-10	P-BN-10
Empirical formula	C ₄₀ H ₅₄ I ₂ N ₂ O ₂	C ₄₄ H ₅₄ I ₂ N ₂ O ₂
Formula weight	848.65	896.70
Crystal System	Triclinic	Triclinic
a, Å	7.728(3)	8.608(3)
b, Å	9.453(4)	10.221(4)
c, Å	14.800(5)	13.297(5)
α, deg	75.71(3)	97.85(3)
β, deg	84.00(3)	96.79(3)
γ, deg	66.93(4)	113.64(4)
V, Å ³	963.8(6)	1042.2(7)
T, K	150(2)	150(2)
Space group	P-1	P-1
Z	1	1
μ(Mo Kα), mm ⁻¹	1.666	1.429
θ range, deg	2.84 / 24.71	2.97 / 26.37
Refl. collected	5810	7425
Uniq reflect / R _{int}	3282 / 0.1458	4262 / 0.1884
R ^a /wR ^b (I>2σ)	0.1115 / 0.1637	0.1092 / 0.2913
R ^a /wR ^b (all data)	0.2226 / 0.2118	0.1476 / 0.2204
Max. shift/esd	0.002	0.016
Residual ρ/e Å ⁻³	-0.690 / 1.081	-1.552 / 0.746

5.10 Bibliography

- [1] F. Reinitzer, *Monatshefte für Chemie und verwandte Teile anderer Wissenschaften* **1888**, 9, 421-441.
- [2] a) H. Sackmann, *Kristall und Technik* **1981**, 16, 527-527; b) R. T. a. G. ATTARD in *The World of Liquid Crystals: The fourth state of matter Vol. 1991*; c) P. J. Collings., *Liquid Crystals, Nature's Delicate Phase of Matter*, IOP Publishing Ltd., England, **1990**, p.
- [3] a) J. P. F. Lagerwall and G. Scalia, *Current Applied Physics* **2012**, 12, 1387-1412; b) A. M. Lowe and N. L. Abbott, *Chem. Mat.* **2012**, 24, 746-758; c) J. A. Castellano in *The Story of Liquid Crystal Displays and the Creation of an Industry*, Vol. World Scientific Publishing, **2005**.
- [4] J. W. Steed and J. L. Atwood in *The Supramolecular Chemistry of Life*, Vol. John Wiley & Sons, Ltd, **2009**, pp. 49-104.
- [5] J. W. Goodby, P. J. Collings, T. Kato, C. Tschierske, H. F. Gleeson and P. Raynes in *Ionic Self Assembly and Amphotropic Ionic Liquid Crystals Vol. 6: Nanostructured and Amphiphilic Liquid Crystals PART II - Amphiphilic Liquid Crystals and Hydrogen-Bonded Systems: Discrete Defined Aggregates and Intramolecular H-Bonding, Amides, Carboxylic Acids, Heterocycles Vol. 5: Non-Conventional Liquid Crystals. In Handbook of liquid crystals.*, Vol. 8 Wiley, **2014**.
- [6] a) T. Kato and J. M. J. Frechet, *Liq. Cryst.* **2006**, 33, 1429-1433; b) T. Kato, N. Mizoshita and K. Kishimoto, *Angew. Chem. Int. Ed.* **2006**, 45, 38-68; c) D. Broer, G. P. Crawford and S. Zumer, *Cross-Linked Liquid Crystalline Systems: From Rigid Polymer Networks to Elastomers*, Boca Raton, FL, **2011**, p.
- [7] a) T. Kato and J. M. J. Frechet, *J. Am. Chem. Soc.* **1989**, 111, 8533-8534; b) T. Kato, P. G. Wilson, A. Fujishima and J. M. J. Frechet, *Chem. Lett.* **1990**, 2003-2006; c) B. Feringán, P. Romero, J. L. Serrano, R. Giménez and T. Sierra, *Chem. Eur. J.* **2015**, 21, 8859-8866.
- [8] a) N. Gimeno, M. B. Ros, J. L. Serrano and M. R. de la Fuente, *Angew. Chem. Int. Ed.* **2004**, 43, 5235-5238; b) J. Barbera, N. Gimeno, I. Pintre, M. B. Ros and J. L. Serrano, *Chem. Commun.* **2006**, 1212-1214; c) A. Perez, N. Gimeno, F. Vera, M. B. Ros, J. L. Serrano and M. R. De la Fuente, *Eur. J. Org. Chem.* **2008**, 826-833; d) N. Gimeno, M. B. Ros, J. L. Serrano and M. R. De la Fuente, *Chem. Mat.* **2008**, 20, 1262-1271; e) L.-Y. Wang, I. H. Chiang, P.-J. Yang, W.-S. Li, I. T. Chao and H.-C. Lin, *J. Phys. Chem. B* **2009**, 113, 14648-14660; f) L.-Y. Wang, H.-Y. Tsai and H.-C. Lin, *Macromolecules* **2010**, 43, 1277-1288; g) P.-J. Yang, L.-Y. Wang, C.-Y. Tang and H.-C. Lin, *J. Polymer Science Part a-Polymer Chem.* **2010**, 48, 764-774; h) W.-H. Chen, W.-T. Chuang, U. S. Jeng, H.-S. Sheu and H.-C. Lin, *J. Am. Chem. Soc.* **2011**, 133, 15674-15685.
- [9] L. C. Gilday, S. W. Robinson, T. A. Barendt, M. J. Langton, B. R. Mullaney and P. D. Beer, *Chem. Rev.* **2015**, 115, 7118-7195.
- [10] a) F. Guthrie, *J. Chem. Soc.* **1863**, 16, 239; b) I. Remses, J. F. Norris and *Am. Chem. J.* **1896**, 18, 90.
- [11] a) O. Hassel and J. Hvoslef, *Acta Chemica Scandinavica* **1954**, 8, 873-873; b) O. Hassel and C. Romming, *Quarterly Rev.* **1962**, 16, 1-18; c) H. A. Bent, *Chem. Rev.* **1968**, 68, 587-&.
- [12] a) P. Auffinger, F. A. Hays, E. Westhof and P. S. Ho, *Proc. Natl. Acad. Sci. U. S. A.* **2004**, 101, 16789-16794; b) P. Metrangolo, H. Neukirch, T. Pilati and G. Resnati, *Acc. Chem. Res.* **2005**, 38, 386-395; c) A. R. Voth and P. S. Ho, *Curr. Top. Med. Chem.* **2007**, 7, 1336; d) P. Metrangolo, F. Meyer, T. Pilati, G. Resnati and G. Terraneo, *Angew. Chem. Int. Ed.* **2008**, 47, 6114-6127; e) M. Fourmigue, P. Metrangolo and G. Resnati, *Halogen Bonding Fundamentals and Applications*, **2008**, p; f) L. A. Hardegger, B. Kuhn, B. Spinnler, L. Anselm, R. Ecabert, M. Stihle, B. Gsell, R. Thoma, J. Diez, J. Benz, J. M. Plancher, G. Hartmann, D. W. Banner, W. Haap and F. Diederich, *Angew. Chem. Int. Ed. Engl.* **2011**, 50, 314-318.
- [13] H. L. Nguyen, P. N. Horton, M. B. Hursthouse, A. C. Legon and D. W. Bruce, *J. Am. Chem. Soc.* **2004**, 126, 16-17.
- [14] T. Kato, T. Yasuda, Y. Kamikawa and M. Yoshio, *Chem. Commun.* **2009**, 729-739.

Liquid Crystals: Promesogenic Calamitic, Bent-core and Discotic Shapes by Halogen Bonding

- [15] a) K. Willis, D. J. Price, H. Adams, G. Ungar and D. W. Bruce, *J. Mat. Chem.* **1995**, *5*, 2195-2199; b) D. J. Price, K. Willis, T. Richardson, G. Ungar and D. W. Bruce, *J. Mat. Chem.* **1997**, *7*, 883-891.
- [16] a) J. W. Xu, C. L. Toh, X. M. Liu, S. F. Wang, C. B. He and X. H. Lu, *Macromolecules* **2005**, *38*, 1684-1690; b) J. W. Xu, X. M. Liu, J. K. P. Ng, T. T. Lin and C. B. He, *J. Mat. Chem.* **2006**, *16*, 3540-3545; c) P. Metrangolo, C. Prasang, G. Resnati, R. Liantonio, A. C. Whitwood and D. W. Bruce, *Chem. Commun.* **2006**, 3290-3292; d) D. W. Bruce, P. Metrangolo, F. Meyer, C. Prasang, G. Resnati, G. Terraneo and A. C. Whitwood, *New J. Chem.* **2008**, *32*, 477-482; e) C. Prasang, A. C. Whitwood and D. W. Bruce, *Chem. Commun.* **2008**, 2137; f) D. W. Bruce in *Halogen-bonded liquid crystals*, Vol. 126 Eds.: P. Metrangolo and G. Resnati), **2008**, pp. 161-180; g) D. W. Bruce, P. Metrangolo, F. Meyer, T. Pilati, C. Prasang, G. Resnati, G. Terraneo, S. G. Wainwright and A. C. Whitwood, *Chem. Eur. J.* **2010**, *16*, 9511-9524.
- [17] L. J. McAllister, C. Prasang, J. P. W. Wong, R. J. Thatcher, A. C. Whitwood, B. Donnio, P. O'Brien, P. B. Karadakov and D. W. Bruce, *Chem. Commun.* **2013**, *49*, 3946.
- [18] L. Gonzalez, N. Gimeno, R. Maria Tejedor, V. Polo, M. Blanca Ros, S. Uriel and J. Luis Serrano, *Chem. Mat.* **2013**, *25*, 4503-4510.
- [19] Y. Chen, H. Yu, L. Zhang, H. Yang and Y. Lu, *Chem. Commun.* **2014**, *50*, 9647-9649.
- [20] a) C. Laurence, M. Queigneccabanetos, T. Dziembowska, R. Queignec and B. Wojtkowiak, *J. Am. Chem. Soc.* **1981**, *103*, 2567-2573; b) C. Laurence, M. Queigneccabanetos and B. Wojtkowiak, *J. Chem. Soc. Perkin Trans. 2* **1982**, 1605-1610; c) C. Laurence, M. Queigneccabanetos and B. Wojtkowiak, *Can. J. Chem.* **1983**, *61*, 135-138.
- [21] a) H. M. Yamamoto, Y. Kosaka, R. Maeda, J. Yamaura, A. Nakao, T. Nakamura and R. Kato, *ACS Nano* **2008**, *2*, 143-155; b) J. Lieffrig, H. M. Yamamoto, T. Kusamoto, H. Cui, O. Jeannin, M. Fourmigue and R. Kato, *Cryst. Growth Des.* **2011**, *11*, 4267-4271.
- [22] A. W. Sun, J. W. Lauher and N. S. Goroff, *Science* **2006**, *312*, 1030-1034.
- [23] L. Luo, C. Wilhelm, A. Sun, C. P. Grey, J. W. Lauher and N. S. Goroff, *J. Am. Chem. Soc.* **2008**, *130*, 7702-7709.
- [24] A. Brun and G. Etemad-Moghadam, *Synthesis* **2002**, 1385-1390.
- [25] a) J. Ruokolainen, J. Tanner, G. Tenbrinke, O. Ikkala, M. Torkkeli and R. Serimaa, *Macromolecules* **1995**, *28*, 7779-7784; b) J. Ruokolainen, G. tenBrinke, O. Ikkala, M. Torkkeli and R. Serimaa, *Macromolecules* **1996**, *29*, 3409-3415.
- [26] a) X. Zhou, S. H. Goh, S. Y. Lee and K. L. Tan, *Appl. Surf. Sci.* **1997**, *119*, 60-66; b) F. Wang, N. Ma, Q. Chen, W. Wang and L. Wang, *Langmuir* **2007**, *23*, 9540-9542.
- [27] A. Priimagi, G. Cavallo, A. Forni, M. Gorynsztein-Leben, M. Kaivola, P. Metrangolo, R. Milani, A. Shishido, T. Pilati, G. Resnati and G. Terraneo, *Adv. Funct. Mater.* **2012**, *22*, 2572-2579.
- [28] A. L. Barres, A. El-Ghayoury, L. V. Zorina, E. Canadell, P. Auban-Senzier and P. Batail, *Chem. Commun.* **2008**, 2194-2196.
- [29] a) S. K. Maity, S. Bera, A. Paikar, A. Pramanik and D. Haldar, *Chem Commun (Camb)* **2013**, *49*, 9051-9053; b) N. Nagels, D. Hauchecorne and W. A. Herrebout, *Molecules* **2013**, *18*, 6829-6851.
- [30] a) A. Velazquez-Campoy and E. Freire, *Nat. Protocols* **2006**, *1*, 186-191; b) A. Velazquez-Campoy, S. Leavitt and E. Freire in *Characterization of Protein-Protein Interactions by Isothermal Titration Calorimetry*, Vol. 1278 Eds.: C. L. Meyerkord and H. Fu), Springer New York, **2015**, pp. 183-204.
- [31] S. M. Walter, F. Kniep, L. Rout, F. P. Schmidtchen, E. Herdtweck and S. M. Huber, *J. Am. Chem. Soc.* **2012**, *134*, 8507-8512.
- [32] A. Eremin, S. Diele, G. Pelzl, H. Nadasi, W. Weissflog, J. Salfetnikova and H. Kresse, *Phys. Rev. E* **2001**, *64*.
- [33] B. K. Sadashiva, R. A. Reddy, R. Pratibha and N. V. Madhusudana, *J. Mat. Chem.* **2002**, *12*, 943-950.

- [34] a) R. A. Reddy and B. K. Sadashiva, *J. Mat. Chem.* **2004**, *14*, 310-319; b) D. Pociecha, M. Cepic, E. Gorecka and J. Mieczkowski, *Phys. Rev. Lett.* **2003**, *91*.
- [35] Y. Shimbo, E. Gorecka, D. Pociecha, F. Araoka, M. Goto, Y. Takanishi, K. Ishikawa, J. Mieczkowski, K. Gomola and H. Takezoe, *Phys. Rev. Lett.* **2006**, *97*.
- [36] a) K. Gomola, L. Guo, D. Pociecha, F. Araoka, K. Ishikawa and H. Takezoe, *J. Mat. Chem.* **2010**, *20*, 7944-7952; b) L. Guo, S. Dhara, B. K. Sadashiva, S. Radhika, R. Pratibha, Y. Shimbo, F. Araoka, K. Ishikawa and H. Takezoe, *Phys. Rev. E* **2010**, *81*.
- [37] S. Tsuzuki, A. Wakisaka, T. Ono and T. Sonoda, *Chem. Eur. J.* **2012**, *18*, 951-960.
- [38] K. Wendler, J. Thar, S. Zahn and B. Kirchner, *J. Phys. Chem. A* **2010**, *114*, 9529-9536.
- [39] a) P. Politzer, J. S. Murray and P. Lane, *Int. J. Quantum Chem.* **2007**, *107*, 3046-3052; b) P. Politzer, J. S. Murray and T. Clark, *Phys. Chem. Chem. Phys.* **2010**, *12*, 7748-7757.
- [40] G. W. T. J. Frisch, H. B. Schlegel, G. E. Scuseria, M. A. Robb, J. R. Cheeseman, G. Scalmani, V. Barone, G. A. Petersson, H. Nakatsuji, X. Li, M. Caricato, A. Marenich, J. Bloino, B. G. Janesko, R. Gomperts, B. Mennucci, H. P. Hratchian, J. V. Ortiz, A. F. Izmaylov, J. L. Sonnenberg, D. Williams-Young, F. Ding, F. Lipparini, F. Egidi, J. Goings, B. Peng, A. Petrone, T. Henderson, D. Ranasinghe, V. G. Zakrzewski, J. Gao, N. Rega, G. Zheng, W. Liang, M. Hada, M. Ehara, K. Toyota, R. Fukuda, J. Hasegawa, M. Ishida, T. Nakajima, Y. Honda, O. Kitao, H. Nakai, T. Vreven, K. Throssell, J. A. Montgomery, Jr., J. E. Peralta, F. Ogliaro, M. Bearpark, J. J. Heyd, E. Brothers, K. N. Kudin, V. N. Staroverov, T. Keith, R. Kobayashi, J. Normand, K. Raghavachari, A. Rendell, J. C. Burant, S. S. Iyengar, J. Tomasi, M. Cossi, J. M. Millam, M. Klene, C. Adamo, R. Cammi, J. W. Ochterski, R. L. Martin, K. Morokuma, O. Farkas, J. B. Foresman, and D. J. Fox, in *Gaussian 09*, Vol. Gaussian Inc., Wallingford CT, **2009**.
- [41] a) P. M. W. Gill, *Mol. Phys.* **1996**, *89*, 433-445; b) J. P. Perdew, K. Burke and M. Ernzerhof, *Phys. Rev. Lett.* **1996**, *77*, 3865-3868.
- [42] W. J. Hehre, L. Radom, S. P. V. R. and J. A. Pople in *Ab initio Molecular Orbital Theory*, Vol. Wiley, New York, **1986**.
- [43] N. Godbout, D. R. Salahub, J. Andzelm and E. Wimmer, *Can. J. Chem.* **1992**, *70*, 560-571.
- [44] J. P. Merrick, D. Moran and L. Radom, *J. Phys. Chem. A* **2007**, *111*, 11683-11700.
- [45] S. F. Boys and F. Bernardi, *Mol. Phys.* **1970**, *19*, 553-566.
- [46] A. E. Reed, L. A. Curtiss and F. Weinhold, *Chem. Rev.* **1988**, *88*, 899-926.
- [47] Siemens, *XSCANS 1994*, Siemens Analytical X-ray Instruments Inc., Madison, Wisconsin, USA.
- [48] in *CrysAlis Vol.* **2006**.
- [49] G. Sheldrick, *Acta Cryst A* **2008**, *64*, 112-122.

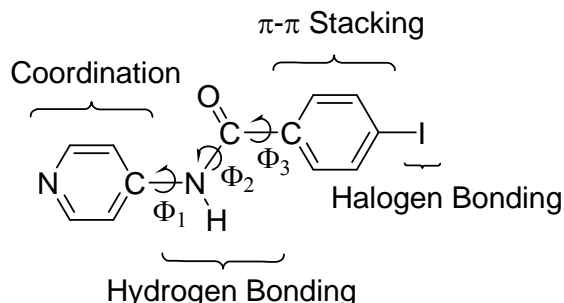
Chapter 6 Coordination Metal Complexes Based on 4-Iodo-N-(4-pyridyl)benzamide, a Polyfunctional Ligand

6.1 Introduction.

The construction of metal-organic coordination polymers with a variety of topologies and structural diversity, which affect and control the macroscopic properties,^[1] has given rise to electrical,^[2] optical,^[3] photoluminescence, gas storage,^[4] and ion exchange materials. One of the most powerful strategies employed to regulate the solid-state structure is the arrangement of metallotectons by non-covalent interactions. The coexistence of metal coordination bonds and hydrogen bonds has resulted in a wide variety of one-dimensional to three-dimensional^[5] structures. Recently, halogen-related interactions, including halogen bonding and related halogen···halogen and halogen···π intermolecular interactions, have become attractive tools in crystal engineering. However, the presence of halogen bonding in metal coordination polymers has not received a great deal of attention.^[6]

This chapter is a continuation of the work begun by Sara Graus,^[7] who explored the design of solid state structures based on molecules that use metal-ligand coordination, hydrogen and halogen bonding, and π-π stacking interactions as directional motifs to guide the self-assembly of network structures. To this end, we considered it of value to employ the ligand 4-iodo-N-(4-pyridyl)benzamide (**INPBA**) (Scheme 6.1), which possesses one pyridine ring for coordination to metal centers, a carboxamide group that can act as a hydrogen bond donor and acceptor and one iodine atom that is potentially capable of partaking in oxygen (or nitrogen), C–I···π and C–I···X–M halogen bonding. Metal-bound halides and pseudohalides are strongly nucleophilic and serve as halogen bonding acceptors – as reported by the Brammer and Ward groups, who employed halometallates and cyanometallates as halogen bond acceptors.^[8]

Coordination Metal Complexes Based on 4-Iodo-N-(4-pyridyl)benzamide, a Polyfunctional Ligand

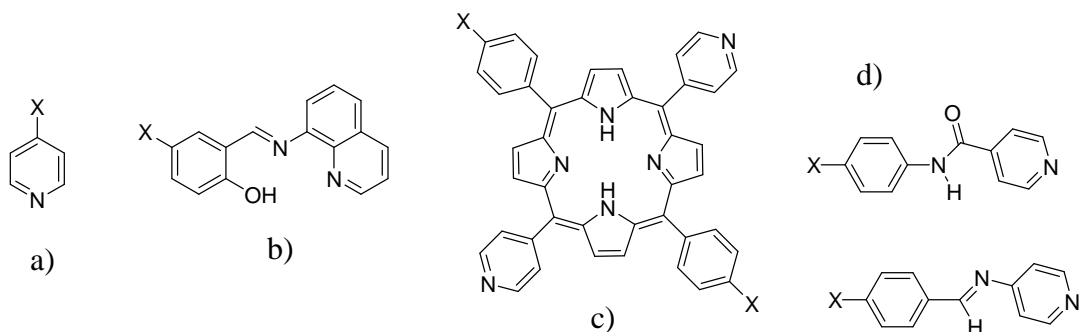


Scheme 6.1 4-Iodo-N-(4-pyridyl)benzamide (INPBA)

We examined the interactions of **INPBA** with metal ions that are known to form complexes with low coordination numbers, such as Ag(I), Zn(II), and Hg(II) centers, by the reaction of **INPBA** with AgNO_3 , ZnBr_2 , $\text{Zn}(\text{NO}_3)_2$ in the presence of sodium benzoate (NaOCOPh) and HgI_2 .

6.2 Previous works

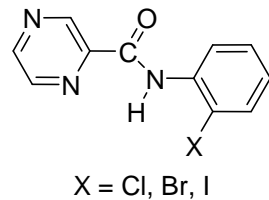
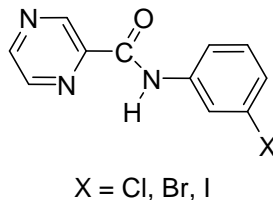
The tailored introduction and evaluation of noncovalent assembly in metal-organic coordination polymers enable the identification and effective use of supramolecular synthons and facilitates a better comprehension of the crystal structures for the systematic design of related materials.^[9] To achieve such a target, a wide variety of pyridyl or carboxylate functional groups have been extensively used for the construction of coordination polymers, which bear substituents that can participate in strong and directional supramolecular synthons such as those involving hydrogen and/or halogen bonds. Among the systems that can form halogen bonds, halobenzoate salts have been employed extensively because the carboxylate group is a good coordinating and electron-withdrawing group. The latter property favors the formation of strong halogen bonds. Among the most widely used neutral ligands are halopyridines, 5-halo-quinolylsalicylaldimines, porphyrins, 4-halo-N-(pyridin-4-ylmethylene)aniline and N-(4-halophenyl)pyridinecarboxamide.(See Scheme 6.2)



Scheme 6.2 The most widely used neutral ligands: a) halopyridines, b) 5-halo-quinolylsalicylaldimines, c) porphyrins, d) 4-halo-N-(pyridin-4-ylmethylene)aniline and N-(4-halophenyl)pyridinecarboxamide

The metal complexes with neutral ligands that contain groups that can form coordination bonds and hydrogen bonding groups and halogens are very scarce. The largest number of structures described correspond to the halophenyl pyrazine carboxamide complexes with mercury(II) halides^[10] (Scheme 6.3).

Coordination Metal Complexes Based on 4-Iodo-N-(4-pyridyl)benzamide, a Polyfunctional Ligand



Scheme 6.3 N-(3-halophenyl)-2-pyrazinecarboxamide and N-(2-halophenyl)-2-pyrazinecarboxamide.

In the halophenyl pyrazine carboxamide structures with mercury(II) halides the mercury atom has a wide variety of environments. For example, of the thirteen structures described in the Cambridge Structural Database (CSD), the T-coordinated structure is the most common, while in eight of them the mercury halide forms one-dimensional polymers. The coordination spheres of the mercury atom in the structures of halophenylpyrazine carboxamide complexes with mercury(II) halides reported to date are shown in Figure 6.1 (T-shaped Figure 6.1 (a), octahedral Figure 6.1 (b) and square-based pyramidal Figure 6.1 (c) and (d)).^[10a]

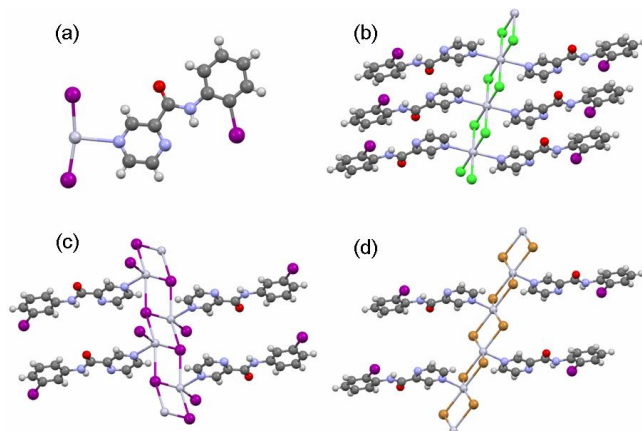


Figure 6.1 (a) Coordination type T [HgI_2 ($\text{N}(\text{-2-iodophenyl})\text{-2-pyrazinecarboxamide}$)], (b) Octahedral coordination [HgCl_2 ($\text{N}(\text{-2-iodophenyl})\text{-2-pyrazinecarboxamide}$)], (c) Square-based pyramidal coordination [HgI_2 ($\text{N}(\text{-3-iodophenyl})\text{-2-pyrazinecarboxamide}$)] and (d) Square-based pyramidal coordination [HgBr_2 ($\text{N}(\text{-2-iodophenyl})\text{-2-pyrazinecarboxamide}$)].^[10a]

In the structures of mercury(II) halide complexes with N-(2-iodophenyl)-2-pyrazinecarboxamide. The iodine atom of the ligand forms very weak interactions. In contrast, in the crystal structures of mercury complexes with the N-(3-iodophenyl)-2-pyrazinecarboxamide, the iodine atom acts as a C–I…N halogen bonding donor and NH…I hydrogen bond acceptor. This leads to the formation of dimers, as shown in Figure 6.2 (a). These dimers bind the one-dimensional polymers to give rise to supramolecular organizations of different dimensionality. For instance, the structure of $[\text{HgI}_2 \text{ (N-(3-iodophenyl)-2-pyrazinecarboxamide)}]$ is formed by two-dimensional networks, as shown in Figure 6.2 (b), by the union of the one-dimensional mercury iodide polymers through the aforementioned dimers.

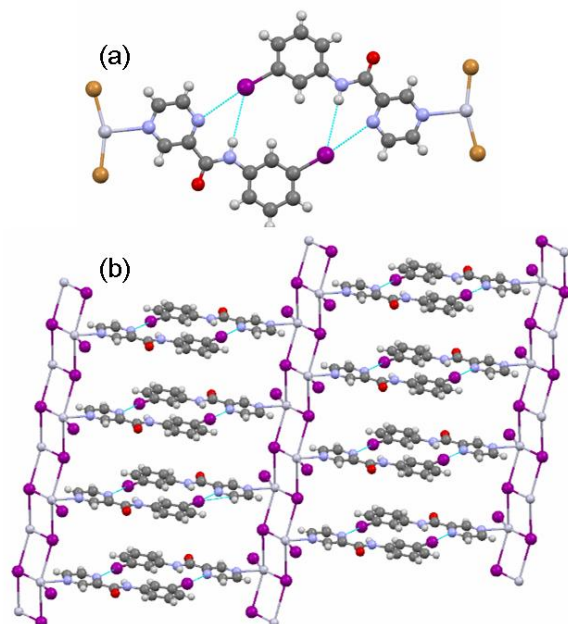


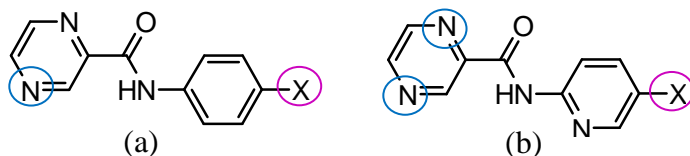
Figure 6.2 (a) Dimers formed by hydrogen and halogen bonds $[\text{HgBr}_2 \text{ (N-(3-iodophenyl)-2-pyrazinecarboxamide)}]$ and **(b)** Two-dimensional network $[\text{HgI}_2 \text{ (N-(3-iodophenyl)-2-pyrazinecarboxamide)}]$.

None of the neutral ligands depicted in Scheme 6.3 are good halogen bonding donors, since they lack electron-withdrawing groups attached to the aromatic ring that contains the halogen atom. Aakeroey and co-workers described the 1-(4-

Coordination Metal Complexes Based on 4-Iodo-N-(4-pyridyl)benzamide, a Polyfunctional Ligand

pyridyl)-2-(2,3,5,6-tetrafluoro-4-iodophenyl)ethene ligand, which has a strong halogen bonding donor group, but all of their attempts to incorporate multiple supramolecular interactions failed. The reason for this is that only metal coordination was produced, while the halogen···halogen or halogen···N_(heterocycle) interactions failed to occur.^[11]

To increase the halogen bonding donor character of the N-(halophenyl)pyrazine-2-carboxamide derivatives, Khavasi and co-workers,^[12] based on previous studies,^[13] replaced a CH group in the framework of the phenylpyrazinamide system by an isoelectronic nitrogen atom (Scheme 6.4 (a)). The nitrogen atom of the pyridine ring in the N-(5-halo-2-pyridinyl)pyrazine-2-carboxamide molecule (Scheme 6.4 (b)) imparts new features into the crystal engineering of phenylpyrazinamide derivatives.



Scheme 6.4 N-(4-halophenyl)pyrazine-2-carboxamide structures, X-ph, (a) and N-(5-halo-2-pyridinyl)pyrazine-2-carboxamide structures, X-Py (b). The halogen bond donor and halogen bond acceptors are shown in purple and blue circles, respectively.

Our starting hypothesis for using 4-iodo-N-(4-pyridyl)benzamide (**INPBA**) (Scheme 6.1) is that the orientation of the amide group with respect to the donor and acceptor halogen bonding moieties may be important in its coordination and halogen bonding donor features. Thus, the nitrogen atom of the amide group is an electron donor that will favor the ability of the pyridyl fragment to form coordination bonds, while the carbonyl group is electron withdrawing, which will favor the formation of a σ-hole on the iodine atom. Our hypothesis is that the orientation of the amide group with respect to the donor and acceptor halogen bonding moieties would improve their features.

We report the synthesis and crystal structure of **INPBA** (**1**) and four metal INPBA coordination supramolecular and polymeric structures [**Ag(INPBA)₂NO₃**] (**2**), [**ZnBr₂(INPBA)₂**] (**3**), [**Zn(OCOPh)₂(INPBA)₂**] (**4**), and [**HgI₂(INPBA)**]_n (**5**). In **4**, benzoic acid was used as an ancillary ligand. The interactions and contacts in structures were analyzed by Hirshfeld surface calculations. The capacity of **INPBA** as a halogen bonding donor was evaluated by DFT calculations and comparison with crystal structures of other halogen bonding donors.

6.3 X-ray Crystallography

6.3.1 4-iodo-N-(4-pyridyl)benzamide (INPBA).

4-Iodo-N-(4-pyridyl)benzamide (**INPBA**) consists of four structural parts: (1) a pyridyl group that can coordinate to a metal, (2) a carboxamide group can serve as both a hydrogen bond donor and acceptor, (3) an iodine atom, which can be involved in halogen bonding interactions as a donor and/or an acceptor and (4) two aromatic rings, which can participate in π - π stacking interactions. Furthermore, **INPBA** has three planar regions, the pyridyl, the carboxamide, and the phenyl group, with conformational degrees of freedom defined by the torsion angles Φ_1 ($\Phi_1 = C(9)-C(8)-N(1)-C(7)$), Φ_2 ($\Phi_2 = C(8)-N(1)-C(7)-C(4)$) and Φ_3 ($\Phi_3 = N(1)-C(7)-C(4)-C(3)$), which allow it to fit the local environment (Figure 6.3).

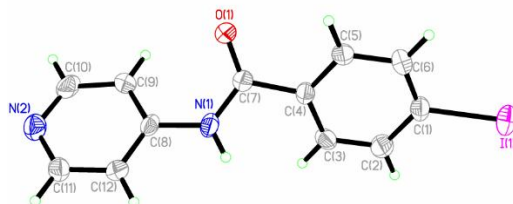


Figure 6.3 ORTEP diagram and numbering scheme for the **INPBA** crystal structure

This compound crystallizes in the monoclinic $P2_1/c$ space group, with one independent molecule in the asymmetric unit. The bond distances and angles for **INPBA** were as expected and the central C–C–N–C spacer unit is nearly planar, as shown by the torsional angle ($\Phi_2 = -177.3(5)^\circ$). However, the aromatic rings are markedly twisted out of this plane ($\Phi_1 = 33.7(8)$ and $\Phi_3 = 28.4(7)^\circ$) (Table 6.1). This conformation is similar to that shown by N-(4-pyridyl)benzamide (**NPBA**) in its crystal structure ($\Phi_1 = -16.8(2)$, $\Phi_2 = 178.4(1)$ and $\Phi_3 = -34.3(2)^\circ$).^[14]

Table 6.1 Torsional angles of INPBA in 1–5 and N-(4-pyridyl)benzamide (NPBA)

	Conform.	Φ_1	Φ_2	Φ_3	Φ_4	Φ'_4	Φ_5^b
NPBA ^a		-16.8	-178.4	-34.3			
INPBA		33.7	-177.3	28.4			
[Ag(INPBA) ₂]NO ₃	<i>cis</i>	-6.0	174.5	4.3	35.7	-62.5	36.5
		16.6	-179.8	14.9			
[ZnBr ₂ (INPBA) ₂]	<i>trans</i>	4.5	171.5	35.7	-	-68.6	87.3
		-18.4	-172.8	-26.8			
[Zn(OCOPh) ₂ (INPBA) ₂]	<i>trans</i>	-4.4	172.1	-21.9	61.6	61.6	86.8
[HgI ₂ (INPBA)] _n	-	21.0	176.1	32.0			

(a) Ref.^[14]; (b) Φ_5 angle between the planes containing the benzene rings.

The supramolecular arrangement of **INPBA** consists of chains, along the *b* axis, of molecules aligned head-to-tail by halogen bonding C—I···N (2.989 Å, 175.3°). This halogen bond distance is shorter than those observed in N-(4-iodophenyl)pyrazine-2-carboxamide (3.45 Å, 166.7°)^[15] and N-(5-iodopyridin-2-yl)pyrazine-2-carboxamide (3.11 Å, 175.9°).^[15] This seems to confirm our hypothesis that the orientation of the amide group with respect to the donor and acceptor halogen bonding moieties would improve the features.

The halogen bonded polymers are joined by hydrogen bonds (between carboxamide groups) and this results in layers in the *ab* plane, which pack in an anti-parallel fashion to afford a centric crystal (Figure 6.4(a)). The layers are practically isolated from each other and, despite the presence of phenyl moieties in **INPBA**, they do not exhibit π - π -stacking interactions due to the twisted conformation (Figure 6.4(b)).

Coordination Metal Complexes Based on 4-Iodo-N-(4-pyridyl)benzamide, a Polyfunctional Ligand

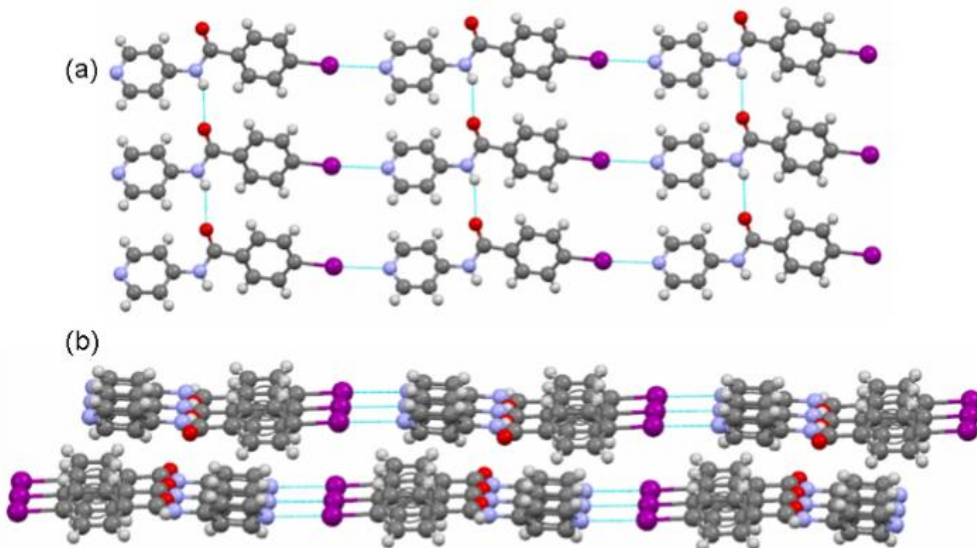


Figure 6.4 INPBA structure (a) 2-D sheets formed by C–I…N_{pyr} halogen bonding and perpendicular N–H…O=C carboxamide hydrogen bond; (b) Isolated layers.

6.3.1.1 [Ag(INPBA)₂]NO₃

The reaction of INPBA with AgNO₃ afforded the complex [Ag(INPBA)₂]NO₃ and this crystallizes in the *P*-1 triclinic space group. The asymmetric unit contains two ligand molecules coordinated to a silver atom and one nitrate anion (Figure 6.5). The Ag(I) atom is almost linearly coordinated to the pyridyl nitrogen of two ligands. Interestingly, both carbonyl groups are projected in the same direction (Figure 6.5). In contrast, the NPBA (N-(4-pyridyl)benzamide) ligands in the [Ag(NPBA)₂]NO₃ crystal structure have a *trans* conformation – as in all structures of NPBA described to date.^[14, 16]

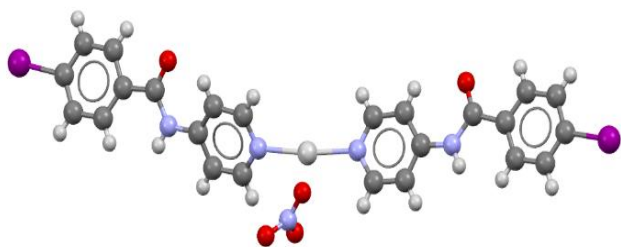


Figure 6.5 A view showing Ag(I) coordination in the $[\text{Ag}(\text{INPBA})_2]\text{NO}_3$ complex.

The Ag(I) atom interacts with iodine atoms of ligands and anions, in addition to the pyridyl nitrogen atoms. The coordination environment of the Ag(I) atom is pseudo trigonal bipyramidal with two C–Is and two nitrate Os (counts as one) in the plane and the two pyridyl Ns occupying the apical positions (Figure 6.6(a)).

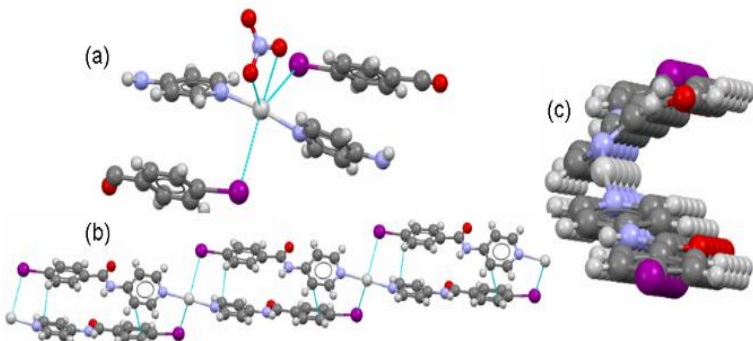


Figure 6.6 (a) Ag(I) coordination environment in 2 with two pyridyl groups, one nitrate counterion and two iodine atoms, only the moiety of the ligands that interact with Ag(I) is represented for the sake of clarity; (b) strands with a ‘half pipe’ shape along $[1\ 1\ 0]$

The equatorial electronegative and polar electropositive regions of the iodine halogen atom point towards the metallic cation and anion centers, respectively. This is consistent with the charge polarization model at the heavy halogen. Silver(I) shows a great tendency to receive electron density from the iodine atoms, as evidenced by the fact that of the 73 structures listed in the Cambridge Structural

Coordination Metal Complexes Based on 4-Iodo-N-(4-pyridyl)benzamide, a Polyfunctional Ligand

Database (update Nov-2014) having metal···I–C interactions, 53 correspond to silver complexes. The C–I···Ag distances in **2** (3.472 Å, 3.585 Å) and angles close to 90° (97.9 and 108.6°) mean that the ligands are arranged in an almost antiparallel fashion in which the planes defined by the amide groups form an angle of 24.20° (Figure 6.6(b)). These features give rise to strands with a ‘half pipe’ shape along the [1 1 0] direction and such half pipes interdigitate along the concave surface, while the convex surfaces are connected by the nitrate anions through hydrogen and halogen bonds (Figure 6.7). The presence of C–I···Ag interactions does not affect the N···Ag bond distance (2.145 Å) in comparison with the distance of such bonds in the crystal structure of *trans*-[Ag(NPBA)₂]NO₃ (2.149 Å).^[14]

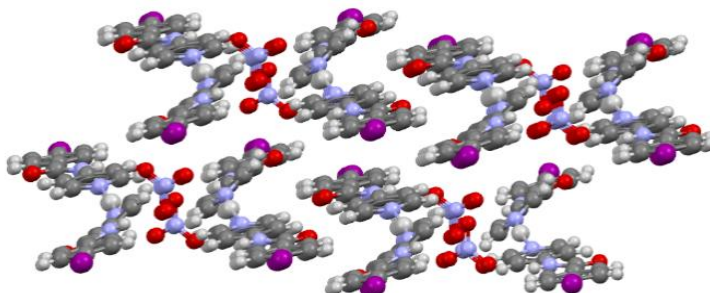


Figure 6.7 2-D supramolecular aggregation of **2**

The nitrate anion plays an important role in the supramolecular architecture of *cis*-[Ag(INPBA)₂]NO₃. Two consecutive complexes are joined by hydrogen bonding (N(2)–H···O(5) 3.024 Å, 158.8°; N(4)–H···O(4) 2.958 Å, 161.3°) and this provides stability to the strands formed by the C–I···Ag interaction. On the other hand, the anion connects one chain with two others, one through the Ag···O bifurcated interaction (Ag(1)···O(3) 2.856 Å; Ag(1)···O(4) 2.934 Å) and the other by C–I(2)···O (5) halogen bonding (3.498 Å, 152.5°).

6.3.1.1 $[\text{ZnBr}_2(\text{INPBA})_2]$

The complex $[\text{ZnBr}_2(\text{INPBA})_2]$ was obtained by reaction of INPBA with ZnBr_2 in a 2:1 stoicheometric ratio. $[\text{ZnBr}_2(\text{INPBA})_2]$ crystallizes in the $P2_1/c$ monoclinic space group. In the crystal structure of **3** the $\text{Zn}(\text{II})$ ion has a distorted tetrahedral geometry with a ZnBr_2N_2 core. INPBA ligands exhibit a *trans* configuration with respect to the orientation of the carbonyl groups. The main features of **3** are the $\text{C}-\text{I}\cdots\text{I}$ halogen bonding and hydrogen bonds between the amide groups. Each iodine atom in the $[\text{ZnBr}_2(\text{INPBA})_2]$ structure has a different role: one is a halogen bond donor while the other acts as an acceptor ($\text{C}-\text{I}(2)\cdots\text{I}(1)$ 3.938 Å, 166.2°). The donor is oriented towards the equatorial part of the acceptor, forming an angle close to 90° ($\text{C}-\text{I}_{\text{donor}}\cdots\text{I}_{\text{acceptor}}$ 75.1°), which promotes the formation of a chiral propeller along a 2_1 axis. The distance between Zn atoms in the propeller is 27.758 Å along the *b* axis and 24.235 Å along the diagonal (Figure 6.8(a)).

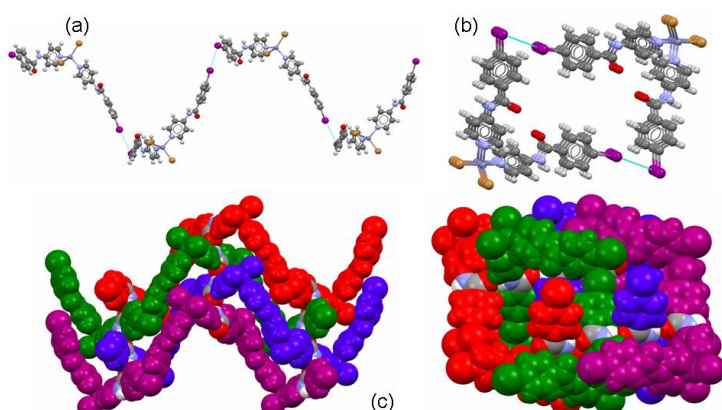


Figure 6.8 (a) A view along the *b*-axis of a helical strand of **3** formed by $\text{C}-\text{I}\cdots\text{I}$ halogen bonding. (b) View along the *c*-axis. (c) Enantiomeric helical strands hydrogen bonded along the *b*- and *c*-axes.

Each chain is joined to two enantiomeric helices through hydrogen bonds between the amide group along the *c* axis ($\text{N}(4)-\text{H}\cdots\text{O}(2)$ 2.795 Å, 149.2°) of the **INPBA**

Coordination Metal Complexes Based on 4-Iodo-N-(4-pyridyl)benzamide, a Polyfunctional Ligand

ligand with the more tilted conformation with respect to carboxamide group ($\Phi_1 = -18.4(8)^\circ$; $\Phi_3 = -26.8 (9)^\circ$), as shown in Figure 6.8(c).

The carboxamide of the second **INPBA** ligand gives rise to coplanar dimers through weak hydrogen bonds C(5)–H \cdots O(1)=C (3.577 Å, 158.1°). These dimers are connected to each other by N(2)–H \cdots Br(1)^[9a] interactions (3.743 Å, 150.9°), which leads to a ladder with parallel offset stacking of pyridine rings (3.45 Å) (Figure 6.9). The different environments of the carbonyl groups are evidenced by two bands at 1695 and 1970 cm⁻¹ in the ATR-IR spectra.

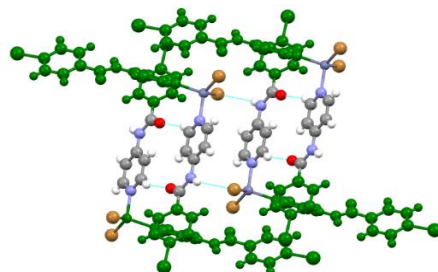


Figure 6.9 A view of the ladder structure formed by amide hydrogen bonds in **3**.

6.3.1.2 [Zn(OCOPh)₂(INPBA)₂]

The metal complex **Zn(OCOPh)₂(INPBA)₂** was obtained by reacting ZnBr₂ with INPBA in the presence of sodium benzoate. The crystal structure of **Zn(OCOPh)₂(INPBA)₂** (**4**) was solved in the orthorhombic Pbcn space group. The zinc(II) ion has a distorted tetrahedral geometry with a ZnO₂N₂ core. In **3** and **4** the INPBA ligands exhibit a *trans* configuration with respect to the orientation of the carbonyl groups. As shown in Figure 6.10, the different conformation of **INPBA** means that the iodine-to-iodine distances in **3** and **4** are 19.3 and 23.3 Å, respectively.

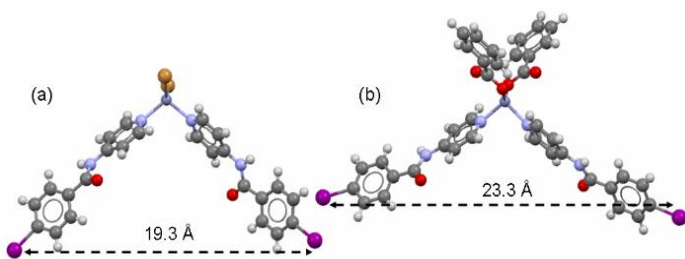


Figure 6.10 Coordination environment of zinc(II) in 3 (a) and 4 (b)

The supramolecular organization of **Zn(OCOPh)₂(INPBA)₂** is determined by the halogen and hydrogen bonds. The halogen bonding between the iodine atom and the carbonyl oxygen atom of the carboxamide group, C—I(1)···O(3)=C (3.257 Å, 148.8°), provides corrugated layers that extend along the *ac* plane. These planes are stacked along the *b* axis and are connected by N(2)—H···O(2)=C (2.822 Å, 167°) hydrogen bonds in which the donor is the carbonyl oxygen of the ester group (Figure 6.11). This organization leaves a small cavity around the Zn(II) atoms of 154 Å³ per cell, which represents about 4% of the volume.

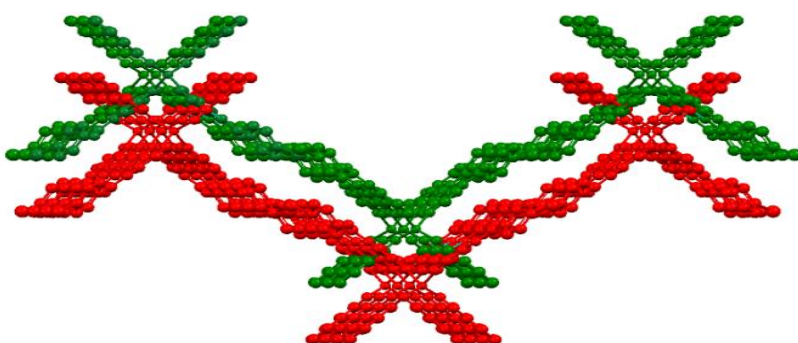


Figure 6.11 Corrugated layers stacking along the *b*-axis in **[Zn(OCOPh)₂(INPBA)₂].**

6.3.1.3 **[HgI₂(INPBA)]_n**

[HgI₂(INPBA)]_n crystallizes in the *P2₁/c* monoclinic space group. The bond distances, angles and even torsion angles, $\Phi_1 = 21^\circ$ and $\Phi_3 = 32^\circ$, of the ligand

Coordination Metal Complexes Based on 4-Iodo-N-(4-pyridyl)benzamide, a Polyfunctional Ligand

(**INPBA**) are very similar to those determined in the crystal structure of **INPBA**. This situation is unusual in previously described metal complex structures of N-(4-pyridyl)benzamide (**NPBA**).^[14, 16]

The mercury cation has a rhomboidal-based pyramidal coordination sphere, with four iodide ligands in the base plane and the substituted pyridine in the apical position. The rhomboidal base has sides of 4.35 and 4.30 Å and diagonals of 5.11 and 6.98 Å (Figure 6.12a). The Hg–N distance is 2.368(9) Å. Two Hg–I bonds (2.651(1) and 2.666(1) Å) are shorter than the other two distances (3.238(1) and 3.867(1) Å). The very long Hg–I interatomic distance (3.867 Å) is too long to be considered as a bond, which is often quoted to have a van der Waals radius range from 1.82^[17] to 2.24 Å^[18] for mercury and 2.1 Å for iodine. However, the distance is too short to warrant comment (dashed solid lines in Figure 6.12(a)). The mercury rhomboid-pyramidal coordination shares the edges of the base (Figure 6.12(a)) and all apical ligands point to the same side of the polymer chain along the *c* axis, as shown in Figure 6.12 (b).

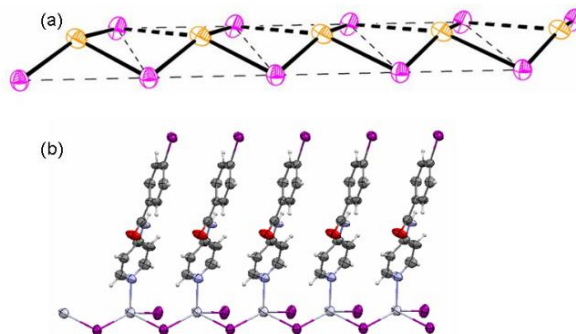


Figure 6.12(a) A view showing the rhomboidal base of the coordination sphere of mercury(II) and edge-sharing (b) Rhomboid-pyramidal coordination of mercury cations and the 1D polymer chain.

This organization promotes π - π stacking since the adjacent molecules of **INPBA** are related by a translation along the *a* axis and the distance between planes

containing pyridyl moieties is 3.559 Å and between the planes containing phenyl rings is 3.587 Å. These interactions are different to the five types of π - π stacking described previously for **NPBA** metal complex structures.^[14, 16] In addition, 1D chains are linked by C(1)–I(1)…I(3) (3.86 Å and 175°) halogen bonding (Figure 6.13(a)). This XB gives rise to corrugated planes and the adjacent chains inside the plane form an angle that is almost perpendicular (84.5°), as shown in Figure 6.13(b). These corrugated planes are joined through weak hydrogen bonding between the amide oxygen and pyridyl hydrogen atom of an **INPBA** molecule with an inversion center relationship. This gives rise to a 3D structure in which **INPBA** is involved in a coordination bond, hydrogen and halogen bonding and π - π stacking (Figure 6.13(b)).

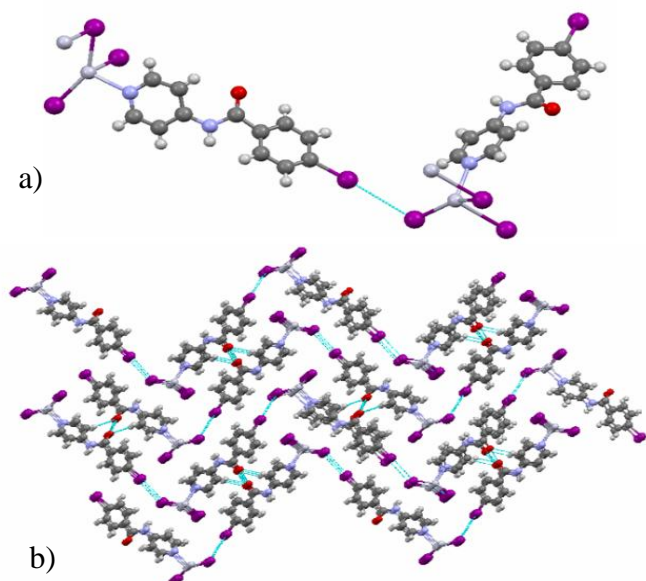
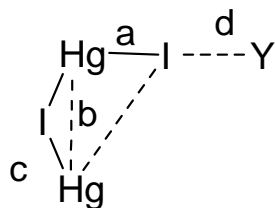


Figure 6.13 Crystal structure of $[\text{HgI}_2(\text{INPBA})]_n$. (a) Detail of C–I…I halogen bonding; (b) 3D organization of corrugated planes formed by halogen bonding.

The formation of halogen bonding gives rise to a 3D organization and is responsible for the variation in the bond distances and angles as well as the coordination geometry, when compared to others structures in which a mercury

Coordination Metal Complexes Based on 4-Iodo-N-(4-pyridyl)benzamide, a Polyfunctional Ligand

atom has a similar coordination. Seven structures were found in the Cambridge Structural Database (update Nov-2014), five with pyridine derivatives,^[19] one with a triazole derivative (refcode: VUJYUV)^[20] and one with an imidazole moiety (refcode: TAWREP).^[21] Selected distances and angles of such structures are gathered in Table 6.2 and Scheme 6.5 to facilitate comparison.



Scheme 6.5 Halogen bond with Mercury

Table 6.2 Bond lengths [Å] and angles [°] for the coordination sphere around Hg(II)

Refcode	a (Å)	b (Å)	c (Å)	d (Å)	Hg (base)	Hg-N (°)	Ref
TAWREP	2.632	4.528	4.408	3.01	0.71	2.228	89.4
LEQRAB	2.615	3.682	4.425	-	0.40	2.507	62.9
NIKBUF	2.631	3.697	4.340	-	0.39	2.489	76.0
VUJYUV	2.612	3.869	4.340	-	0.52	2.391	78.6
ADOKUA	2.614	3.766	4.308	-	0.39	2.532	89.6
ADOLAH	2.625	3.800	4.312	-	0.58	2.404	86.9
ADOKOU	2.627	3.710	4.266	-	0.41	2.503	87.8
$[\text{HgI}_2(\text{INPBA})]_n$	2.651	3.867	4.303	3.858	0.66	2.368	68.14
This							

TAWREP: 1H-benzimidazole; NIKBUF: 3-ethoxycarbonylpyridine; LEQRAB: 4,4'-Bipyridine; ADOLAH: 3,5-dimethylpyridine; ADOKUA: 3,5-dibromopyridine ADOKOU: 3,5-dichloropyridine; NIKBUF: 3-ethoxycarbonylpyridine; VUJYUV: 9-ethyl-3,6-bis(1,2,4-triazol-1-yl)-9H-carbazole

Comparison of the structures shows that the establishment of halogen bonding causes an elongation of the Hg–I bond, shortening of the Hg–N bond and a shift of the Hg atom from the plane defined by the iodine atoms (base in Table 6.2). Thus, the structure of $[\text{HgI}_2(\text{INPBA})]_n$ has the longest Hg–I distance (2.651 Å), the shortest Hg–N bond distance (2.368 Å) and the longest distance from the mercury atom to the plane defined by the iodine atoms (0.66 Å). These effects are consistent with halogen bonding wherein the iodine atom attached to the phenyl moiety behaves as an XB donor and the iodine atom attached to mercury as a XB acceptor.

6.4 Hirshfeld Surface Analysis

Hirshfeld surface analysis, which was carried out using the Crystal Explorer program,^[23] was used to evaluate intermolecular contacts in the crystal structures of **INPBA** and coordination polymers $[\text{Ag}(\text{INPBA})_2]\text{NO}_3$ (**2**), $[\text{ZnBr}_2(\text{INPBA})_2]$ (**3**), $[\text{Zn}(\text{OCOPh})_2(\text{INPBA})_2]$ (**4**), and $[\text{HgI}_2(\text{INPBA})]_n$ (**5**). As expected, the Hirshfeld surfaces of each crystallographically independent **INPBA** ligand in structures **1** to **5** reveal the close contacts of halogen and hydrogen bonding, along with other weaker interactions and contacts. The relative contributions of the different contacts to the Hirshfeld surface were calculated and these account for around 98% of the surface. The main contributors are weak $\text{H}\cdots\text{H}$, $\text{C}\cdots\text{H}$, and $\text{I}\cdots\text{H}$ dispersion forces. Comparison of the contributions of different contacts of **INPBA** and **NPBA** to Hirshfeld surfaces shows that the presence of the iodine atom increases the contact types. Specifically, the contacts involving the iodine atom represent approximately 20% of the Hirshfeld surface

The fingerprint plot (Figure 6.14) for each **INPBA** ligand is different – including that belonging to the same crystal structure – and they are characterized by spikes that correspond to $\text{O}\cdots\text{H}$, $\text{C}\cdots\text{H}$ and $\text{I}\cdots\text{H}$ interactions denoted as **a**, **b**, **c** in the fingerprint plots, respectively (Figure 6.14). The major differences between the graphs are the presence or absence of a clear area close to the center of the plot, in the vicinity of $(d_i, d_e) \approx 1.8\text{--}2.0 \text{ \AA}$ (**d**). This is related to the planar $\pi\text{-}\pi$ stacking ($\text{C}\cdots\text{C}$ and $\text{C}\cdots\text{N}$ interactions).

The $\pi\text{-}\pi$ stacking contribution to Hirshfeld surface of structures **1** to **5** ranged from 0 to almost 14% in **1** and **2**, respectively, as shown in Figure 6.14. Such a contribution is different in each crystallographically independent **INPBA** in structures **2** and **3**. Although in the silver complex the ligand that has a flatter conformation has a greater $\pi\text{-}\pi$ interaction, there is no correlation between the conformation and $\pi\text{-}\pi$ stacking in the structures studied.

Coordination Metal Complexes Based on 4-Iodo-N-(4-pyridyl)benzamide, a Polyfunctional Ligand

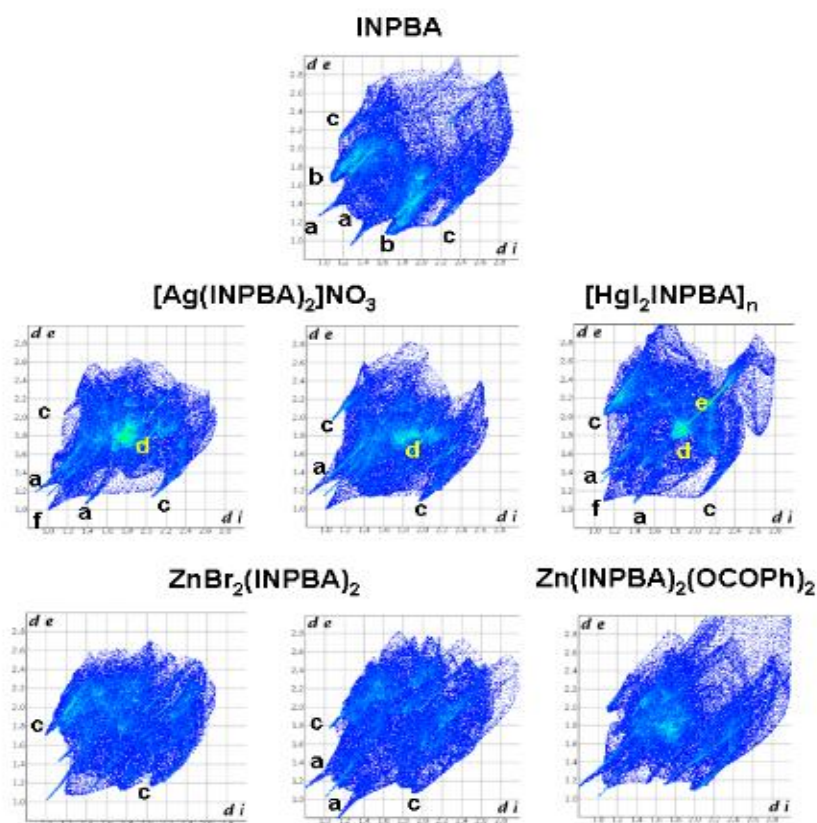


Figure 6.14 Fingerprint plots of the INPBA ligand (crystallographically different) in structures 1 to 5.

6.5 Quantum Mechanical Calculations

The complex **INPBA–INPBA** was optimized in order to verify theoretically the existence, nature, and strength of the halogen bonding. The calculations were carried out using the B98 exchange and correlation functional combined with the DGDZVP basis set for iodine and 6-311+G(d,p) basis set for the other atoms. The molecular conformations taken from the crystal structure were geometrically optimized in gas-phase conditions. The electrostatic potential map of the complex partner **INPBA** (Figure 6.15) shows a region of positive electrostatic potential (blue) located on the iodine atom along the axis of the C–I bond (σ -hole) and a negative electrostatic potential (red) located on the pyridine nitrogen atom.

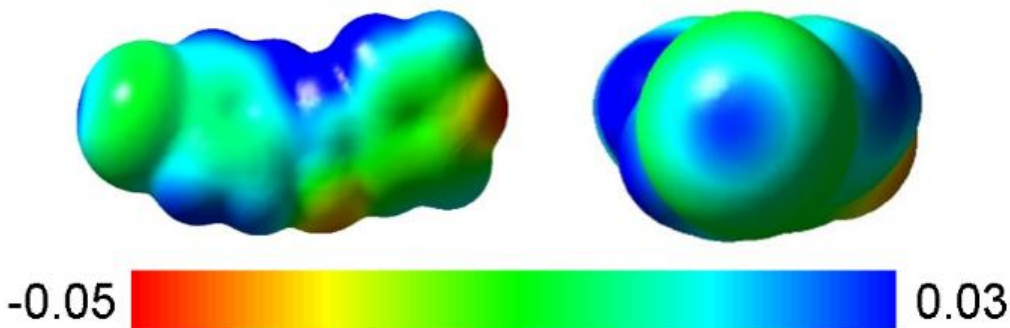


Figure 6.15 Computed electrostatic potential of minimized **INPBA**

The degree of polarization of the iodine is a function of the arene substitution pattern of electron-withdrawing groups at the para positions.^[24] Supposing that most halogen bonding is dominated by electrostatic attractions, the higher the polarization of iodine the better the halogen bond donor.^[25] The maximum value of the relative electrostatic potential on the iodine atom is 16.3 kcal/mol. This value is close to the relative potential calculated for other halogen-bonding donors such as 4-iodophenone (10.0 kcal/mol), phenyl 4-iodobenzoate (6.8 kcal/mol) and 1,4-di(iodoethynyl)benzene (24.6 kcal/mol)^[26] and corresponds to an intermediate

Coordination Metal Complexes Based on 4-Iodo-N-(4-pyridyl)benzamide, a Polyfunctional Ligand

halogen bonding donor. The key features of the B98-calculated geometries and the interaction energy between the XB-donor and XB-acceptor are gathered in Table 6.3.

Table 6.3. Interaction Energy (ΔE_{int}), Basis Set Superposition Error (BSSE) and Halogen Bonding Distance (DI…N) and Angle (ZC–I…N) of the Complex.

Partner/Complex	ΔE_{int} kcal/mol	BSSE kcal/mol	$D_{I\cdots N}$ Å	D_{I-C} Å	$Z_{C-I\cdots N}$ deg	q_N e	q_I e
INPBA				2.123		-0.472	0.195
Complex INPBA	-4.0	0.8	3.071	2.130	178.9	-0.494	0.223

The calculated noncovalent bond angle ZC–I…N is almost linear (178.8°). Moreover, the halogen-bonding distance DI…N (3.071 Å) is noticeably shorter than the sum of the van der Waals radii (3.53 Å). These data are consistent with the angle (175.3°) and the distance (2.99 Å) measured in the crystal structure. The interaction energy (ΔE_{int}) was -4.0 kcal/mol, as calculated using the equation:

$$\Delta E_{int} = E_{complex} - \sum E_{partner}$$

6.6 Conclusions

In this chapter we present the preparation and crystal structure of 4-iodo-N-(4-pyridyl)benzamide (**INPBA**), three metal complexes, namely $[\text{Ag}(\text{INPBA})_2]\text{NO}_3$, $[\text{ZnBr}_2(\text{INPBA})_2]$, $[\text{Zn}(\text{OCOPh})_2(\text{INPBA})_2]$, and the coordination polymer $[\text{HgI}_2(\text{INPBA})]_n$. The ligand **INPBA** shows a great ability to form different types of interactions such as coordination, hydrogen and halogen bonds and $\pi\cdots\pi$ stacking. This ability promotes increased dimensionality as well as the stability of the structures in compounds **1–5**. Furthermore, the interplay of coordination, halogen bonding, hydrogen bonds and $\pi\cdots\pi$ interactions in these complexes also highlights the complexity and challenge in programming the supramolecular assembly of metal organic networks.

6.7 Experimental Section

4-Iodobenzoyl chloride, 4-aminopyridine, triethylamine, silver nitrate, zinc bromide and mercury(II) iodide were used as received from commercial sources (Sigma-Aldrich or Acros). ^1H - and ^{13}C -NMR spectra were recorded on a Bruker Avance 300 spectrometer. Infrared (IR) spectra were recorded on an ATR-unit-upgraded (Golden Gate) Bruker FT-IR Vertex 70 spectrophotometer. Mass spectra were recorded on a VG Auto-spec instrument, with the ESI technique. C, H, and N analyses were carried out with a Perkin-Elmer 2400 microanalyzer.

- **4-Iodo-N-(4-pyridyl)benzamide(INPBA).**

A solution of 4-iodobenzoyl chloride (1.32 g, 5.0 mmol) and triethylamine (0.50 g, 5.0 mmol) in 50 mL of chloroform was cooled to 0 °C in an ice bath for 10 min. 4-Aminopyridine (0.470 g, 5.0 mmol) was added slowly to the cold solution over a period of 10 min. The reaction mixture was stirred at room temperature for 16 h. The solution was concentrated and a white precipitate was obtained. The solid was filtered off and washed several times with cold chloroform. Yield 1.33 g (82%). ^1H NMR spectrum (d_6 -DMSO, 300 MHz) δ from TMS: 7.63 (m, 3H, Bz), 7.78 (d, 2H, Py), 7.95 (d, 2H, *o*-Bz), 8.47 (d, 2H, Py), 10.60 (s, NH). ^{13}C NMR spectrum (d_6 -DMSO, 62.5 MHz): 114.70, 128.56, 129.15, 132.76, 134.96, 146.66, 150.97, 167.19. IR (ATR) ν_{max} (neat) / cm^{-1} : 3332, 1660, 1587, 1502, 1477, 1413, 1330, 1282, 1210, 822, 748. High resolution positive ESI-MS (amu): Calcd. for M + H 324.9834 Found: 324.9827. Anal. Calcd. for $\text{C}_{12}\text{H}_9\text{IN}_2\text{O}$: C 44.47, H 2.80, N 8.64. Found: C 44.22, H 2.67, N 8.61.

- **Preparation of INPBA metal complexes**

A solution of INPBA (32 mg, 0.10 mmol) in 10 mL of THF was added to 5 mL of a methanolic solution of inorganic salt (0.1 mmol). The solution was allowed to slowly evaporate with orbital stirring over a period of 48 h, during which time colorless crystals formed.

[Ag(INPBA)₂](NO₃) Yield 36.0 mg, 73%. IR (ATR) ν_{max} (neat) / cm⁻¹: 3342, 1680, 1591, 1509, 1478, 1425, 1378, 1323, 1288, 1209, 1091. High resolution positive ESI-MS (a.m.u.): Calcd. for Ag(INPBA)₂ 754.8570 Found: 754.8599. Anal. Calcd. for C₁₂H₉IN₂O: C 44.47, H 2.80, N 8.64. Found: C 44.22, H 2.67, N 8.61. Anal. Calcd. for C₂₄H₁₈I₂N₅O₅Ag: C 35.23, H 2.22, N 8.56. Found: C 34.89, H 2.14, N 8.54.

[ZnBr₂(INPBA)₂] Yield 39.1 mg, 71%. IR (ATR) ν_{max} (neat) / cm⁻¹: 3349, 1695, 1670, 1613, 1585, 1510, 1497, 1478, 1427, 1332, 1294, 1262, 1207, 1092. High resolution positive ESI-MS (a.m.u.): Calcd. for [ZnBr₂(INPBA)₂] + Na: 894.7055 Found: 894.7036. Anal. Calcd. for C₂₄H₁₈Br₂I₂N₄O₂Zn: C 33.00, H 2.08, N 6.41. Found: C 30.52, H 2.01, N 5.85.

[HgI₂(INPBA)]_n Yield 63.1 mg, 81%. IR (ATR) ν_{max} (neat) / cm⁻¹: 3368, 1702, 1603, 1585, 1578, 1497, 1475, 1419, 1327, 1264, 1208, 1091. Anal. Calcd. for C₁₂H₉I₃N₂OHg: C 18.51, H 1.17, N 3.60. Found: C 18.97, H 1.07, N 3.58.

[Zn(OCOPh)₂(INPBA)₂]₍₄₎ X-ray quality single crystals of **[Zn(OCOPh)₂(INPBA)₂]₍₄₎** were obtained by three layer diffusion: INPBA in MeOH, NaOCOPh in EtOH and Zn(NO₃)₂ in water.

• X-ray crystallographic analysis

X-ray diffraction experiments were carried out on Oxford-diffraction Xcalibur S and Bruker AXS D8 Venture diffractometers. Mo-K α radiation was used for data collection for **1**, **2**, **4** and **5** and Cu–K α for **3**. Software packages XSCANS^[27] and CrysAlis^[28] were used to process data.

Final cell parameters were obtained by global refinement of reflections obtained by integration of all the frames data. The structures were solved by direct methods and refined by the full-matrix method based on F² using the SHELXTL program.^[29] The non-hydrogen atoms of **1** to **5** were refined anisotropically, the hydrogen atoms

Coordination Metal Complexes Based on 4-Iodo-N-(4-pyridyl)benzamide, a Polyfunctional Ligand

of **2**, **4**, **5** were observed in difference electron density maps and refined isotropically. Hydrogen atoms of **1** and **3** were included at idealized positions by using a riding model and refined isotropically. The crystal parameters and basic information relating data collection and structure refinement are summarized in Table 6.4.

Table 6.4 Crystallographic data for INPBA, [Ag(INPBA)2]NO₃(2**), [ZnBr₂(INPBA)2] (**3**), [Zn(OCOPh)₂(INPBA)2] (**4**) and [HgI₂(INPBA)]n (**5**)**

Compound	INPBA	2	3^(a)	4	5
Empirical formula	C ₁₂ H ₉ IN ₂ O	C ₂₄ H ₁₈ N ₅ O ₅ I ₂ Ag	C ₂₄ H ₁₈ N ₄ O ₂ Br ₂ I ₂ Zn	C ₃₈ H ₂₈ I ₂ N ₄ O ₆ Zn	C ₁₂ H ₉ HgI ₃ N ₂ O
Formula weight	324.11	818.10	873.41	955.81	778.50
Crystal System	Monoclinic	Triclinic	Monoclinic	Orthorhombic	Monoclinic
a, Å	5.3119(3)	9.3872(5)	9.7184(2)	14.2615(6)	4.303(12)
b, Å	14.3087(6)	11.4744(4)	27.7576(6)	8.9996(3)	14.824(5)
c, Å	15.0594(9)	13.2529(6)	9.8707(2)	29.6078(13)	25.840(8)
α, deg		107.591(4)			
β, deg	90.017(5)	110.075(5)	91.040(2)		
γ, deg		94.437(4)			
V, Å³	1144.61(11)	1251.65(10)	2662.27(10)	3800.1(3)	1648.3(9)
T, K	248(2)	292(2)	100(2)	100(2)	293(2)
Space group	<i>P</i> 2 ₁ /c	<i>P</i> ī	<i>P</i> 2 ₁ /c	<i>P</i> bcn	<i>P</i> 2 ₁ /c
Z	4	2	4	4	4
μ(Mo Kα), mm⁻¹	2.777	3.318	23.252	2.321	14.950
Θ range, deg	1.96 to 28.32	1.75 to 26.37	3.18 to 74.29	2.68 to 26.37	3.15 to 25.00
Refl. collected	8308	8687	20071	40876	5264
Uniq reflect / R_{int}	2604 / 0.0384	5123 / 0.0239	5330 / 0.0612	3879 / 0.0326	2884 / 0.0340
R1/wR2 (I>2σ)	0.0376 / 0.0655	0.0295 / 0.0638	0.0500 / 0.1287	0.0315 / 0.0726	0.0420 / 0.0778
R1/wR2 (all data)	0.0529 / 0.0703	0.0336 / 0.0677	0.0521 / 0.1304	0.0382 / 0.0764	0.0666 / 0.0872
Max. shift/esd	0.001	0.009	0.001	0.001	0.004
Residual ρ/e Å⁻³	0.669 and -0.633	1.181 and -0.975	1.895 and -2.123	2.016 and -1.927	1.161 and -1.361

• Hirshfeld Surface Analysis

Hirshfeld surfaces and the associated fingerprint plots were calculated using CrystalExplorer,^[23a] which accepts a structure input file in the CIF format. Bond lengths to hydrogen atoms were set to typical neutron values (C–H = 1.083 Å,

$\text{N-H} = 1.009 \text{ \AA}$, $\text{O-H} = 0.983 \text{ \AA}$). The distance from the Hirshfeld surface to the nearest atoms outside and inside the surface are characterized by the quantities d_e and d_i , respectively, and the normalized contact distance based on these, $d_{norm} = (d_i - r_i^{vdW})/r_i^{vdW} + (d_e - r_e^{vdW})/r_e^{vdW}$, with r_i^{vdW} and r_e^{vdW} are the van der Waals radii of the atoms. The 2D histograms, fingerprints, plot distance external to the surface (d_e) versus distance internal to the surface (d_i): is the distance from the surface to the nearest atom in the molecule itself.

• Computational Methods.

Quantum chemical calculations were performed using the Gaussian 09^[30] suite of programs. Geometry optimizations were carried out in the gas phase with the B98^[31] method, employing the 6-311G+(d,p)^[32] basis set for all atoms except iodine, for which the DGDZVP^[33] basis set was used. Geometry optimizations were carried out without constraints, using the default convergence criteria for the Gaussian software. The natural bond orbital (NBO) analysis^[34] using the NBO module contained in the Gaussian 09 program was performed on the basis of the minimized structures in order to calculate the NBO charges. The resulting electronic energies of interaction were corrected for scale (0.9884),^[35] zero point differences and for basis set superposition errors.

6.8 Bibliography

- [1] M. D. Allendorf and V. Stavila, *CrystEngComm* **2015**, *17*, 229-246.
- [2] S. Q. Liu, T. Kuroda-Sowa, H. Konaka, Y. Suenaga, M. Maekawa, T. Mizutani, G. L. Ning and M. Munakata, *Inorg. Chem.* **2005**, *44*, 1031-1036.
- [3] M. D. Allendorf, C. A. Bauer, R. K. Bhakta and R. J. Houk, *Chem Soc Rev* **2009**, *38*, 1330-1352.
- [4] a) O. M. Yaghi, M. O'Keeffe, N. W. Ockwig, H. K. Chae, M. Eddaoudi and J. Kim, *Nature* **2003**, *423*, 705; b) J. L. C. Rowsell and O. M. Yaghi, *J. Am. Chem. Soc.* **2006**, *128*, 1304-1315; c) K. Sumida, D. L. Rogow, J. A. Mason, T. M. McDonald, E. D. Bloch, Z. R. Herm, T.-H. Bae and J. R. Long, *Chem. Rev.* **2012**, *112*, 724-781; d) M. P. Suh, H. J. Park, T. K. Prasad and D.-W. Lim, *Chem. Rev.* **2012**, *112*, 782-835.
- [5] C. B. Aakeröy, A. M. Beatty and D. S. Leinen, *Angew. Chem. Int. Ed.* **1999**, *38*, 1815-1819.
- [6] a) L. Brammer, G. M. Espallargas and S. Libri, *CrystEngComm* **2008**, *10*, 1712-1727; b) R. Bertani, P. Sgarbossa, A. Venzo, F. Lelj, M. Amati, G. Resnati, T. Pilati, P. Metrangolo and G. Terraneo, *Coord. Chem. Rev.* **2010**, *254*, 677; c) R. Bertani, P. Sgarbossa, A. Venzo, F. Lelj, M. Amati, G. Resnati, T. Pilati, P. Metrangolo and G. Terraneo, *Coord. Chem. Rev.* **2010**, *254*, 677-695; d) R. W. Troff, T. Mäkelä, F. Topič, A. Valkonen, K. Raatikainen and K. Rissanen, *Eur. J. Org. Chem.* **2013**, *2013*, 1617; e) B. Li, S.-Q. Zang, L.-Y. Wang and T. C. W. Mak, *Coord. Chem. Rev.* **2016**, *308*, 1-21.
- [7] S. Graus in *Sintones supramoleculares clásicos: nuevas arquitecturas cristalinas y determinación de estructuras absolutas*, Vol. Thesis Zaragoza, University of Zaragoza, **2015**.
- [8] a) M. D. Ward, *Dalton Trans.* **2010**, *39*, 8851-8867; b) J. E. Ormond-Prout, P. Smart and L. Brammer, *Cryst. Growth Des.* **2012**, *12*, 205-216.
- [9] a) K. Biradha, C.-Y. Su and J. J. Vittal, *Cryst. Growth Des.* **2011**, *11*, 875-886; b) G. R. Desiraju, J. J. Vittal and A. Ramanan, *Crystal Engineering: A Textbook*, World Scientific Pub. Co. Inc. **2011**.
- [10] a) H. R. Khavasi and A. A. Tehrani, *CrystEngComm* **2013**, *15*, 5799-5812; b) H. R. Khavasi and A. A. Tehrani, *Inorg. Chem.* **2013**, *52*, 2891-2905.
- [11] C. B. Aakeroy, N. Schultheiss, J. Desper and C. Moore, *CrystEngComm* **2007**, *9*, 421-426.
- [12] H. R. Khavasi, M. Hosseini, A. A. Tehrani and S. Naderi, *CrystEngComm* **2014**, *16*, 4546.
- [13] A. Collas, R. De Borger, T. Amanova and F. Blockhuys, *CrystEngComm* **2011**, *13*, 702-710.
- [14] J. C. Noveron, M. S. Lah, R. E. Del Sesto, A. M. Arif, J. S. Miller and P. J. Stang, *J. Am. Chem. Soc.* **2002**, *124*, 6613-6625.
- [15] H. R. Khavasi, M. Hosseini, A. A. Tehrani and S. Naderi, *CrystEngComm* **2014**, *16*, 4546-4553.
- [16] J. C. Noveron, A. M. Arif and P. J. Stang, *Chem. Mat.* **2003**, *15*, 372-374.
- [17] H. J. Bohórquez and R. J. Boyd, *Chem. Phys. Lett.* **2009**, *480*, 127-131.
- [18] a) S. Nag, K. Banerjee and D. Datta, *New J. Chem.* **2007**, *31*, 832-834; b) S.-Z. Hu, Z.-H. Zhou and B. E. Robertson, *Z. Kristallogr.* **2009**, *224*, 375-383.
- [19] a) C. Hu, I. Kalf and U. Englert, *CrystEngComm* **2007**, *9*, 603-610; b) W.-T. Chen, M.-S. Wang, X. Liu, G.-C. Guo and J.-S. Huang, *Cryst. Growth Des.* **2006**, *6*, 2289-2300; c) Q.-Y. Du, J.-H. Qin and H.-X. Wu, *Chin. J. Struct. Chem.* **2007**, *26*, 817-821.
- [20] H.-P. Zhou, J.-H. Yin, L.-X. Zheng, P. Wang, F.-Y. Hao, W.-Q. Geng, X.-P. Gan, G.-Y. Xu, J.-Y. Wu, Y.-P. Tian, X.-T. Tao, M.-H. Jiang and Y.-H. Kan, *Cryst. Growth Des.* **2009**, *9*, 3789-3798.
- [21] Y.-H. Shen, J.-G. Liu and D.-J. Xu, *Acta Cryst. E: Structur. Rep. Online* **2005**, *61*, m1880-m1882.
- [22] Y. H. Shen, J. G. Liu and D. J. Xu, *Acta Crystallogr., Sect. E: Struc. Rep. Online* **2005**, *61*, M1880-M1882.
- [23] a) S. K. Wolff, D. J. Grimwood, J. J. McKinnon, M. J. Turner, D. Jayatilaka and M. A. Spackman in *CrystalExplorer Vol. (Ed. CrystalExplorer)*, University of Western Australia, **2012**; b) M. A. Spackman and D. Jayatilaka, *CrystEngComm* **2009**, *11*, 19-32.

- [24] C. B. Aakeroey, M. Baldrighi, J. Desper, P. Metrangolo and G. Resnati, *Chem. Eur. J.* **2013**, *19*, 16240-16247.
- [25] F. C. Pigge, V. R. Vangala, D. C. Swenson and N. P. Rath, *Cryst. Growth Des.* **2010**, *10*, 224–231.
- [26] L. Gonzalez, N. Gimeno, M. R. Maria Tejedor, V. Polo, M. B. Ros, S. Uriel and J. L. Serrano, *Chem. Mat.* **2013**, *25*, 4503-4510.
- [27] XSCANS in Vol. Madison, Wisconsin USA., **1994**.
- [28] CrysAlis and CCD in *Oxford Diffraction Ltd*, Vol. Abingdon, England, **2006**.
- [29] G. M. Sheldrick, *Acta Cryst. A* **2008**, *64*, 112-122.
- [30] M. J. Frisch, G. W. Trucks, H. B. Schlegel, G. E. Scuseria, M. A. Robb, J. R. Cheeseman, G. Scalmani, V. Barone, B. Mennucci, G. A. Petersson, H. Nakatsuji, M. Caricato, X. Li, H. P. Hratchian, A. F. Izmaylov, J. Bloino, G. Zheng, J. L. Sonnenberg, M. Hada, M. Ehara, K. Toyota, R. Fukuda, J. Hasegawa, M. Ishida, T. Nakajima, Y. Honda, O. Kitao, H. Nakai, T. Vreven, J. Montgomery, J. A., J. E. Peralta, F. Ogliaro, M. Bearpark, J. J. Heyd, E. Brothers, K. N. Kudin, V. N. Staroverov, R. Kobayashi, J. Normand, K. Raghavachari, A. Rendell, J. C. Burant, S. S. Iyengar, J. Tomasi, M. Cossi, N. Rega, J. M. Millam, M. Klene, J. E. Knox, J. B. Cross, V. Bakken, C. Adamo, J. Jaramillo, R. Gomperts, R. E. Stratmann, O. Yazyev, A. J. Austin, R. Cammi, C. Pomelli, J. W. Ochterski, R. L. Martin, K. Morokuma, V. G. Zakrzewski, G. A. Voth, P. Salvador, J. J. Dannenberg, S. Dapprich, A. D. Daniels, Ö. Farkas, J. B. Foresman, J. V. Ortiz, J. Cioslowski and D. J. Fox in *Gaussian 09*, Vol. Gaussian Inc., Wallingford CT, **2009**.
- [31] a) P. M. W. Gill, *Mol. Phys.* **1996**, *89*, 433-445; b) J. P. Perdew, K. Burke and M. Ernzerhof, *Phys. Rev. Lett.* **1996**, *77*, 3865-3868; c) M. G. Chudzinski and M. S. Taylor, *J. Org. Chem.* **2012**, *77*, 3483-3491.
- [32] W. J. Hehre, L. Radom, S. P. V. R. and J. A. Pople in *Ab initio Molecular Orbital Theory*, Vol. Wiley, New York, **1986**.
- [33] N. Godbout, D. R. Salahub, J. Andzelm and E. Wimmer, *Can. J. Chem.* **1992**, *70*, 560-571.
- [34] A. E. Reed, L. A. Curtiss and F. Weinhold, *Chem. Rev.* **1988**, *88*, 899-926.
- [35] J. P. Merrick, D. Moran and L. Radom, *J. Phys. Chem. A* **2007**, *111*, 11683-11700.

Chapter 7 Conclusions

General Conclusions

The haloethynyl group form strong halogen bond interactions comparable to the well known Iodopentafluorobenzene moieties. The ethynyl group acts as a good electron withdrawing increasing the sigma hole in the halogen, mainly in the Iodine atom.

Haloethynyl derivatives behave as excellent building blocks in supramolecular chemistry, thanks to the halogen bond interaction and the anisotropy of the bond. Furthermore, haloethynyls groups act as heteroditopic tectons.

Halogen bond is useful in different applications like liquid crystals or porous materials, opening new possibilities in organic chemistry materials.

Capítulo 2

Se han sintetizado y caracterizado diferentes alquinos yodados. Además se ha realizado un estudio comparativo de las estructuras cristalinas de estos alquinos yodados con sus precursores con el grupo etinilo.

Los estudios realizados permiten concluir que cuando las moléculas son rígidas y planas tanto los derivados iodados como sus precursores pueden dar lugar organizaciones supramoleculares isoestructurales. Las diferencias entre las estructuras de los derivados alquínicos y sus yododerivados homólogos están relacionadas con el número de grupos etinilos y su proximidad.

Por otro lado, las moléculas flexibles no llegan a presentar isostructuralismo. En estos derivados la organización supramolecular no está gobernada únicamente por la interacción más fuerte, por ejemplo el enlace de halógeno o el enlace de hidrógeno ($C_{sp}-I \cdots Y$ and $C_{sp}-H \cdots Y$), cobrando mayor importancia en el empaquetamiento final de la estructura cristalina otras interacciones débiles como $C_{sp^2}-H \cdots Y$.

Capítulo 3

Los derivados yodados de la base de Tröger “2,8-diido-4,10-dimethyl-6H,12H-5,11-methano-dibenzodiazocine” (*rac*-**I**) y (*5S,11S*)-**I**) quiral son tetraheterotópicos y autocomplementarios mediante enlaces de halógeno, siendo adecuados para obtener tanto de estructuras supramoleculares tipo clatrato como materiales cristalinos compactos.

Además, se han obtenido estructuras porosas tipo diamante cuando *rac*-**I** es cristalizado a partir de una solución de diclorometano. Las arquitecturas supramoleculares de las estructuras compactas *rac*-**I** y (*5S,11S*)-**I** presentan algunas similitudes aunque el enlace de halógeno juegue en diferentes roles en cada estructura. Así, en *rac*-**I** son observadas las interacciones de enlace de halógeno

N···I y I···I, mientras que en **(5S,11S)-1** solo esta presente la interacción I···I. Estas son las primeras estructuras de derivados yodados de la base de Tröger que presentan interacciones tipo I···I.

Por otro lado, el derivado de base de Tröger “*2,8-diiodoethynyl-4,10-dimethyl-6H,12H-5,11-methanodibenzodiazocene*” (***rac*-2**) cristaliza en el grupo espacial monoclinico P2₁/c mostrando canales nanométricos los cuales representan el 20% de volumen de la celda. Estos canales están ocupados por moléculas de disolvente. Los dos grupos yodoetinilos se comportan como fuertes dadores de enlaces de halógeno I···N y I···π_(Ar). Estas interacciones forman unidades dímeras formadas por los dos enantiómeros **(5S,11S)-2** y **(5R,11R)-2** que juegan un papel fundamental en la obtención de organizaciones cristalinas nanoporosas.

Capítulo 4

En este capítulo se han descrito once estructuras basadas en complejos de enlace de halógeno a partir de “*bis(haloethynyl)benzene*” con moléculas cuyos aceptores de enlace de halógeno eran: nitrógeno, oxígeno y bases halogenadas. Todo ello además del análisis de las superficies de Hirshfeld y los cálculos de química cuántica nos permite establecer que **pBIEB**, **pBBrEB** y **mBIEB** son buenos dadores de XB, haciendo de ellos una herramienta muy útil en el diseño de estructuras supramoleculares.

La distancia del enlace de halógeno C_{sp}–I···N depende de la hibridación del átomo de nitrógeno y decrece siguiendo la tendencia desde *sp* a *sp*³ a *sp*². Además, la distribución electrónica del grupo haloetinil muestra un área nucleofílica cilíndrica alrededor del triple enlace y del átomo de halógeno lo que permite la formación de enlaces de hidrógeno del tipo C_{sp2}–H···X y C_{sp2}–H···π_(alkyne) con hidrógenos del anillo aromático, que impide la formación de organizaciones tipo espiga. La energía de estabilización de estas estructuras supramoleculares varía entre 2.9 a 5.7 kcal mol⁻¹. A pesar de ser interacciones débiles, sus efectos en la estructura

cristalina y el empaquetamiento es relevante y en combinación con los enlaces de halógeno son herramientas muy útiles para el aumento de la dimensionalidad en los cocristales teniendo un gran interés en el desarrollo de materiales orgánicos.

El ITC es una herramienta útil para estudiar las interacciones de los enlaces halógenos, ayudando a entender la esfera de coordinación, en este caso, del bromuro.

Capítulo 5

Los derivados de yodoetinilbenceno han demostrado ser buenos dadores de enlaces de halógeno. La unión de un átomo de yodo a un átomo de carbono con hibridación sp conduce a la formación de interacciones no covalentes con derivados de piridina fuertes ($\Delta E_{int} = -10$ kcal / mol) e interacciones un poco más débiles con los benzonitrilos ($\Delta E_{int} = -7,5$ kcal / mol).

El pBIEB al ser una molécula lineal forma complejos de enlace de halógeno con aceptores basados en piridina que llevan uno o dos anillos aromáticos para dar complejos que muestran fases calamíticas ordenadas (SmB y CrG) en amplios intervalos de temperatura. Por otra parte, el mBIEB al ser una molécula angular forma complejos de enlace de halógeno con derivados de piridina que contienen tres anillos aromáticos para dar complejos que muestran fases de tipo banana. Además, el 1,3,5-TIEB tipo disco forma complejos de enlace de halógeno con derivados de piridina con aminas como conectores. Los estudios XRD, ITC, Raman y de modelización apoyan los resultados experimentales y también explican las interacciones más débiles de estos dadores de halógeno con un aceptor basado en benzonitrilo. Se encontró experimentalmente que esta interacción más débil impide la formación de complejos homogéneos de enlace de halógeno tras la fusión.

Capítulo 6

En este capítulo se ha presentado la preparación y síntesis de la estructura cristalina de “*4-iodo-N-(4-pyridyl)benzamide*” (**INPBA**), tres complejos metálicos, $[\text{Ag}(\text{INPBA})_2]\text{NO}_3$, $[\text{ZnBr}_2(\text{INPBA})_2]$, $[\text{Zn}(\text{OCOPh})_2(\text{INPBA})_2]$, y un polímero de coordinación $[\text{HgI}_2(\text{INPBA})]_n$. El ligando **INPBA** da lugar a diferentes tipos de interacciones tales como: coordinación, enlaces de hidrógeno y de halógeno e interacciones de apilamiento $\pi\cdots\pi$. Esto favorece el aumento de la dimensionalidad así como la estabilidad de la estructura en los compuestos. Además, la interacción de la coordinación, el enlace de halógeno, los enlaces de hidrógeno y las interacciones $\pi\cdots\pi$ en estos complejos también pone de manifiesto la complejidad y desafío en el diseño de la organización supramolecular de redes orgánicas metálicas.

